

Comparing Physical and Virtual Methods for Daylight Performance Modelling Including Complex Fenestration Systems

THÈSE N° 4130 (2008)

PRÉSENTÉE LE 3 SEPTEMBRE 2008

À LA FACULTE ENVIRONNEMENT NATUREL, ARCHITECTURAL ET CONSTRUIT
LABORATOIRE D'ÉNERGIE SOLAIRE ET PHYSIQUE DU BÂTIMENT
PROGRAMME DOCTORAL EN ENVIRONNEMENT

ÉCOLE POLYTECHNIQUE FÉDÉRALE DE LAUSANNE

POUR L'OBTENTION DU GRADE DE DOCTEUR ÈS SCIENCES

PAR

Anothai THANACHAREONKIT

Master of Architecture, Chulalongkorn University, Bangkok, Thaïlande
et de nationalité thaïlandaise

acceptée sur proposition du jury:

Prof. A. Mermoud, président du jury
Prof. J.-L. Scartezzini, directeur de thèse
Prof. M. Andersen, rapporteur
M. Bodart, rapporteur
Prof. L. Ortelli, rapporteur



ÉCOLE POLYTECHNIQUE
FÉDÉRALE DE LAUSANNE

Suisse
2008

Acknowledgements

Throughout my stay at LESO-PB for my PhD, I worked with some very wonderful people. I take this opportunity at the most important junction of my life to acknowledge my gratitude to all of them directly or indirectly involved in my work throughout the course of my PhD.

Prof. Jean-Louis Scartezzini, my supervisor provided me with an excellent guidance and advice that greatly helped me presenting the thesis in its present form. Working under him has not only equipped me technically to excel in the field of science and research but has also matured me into a better human being. I can only say that my vocabulary is not enough to thank him.

Prof. Andre Marmoud, Prof. Luca Otelli, Prof. Marilynne Andersen and Dr Magali Bodart deserve special thanks as the president of the Jury and thesis committee members for their attention, their comments and suggestions in this thesis. In particular, I would like to thank Prof. Marilynne for her support in the early stage of my research. Her advice and supervision broadened my perspective on the practical aspects of my study.

I would also like to thank the Swiss Federal Commission for Scholarships for Foreign Students(FCS) who gave me the opportunity to come to study in Switzerland. I would also like to thank the Velux Foundation for the financial support for this thesis.

Many thanks go in particularly to Christian Roecker, Pierre Loesch and Yonel Teodorescu for helping the research to run smoothly and for assisting me in many different ways. I would also like to thank Laurent Deschamps and his team for their assistance with all the computer stuffs.

I also thank Dr. Laurent Michel for his valuable advice in the research equipments, spending his precious time to answer my questions and even visiting me to help and set up the scientific devices. Dr. Raphael Compagnon for his introduction to the Radiance program and his helps to employ it afterwards was very helpful. Thanks also to Dr. Darren Robinson for teaching me various sky models and David Lindelof for the technical inputs he gave me from time to time.

I benefited a lot in the field of various imaging technique from Steve Selkowitz, Eleanor Lee and Luis Fernandes. Their kind assistance deserves special mention here.

I would also like to thank Dai Jones who carefully reread all the chapters in this thesis, gave me several useful advice until the last day of the writing, to Margaret Howett who always supported me and taught me technical writing in English.

It is also a pleasure to thank all my colleagues for providing an unforgettable environment, warmth and fun:

I am grateful to the secretaries in LESO-PB, Suzanne L'Eplattenier, Sylvette Renfer and Barbara Smith, for facilitating the laboratory and assisting me in many ways.

Many thanks to Jerome Kaempf for his helps, advice in daylighting simulations with Radiance and translating the summary from English to French of this thesis, to Adil Rasheed for rereading parts of the thesis. Thanks again to both of them for their fun zone in their office where I could stop to have a drink, listen to some jokes while I was tired.

Thanks to Natalia Filchakova and Apiparn Borisuit for their constant support during the compilation of my thesis and accompanying me for relaxation.

II

Last but not the least I would like to thank Maria Cristina Munari Probst, Paula Tosolini, Marylene Montavon, Mario Germano, Jessen Page and Frederic Haldi for their constant source of encouragement during my study.

I would also like to thank all the members in LESO-PB for such a pleasure working environment.

Further more, I wish to thank my friends in Thailand and Switzerland, Pariyaree, Patrawan, Sirinute, Sukhwan, Mali, Wanlaya, Takeru Bessho, Mio Tsuneyama, Sawarin Wirojchoochut, Mingkwan Nipitwatanaphon and Sandeep Dhanik for their emotional support, entertainment, friendship and care.

My deepest gratitude goes to my boyfriend, Adam Machacek who patiently helped me in this work, always supported me in many ways. His help was instrumental in providing a visual boost to my PhD. Thesis. His sweet smiles were very effective to ease out the pressure in tough times that I faced occasionally.

I wish to thank my entire family, my grand-parents, my uncles and aunts, my cousins for providing a caring and loving family environment for me. Really special thanks to my parents and brother. I would not have seen this day without them and their support.

Summary

III

Physical or virtual models are commonly employed to visualize the conceptual ideas of architects, lighting designers and daylighting researchers. The models are also used to assess the daylighting performance of their buildings, particularly when Complex Fenestration Systems (CFS) are considered. Recent studies have revealed a general tendency of physical models to over-estimate the performance, usually expressed through work plane illuminance and daylight factor profiles, when compared to that of the real building. These discrepancies can be attributed to several experimental errors. To analyze the main sources of error, a set of comparisons between a real building, a virtual model and a physical model was undertaken. The real building in our case consisted of a full scale test module with a south-facing windows designed for experimentation on daylighting systems. A virtual model was a computed model created in Radiance program while the physical model was a scale model (1:10) of the real case. The fenestration systems considered in this study were a simple window (double glazing) and two CFS (Laser-cut panel and Prismatic film).

The physical model was placed in outdoor conditions similar to that of the real building as well as under a scanning sky simulator (for both real sky luminance distribution and CIE standard sky); the virtual model simulations were carried out with the program Radiance using the GenSky function (for CIE standard sky) and the Partial Daylight Factor (PDF) method, the later using the real sky luminance distribution acquired by a digital sky scanner at the same time as the the real building's daylight performance was assessed. The daylighting performances of the building, daylight factor (DF) for overcast sky and illuminance ratio (IR) for clear sky, were monitored using illuminance meters: a set of sensors for exterior illuminance and another set of equally spaced 7 sensors placed at 1m intervals starting from the window plane for the interior space were used for that purpose. The interior surface luminance of both real building and physical model was measured using a luminance meter and a High Dynamic Range (HDR) imaging technique (within the Photosphere program). The Radiance program was used to determine the interior surface luminance within the virtual model. The measured performance of the real case, physical models and virtual models were compared, the causes of discrepancies between the real building and models were analyzed. The causes of errors that were evaluated were modeling of building details and dimensions, CFS modeling, mocking-up of the photometric properties (surface reflectance and window transmittance), model location as well as photometer features. To study the impact of these error sources on daylighting performance assessment, virtual models created using the Radiance program were used to achieve a sensitivity analysis of modeling errors. The significant factors were considered, leading to a set of modeling guidelines.

The experimental study shows that large discrepancies can occur in daylighting performance figures. For example if glazings are omitted from the model's window, a relative divergence of 25% to 40% can be found at different points in the room, suggesting more light entering than actually measured in the real building. Inaccuracy in window transmittance inaccuracy is a major cause of errors commonly found in daylight modeling. In addition, significant discrepancies can be caused by even slight error in surface reflectance values. Only 10% overestimation of surface reflectance modeling leads up to 80% relative errors in work plane illuminance for a simple window and up to 90% for the assessment of CFS. Continuous sky distribution presented more accurate results than 145 sky sectors simulation, particularly when CFS were evaluated. These discrepancies can be reduced by making an effort to mock up the geometric and photometric features including the daylight simulation of the models carefully. A checklist presented in this thesis can be used as a guideline to help the daylight designers to estimate and avoid errors when assessing daylighting performance.

Key words: Daylighting, scale model, virtual model, errors sources, daylighting performance assessment, modelling guidelines

Résumé

Les modèles physiques ou virtuels sont communément employés pour visualiser les idées projectuelles des architectes, des concepteurs d'éclairage et des chercheurs en d'éclairage naturel. Ils sont de même utilisés pour déterminer les performance des bâtiment, et plus particulièrement des systèmes complexes de fenêtres (CFS).

Des études récentes ont montré une tendance générale dans les modèles physiques à la sur -estimation de la performance en lumière naturelle en comparaison avec des bâtiments réels, à travers des profils d'éclairement sur le plan de travail et de facteurs lumière du jour; plusieurs sources d'erreur en sont la cause.

Pour analyser les principales sources d'erreur, un ensemble de comparaison d'un cas réel (un module de test grandeur nature destiné à l'expérimentation de systèmes de lumière naturelle), d'un model virtuel crée à l'aide du programme Radiance ainsi qu'un modèle physique à l'échelle 1:10 a été entrepris. Les systèmes de fenêtres considérés dans cette étude étaient une fenêtre latérale (double vitrage) et deux CFS (Laser-cut panel et film prismatique).

Le modèle physique a été placé dans des conditions extérieures identiques au bâtiment réel, ainsi que sous un ciel artificiel afin de reproduire la distribution de luminance du ciel réel et de ciels standard CIE. Des simulations numériques ont été réalisées en utilisant la fonction Radiance GenSky (pour le ciel CIE standard) et la méthode des Facteurs de Lumière du Jour partiels, cette dernière utilisant la distribution de luminance du ciel réel obtenue à l'aide un scanneur numérique de ciel au (mesure simultanée sur le bâtiment réel).

Les performances en lumière naturelle du bâtiment, les facteurs de lumière du jour (FLJ) pour les ciels couverts et le facteur d'éclairement pour les ciels sereins, ont été mesurés par un ensemble de luxmètres pour l'éclairement extérieur et, pour l'éclairement intérieur, 7 senseurs individuels placés à 1m d'intervalle depuis la fenêtre. Les distributions de luminance du ciel ont été mesurées par le biais d'un scanneur numérique de ciel. La luminance des surfaces intérieures des modèles réels et virtuels ont été mesurée par un luminance-mètre et des techniques d'imagerie High Dynamic Range (à l'aide du logiciel Photosphere). Le programme Radiance a été utilisé pour déterminer la luminance des surfaces intérieures dans le cas du modèle virtuel. Finalement, une comparaison a été effectuée pour les valeurs obtenues dans les cas réel, physique et virtuel.

Les causes des différences obtenues entre les valeurs du cas réel et des modèles furent analysées. Plusieurs causes d'erreur furent trouvées : la modélisation des détails du bâtiment et de ses dimensions, la modélisation du CFS, la reproduction des propriétés photométriques (réflectance des surface et transmittance des fenêtres), la position du modèle ainsi que les caractéristiques des sondes photométriques.

Pour étudier l'impact de ces sources d'erreur sur l'évaluation de la performance de la lumière naturelle, des modèles virtuels créés à l'aide du logiciel Radiance ont été utilisés afin de réaliser une étude de sensibilité des imprécisions des modèles. Les facteurs les plus importants furent considérés, ce qui a mené à proposer des règles de conception pour les modèles.

V

L'étude expérimentale montre que de grandes différences peuvent apparaître pour les grandeurs qui caractérisent la performance en lumière naturelle. Pour exemple, si le vitrage est omis dans la modélisation de la fenêtre (un cas relativement fréquent), une différence relative de 25 et 40% peut être trouvée à différents endroits de la pièce, ce qui suggère que plus de lumière n'entre par rapport au bâtiment réel. L'inexactitude dans le coefficient de transmission des fenêtres est une cause commune d'erreurs dans la modélisation en éclairage naturel, bien que son impact soit très important par rapport aux autres. De surcroît, de grosses incertitudes peuvent être dues à de petites différences dans les facteurs de réflexion des surfaces intérieures.

Rien que 10% de sur-estimation dans la modélisation de la réflectance de la surface conduise jusqu'à 80% d'erreurs relatives dans les mesures d'éclairement sur le plan de travail pour une simple fenêtre, et jusqu'à 90% pour des CFS. En outre, la méthode de simulation pour la lumière du jour utilisée pour l'évaluation doit être choisie avec soin. Une distribution continue pour le ciel a donné des résultats plus précis que la simulation à l'aide des 145 secteurs du ciel, particulièrement lorsque les CFS ont été considérés.

Ces différences peuvent être réduites en faisant l'effort de faire correspondre la géométrie et la photométrie des modèles en incluant la simulation pour la lumière du jour. Une check-list présentée dans cette thèse peut être utilisée comme guide pour aider le concepteur en lumière naturelle à estimer et éviter les erreurs lors d'une étude de performance.

Mot clés : Lumière du jour, modèles physiques, modèles virtuels, erreurs d'évaluation de performance lumineuse, guide de modélisation

Contents

Acknowledgements	II
Summary	III
Chapter 1: Introduction	1
1.1 Daylight and architecture	3
1.2 Physical and virtual models for daylighting performance assessment	9
1.3 Research objectives	13
1.4 Structure of the report	14
Chapter 2: Daylighting design tools: physical and virtual models	15
2.1 Daylighting design tools	17
Physical model	17
Virtual model	21
High Dynamic Range imaging technique	23
2.2 Main causes of error in daylighting design tools	25
Model geometry	25
Photometric properties of materials	27
Daylight source simulation	33
Photometric sensors	36
Chapter 3: Daylighting performance assessment of buildings	39
3.1 The real building	41
Type of building	41
Location and surroundings	42
Geometry and dimensions	44
Interior Features	45
Fenestration details	47
Equipment set-up	52
Summary of test model's features (real building)	57
3.2 The physical model	59
Scale of physical model	59
Geometry and dimensions	60
Interior Features	60
Fenestration details	63
The scale model under real sky conditions	64
The scale model under simulated sky	65
Equipment set-up	66
Daylight simulation	68
Tables summarising the scale model's features	70
Comparison of geometry and photometry features between the real building and its scale model	73
3.3 The virtual model	74
Computer simulation program	74
Surroundings	74
Geometry and dimensions	75
Interior details	76
Fenestration details	76
Experimental set-up	77
Daylight simulation	78
Tables summarising the virtual model's features	79
Comparison of geometry and photometry features between the real building and its virtual model	80
3.4 Photometric variables	81
Lighting units	81
Daylighting performance	82

Chapter 4: Identification of potential sources of errors	83
4.1 Parameters of physical and virtual models under study	85
4.2 Sky conditions used in the assessments	88
Overcast sky	90
Daylighting simulation for overcast sky	97
Clear sky	98
Daylighting simulation for clear sky	117
4.3 Discrepancies in daylighting factors (DF) or illuminance ratio (IR)	120
Comparison of the daylight factor (DF) or the real building and its models under overcast sky conditions	120
Daylight factors and relative divergences of the models	125
Potential sources of error in daylighting performance assessment under overcast sky condition	126
Comparison of the illuminance ratio (IR) or the real building and its models under clear sky conditions	129
Illuminance ratios and relative divergences of the daylighting performance assessment of double glazing under clear sky conditions	140
Illuminance ratios and relative divergences of the daylighting performance assessment of laser cut panel under clear sky conditions	141
Illuminance ratios and relative divergences of the daylighting performance assessment of prismatic film under clear sky conditions	142
Potential sources of error in daylighting performance assessment under clear sky condition	143
4.4 Luminance measurement of the interior surfaces	148
4.5 Dissimilarity between models and real buildings	157
Chapter 5: Daylighting models reliability and accuracy	159
5.1 Sets of parameters	161
5.2 Geometric measurement	163
Window dimensions	163
Model dimensions	167
5.3 Geometric details	170
Lighting fixtures	170
Window details	171
5.4 Photometric measurement	174
Interior surface reflectance	174
Ground reflectance	180
Window transmittance	186
5.5 Photometric sensors	190
The sensitive area of the sensor	190
Sensor positioning	193
5.6 Surroundings	199
Chapter 6: Conclusion	209
6.1 Putting the results into application	211
A checklist to avoid daylighting modelling errors	212
Charts to help estimate the level of assessment inaccuracy	218
6.2 Further study	220
Appendices	221
A CIE standard general sky	223
B Impact on daylighting performance assessment of CFS placement within scale models	227
C Impact of the different CIE standard skies on daylighting performance assessment	229
Nomenclature	233
Bibliography	235
Curriculum vitae	241

chapter

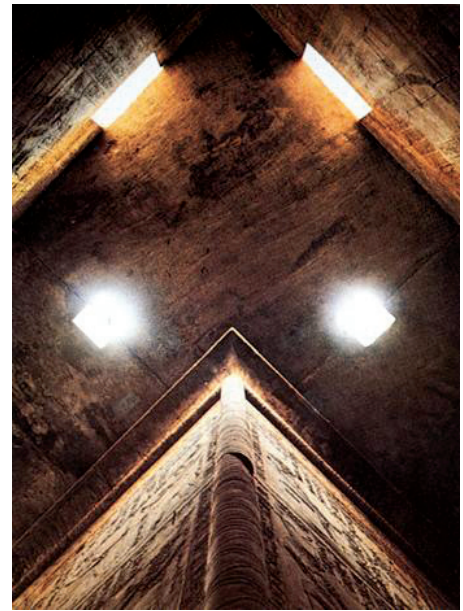
1

introduction

Fig. 1.1
The clerestories of the great temple of Amon at Karnak, Egypt (1530-323 BC)



Fig. 1.2 →
Guiding light into the temple of Horus at Edfu, Egypt (237-57 BC)



1.1 Daylight and architecture

Daylight is a primary source of energy for living beings and is the primary means of illumination by which we see. Because daylight is important for visual perception it is always a requirement in architecture, so architecture usually aims for optimal daylight quality.

Since humans started building shelters, the development of daylighting has been integrated with that of architecture itself. Fenestration as a means of transmitting daylight is always considered in conjunction with the structure of buildings. As a very early challenge, in Egyptian architecture from 1530 to 323 BC, *the Great Temple of Amon at Karnak* (Fig. 1.1), shows an attempt to bring daylight into the temple by the design of the clerestory whose columns are arranged in two rows of differing heights. In *the Temple of Horus at Edfu* (237-57 BC) several light openings were employed to bring daylight into the temple, as shown in Fig. 1.2.

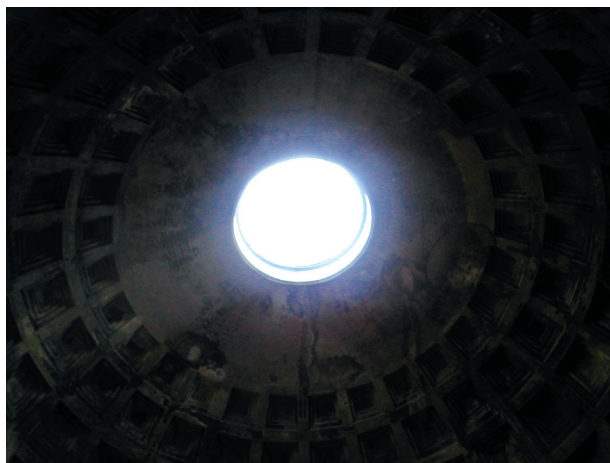


Fig. 1.3 The eye or "oculus" of the Pantheon, Rome (118-128 AD)

Subsequently, in the architecture of Rome, *the eye or "oculus" of the Pantheon* (118-128 A.D.), (Fig. 1.3) and *the three groin vaults of the Bath of Caracalla* (212-216 A.D.) (Fig. 1.4), correspond to the discovery of structures which permit daylight through their enclosures. Additionally, in the Bath of Caracalla a bronze mirror was used to reflect daylight in order to brighten the interior space, thus illustrating the effort to transport a maximum flux of light.

In Gothic architecture, the insistent demand to bring daylight into buildings was met by the discovery of the combination of rib vault and pointed arch as well as that of flying buttresses. These luminous structures allowed Gothic churches to

4

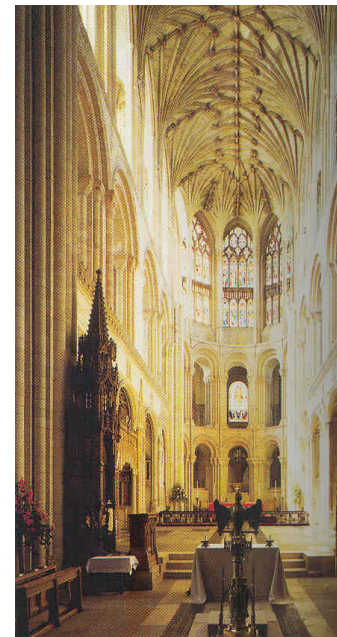
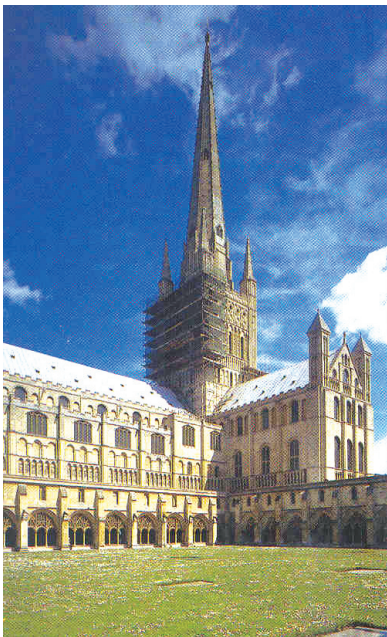


Fig. 1.4 Light streaming into the Bath of Caracalla, Rome (212-216 AD)

instance in the horizontal ribbon window of his work *Villa Savoye*, Poissy (1928-1931) (Fig. 1.10), which he was convinced provided better illumination of the interior.

Even in the second half of the twentieth century, when affordable electricity and artificial lighting became available, most buildings showed a preference for natural lighting in architecture. In public buildings such as *the Guggenheim Museum* (1943-1959) (Fig. 1.11) in New York, designed by the architect

Fig. 1.5 Norwich cathedral, Great Britain, and its glass windows (1096 AD)



open their walls to huge panels of stained glass, as shown in *Norwich Cathedral* (1096) (Fig. 1.5) and *Notre-Dame de Paris* (1163-1250), (Fig. 1.6).

Nineteenth century building design achieved optimal daylighting. Industrialisation had a great impact on architecture; modular cast iron columns and beams as well as glass panels led to the innovative *Crystal Palace* (1851-1963) (Fig. 1.7). This grand oversized greenhouse was built effectively to allow a maximum of daylight to enter the exposition building without hindering the view out from inside.

Early in the twentieth century, *Walter Gropius* (1883-1969) and *Adolf Meyer* created the administrative office of *the Fagus Factory* (1909) (Fig. 1.8) in Germany. The inward-tapering structure of this building allowed the merging of glass curtain walls and a significant transparent corner, thus improving illumination in the building. The same concept was also used in the working wing of *the Bauhaus* (1925-1926) (Fig. 1.9), where the entire glass wall hung away from the supporting structure. In 1926 the Swiss architect *Le Corbusier* specified the five points of his architectural discipline. One, exemplified in free fenestration, can be seen for instance

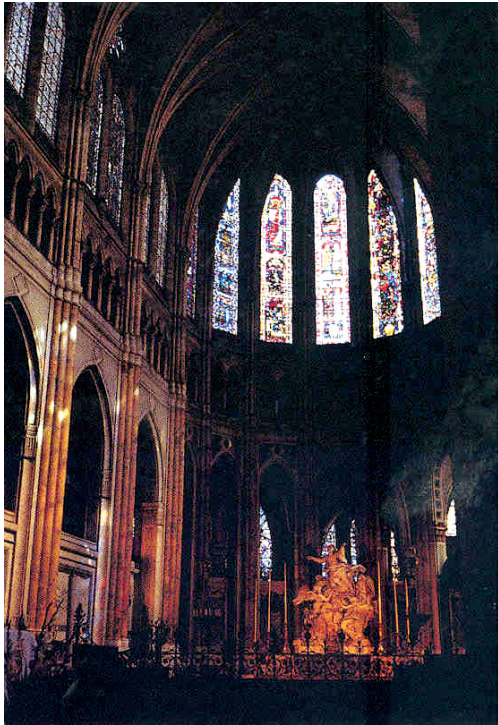


Fig. 1.6
The glass windows of
Notre-Dame de Paris, Paris
(1163-1250)

Fig. 1.7
Modular cast iron columns
and beams allowed
the composition of the
transparent Crystal Palace,
Great Britain, in industrial
times (1851-1963)

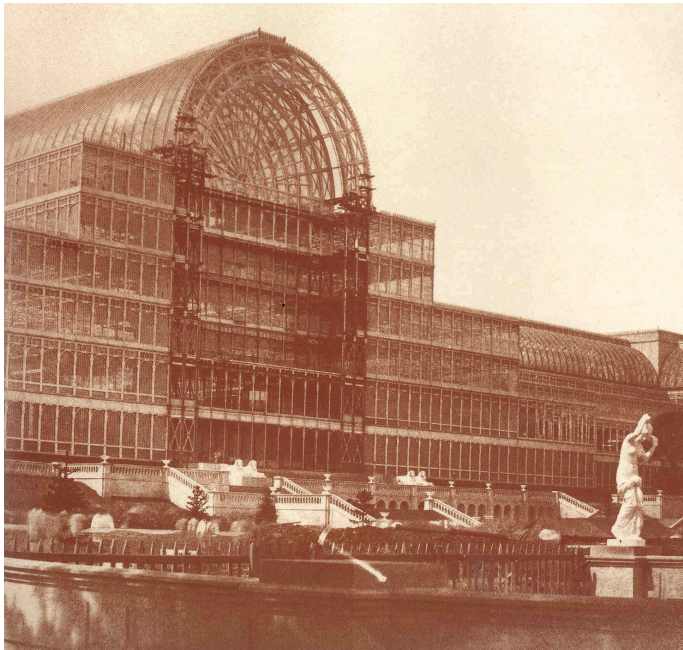


Fig. 1.8
Glass curtain walls of the
Fagus Factory, Germany
(1909)



6



Fig. 1.9
Entire glass walls of
the Bauhaus, Germany
(1925–1926)

Frank Lloyd Wright, skylights have been wisely used to illuminate the paintings. In religious architecture, for instance *the Notre-Dame-du-Haut* (1950-1955) (Fig. 1.12) at Ronchamp and the *Monastery of Sainte Marie de la Tourette* (1952-1959) (Fig. 1.13) at Evreux-sur-l'Arbresle, designed by *Le Corbusier*, daylight also plays an important role in buildings. In both structures splendid fenestrations were used to reveal the spiritual interior space.

In Eastern architecture, too, fenestrations bring a sacred light into the religious space, as often shown in *Thai temples* (Fig. 1.14) where daylight is guided in to increase the holy ambience of the gilt image of the Buddha. In residential buildings such as traditional Japanese houses, the *shoji* movable screen made of translucent paper (Fig. 1.15) is commonly employed to allow daylight to illuminate the interior.

The concepts of daylighting in architecture have been considered by many architects. The architect *Louis I. Kahn* said in his theory regarding *Silence and Light* that “a room is not a room without natural light”, the changeable quality of daylight giving life to architecture because one’s relationship to a building changes according to the light surrounding and penetrating it. Kahn had practiced as a lighting designer for many years, trying to subjugate the fierceness of light and to deal with the unpredictability of its nature. He considered that the amount of light reaching the interior should be controlled in relation to the angle of the sun, giving rise to the adjustable fenestration devices used in his work. A notable example can be seen in the wooden shutters used at *the Salk Institute laboratory building* (1959-1965) (Fig. 1.16) in San Diego, California. These sunlight control devices were installed on windows facing west onto the Pacific Ocean to avoid problems of glare and also to provide shade from the head-on sun.

Naturally, fenestration is under constant deliberation. Thanks to the progress of building technology many advanced techniques known as Complex Fenestration Systems (CFS) have been developed and are currently in use in buildings. For instance, architects *Herzog & de Meuron* applied prismatic external panels to the façade of the *CNA-SUVA building* in Basle (Fig. 1.17), Switzerland (1993). The prismatic panel is a CFS which reflects sunlight outwards while permitting diffuse light into the deeper parts of a room to improve the daylight quality.

The development of CFS does not only enhance daylight quality in architecture, it presents a simple form of preventive medicine, improving health without compromising efficiency, thus providing a new challenge for the lighting community (Wilkins, 1993) (Begemann et al, 1966). In addition CFS contribute significantly to curbing a building's energy consumption, and associated carbon emissions, by substituting for electricity. Recent surveys show on average 15-40 % of the energy consumed in non-residential buildings in Switzerland and the United States goes on electric lighting (Scartezzini, 2003). By increasing the use of CFS in buildings one can appreciably reduce electric lighting energy consumption.

The integrated anidolic system (Fig. 1.18) used in the *LESO solar experimental building* of the Swiss Federal Institute of Technology in Lausanne (EPFL), shows that lighting power densities lower than 5 W/m^2 can be achieved within office rooms thanks to advanced daylighting technology (typical values for Swiss buildings reach $10\text{--}12\text{ W/m}^2$) (Linhart and Scartezzini, 2007).

Efforts by the natural lighting research community to improve the performance and photometric properties of novel CFS, as well as attempts by architects to integrate them in their projects, continue. Several CFS were created during the last decade (International Energy Agency, 2000). A certain number of daylighting design tools are used to assess their daylight performances (International Energy Agency, 1999). Physical models are usually employed by the daylighting researchers and architects for that purpose. Virtual models have become standard tools within architectural design, too, the capability of computer simulation programmes for daylighting design having been significantly enhanced in the last decade (Compagnon, 1993) (Erhorn and Dirksmöller, 2000). To ease daylighting performance assessment these models are, of course, elaborated to achieve maximal accuracy when compared to reality.



Fig 1.10
The horizontal ribbon windows of the Villa Savoye, Poissy (1928–1931)

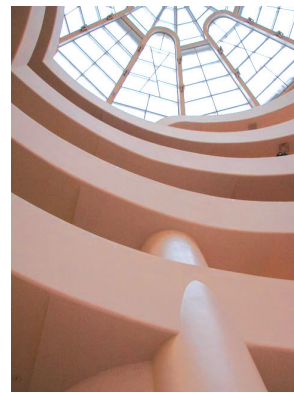


Fig 1.11 Skylight at the Guggenheim museum, New York (1943–1959)



Fig 1.12
Fenestrations at Notre-Dame-du-Haut, Ronchamp (1950–1955)



Fig. 1.13
Fenestrations of the Monastery of Sainte Marie de la Tourette, Evreux-sur-l'Arbresle (1952–1959)



8

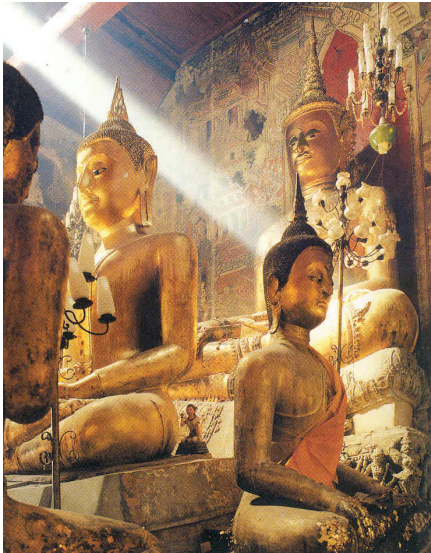


Fig 1.14
Divine light in
a Thai temple

Fig 1.15 →
Bamboo screens (shoji)
traditionally used in
Japanese houses



Fig 1.17
Prismatic panels
on the CNA-SUVA
building, Basle (1993)

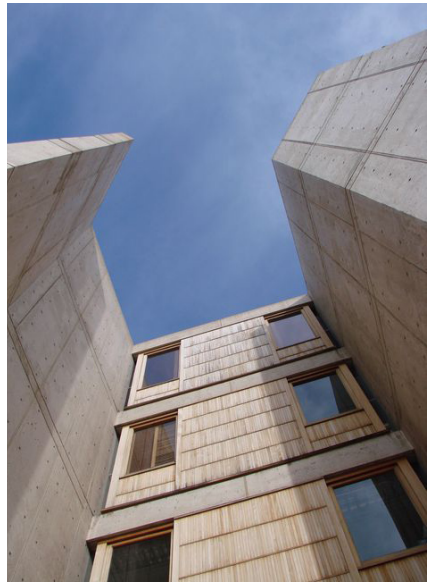
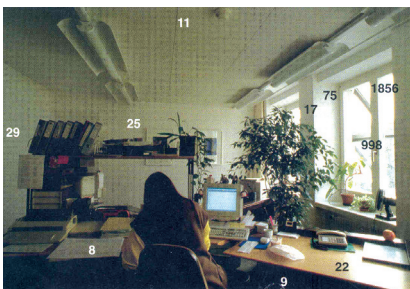


Fig 1.16 →
Wooden shutters
at the Salk Institute
laboratory building,
San Diego (1959-1965)



Fig 1.18 →
An anidolic system
integrated into
the LESO solar
experimental
building on the EPFL
campus (Lausanne,
Switzerland) (1999)



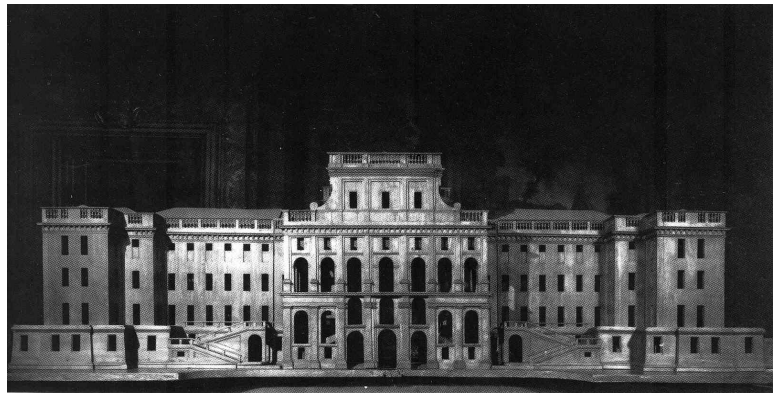
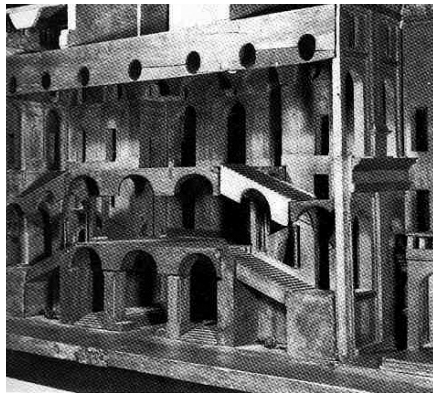


Fig 1.19
The scale model of Rivoli Castle by Fillippo Juvarra (1718). The model can be opened in sections to assessment interior performance.

1.2 Physical and virtual models for daylighting assessment

In order to visualize conceptual ideas, architects and daylighting designers usually rely on physical and virtual models; these are particularly needed to assess the daylighting performance of Complex Fenestration Systems (CFS).

Physical models are tools commonly used in the architectural design process, and reflect the engineering aspect of daylighting design. They play an important role for decision-making throughout the development of the schematic design as well as in project presentation. Architects also use scale models to evaluate the lighting environment of buildings. They are among the primary design tools used for daylighting strategies before their integration into a real building (Chauvel, 1985). Daylighting researchers require even more detailed scale models to assess the daylighting performance of CFS.

Since scale models are one of the most easily understood techniques for presenting a building project, they were used as part of the design process from early on. Already in the 1300s documents mention 'models', derived from the Latin root *modus* or *modular* (Pacciani, 1987). By the Renaissance period the use of physical models (for size and interior assessment, materials) was already basic. However, scale models were mostly used to assist structure development and building construction.

Since that time, designers have tried to make the models correspond as closely as possible to real buildings. The interior building performance and detailed assessment were often taken into account. As in the scale model of *Rivoli Castle* (architect: *Filippo Juvarra*), made by *Carlo Maria Ugliengoin* in 1718 (Fig. 1.19) - this scale model allowed people to assess exterior and interior building performance. The model aided the design team in their conception of the building. Detailed scale models were often included to help see how the building would perform; a model of the façade and windows of *the Duomo of Milan*, designed by *Giulio Gallioni* in 1786, was employed to assess the façade detail during the cathedral's development and renovation (Fig. 1.20).

Scale models were commonly used as a major design tool. When a very complex building was built scale models were obligatory. The *Sagrada Familia*, the master work of *Antonio Gaudi*, is a case in point; development was long drawn out, beginning in 1901. To achieve this complex sculptural architecture, scale models were used to visualize the three-dimensional performance of the building. Fig. 1.21 presents the overall scale model of the church together with a detailed model of the hyperbolic and parabolic windows.

Fig 1.20
The scale model of the Duomo of Milan by Giulio Gallioni (1786) which was used to evaluate the detailed structure of the windows and façade

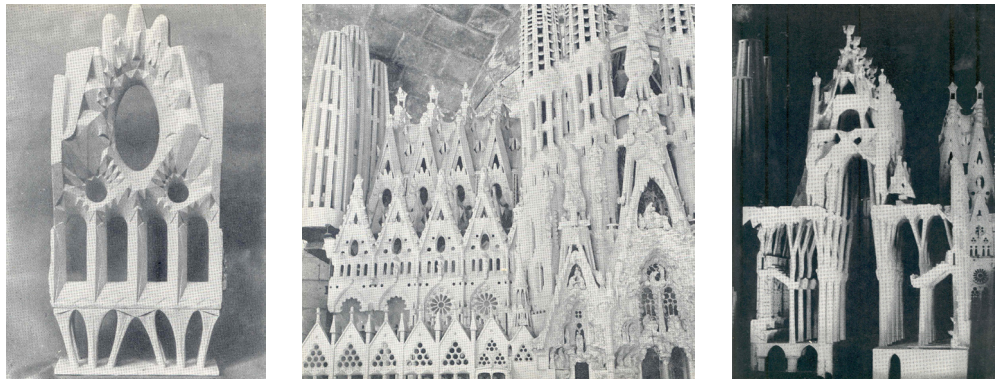
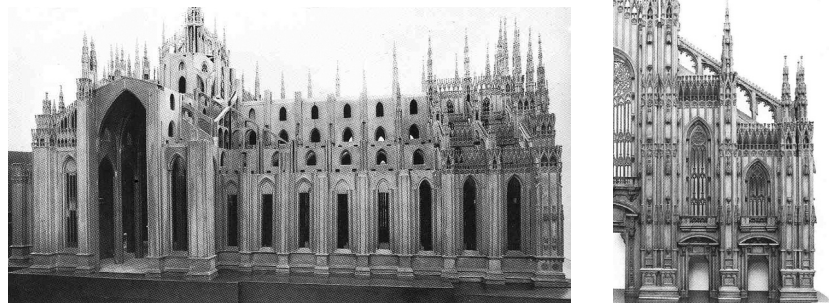


Fig 1.21
Antoni Gaudí's scale models of the façade and window of the Sagrada Família (1901) help understand his requirements

Scale models are important tools for building assessment when investigating a novel system. The study models of *Notre-Dame-du-Haut* at Ronchamp by *Le Corbusier* show various uses of modelling. Some were used to appraise shade and shadow and a specific model was used to assess the building's construction and structure (Fig. 1.22).

Design teams employed scale models for several aspects of building assessment. Daylighting performance assessment was usually one of the main aspects. Several detailed models for the evaluation of the daylighting component were used in *Louis I Kahn's* building projects. The scale model of the roof of sanctuary of *the First Unitarian church and school*, New York (1959-1969), (Fig. 1.23) is an example. This scale model showed how daylight would penetrate the sanctuary.

In a complex building such as the *Salk Institute*, San Diego (1959-1969), different sizes and types of models were used to evaluate the building's performance (Fig. 1.24). A mass model was used for overall shade and shadow, a section model demonstrated daylight penetration, while a detailed model was used to judge the influence of the sunshield. Moreover, to simulate how natural light illuminates a building with complex daylighting systems, precise scale models can represent the real building and help simulate the lighting aspect, such as in the double skylight flanking used in Yale centre for British Art in Connecticut (1969-1974) (Fig. 1.25).

Scale models are commonly used to provide qualitative assessment, as in a visual presentation of a building project. Quantitative lighting measurement has been widely used by engineers and architects since the invention of inexpensive photometers in the 1930s; scientifically used scale models assess daylight properties as, for example, when measuring building illuminance. Fig. 1.26 shows the daylighting scale model of the *Building Research Station*, London, which was built in 1966 specifically for daylight assessment under both real sky and sky simulator conditions.

Another example of physical model employment in daylighting is shown in Fig. 1.27: the scale model of *the Church of Light* (1989) designed by the architect *Tadao Ando*. It played an important role during the design procedure, in particular for the study of the building's daylight quality. More detailed scale models were diligently constructed to exactly assess daylighting performance of CFS, such as for the anidolic systems (Fig. 1.28), which were installed on the *LESO solar experimental building*.

Even if the scale models used by architects and daylighting researchers are carefully constructed with geometrical and photometrical properties very close to those of the real buildings, small discrepancies in the scale model compared to the reality can lead to inaccurate daylighting performance assessment. There are many reasons: duplication of details, a difference in furnishings, and so on.

Several recent studies (Schiler et al., 1987), (Love and Navvab, 1991), (Cannon Brookes S. W. A., 1997) have reported errors caused by these dissimilarities. The main causes of discrepancies compared to reality, such as surface reflectance and glazing transmittance, were analysed. An attempt to find out the best way to produce a daylighting scale model was investigated. They found the complexity of the experimental construction of the scale model remained the problem. Moreover, if CFS are needed in these representations the difficulty of modelling them can be a significant source of errors; no detailed study of CFS with physical models has been reported yet.

Virtual models have recently become a universal design tool for architects and daylighting researchers. Many validations of daylighting simulation programs have been carried out (International Energy Agency, 1999). Computer simulation was first used in the 1970s to create simple 3D shapes and shadows for lighting performance assessment (Fig. 1.29). In the 1980s the invention of pixelised bitmap images helped create a better simulation. Since the late 1980s, thanks to the development of the Video Graphics Array (VGA) and the Super Video Graphics Array (SVGA), photorealistic images and rendering, together with computer graphic lighting and daylighting simulation, have become an important part of daylighting research.

During the same period artificial light source and reflectance models for rendering were introduced, followed by mirror and transparent effects. Consequently, computers began to simulate natural light. The inter-reflection of light was also pioneered at this time. However computer simulations only really became common in the 1990s when personal computers became more popular and inexpensive.

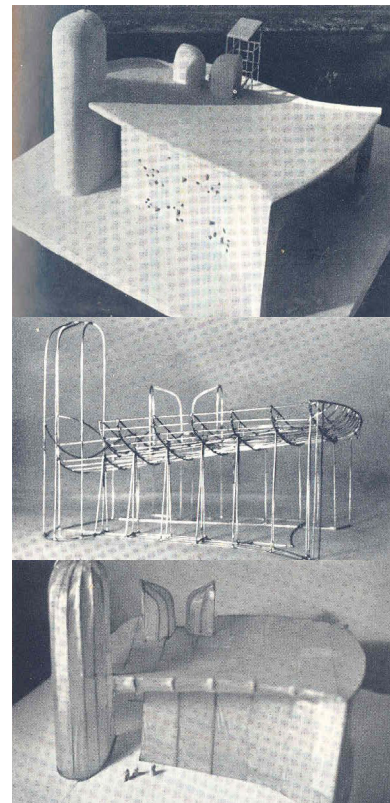


Fig 1.22
For Le Corbusier's Notre-Dame-du-Haut at Ronchamp (1950–1953) various types of scale model were used for different building performance assessments

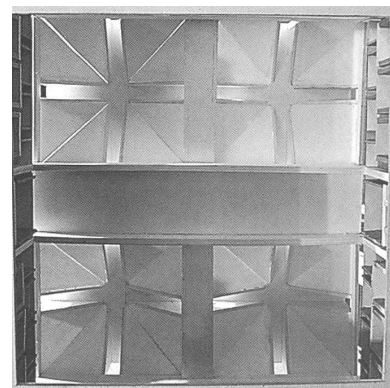


Fig 1.23
The detailed model of the Sanctuary, First Unitarian church and school, by Louis I. Kahn, demonstrates how daylight penetrates into the building (1959–1969)

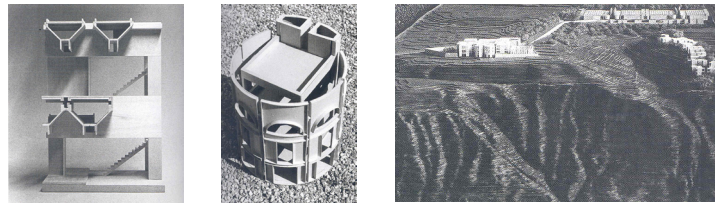
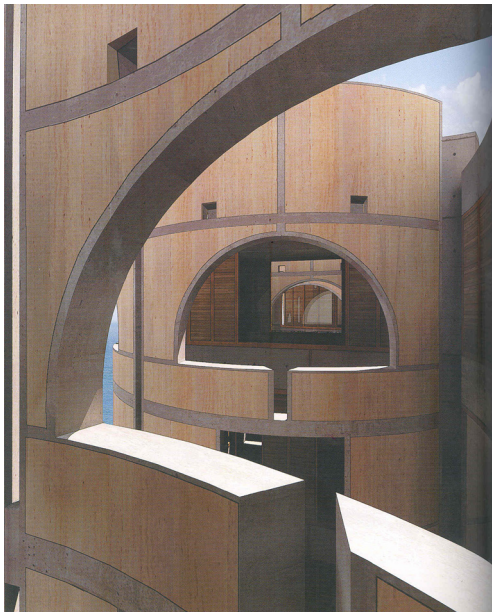
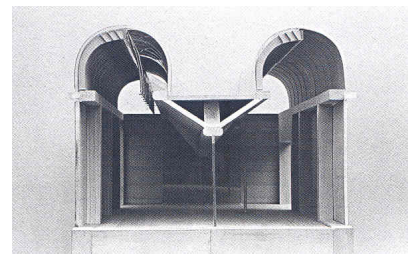


Fig 1.24 Different daylighting models of the Salk Institute by Louis I. Kahn (1959-1969): the mass model for assessment of shadow and shade; the section model for assessment of daylight penetrating into the building; a detail of the sunshield used in comparing the building with the computer simulation

Fig 1.25 Scale model of the double skylight flanking in the Yale Centre for British Art by Louis I. Kahn (1971)



Radiance, which is a set of programs for lighting analysis and visualization, is currently one of the best suites and is widely used in the daylighting research community. Fig. 1.30 shows the daylighting simulation of the sun roof of a factory hall (Scartezzini and Compagnon, 1994). This rendering provided both qualitative information (visual feedback of a given integrated daylighting technology) and quantitative Figures (workplane illuminance and daylighting factors).

However, divergences in daylighting performance Figures between virtual model and real building are often mentioned. These result from the virtual model's parameters not conforming to the real situation. The sky luminance models, the virtual model's geometrical and photometrical properties, as well as the modelling of CFS, are some of the major causes of errors. Detailed studies of these causes have not yet been presented even though they are fundamental to the architects' and daylighting researchers' daylighting modelling.

The goal of this thesis is the identification of the main causes of inaccuracies when using physical and virtual models in the assessment of a building's daylighting performance. These principal causes were identified by pursuing sensitivity analysis so as to discover and quantify the inaccuracies. The results are translated into a checklist to assist the elaboration of daylighting models by architects and researchers.

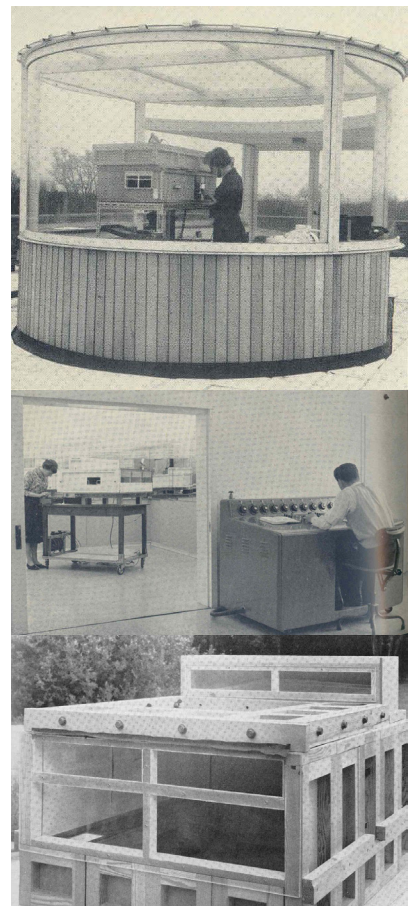


Fig 1.26 The daylighting scale model by R.G. Hopkinson was built mainly for daylighting performance assessment (1966). It was placed under both real sky observation and a sky simulator.

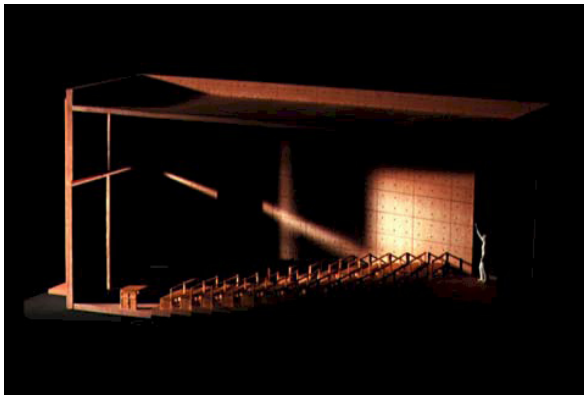


Fig 1.27
The scale model of the Church of Light by Tadao Ando demonstrates how daylight penetrates the building's fenestration (1989)

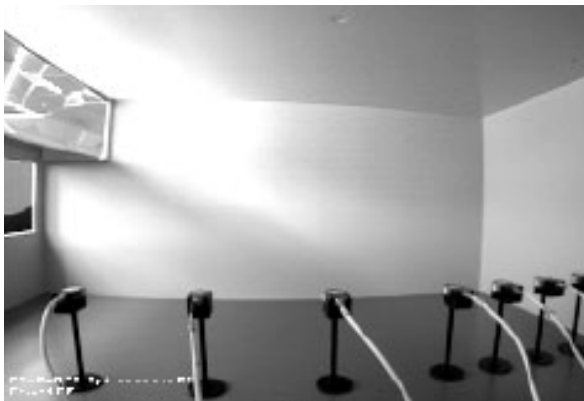


Fig 1.28
The physical model of an anidolic integrated system being analysed under an artificial sky (1999)

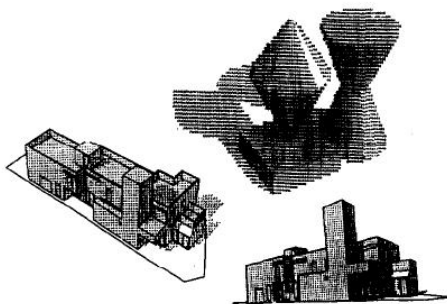


Fig 1.29
Rudimentary virtual models used for simple 3D shape and shadow (1970s)

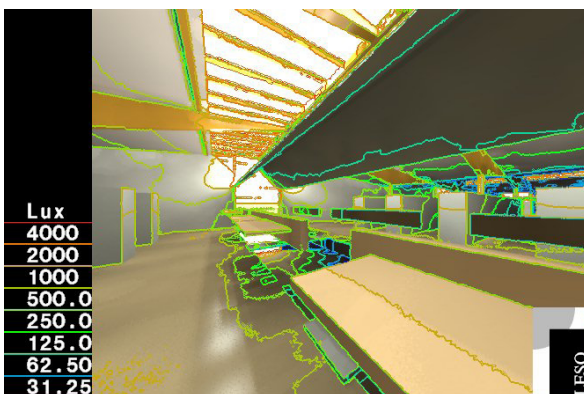


Fig 1.30
The virtual model of a factory hall produced by the Radiance suite of programs (1994)

1.3 Research objectives

13

Since models are important in assessing daylighting performance, development of daylighting models has evolved progressively over the years. Accurate models now appear to resemble the real situation very well. However, the degree of any inaccuracies should be predictable.

The main objective of this thesis is to assist the daylighting designer by improving the performance assessment on an experimental basis by:

—Identifying the main causes responsible for experimental errors within scale models of buildings, including the daylight performance assessment of CFS integral to buildings.

—Pursuing a similar study for the main factors responsible for numerical errors within virtual models, including the daylight performance assessment of CFS integral to buildings.

—Comparing physical and virtual models with real buildings as regards to their accuracy and reliability when assessing the performance of advanced daylighting technology.

—Establishing a practical checklist for daylighting designers who use physical or virtual models.

1.4 Structure of the report

14

This document is arranged as follows:

Chapter 1 shows the importance of daylight in architecture and daylighting research. It introduces physical and virtual models used in the daylighting design process, as well as defining the main objectives and structure of the thesis.

Chapter 2 presents the models, both physical and virtual, currently used in daylighting design as well as the High Dynamic Range (HDR) imaging technique. The main causes of errors are also listed and explained.

Chapter 3 gives an overview of how the real building, physical model and virtual model were equipped in the experiments for this thesis. The chapter ends with a description of the photometric variables.

Chapter 4 explains the sky luminance monitoring used in the research as well as giving an overview of sky luminance models. Comparisons of the various modelling approaches are given, the results being analysed and validated using relative divergences of the models' monitored values from those of the real building. Results of analysis using the High Dynamic Range imaging technique are included.

Chapter 5 describes the sensitivity study carried out on models: their location, geometric and photometric properties, design details and placement of photometric sensors.

Chapter 6 presents a checklist for physical and virtual daylighting models based on the results of this thesis, discusses future research in this field and brings the work to a conclusion.

chapter

2

daylighting design tools: physical and virtual models

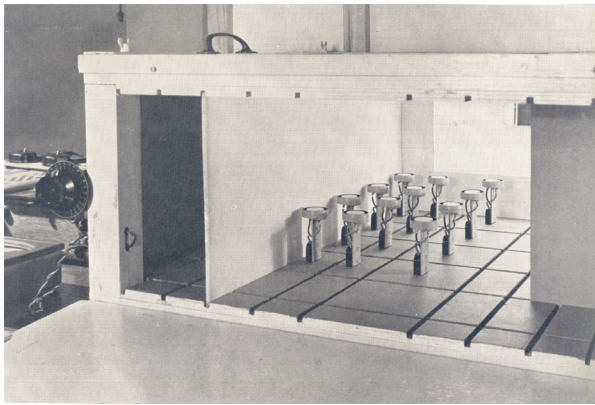


Fig. 2.1
Daylighting scale model by *Hopkinson et al.*, equipped with illuminance sensors for measuring a building's lighting

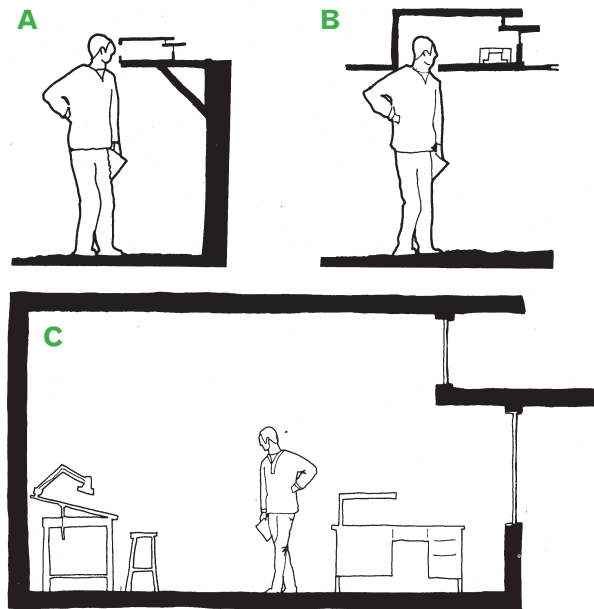


Fig. 2.2
The study of C. Robbins shows how the scale and size of a physical model depends on the requirements:
a) Small scale model for observing from the exterior
b) Medium scale model for internal observation
c) Full scale model for accurate daylight simulation

2.1 Daylighting design tools

Physical models

During the architectural design process of a building architects commonly require tools such as drawings, mathematical calculation or physical modelling, to facilitate their planning. Physical models are frequently used during different phases of the design process, from the small-scale mass models for studying the building in its surroundings to the large-scale models for evaluating details of the construction. However, scale models for lighting purposes may differ somewhat from the habitual architectural model. Daylighting scale models usually play an important role throughout the decision-making; they do not require high-technology though they do provide both quantitative figures (workplace illuminance and daylighting factors) and qualitative information (visual feedback from a given integrated daylighting technology) to the building's designer. They are certainly important tools and have an impact on the building's performance.

Ever since simple and inexpensive lighting measurement instruments became available in the early 1900s they have been used to measure lighting properties in buildings and streets (Johnston, 2001); subsequently they were also used in daylight measurement. *R. G. Hopkinson et al.* mentioned that the scale and detail of physical models depend upon the purpose of the models (Hopkinson, 1966); he was the first to suggest some rules to improve their design. If the models are used for measurement, both precise scale and internal surface reflectance including window details should be considered. The photometer sensors had also a great effect in the lighting measurement; the size and positioning of the sensor should correspond to the size of the model.

The length and width of the model should be at least 10-12 times the diameter of the photometer's sensitive area. On the other hand, when models are built for subjective evaluation, the scale of the models should be appropriate to the observers' view. The range of scales of 1:12-1:20 to 1:5-1:4 was suggested as adequate (Fig. 2.1), bearing in mind that the scale of the model should be chosen according to the dimensions of the considered interior space.

However, creating an accurate physical model is not easy. *C. Robbins* produced a study of scale modelling of daylighting systems (Robbins, 1986) which gave a number of major factors the modeller must take into account when constructing daylighting scale models. It was mentioned in the study that the scale and detail of the model depend to a large extent on the information required. Mass models for shade and shadow analysis should have scales between 1:400 and 1:50 while scale models for studying the penetration and distribution of sun and sky light should be between 1:24 and 1:16. The floor-to-ceiling height should not be less than 13 cm so that photometers can be used. If precision data is required, scales between 1:24 and 1:12 can be used for observations from the outside, but if a photograph is needed from inside then models scaled in the range 1:8 to 1:4 are necessary. A full 1:1 scale model is generally called for when the observers themselves need to be inside and very accurate data is needed (Fig. 2.2).

Besides geometry, the transmittance replication of the building materials, reflectance and surrounding context can play significant roles, depending on the objective of the models. In particular the photometry properties, such as reflectance and transmittance, of the building materials should be considered since they are the main factors which modify the daylight distribution within the building. Moreover, the daylight source is one of the factors with which the modeller should be concerned. The type of sky (real or artificial) and sky conditions (e.g. luminance sky distribution) have an important effect on the daylighting performance assessment of buildings. The awareness in constructing a scale model, which was resumed in the study, was based on the author's experience but, however, no details or quantitative results that could be used as a daylighting model checklist were reported in this work.

In a manner similar to that of the previous studies, *M. Schiler et al.* established a manual for architectural models used within daylighting simulations (Schiler et al., 1987). The modeller is strongly advised to construct model details such as window frames and mullions adequately (Fig. 2.3). The scale of the model should be carefully considered; a massing model between 1:100 and 1:200 should be used during preliminary design and concept development, while a scale of 1:10 to 1:1 is required for a detailed study. These authors identify the difficulty of accurately reproducing internal surface reflectances as well as the penetration of parasitic light into scale models as the common error sources in daylighting performance assessment. In addition, a step by step instruction for scale modelling approach is

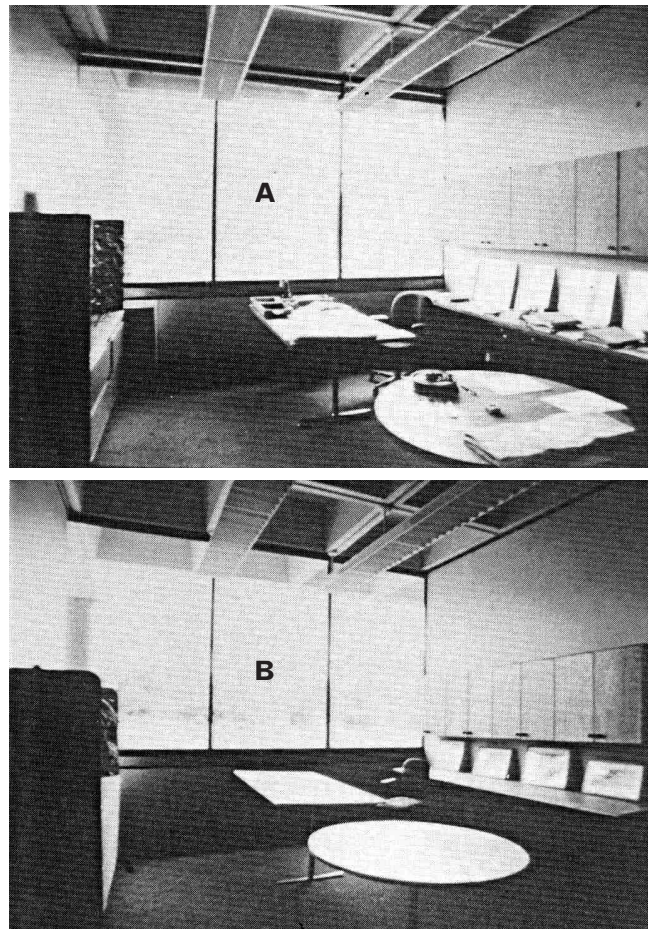


Fig. 2.3
M. Schiler et al. strongly advised the reproduction of the building's critical details: (a) reality (b) scale model

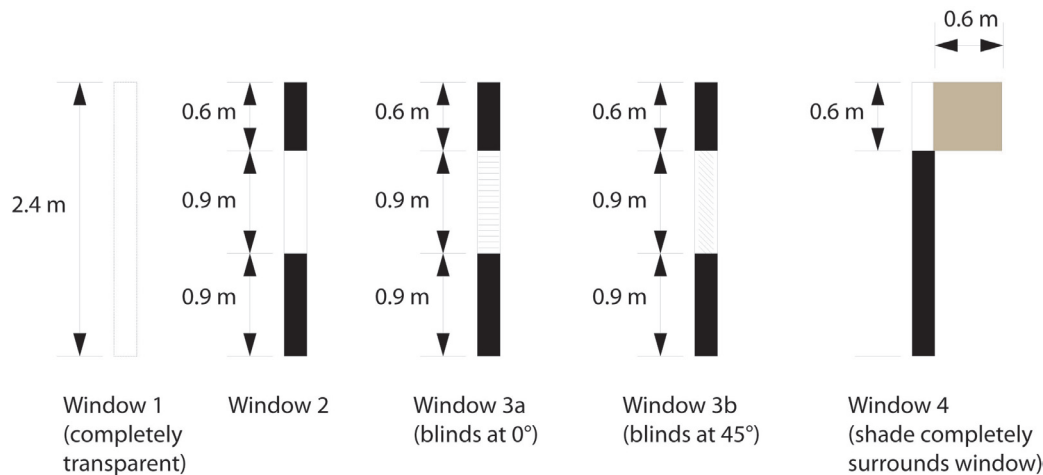


Fig. 2.4
More complex windows were assessed in the study of J.A. Love and M. Navvab

mentioned in this manual; for instance, model construction, sky simulation and data monitoring are discussed. In the study, several significant sources of errors were addressed. However, the correlation between the scale model precision and errors in assessing daylighting performances was not reported. An appropriate guideline for scale modelling was still missing.

A further study carried out by *J. A. Love and M. Navvab* confirmed the previous results (Love and Navvab, 1991); in addition, errors that can be attributed to the sensors used in the model are mentioned. By comparing a simple building with its scale model under real sky conditions (overcast and clear sky) these errors can be avoided by sensor calibration. Other causes of errors mentioned are the precision of the sensor's levelling and its position in the scale models.

A more detailed analysis of the impact of a model's surface reflectance was done by the same authors by comparing two test spaces of differing reflectance. Assorted windows (Fig. 2.4) were also compared in order to have an in-depth analysis of rather complex fenestration systems. The results of this study showed that the general estimation of daylighting performance in physical models differed by 10 to 50 percent from that of the real building (full-scale space) depending on the fenestration types and photometer position in the space. Therefore, these comparative studies gave remarkable results in spite of the fact that they were only evaluated qualitative.

A more recent paper from *Cannon-Brookes* (Cannon-Brookes, 1997) corroborates these earlier studies by assessing more complex buildings (e.g. a gallery) (Fig. 2.5). A comprehensive study of a real building and its 1:20 scale model was held under real sky conditions (overcast and clear sky). Besides the geometric and photometric properties of the scale models, which the previous authors had presented, the study pointed out other physical parameters, such as maintenance and dirt in the building, as contributors to discrepancies. This study strives to guide the modeller who constructs a physical daylighting model. Some quantitative results were reported; relative divergences of +10 to +25% can happen, for instance, if the surface reflectance of the scale model is not accurate.

As shown by these earlier studies, the development of daylighting design tools is progressing. However, thorough sensitivity analysis has not yet been fully reported. No attempt has considered Complex Fenestration Systems (CFS). Moreover, a complete assessment of real building and scale models under various sky conditions (real sky and artificial sky) is still lacking. To achieve these objectives a wider exploration of the relationship of physical and virtual models of a building to real building should be accomplished, in which CFS need to be included. Table 2.1 summarises the previous studies.

Authors	Main factors	Relative Divergence vs. Real Building
Hopkinson 1966	Scale of model Model details Fenestration details Model dimension accuracy Surface reflectances Window transmittance Lux-meter size (sensing aperture) Sensor placement	N / A
Robbins 1986	Scale of model Model details Model dimension accuracy Surface reflectances Window transmittance Surrounding context Daylight sources	N / A
Schiler et al. 1987	Scale of model Model details Fenestration details Surface reflectances Window transmittance Daylight sources Light leakages	N / A
Love and Navvab 1991	Model details Fenestration details Model dimension accuracy Surface reflectances Sensor calibration Lux-meter size (sensing aperture) Sensor placement	+ 10 to 50%
Cannon-Brookes 1997	Model details Model dimension accuracy Surface reflectances Window transmittance Surrounding context Maintenance and dirt	+ 10 to 25%

Table 2.1
Principal factors that contribute to experimental errors when using scale models, as identified in previous studies

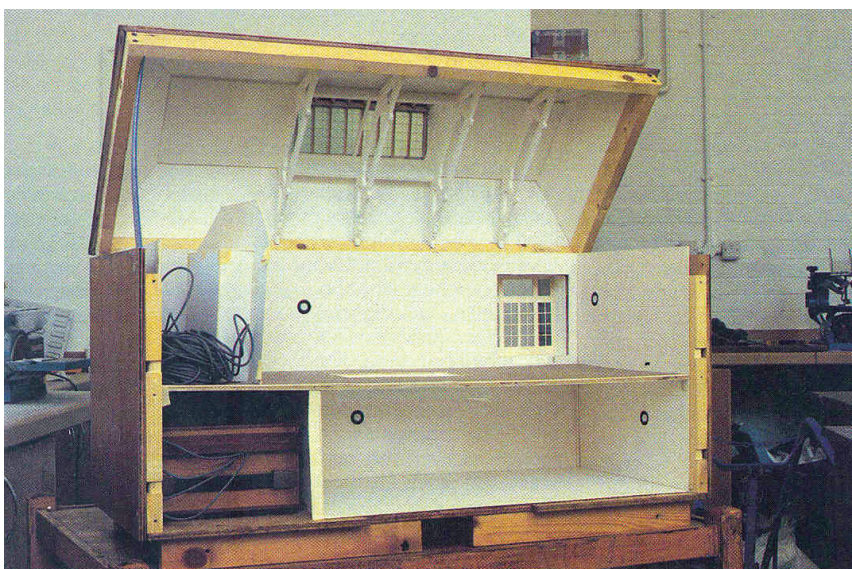


Fig 2.5
The intricacy of a daylighting physical model in the study of Cannon-Brookes

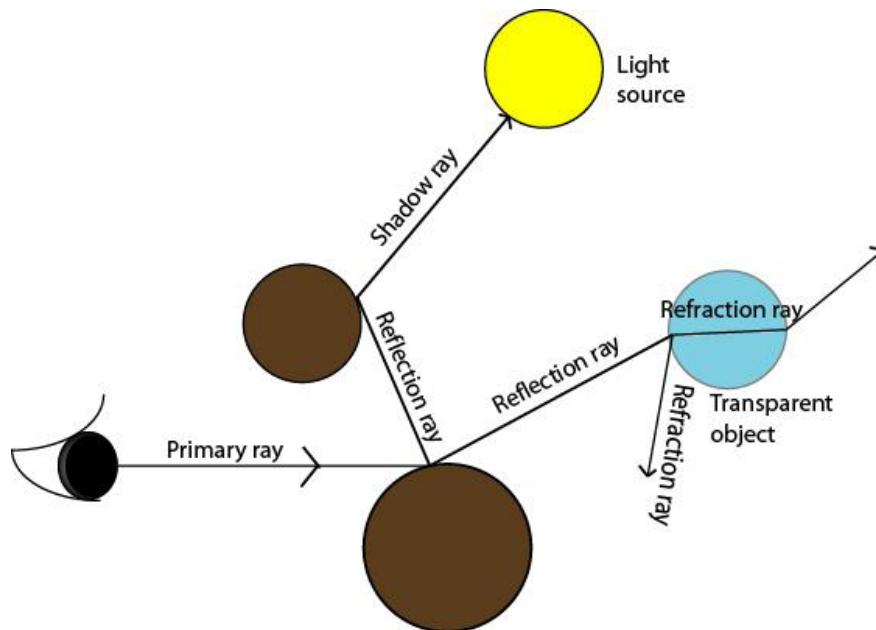


Fig 2.6
Ray tracing process in lighting
simulation (backward process)

Virtual models

Since 3D computer graphics were invented in the 1960s the effort to get photorealistic images has been continuous. The earliest lighting effects were simple shadows and half transparent objects. An attempt to have a computer model to predict luminance and illuminance was presented by *C. G. H. Plant and D. W. Archer* (Plant and Archer, 1973) : only simple simulation cases, for instance lighting simulation in a rectilinear environment, were validated under both natural and artificial light sources. In the early 1980s the ray tracing algorithm was presented as a technique for rendering artificial light sources and modelling reflectance precisely. This algorithm was able to offer very attractive renderings in computer simulation. It gave photorealistic images with mirror and transparent effects accounting for refraction. Shortly afterwards the radiosity algorithm was introduced in order to solve inter-reflection of light between diffuse surfaces and correct global illumination effects (M. Cindy et al., 1984). Subsequently, natural light in computer simulation was widely talked about. Photorealistic images by means of inter-reflecting light rays between the illuminated objects as well as spectral effects of skylight (including atmospheric scattering and absorption) became more familiar in this period. In the 1990s virtual lighting design became more widespread through the use of advanced powerful computers, interactive modelling tools and novel computer techniques (Nakamae and Tadamura, 1995).

Lighting design by computer graphics is an expanding field whose main goal is the accurate solution of global illumination problems (Kopylov and Dmitriev, 2000). With the advent of personal computers (PCs), powerful processors that can handle complex lighting calculation and simulation techniques are today available to nearly all practitioners. In addition to a first generation of simple design tools, several new programs have been developed since the 1980s to address light propagation into buildings; in the last few years they have become capable of handling Complex Fenestration Systems (CFS) such as prismatic panels or prismatic film. Recent surveys have shown that the number of these tools is increasing, as well as their use within the building designer community (de Boer and Erhorn, 1998).

Another category of computer design tools for lighting simulation, distinct from ray-tracing techniques, was also introduced (International Energy Agency, 2000). Originally developed for radiant energy calculations, the radiosity method can be used to determine illuminance and luminance of room surfaces, by dividing them into small finite elements (Fig. 2.7). These surfaces must, however, be perfectly diffusive (i.e. Lambertian reflectors), which in practice reduces the flexibility of the method.

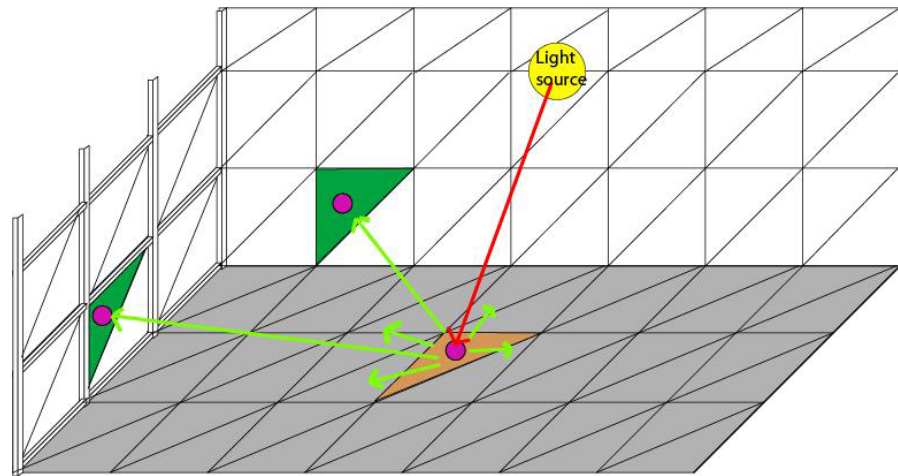


Fig 2.7
Radiosity as a basis of lighting
simulation

The ray-tracing technique, on the other hand, determines the visibility of surfaces by tracing imaginary light rays from a viewer's eye to a rendered visual scene (Fig. 2.6). Thanks to the power of new computer processors, millions of rays can be traced to achieve a high-resolution computer rendering (Compagnon, 1993). Most lighting software, especially that dedicated to calculation of daylight distribution into buildings, currently uses this simulation technique (Erhorn and Dirksmüller, 2000). Several validations of ray-tracing programs have demonstrated its reliability for daylighting performance assessment (Fontoynt et al, 1999).

Thanks to the expansion of computer graphics technology and affordable personal computers, virtual models for lighting performance assessment are now common. Validations of lighting programs have been carried out in an attempt to make the virtual model correspond as closely as possible to reality. Both quantitative and qualitative figures are progressively introduced in order to have the greatest accuracy. Nevertheless, several errors in assessing daylighting performance in virtual model are still present: some of these errors were revised in recent studies.

A validation of computer daylight simulation programs achieved by comparing several leading computer lighting software suites (both radiosity and ray-tracing algorithms) was undertaken by *J. Ashmore and P. Richens*. This study analysed both physical accuracy and visual quality of Lightscape, Radioray, Microstation and Adeline programs. Physical accuracy analysis was done by comparing daylight factors with a physical model under two types of sky simulator (Mirror and Spot light sky simulators). They found average discrepancies of the daylight factor in between the software and the physical model about 30%; these errors comprised also an estimated experimental error between 25% - 40% depending on the location in the room (Ashmore and Richens, 2001). Moreover, rendering parameters such as the exposure were presented in this work as the main cause of errors in lighting simulation.

Recent studies to evaluate the accuracy of different lighting programs compared them with an analytical solution (Maamari et al., 2003); they pointed out relative errors between 10% and 100% depending on the reflectance, transmittance and types of opening. This study suggested that the external light source (sky modelling), the external ground and obstructions can also be the causes of the errors. In a more recent work (Maamari et al., 2004), comparisons of the results of different daylighting programs – Genelux, Inspirer, Lightscape and Desktop Radiance - presented a high accuracy in respect to a given aspect of lighting simulation but not necessarily for other aspects. Concurrently, *J. Mardaljevic* asserted in his work on validation of lighting programs for illuminance modelling, that surface reflectance, sky luminance distribution and imprecision in model parameters can lead to significant errors - about 10% to 25% - in illuminance modelling (Mardaljevic, 2004). Even though recent studies

of daylighting performance assessment have reported virtual models of progressively greater accuracy, no attempt has been made to consider simulations of advanced daylighting technologies (CFS integrated into buildings). Guidelines for computer lighting simulation in order to improve the accuracy of daylighting performance assessment are still lacking. Notably, no study has yet been presented that compares physical and virtual models with a real building under different sky conditions. A study showing a complete set of comparisons of real buildings with both models under the different daylight sources is therefore necessary. Thanks to the scientific equipment (details in chapter 3) available at the EPFL, such a complete assessment could be carried out. The results of these evaluations should help the daylighting research community and architects to incorporate them into their physical and virtual daylighting models. Table 2.2 summarises the previous studies.

Authors	Main factors	Relative Divergence vs. Real Building
Ashmore and Richens 2001	Model dimension accuracy Model details Surface reflectances Lighting simulation Chromatic effect Software error	±25 to 40%
Maamari et al 2002 and 2004	Fenestration type Surface reflectances Window transmittance Surrounding context Daylight sources	±10 to 100%
Mardaljevic 2004	Model details Model dimension accuracy Surface reflectances Window transmittance Surrounding context Daylight sources	±10 to 25%

Table 2.2
Principal factors that contribute to experimental errors when using virtual models, as identified in previous studies

High Dynamic Range imaging technique

The High Dynamic Range (HDR) imaging technique, initially introduced in the 1980s in the cinema industry, was conceived to create a greater dynamic range of exposure for lighting environment scenes than the conventional digital imaging techniques (the dynamic range is the ratio of a scene's maximum radiance to its minimum). It is now also used in lighting design and research (either daylight or artificial lighting) to assess luminance distribution for the evaluation of visual comfort. A greater range of real-world light intensity values than those registered by normal digital camera CCD sensors or displayed by current computer screens can be stored and later analysed without loss of accuracy. Expensive high precision CCD cameras do exist but usually have to be calibrated by the manufacturers, so separate images taken at various under- and over-exposures using a common digital camera are merged into a single HDR image by software.

Even though errors in luminance measurement by HDR cameras are still reported (Anaokar and Moeck, 2005), the technique is widely employed in lighting assessment as a part of the Radiance lighting simulation programme (Ward, 1998) as well as in several software packages used for converting an image to luminance distribution maps. The development of HDR imaging technique is currently expanding, various research projects are under way.

A study of the assessment of luminance distribution using high dynamic range imaging was presented by *L.O. Beltran* (Beltran, 2005). This included the use of luminance ratios to compare the result of various combinations of different light sources (artificial and daylight). Several HDR image builder programs and other image analysis software were evaluated to find how best to assess lighting performance by this method. Both real buildings and scale models were used as case studies. The study concluded that HDR imaging is a simple, quick and affordable technique for luminance distribution assessment. In a short time it gives adequate luminance measurement for quite complex lighting environments.

Another attempt to determine the errors in luminance mapping using the HDR imaging technique was reported by *S. Anaokar and M. Moeck* (Anaokar and Moeck, 2005). The study determined the errors in luminance mapping due to colour and reflectance, the light source's spectrum, optical vignetting of the camera and the object's spatial resolution. The study concluded that although HDR for luminance measurement has many advantages, being handy and inexpensive, it has also certain limitations. By comparing measurements of the luminance mapping of different hues and saturation (using Munsell chips) it shows that the errors on luminance assessment varied according to the reflectance properties of the interior space's surface materials. Warm hue colours gave the least error while cool hues create the largest errors, saturation being another major cause of error. They recommended the use of a luminance meter in the scene to check the HDR imaging technique.

A more recent study by *M.N. Inanici* (Inanici, 2006) performed luminance mapping by HDR using different settings; an office room, a dark room lit variously by incandescent, fluorescent and metal halide lamps, as well as outdoor conditions under cloudy and clear sky were considered. The average relative error with greyscale and coloured targets was reported to be between 4.8 and 11.6%. However, it was concluded in this study that HDR imaging technique cannot entirely replace luminance meters; at least one target should be used in the field in order to calibrate the HDR pictures. In addition, the stability of the lighting condition should be considered; dynamic lighting conditions can give significant errors in luminance distribution measurement.

The use of HDR imaging in luminance measurement is currently expanding due to its remarkable advantages. The daylight quality of a space can be effortlessly evaluated. A luminance mapping system by HDR imaging technique is affordable, simple and convenient. However, even though a certain amount of research comparing luminance measurement by HDR with conventional methods (luminance meter) has been carried out, further study in this domain is still required. In particular, the validation of HDR imaging technique when assessing daylighting performance of CFS integrated into both real buildings and scale models must be carried out.

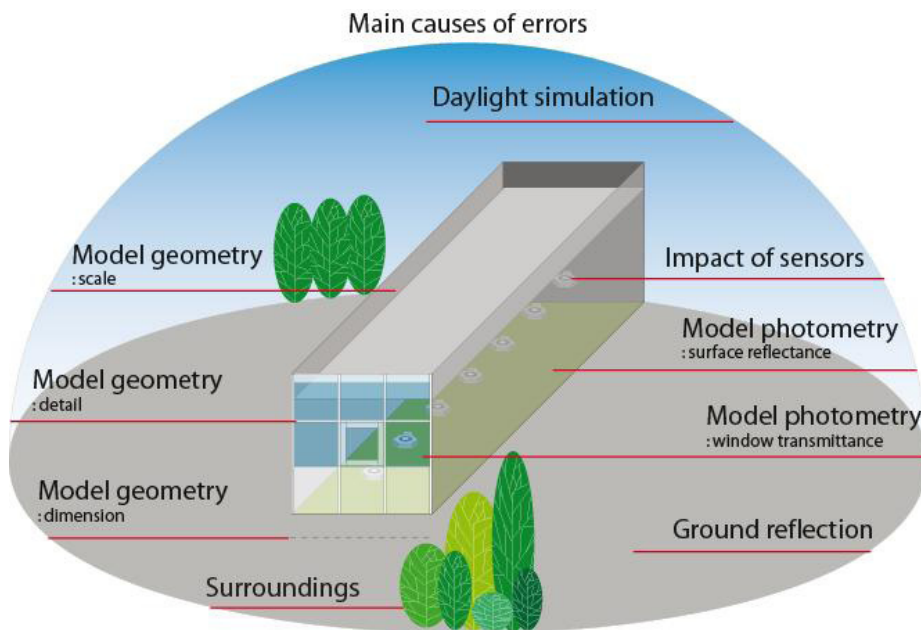


Fig. 2.8
Major causes of error in
daylighting performance
assessment

2.2 Main causes of error in daylighting design tools

According to the aforementioned studies, over or under-estimation in daylighting performance measurement has several causes. The main causes of error, as explained later in this chapter are illustrated on Fig. 2.8, are:

- Model geometry
- Model photometry
- Daylight sources simulation
- Illuminance sensors
- Surroundings

Model geometry

The accuracy of the measurements of daylighting performance depends on how precisely the physical model duplicates the real building. Ideally, a full scale model (1:1) with real details and materials would give to the most accurate evaluation. However, such models are unusual, the common tool being a small-scale model. The scale, details and dimensions of a daylighting model therefore have a great impact on the daylighting assessment of buildings.

Scale

When a physical model is used to assess daylighting performance, the model's scale is usually defined by the requirement of the design or study, as shown in Table 2.3.

Type	Purpose	Scale
Massing model	Shade and shadow analysis	1:400 – 1:50
Study model	Sun and sky light distribution (Observed from outside)	1:50 – 1:10
Detailed model	Sun and sky light distribution (Observed from inside)	1:10 – 1:1

Table 2.3
Scale according to model type

26

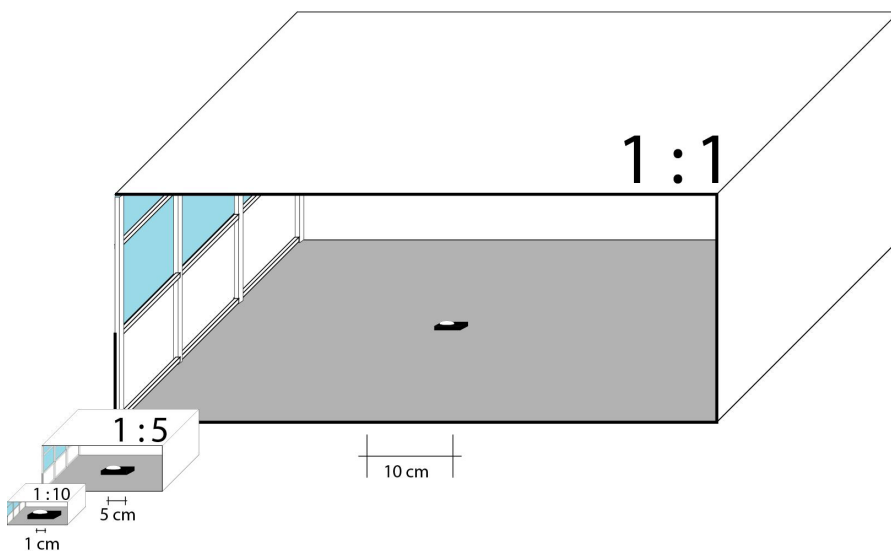


Fig 2.9
A small-scale model can lead to greater error in dimensions and the sensors have a larger impact

When creating a massing model to analyse shade and shadow, the exterior details, the dimensions of the model, the exterior surface reflectance, the surrounding buildings and obstructions are all important. When the model is built to study the sun and sky light distribution, critical design elements must be considered. The size of the scale model has to be suitable for the observation of interior lighting and an even larger size is necessary when photometers and/or cameras are used for interior measurement.

The scale of the model is one of the error sources which can amplify other inaccuracies in daylighting performance assessment, especially if the scale is too small. A very small scale can create difficulties when constructing the model's details. Moreover, a very small scale model also leads to diminished precision when measuring dimensions. For example, an error of 1 cm in a 1:10 scale model equates to an error of 10 cm in reality, while 2 cm in a 1:5 scale model is equal to a real 10 cm. In addition, when photometry sensors and/or cameras are used for daylight observation in the scale model, the presence of the fixed-size measurement tool in a small-scale model will have greater impact than in a larger scale one (Fig. 2.9).



Fig 2.10
Critical details of window elements were accurately constructed in the scale model

Details

Detail reproduction in both scale and virtual models are important when they are critical design elements. It is usually necessary to include any building detail which has an impact on daylight distribution. For example, the precise details of daylighting systems are needed in daylighting model (Fig. 2.10). Modelling the material and texture used in scale model is complicated. Real materials are sometimes used if the model is not too small. Inaccuracy of the texture and material can occur in very small scale model.

Dimensions

Accurate dimensions in scale and virtual models are also important, particularly on critical design elements. For instance, an error of an additional 1 mm on every side of 0.7 m x 0.7 m window frame in a 1: 10 scale model increases the window's glazing area by 6% (Fig. 2.11).

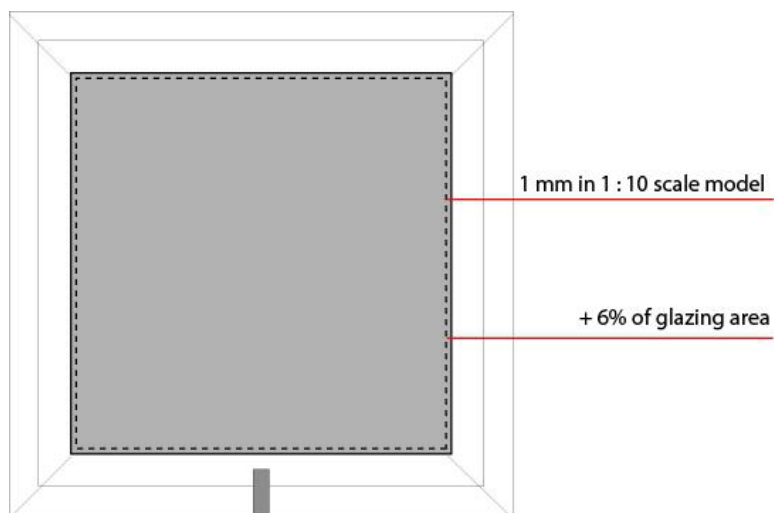


Fig 2.11
The impact of the model's dimensions on a window's glazing area

Photometric properties of materials

When light falls on a surface it can be reflected, absorbed or possibly transmitted (Fig. 2.12).

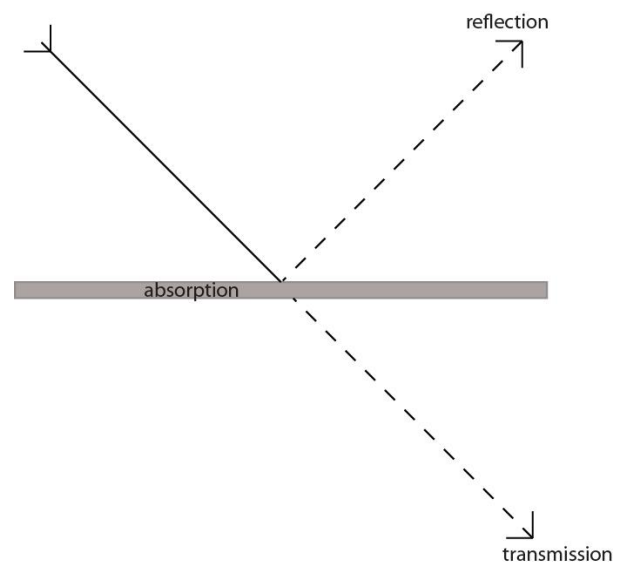


Fig 2.12
Photometrical properties of a material

28

The ratio of the reflected light flux to the incident light flux is reflectance (or ρ).

$$\rho = \Phi_r / \Phi_i \quad (2.1)$$

The ratio of the transmitted light flux to the incident one is transmittance (or τ).

$$\tau = \Phi_t / \Phi_i \quad (2.2)$$

The ratio of the absorbed light to the incident light is absorptance (or a).

$$a = \Phi_a / \Phi_i \quad (2.3)$$

As described below, the properties of a material lead to various forms of reflectance and transmittance by its surface.

Opaque material

The transmittance of an opaque material is nil. For an opaque surface, the reflectance of a perfect black surface is defined as 0 and that of a perfect white surface as 1. The reflectance is proportional to the incident light flux minus the absorbed light flux:

$$\rho = 1 - a \quad (2.4)$$

As a first case, take direct incident light (e.g. direct sun light or a distant point source) falling on an opaque material that reflects a light ray, as shown in Fig. 2.13. Such an opaque surface is called a specular surface. Specular reflectance occurs when light rays obey Snell's law of reflection. A good example is the surface of a mirror, in which the angle of incident light to the normal is equal to the angle of reflected light to the normal. As the reflectance is the ratio of reflected light to the incident light flux, the considered reflectance is direct-direct reflection.

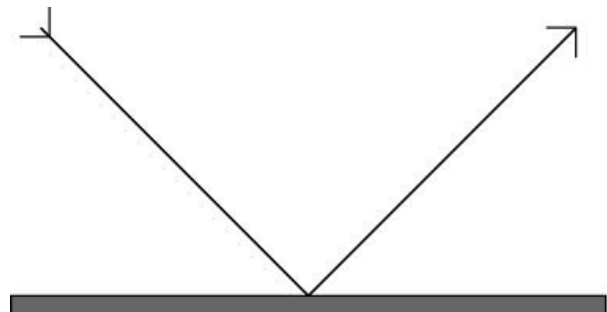


Fig 2.13
Specular reflectance

Fig 2.14
Diffuse reflectance (Lambertian)

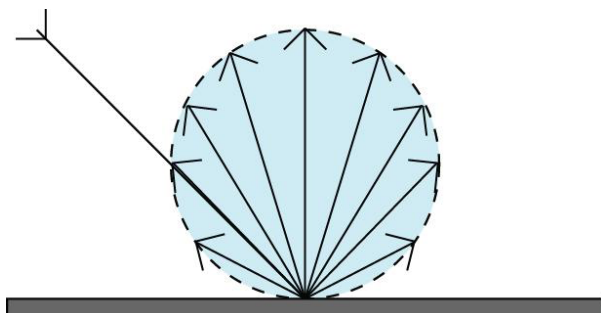
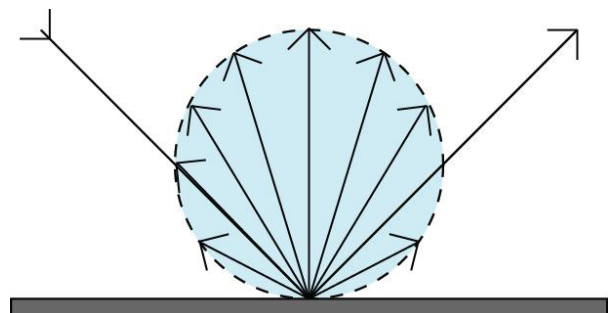


Fig 2.15
Both specular and diffuse reflectance



A further case is when reflected light is distributed in all directions towards the hemisphere even though the incident light is a single light ray. Fig. 2.14 shows an opaque surface diffusing perfectly which is known as Lambertian diffusion. However, perfectly specular or diffused materials are rarely used for building; most materials will have both specular and diffused properties as shown in Fig. 2.15.

Spread reflectance, which is the combination of both specular and diffuse reflectance (Fig. 2.16), is another case. Some materials like aluminium foil can have partial-scattering properties. They have a smooth specular appearance but also keep the directional property as shown in Fig. 2.17. Complex materials such as a prismatic surface can give random reflected light rays as shown in Fig. 2.18.

Diffuse daylight falls from a hemispherical sky vault. In such a case the incident and reflected light can be considered as hemispherical-hemispherical reflectance (Fig. 2.19).

As shown in Fig. 2.21, the specular reflection of the mirror atrium in the Reichstag reflected (in a specular way) most of the daylight entering from the roof above, while the whitewash wall of the British Museum reflected (in a diffuse way) only partially the daylight delivered by the sky roof.

In this thesis reflectance was measured by a reflectometer (Fig. 2.20). The reflectometer used was a Minolta CR-200b chroma meter, a compact tri-stimulus colour analyser which measures reflected light by providing a diffuse light flux, 0° viewing angle geometry lighting over the 8 mm measuring area. The optical fibre received reflected light only perpendicular to the surface. Therefore, reflectance measured in this thesis is hemispherical-direct reflectance.

Surface reflectance is a major factor influencing the daylight distribution in the indoor environment. It is obvious that inaccuracies of reflectance can bring significant errors during the assessment of daylighting performance. As reflectance is an important influence on daylight quality, close care and attention must be brought to it when elaborating scale and virtual models.

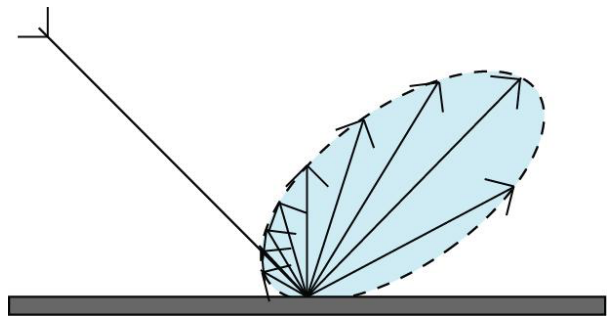


Fig 2.16
Spread reflectance

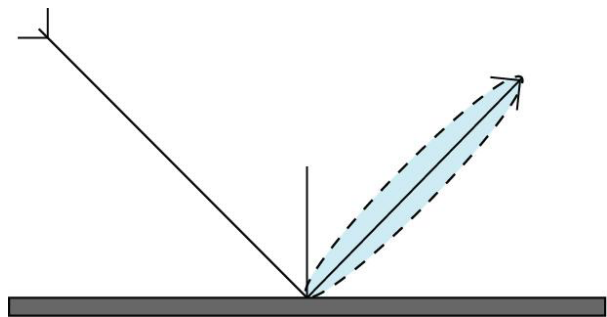


Fig 2.17
Scatter reflectance

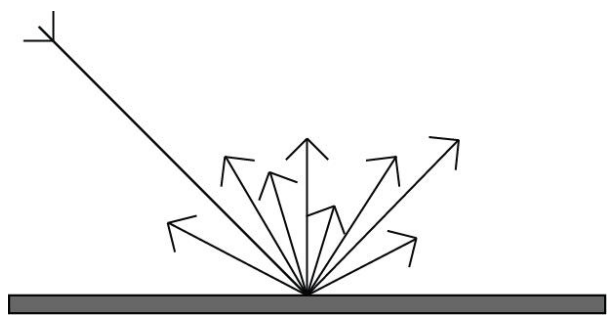


Fig 2.18
Random reflectance

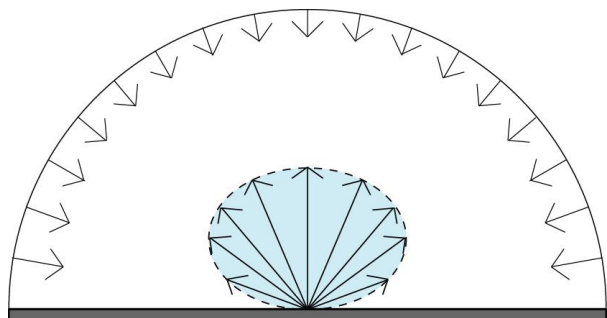


Fig 2.19
Hemispherical-hemispherical reflectance

30

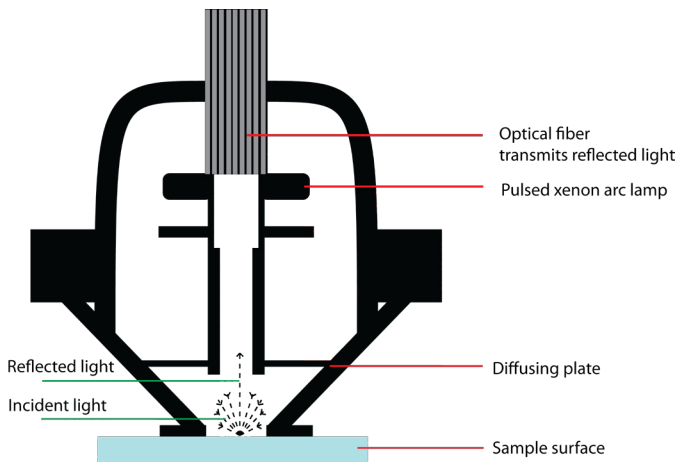


Fig 2.20
The reflectometer used in this thesis



Fig 2.21
(a) The mirrored interior surface in the Reichstag, Berlin, Germany, by architect Lord Norman Foster shows maximal reflection of daylight. (b) The reflection of daylight by the whitewashed wall of the British Museum, London, Great Britain (architect Lord Norman Foster)

Transparent material

When light falls on a transparent material, it is reflected, absorbed and transmitted. The transmittance is equal to the incident light flux minus the absorbed and reflected light fluxes;

$$\tau = 1 - a - \rho \quad (2.5)$$

As an example, a 6 mm clear glass has a normal reflectance equal to 10% and an absorptance of 5%, giving a transmittance equal to 85%.

When the direct incident light falls on a transparent material and it is transmitted without diffusion, it is called regular transmittance, as shown in Fig. 2.22.

And, as with the reflectance of an opaque surface, the transmittance is the ratio of transmitted light to the incident light flux. Such transmittance in this case is called direct-direct transmittance.

When transmitted light is distributed in all directions towards the hemisphere, even though the incident light is direct, it is called diffuse transmittance, as shown in Fig. 2.23.

As noted for reflectance, transparent materials can have both specular and diffused transmittance properties (Fig. 2.24).

Spread transmittance, which is the combination of both specular and diffuse transmittance as shown in Fig. 2.25, also occurs.

Some materials like sanded glass can have partial-scattering properties. They can be smooth specular but also keep the directional property as shown in Fig. 2.26.

Complex materials such as a prismatic surface can give random transmitted light, as shown in Fig. 2.27.

However, daylight falls from a hemispherical sky vault. In such a case the incident and transmitted light can be considered as hemispherical-hemispherical transmittance (Fig. 2.28).

In general the transmittance value depends on the angle of incidence, as explained by Fresnel's law and shown in the graph presented in Fig. 2.29. Transmittance varies considerably with angle of

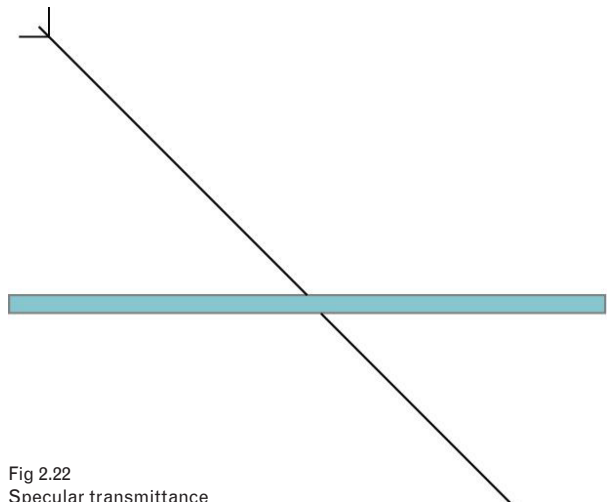


Fig 2.22
Specular transmittance

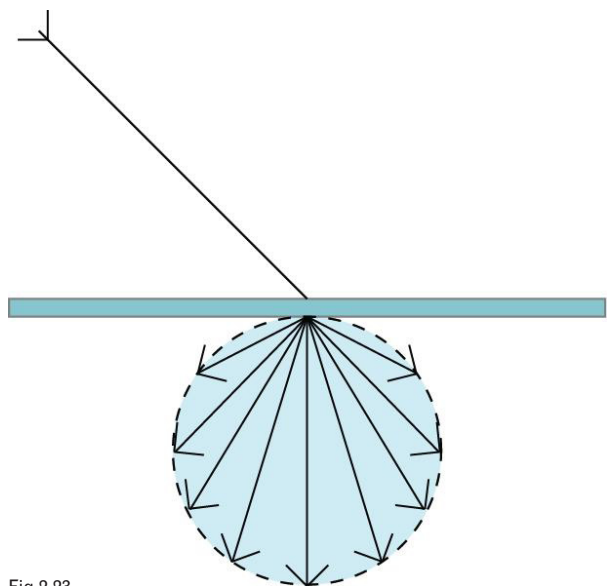


Fig 2.23
Diffuse transmittance

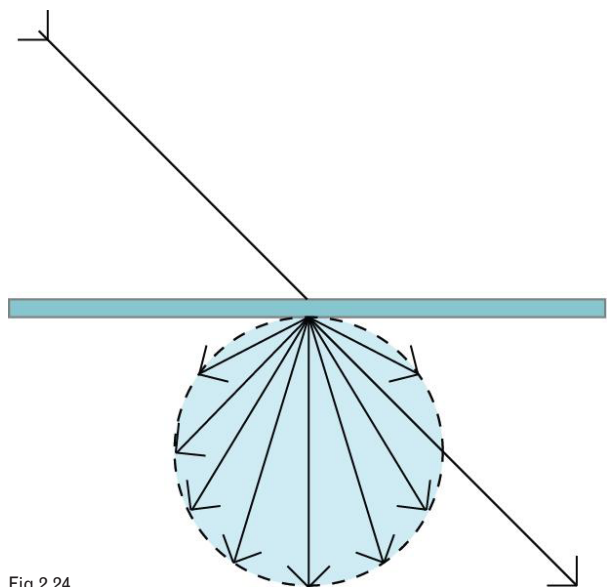


Fig 2.24
Both specular and
diffuse transmittance

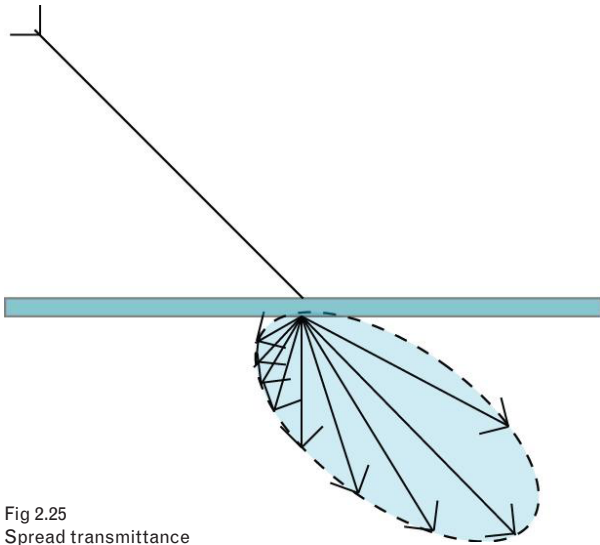


Fig 2.25 Spread transmittance

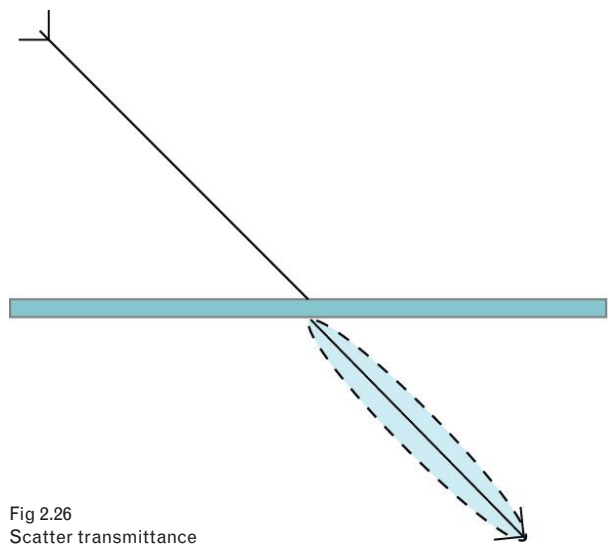


Fig 2.26 Scatter transmittance

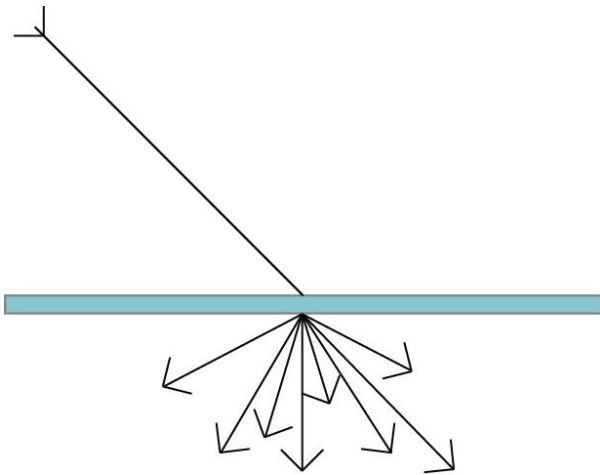


Fig 2.27 Random transmittance

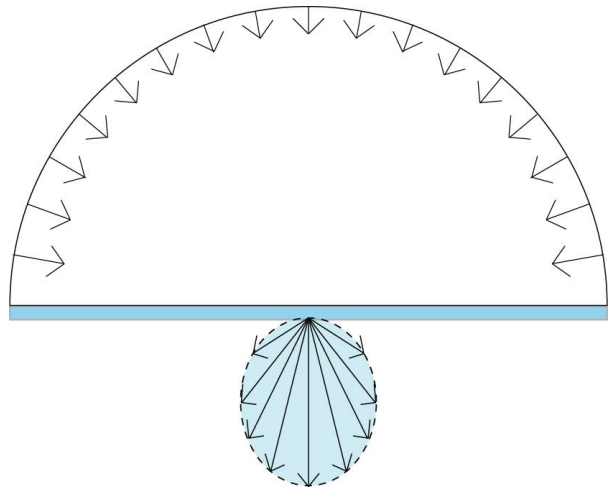


Fig 2.28 Hemispherical-hemispherical transmittance

Fig 2.29 Transmittance depending on the light's angle of incidence

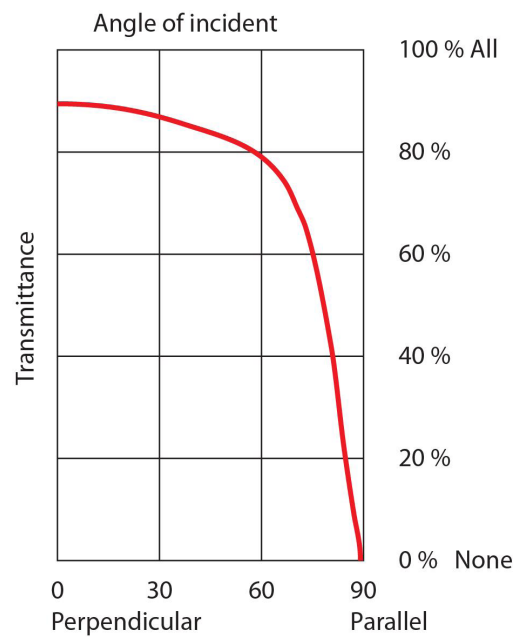




Fig 2.30
Glass fenestration of the Branly museum, Paris, France

incidence of the light rays; that at the normal is usually larger than transmittance at a grazing angle. Fig. 2.30 shows the glass fenestration of the Branly museum in Paris, designed by architect Jean Nouvel so that different angles of sight give different visual impressions due to differing light transmission for different grazing angles.

In this thesis, normal (perpendicular to the surface) glazing transmittance was measured using a calibrated LS-110 Minolta luminance meter (Fig. 2.31).

Glazing transmittance is very important for daylighting performance. In physical models transmittance is tricky to reproduce faithfully, particularly when at a very small scale; dirt and lack of maintenance can significantly influence this parameter (Fig. 2.32). Usually modellers cannot scale down glazing in an appropriate manner while at the same time keeping the glazing transmittance equal to that of the real building components. In the case of more complex fenestration systems, transmittance is even more significant in lighting performance assessment. In virtual models, a correct transmittance value should be used and must correspond to that of the real building. Accordingly the exact transmittance, either measured from the material or simulated in the models, is very important when assessing performance.



Fig 2.31
Luminance-meter

Daylight source simulation

Real sky

To assess daylighting performance of buildings, besides an accurate model, appropriate daylight conditions are also needed. Placing the physical model outdoors is the easiest way to visualise real sky daylighting conditions (Fig. 2.33) but changeable skies can complicate the assessment of daylighting performance. Various sky simulators have been developed to overcome this problem.



Fig 2.32
Dirt can reduce glazing transmittance

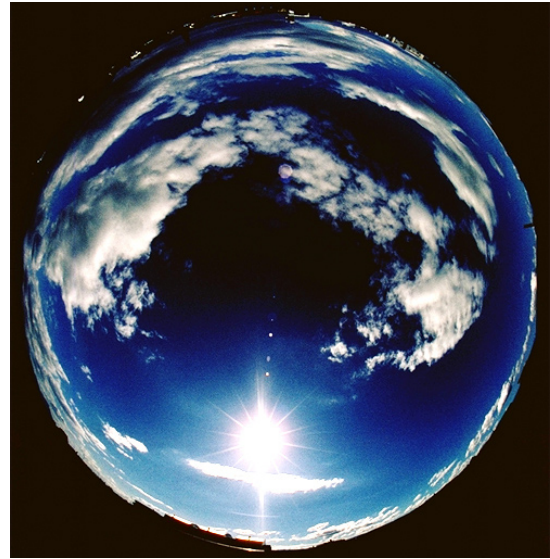


Fig 2.33
Real sky conditions



Fig 2.34
A mirror sky at the Seattle daylighting lab, Washington (USA)



Fig 2.35
A sky dome at the Lawrence Berkeley National Laboratory, California (USA)

Sky simulator

Several types of sky simulator have been invented to reproduce appropriate sky conditions for testing environmental lighting. Most of them can reproduce one or several CIE standard skies (details in Appendix A).

Mirror sky

The mirror sky, which is the most common configuration (Fig. 2.34), consists of a mirrored enclosure with a lighting ceiling (fluorescent tubes and opal diffuser). The advantages of this kind of simulator are its moderate cost and minimisation of horizon error; however it can reproduce only CIE overcast skies and has inter-reflection disturbed by the scale model.

Sky dome

A sky dome (Fig. 2.35) has a diameter of between 3 and 9 metres. Made of an opaque hemisphere illuminated by light sources in a circular groove, it can reproduce different standard sky models (uniform overcast sky or CIE standard skies). Being quite large, it allows very easy access to the scale model. However one drawback is that it is hard and tiresome to calibrate, requiring about one week. Moreover the lamps use a lot of electricity and create frequent maintenance problems.

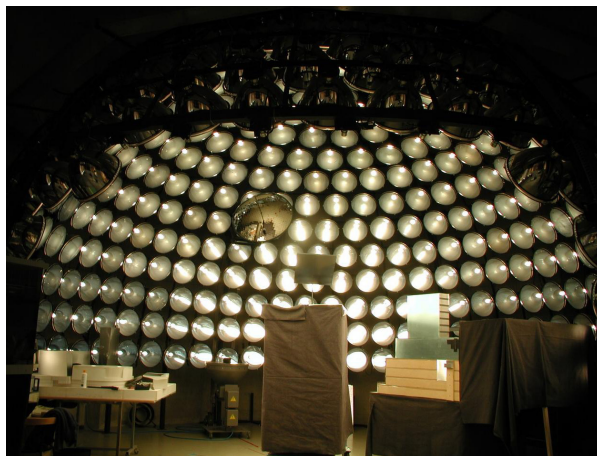


Fig 2.36
Spotlight sky simulator

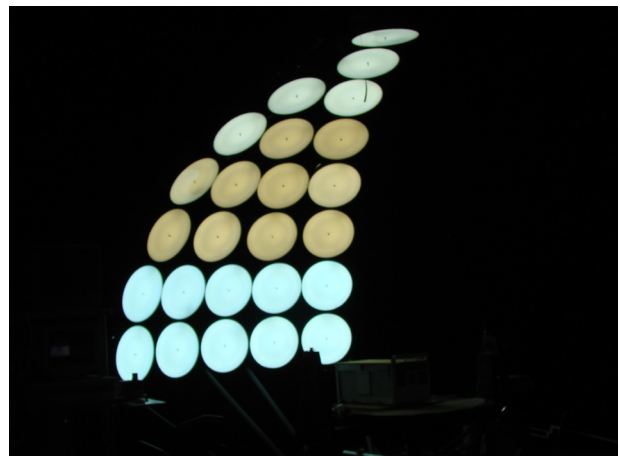


Fig 2.37
Scanning sky simulator

Spotlight sky simulator

Spotlight sky simulators are made of a vault of multiple incandescent lamps or a line of lamps mounted in a quarter-circle arc (Fig. 2.36). They can reproduce all types of sky at moderate cost; however calibration and maintenance are complicated by the light sources aging at different rates. Other disadvantages of this type of sky simulator are the high luminance discontinuity and slow measurement procedure.

Scanning sky simulator

A scanning sky simulator (Fig. 2.37) is made of 25 light sources to create a sixth of the vault. The whole hemisphere is based on Tregenza's model of 145 light sectors, which is reconstructed by a six-step scan (60 degree angular rotation). Quantitative (illuminance) and qualitative (digitised video image) data are summed at the end of the process. This simulator closely matches the IDMP sky luminance measuring format and can reproduce all existing standard or statistical sky models. Costs of construction, maintenance and operation are low; however, it is impossible to visualise or measure instantaneously inside the model. A scanning sky simulator was used in this thesis.

36

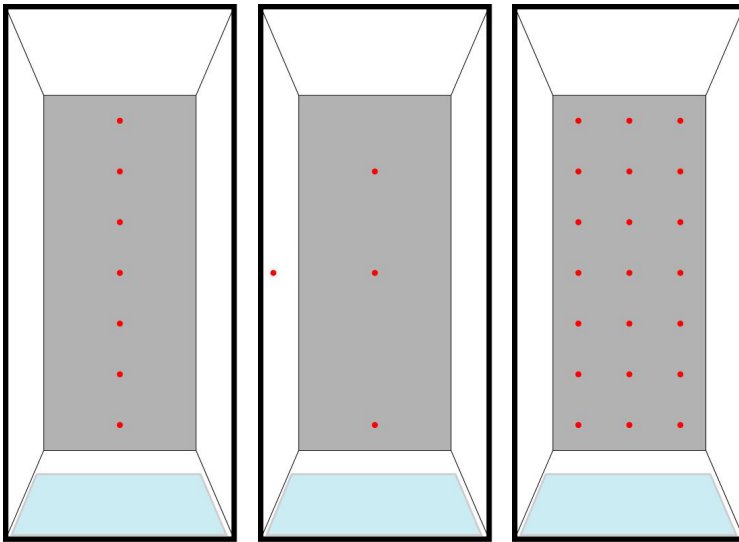


Fig 2.38
Point, line and grid schemes for placement of photometric sensors in both scale and virtual models

Photometric sensors

Photometric sensors are commonly used during daylighting performance assessment to monitor physical variables such as interior illuminance and daylight factors. To measure daylighting performance several sensors at a time are normally used, on either a horizontal or a vertical plane in and outside buildings. In an interior space they are conventionally placed in point, line or grid schemes as shown in Fig. 2.38. Many manufacturers produce photometers and sensors of differing sizes, precision and quality (Fig. 2.39). Even when made by the same manufacturer it is strongly recommended to calibrate the many sensors used in an experimental set-up, otherwise divergence among sensors can lead to significant measurement inaccuracies.



Fig 2.39
A number of different photometers and sensors

The area of sensitivity of the sensors can be a cause of error during assessment. An uneven incident light flux arriving on the sensitive surface (caused by possible gradient, as well as the effect of shade and shadow) can lead to errors in lighting evaluation, as shown in Fig. 2.40.

As with the sensor sensitivity area, the imprecision of sensor positioning and levelling can cause errors in lighting evaluation (Fig. 2.41). Especially with a small model, slight errors in sensor position and levelling can cause significant assessment errors. Moreover, the relative size of the photometric sensor and the scale model are very important (Fig. 2.42).

In virtual models, point-virtual sensors are normally employed so that the accuracy of positioning, levelling and size is not so relevant. However, the position and level of sensors should always be appropriate.

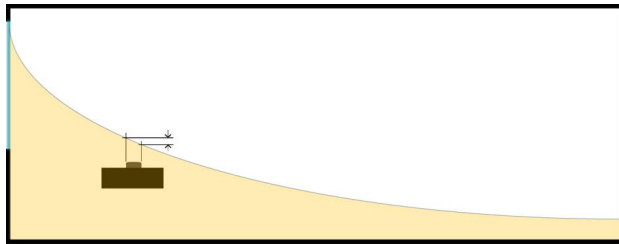


Fig 2.40
The impact of the size of the sensor's sensitive area

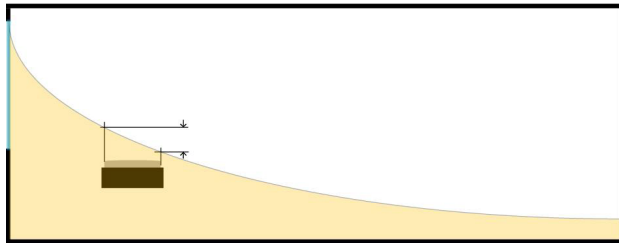


Fig 2.41
The impact of sensor leveling and positioning

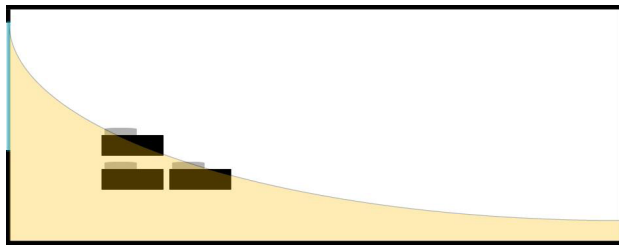
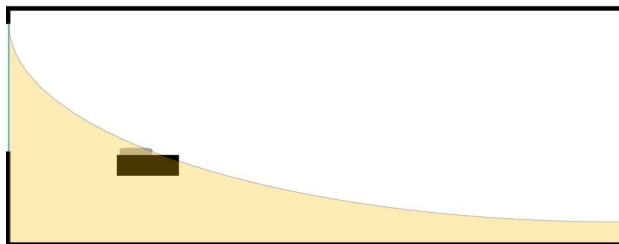
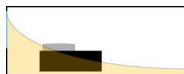


Fig 2.42
The need for an appropriate relative size of scale model and photometric sensor



Surroundings

38

The impact of outdoor environments on scale and virtual models can cause significant errors in daylighting performance assessment. The reflectance from the ground and surroundings, which has a great impact on interior illumination, should not be forgotten. For example, in the simulation of an art gallery by a scale model (Cannon-Brookes S.W.A., 1997) (Fig. 2.43), surrounding trees were modelled by wooden board to minimise errors.



Fig 2.43
The daylighting model
for a gallery included the
surrounding trees



In assessing daylighting performance of buildings using physical or virtual models, the reliability of the evaluation depends on which errors occur and their magnitude. To avoid errors, the modeller should understand their causes, particularly the common and significant causes, which naturally will then be considered during the modelling process. An effort to mock-up the models accurately will help reduce the importance of any errors that may occur.

chapter

3

daylighting performance assessment of buildings



Fig. 3.1
External view of the real building (south facade)



Fig. 3.2
Internal view of the real building towards the south facade

The objective of this thesis is to list and analyse how physical and virtual models give performance measurements differing from those of a real building. Both the daylight factor and the illuminance ratio of a real building and its models were carefully determined and then compared. This chapter documents in detail the real building and its scale and virtual models, and also describes the considered daylighting variables.

3.1 The real building

The real building used in this study was a simple one – a single office room. Its simplicity decreased the overall number of factors usually encountered in buildings so as to concentrate on the main causes of error in daylighting performance assessment. The building was originally a daylighting test module used by the Solar Energy and Building Physics Laboratory at EPFL, Lausanne. It had the necessary monitoring devices for daylighting performance assessment. The flexibility of this test module, such as the movable wheels for orientation change, made the daylighting experiments easier.

Type of building

The real building was an office room, entered by a door on one of the long sides, equipped with a sidelighting window (Fig. 3.1). The room was normally occupied by two desks, but in this study it was emptied to avoid extraneous factors usually encountered in buildings, such as plant shadows, cupboards and so on that disturb daylight factor measurement (Fig. 3.2).

In an efficiently-designed office, the room generally requires adequate horizontal illuminance and uniform light distribution on the task plane (IESNA, 2006). This work focused on the horizontal task plane illuminance. The recommended illuminance for an office room lies between 300 and 1000 lux, depending on the visual tasks involved (Table 3.1).

Table 3.1
Illuminance recommended in office lighting design
(IESNA, 2006)

Visual task requirements	Illuminance (lux)
High contrast and large size	300
High contrast and small size	500
Low contrast and large size	500
Low contrast and small size	1000

Location and surroundings

The real building was situated in the southern car park of EPFL campus, Lausanne (Switzerland), which is located at latitude 46.5°N and longitude 6.6°E, 396 m above sea level (Fig. 3.3).

The location's climate typically gives an average temperature in winter of about 4°C and 22°C in summer. It has an average annual precipitation of 1250 mm and about 1907 hours of sunshine annually. The annual global solar radiation on the horizontal plane is 1176 kWh/m² and the annual diffuse solar radiation on horizontal plane is 255 kWh/m² (Fig. 3.4). The average annual global illuminance is about 14719 lux and diffuse illuminance is about 9253 lux (data using Meteonorm 5.0, 2006) (Fig. 3.5).

To reduce the impact of external obstructions the real building was placed on a concrete platform with its window facing south, such that the angular height of surrounding buildings was less than 10 degrees (Fig 3.6) at the northern side of the car park. It looked on to agricultural fields to the east and south, with Lake Geneva and the Alps on the horizon. On the west side, adjacent to the real building, there was a test module of identical geometrical and photometrical properties, used for experimental assessment of daylighting systems. Figure 3.6 shows a 360° panoramic view of the modules. The ground reflectance and geometry of the platforms are as shown in Table 3.2 and Fig. 3.7.



Fig. 3.3
Location of the real building on the EPFL campus, Lausanne, Switzerland. Credit: Google Earth

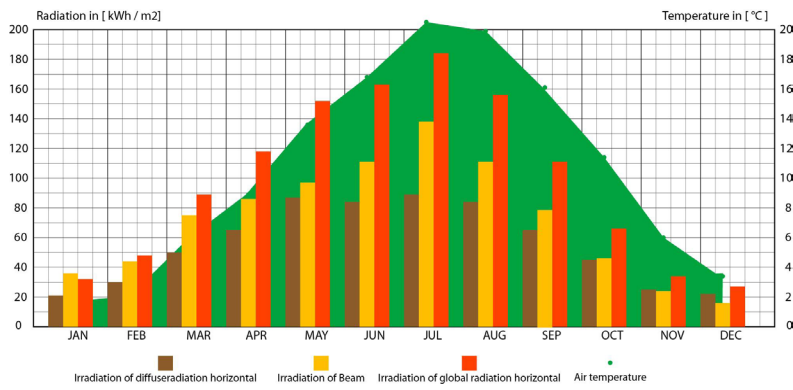


Fig. 3.4 Monthly solar radiation and outdoor temperature of the real building location (Lausanne) simulated by Meteonorm 5.0

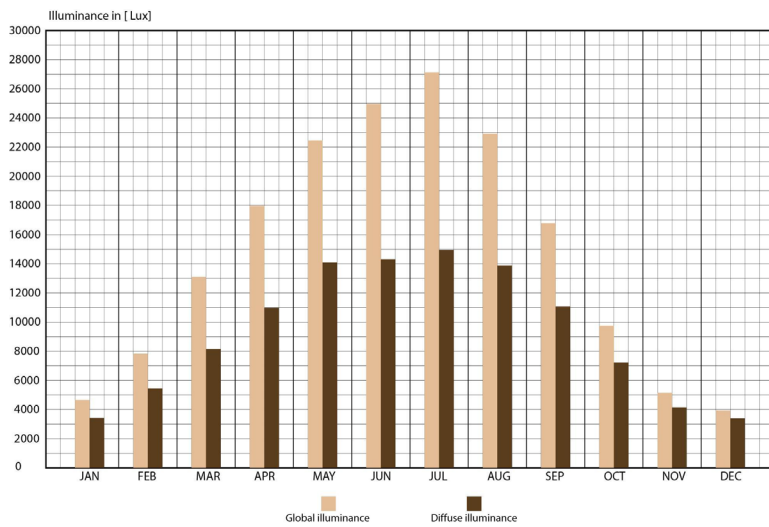
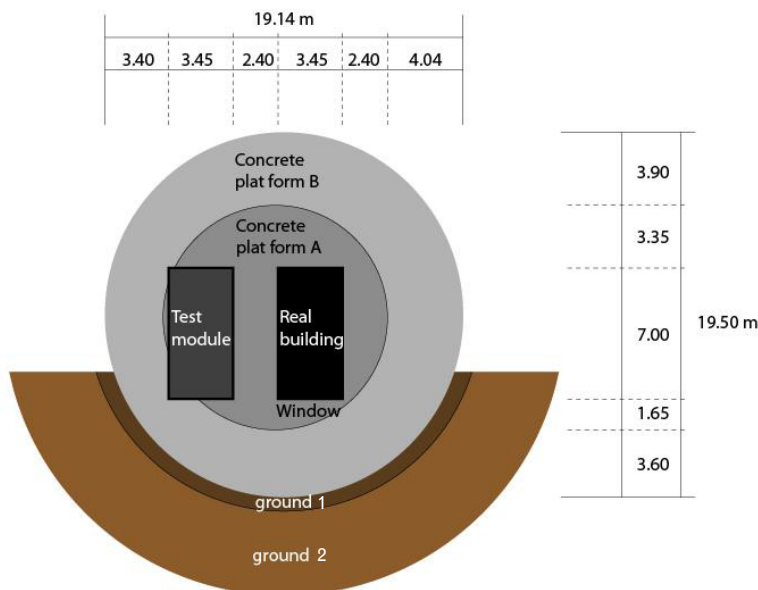


Fig. 3.5 Monthly illuminance of the real building location (Lausanne) simulated by Meteonorm 5.0



↑ Fig. 3.6 Panoramic view of the real building and its surroundings



← Fig. 3.7 Geometrical (dimensions) and photometrical (ground reflectance) properties of the real building and its surroundings

Ground surface	Ground reflectance (%)
Platform A	20.2 ± 2
Platform B	12.4 ± 2
Ground 1	10.2 ± 3
Ground 2	12.8 ± 3

Table 3.2
Ground surface reflectance of platforms and ground

Geometry and dimensions

The real building has a simple rectangular interior space as shown in the drawings of Fig. 3.8. The interior dimensions are shown in Table 3.3.

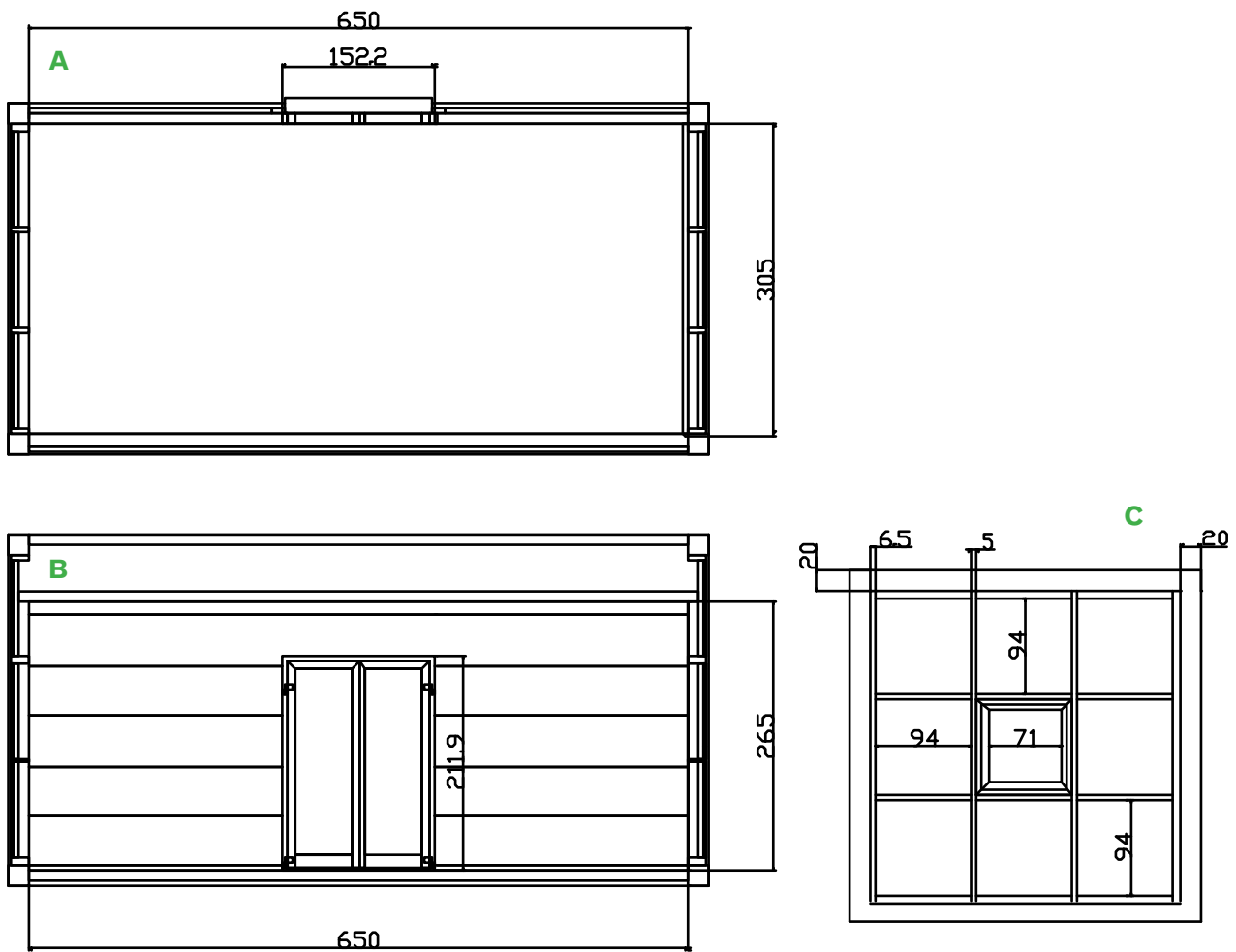


Fig. 3.8
Geometry of the real building (unit: cm): (a) plan view, (b) section view and (c) exterior elevation view

Table 3.3
Dimensions of the real building

Geometry	Dimensions (m)
Width	6.50 ± 0.01
Length	3.00 ± 0.01
Height	2.50 ± 0.01

The window of the real building, shown in Fig. 3.9, is a double insulated glazing one commonly used in Swiss office buildings. It consists of five fixed glazing panels and a workable central window (Fig. 3.10). The details and interior dimensions are shown in Table 3.4 and Fig. 3.11.



Fig. 3.9
Internal view of the real building's windows

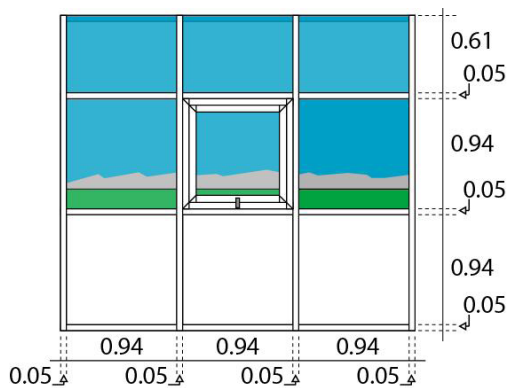


Fig. 3.10
Dimensions (unit: m) of the interior south façade of the real building

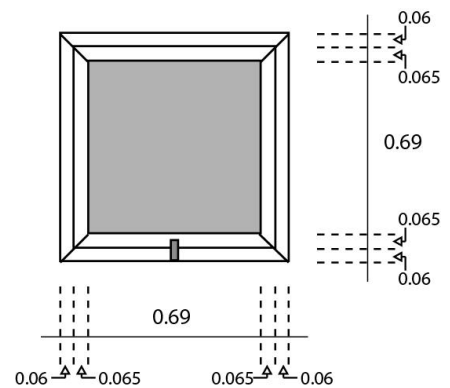


Fig. 3.11
Dimensions (unit: m) of the double-glazing opening window

Table 3.4
Dimensions of the window (real building)

Geometry	Dimensions (m)
Width	3.00 ± 0.01
Height	1.65 ± 0.01

Interior Features

Interior surface reflectance has a strong impact on daylight performance of buildings (Bodart, 2007). The reflectances recommended for office room surfaces are given in Table 3.5, together with the actual interior surface reflectance of the monitored object.

The internal room surfaces are achromatic with white-painted walls and ceiling; the floor is covered by a uniform grey-green carpet. Fig. 3.12 shows an indoor view of the room, with close-ups of the surfaces; the corresponding reflectances are given in Table 3.5 and Fig. 3.13. Table 3.6 shows the furnishing materials used. The chromatic properties of the surfaces monitored using the XYZ CIE Colour Space (i.e. x,y,z chromatic coordinates) are documented in Table 3.7.

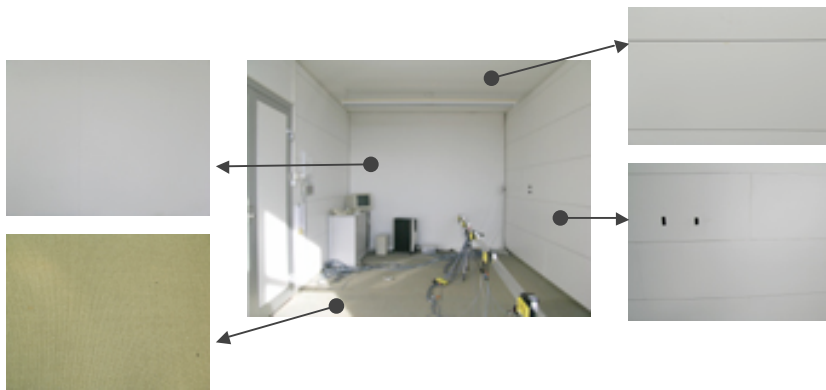


Fig. 3.12 Internal view of the real building (walls, ceiling and floor)

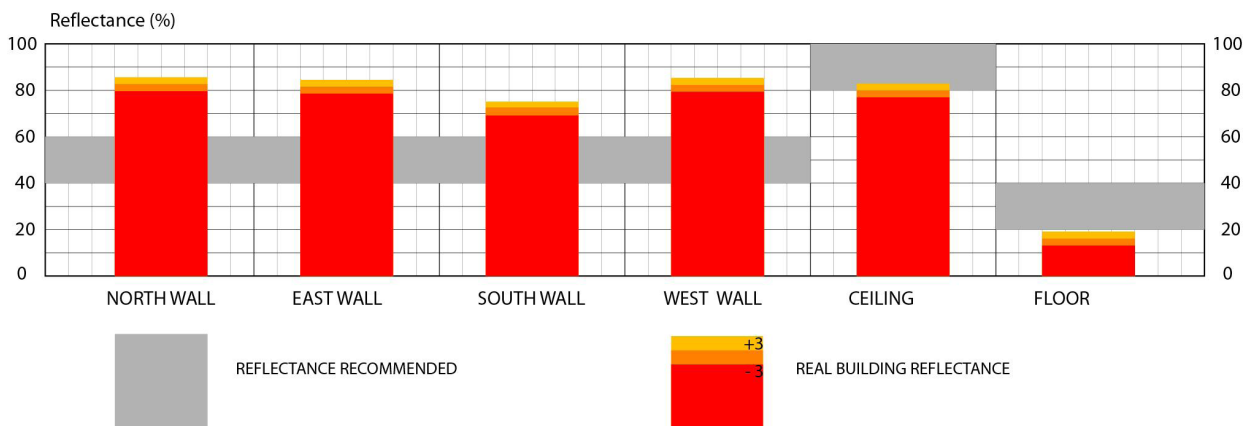


Fig. 3.13 Surface reflectance of the real building (graphically)

Table 3.5 Surface reflectance of the real building

Surfaces	Recommended reflectance (%)	Measured reflectance (%)
North wall	50-70	82.6 ± 3
East wall	50-70	81.5 ± 3
South wall	50-70	72.1 ± 3
West wall	50-70	82.3 ± 3
Ceiling	80 or more	79.9 ± 3
Floor	20-40	16.1 ± 3
Window frame	-	72.1 ± 3

Table 3.6 The furnishing materials of the real building

Surfaces	Materials
North wall	Canvas (white)
East wall	Satin (white)
South wall	Painted metal (white)
West wall	Satin (white)
Ceiling	Satin (white)
Floor	Fitted carpet (grey-green)
Window frame	Painted metal (white)

The materials used in this study are those found in a typical office. The surface reflectance of the materials is close to that recommended (IESNA, 2006). The reflectance and chromatic properties of the materials were measured using a Minolta chromameter (details in Chapter 2).

Surfaces	CIE Chromatic coordinates
North wall	(0.32, 0.34, 0.34)
East wall	(0.31, 0.33, 0.36)
South wall	(0.32, 0.34, 0.34)
West wall	(0.31, 0.33, 0.36)
Ceiling	(0.32, 0.34, 0.34)
Floor	(0.34, 0.36, 0.30)
Window frame	(0.32, 0.34, 0.34)

Table 3.7
Chromatic properties of the surfaces
monitored using the XYZ CIE Colour Space

Additionally, the real building is equipped with two rows of luminaries (2 x 36 W fluorescent, Zumtöbel Licht) suspended across the room's width respectively at 1.7 and 5 m from the window façade as shown in Fig. 3.14. The solar blinds were fully retracted during the monitoring periods; the window was cleaned to eliminate dust.



Fig. 3.14
Surface reflectance of the real building (photo)

Fenestration details

Side window

The test module is habitually equipped with double glazing windows (section shown in Fig. 3.15), giving a glazed ratio to floor area of 0.26. The window façade is oriented due south; its windows are mounted on a 0.94 m high opaque breast wall supported by a metallic frame (Fig. 3.16). The normal-normal window transmittance measured using a Minolta LS 110 luminance meter (details in Chapter 2) is given in Table 3.7. The latter was monitored by pointing the luminance meter on the window and dividing the ratio of the luminance of the targeted point by the value measured for the same point with an open window.

Window	Transmittance (%)
Double glazing	80.5 ± 3

Table 3.7
Transmittance of the double glazing

48

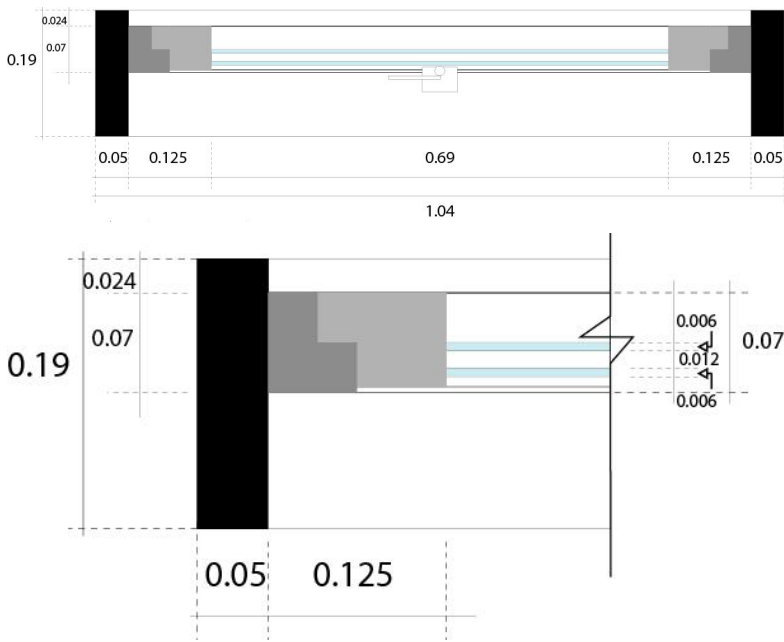


Fig. 3.15 Section of the double-glazing opening window (unit: m)

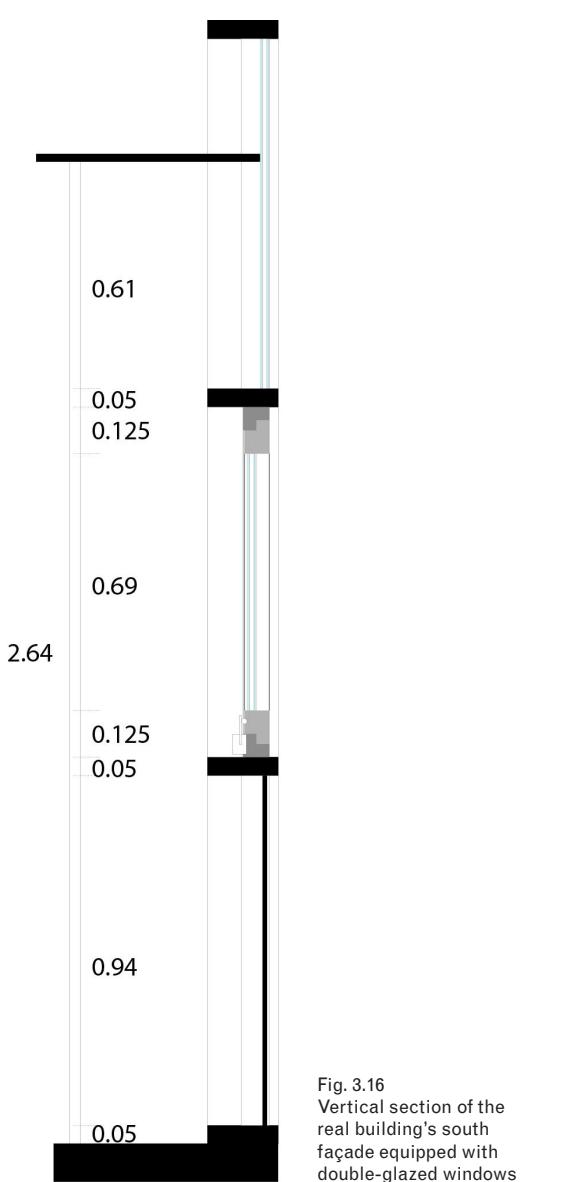


Fig. 3.16 Vertical section of the real building's south façade equipped with double-glazed windows

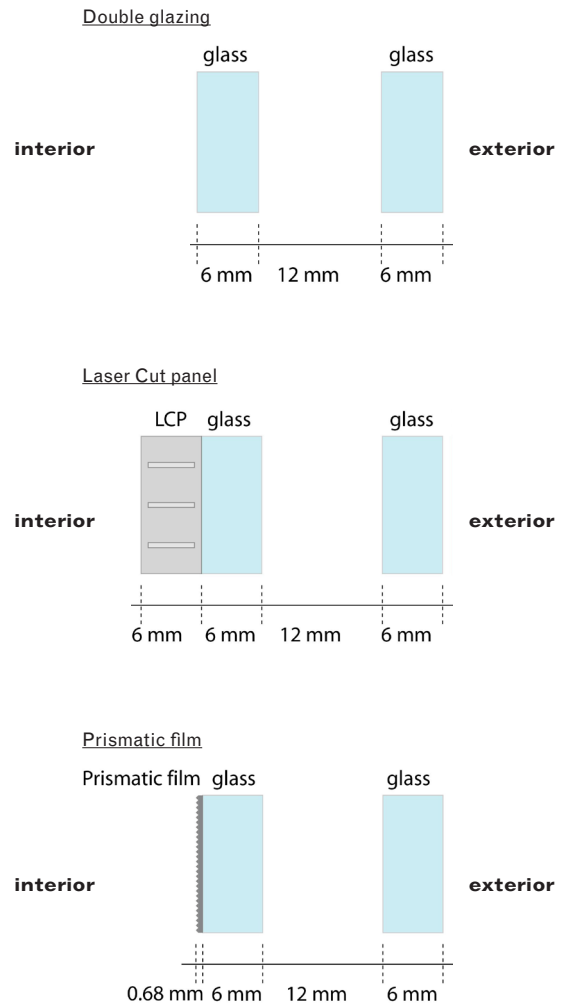


Fig. 3.17 Sections of double glazing, LCP and Prismatic film



Fig. 3.18

Exterior views of the test module equipped with conventional double-glazing, Laser-Cut Panel and Prismatic film respectively

As this work's objective was also to assess the daylighting performance of Complex Fenestration Systems (CFS); two types of CFS were installed. They were attached on the southern facade of the test module, one after the other, on the internal glazing surface of the upper part of the window (Fig. 3.17) to compare CFS daylighting performances. Two direct-light guiding systems (Laser-Cut Panel and Prismatic film) were selected for study. Thus the fenestration systems used in this study were (Fig. 3.18):

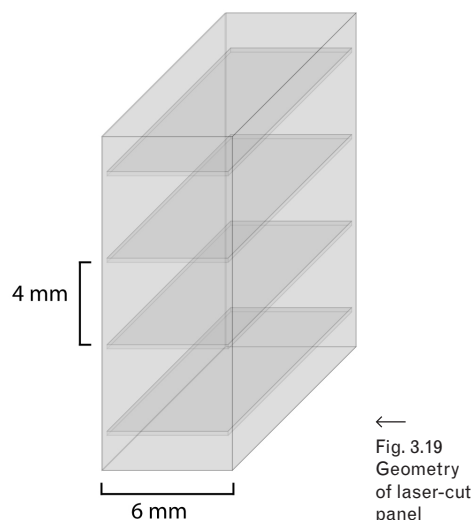
- Double glazing window
- CFS – Laser-Cut Panel
- CFS – Prismatic film

Complex Fenestration Systems

Complex Fenestration Systems are advanced daylighting systems which are nowadays available to the building profession, even though some of these systems are still in the development stage. CFS have different performance figures: their main objectives are to redirect daylight into a room so as to optimise the luminous environment, to improve the daylight flux on the work plane, to improve visual comfort and to control glare (IEA, 2000). It is therefore necessary for researchers and building designers to have accurate design tools in order to be able to assess their daylighting performance.

Laser-Cut Panel

A Laser-Cut Panel (LCP) is a daylight-redirecting system made of a 6 mm thick acrylic panel with parallel laser cuts spaced at 4 mm intervals (Fig. 3.19). Each laser-cut surface obtained performs as a small mirrored surface that deflects daylight passing through the panel (IEA, 2000). Fig. 3.20 shows a view through laser-cut panel.



←
Fig. 3.19
Geometry
of laser-cut
panel



Fig. 3.20
View through the laser-cut panel

50

When a light ray at incidence angle i is refracted into the LCP at angle r , a fraction (f) of the incident light flux is redirected; the remaining fraction ($1-f$) of the light beam is transmitted in the material without any deviation from its original direction of propagation (Fig. 3.21).

The effectiveness of LCP in improving the illumination of rooms depends strongly on the type of window fitting and sky conditions (Edmonds, 1992). The main property of LCP placed in the upper window part is its capacity to redirect sunlight towards the ceiling; when used in skylights, it admits low elevation light rays and rejects high elevation light rays, thus contributing to solar protection. It effectively redirects off-normal light rays through a large angle ($>120^\circ$) and has good viewing transparency in the near-normal direction. The reduction in viewing transparency relative to a conventional window is however perceptible. LCP is usually fixed above eye level (Fig. 3.22) in order to avoid obstruction of the external view as well as discomfort from glare.

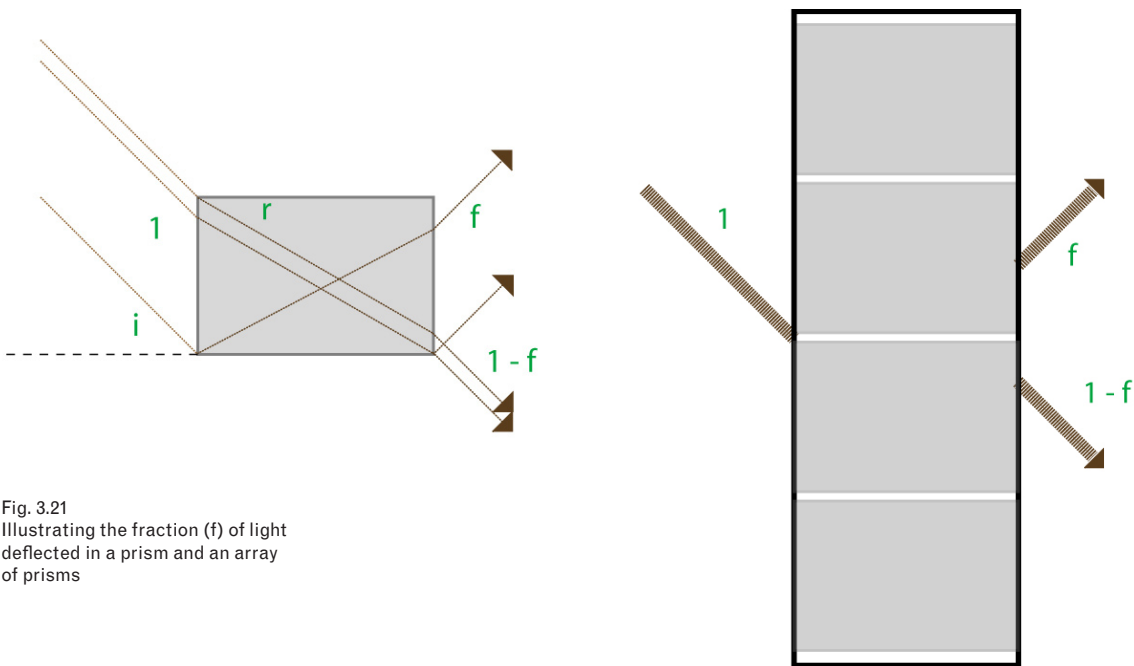


Fig. 3.21
Illustrating the fraction (f) of light deflected in a prism and an array of prisms



Fig. 3.22
The laser-cut panel fixed to the windows above eye level in the real building

Prismatic film

A Prismatic film is a daylight-redirecting system made of acrylic or polycarbonate material; it refracts passing light rays towards the ceiling and illuminates the deeper parts of the room. In this work a 3M prismatic film (3M Brand Optical Lighting Film) was employed. This continuous thin film incorporates microscopic prisms of identical 90° angle geometry, (Fig. 3.23). Fig. 3.24 shows a close-up view of prismatic film.

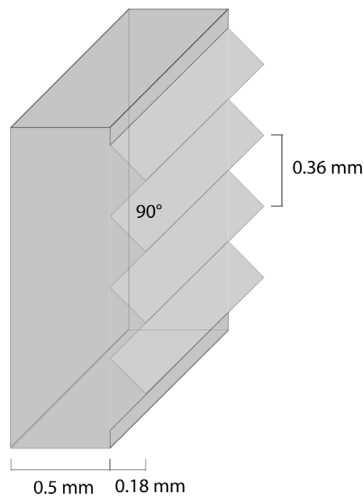


Fig. 3.23
Geometry of prismatic film



Fig. 3.24
Close up view through prismatic film

The advantages of a prismatic film are its longitudinal flexibility, low maintenance and very low light absorption, so allowing the film to transport and distribute light in an effective way.

Under clear sky, the prismatic film refracts sunlight and illuminates the ceiling in the centre of the room. The film performs less well under cloudy sky conditions, but apparently diminishes glare (IEA, 2000) (Fig. 3.25).

Prismatic film is also usually attached to upper windows, above eye level (Fig. 3.26), in order to avoid obstruction of the external view as well as discomfort glare.

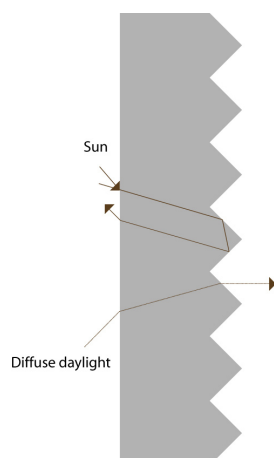


Fig. 3.25
The basic principle of prismatic panels and prismatic film



Fig. 3.26
Prismatic film fixed to the windows above eye level in the real building

Equipment set-up

52

The test module was equipped with the necessary equipment for evaluating both quantitative and qualitative daylighting figures from both interior and exterior viewpoints. Fig. 3.27 illustrates the test module's environment and its instrumentation for the various experimental purposes.

Exterior illuminance

To monitor outdoor illuminance a horizontal LMT/BAP30FCT and 4 vertical Hagner ELV641 illuminance sensors were mounted on a black honeycomb support (Fig.3.28). The sensors were connected to a data logger which stored the illuminance values at intervals of one minute. The outdoor illuminance was used to determine the daylight factors and illuminance ratios.

Sky luminance distribution

The sky luminance distribution around the test module was monitored using a digital sky scanner (Fig. 3.29). This sky scanner, based on digital imaging techniques, was developed at the Solar Energy and Building Physics Laboratory of EPFL, Lausanne (Michel, 1995). It was placed on the construction adjacent to the test module to avoid obstructing the surroundings. (Fig. 3.30).

A mirror-surfaced sphere placed at the base of the scanner, as shown in Fig. 3.31, reflected an image of the whole sky vault which was acquired by a CCD digital camera (Fig. 3.32) hanging over the sphere and then sent to the control unit. The sky luminance distribution from this CCD digital camera were continuously monitored and averaged according to the 145 sectors proposed by Tregenza (Fig. 3.33).

The control unit uses a powerful image analysis software (Image-Pro Plus™) and a user-friendly interface made to facilitate the data acquisition and treatment (Michel L, 1999).

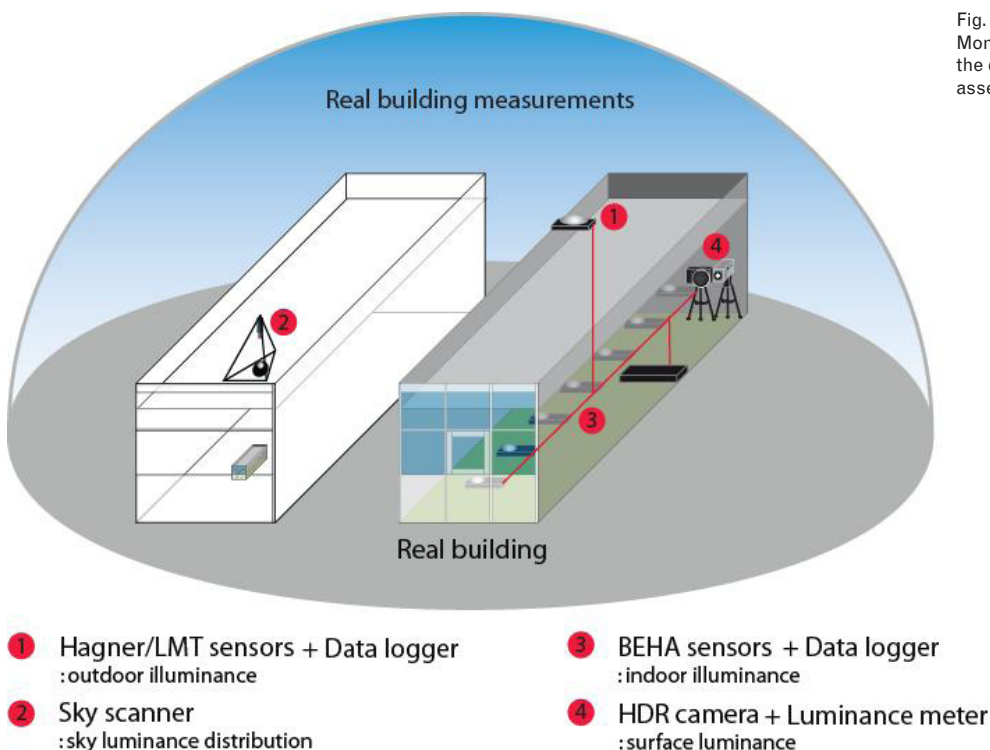


Fig. 3.27
Monitoring equipment used for the daylighting performance assessment of the test module.



Fig. 3.28
A horizontal LMT/BAP30FCT for outdoor illuminance monitoring



→
Fig. 3.29
A digital sky scanner



Fig. 3.30
The digital sky scanner was placed on the roof of the module next to the real building

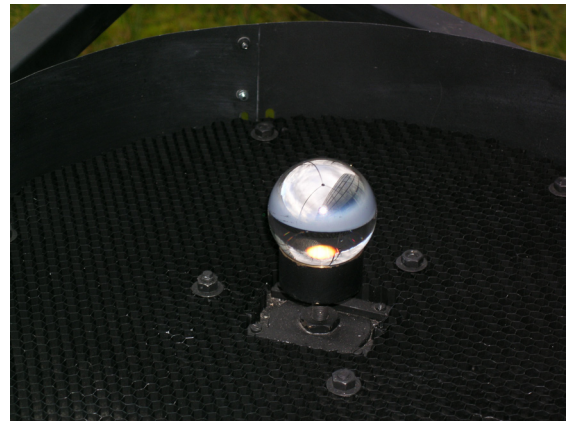


Fig. 3.31
Mirror sphere reflecting the sky vault

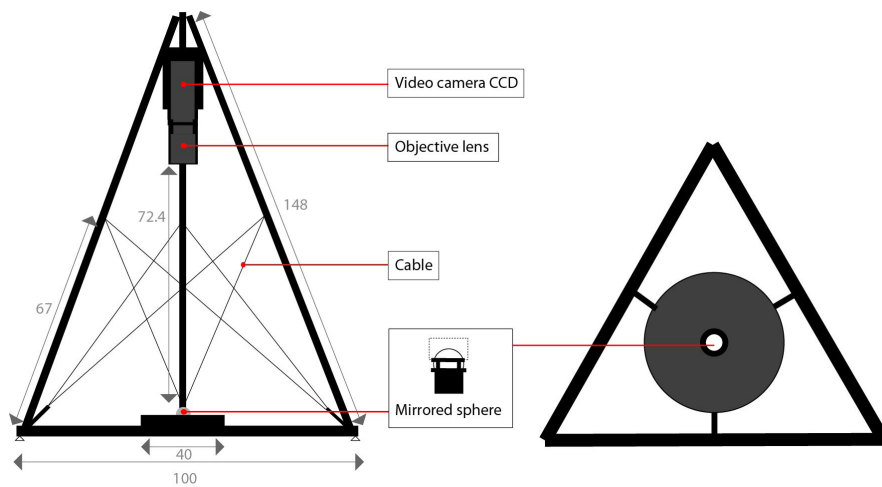


Fig. 3.32
Geometrical properties of the digital sky scanner

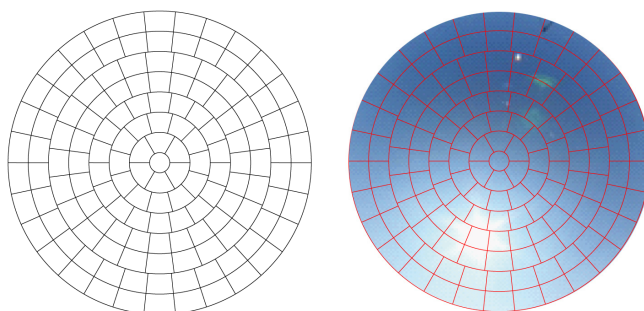


Fig. 3.33
Tregenza's 145 sky sectors

54

Interior illuminance

Seven calibrated BEHA 96408 sensors (Fig. 3.34) were used for indoor illuminance monitoring. They were installed on a metal bar (Fig. 3.35), which lay along the length of the middle of the room at intervals of 1 m distance from the window to deeper in the room, as shown in Fig. 3.36. The sensors were connected to a data logger which collected the illuminance values at one minute intervals. The indoor illuminance was used for daylight factors and illuminance ratios assessment.



Fig. 3.34
Calibrated BEHA 96408 sensor for indoor illuminance monitoring



Fig. 3.35 →
Internal view of the real building and calibrated BEHA 96408 sensors on a metal bar for indoor illuminance monitoring

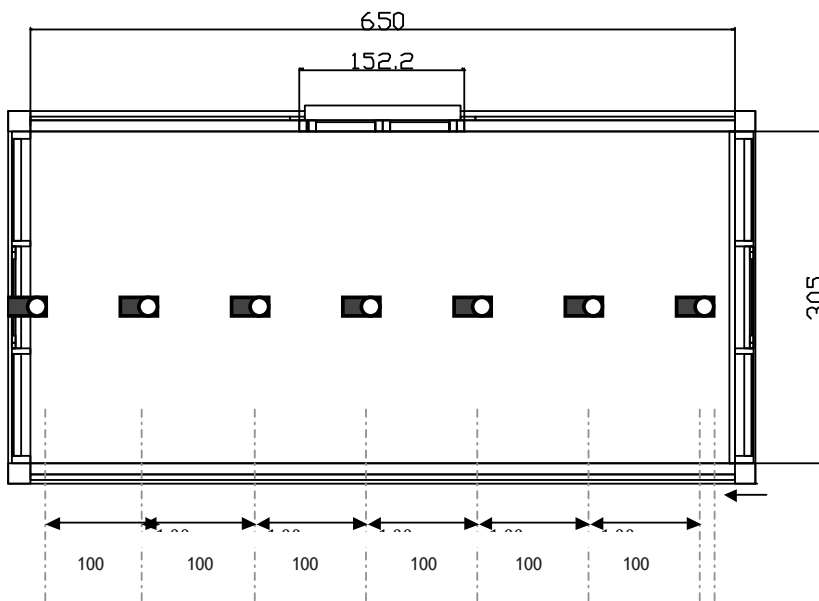


Fig. 3.36
Layout of the calibrated BEHA 96408 sensors monitoring indoor illuminance in the real building (unit: cm)

Interior surface luminance

The luminance property of the interior surfaces is commonly used to analyse indoor luminous quality. The technique habitually used for this purpose is to monitor a surface point after point with a luminance meter (Fig. 3.37).

Fig. 3.38 shows the different points measured using the luminance meter in the test module. The measurements were not made simultaneously but done rapidly, the values of the entire set of points being acquired in less than 5 minutes.



←
Fig. 3.37
A Minolta LS-110 luminance meter

↑ Fig. 3.38
Internal view of the real building presents the surface luminance measured points.

To overcome this luminance meter limitation and facilitate evaluation, a luminance mapper was set up using a High Dynamic Range (HDR) imaging technique. This technique allows a larger dynamic range of exposures than conventional imaging techniques. It also provides greater accuracy for light intensity levels found in real scenes ranging from direct sunlight to deepest shadow (Fig. 3.39).



Fig. 3.39
(upper) Digital images taken conventionally; (lower) High Dynamic Range images

A HDR calibrated camera, a Nikon Coolpix 5400 digital camera was used for that purpose (Fig. 3.40). It was placed on a tripod as close as possible to the luminance meter as shown in Fig. 3.41.

→



Fig. 3.40
Nikon Coolpix 5400 digital camera with its fisheye lens

The camera takes a sequence of multiple exposure images. The series of images was created manually by taking 8-10 digital photographs of differing f-stops, each of 2592 by 1944 pixels. The camera settings are shown in Table 3.8.

Each set of images, such as shown in Fig. 3.42, was merged using the Photosphere image builder program to create an HDR image. Photosphere is a digital image browsing and cataloguing tool. It supports many standard HDR image formats (Ward, 2001) as well as incorporating lens flare removal and ghost removal. Photosphere can also provide the luminance values at specific locations of the HDR image as shown in Fig. 3.43.

Feature	Setting
White balance	Daylight
Best Shot Selector (BSS)	Off
Image adjustment	Normal
Saturation control	Normal
Auto-bracketing	Off
Image size	2592 x 1944
Sensitivity	100 ISO
Image sharpening	Off
Lens (fish eye)	Fisheye
Lens (24 mm)	Off
Noise reduction	Off

Table 3.8
Digital camera parameters for the HDR images



←
Fig. 3.41
Digital camera and luminance meter placed in the real building

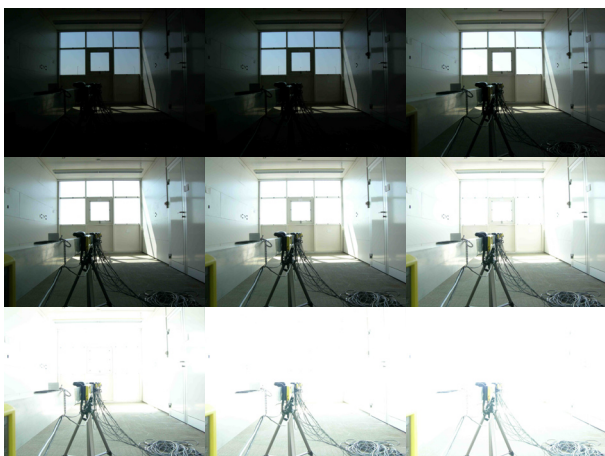


Fig. 3.42
A set of multiple exposure images that will be merged by software

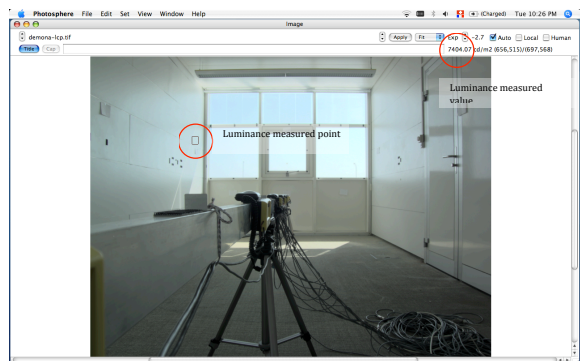


Fig. 3.43
Luminance mapping using Photosphere

Summary of test module's features (real building)

Type of building		single office room
Lighting requirement		300-1000 lux
Location		South car park
		EPFL
		Lausanne
		Switzerland
	Latitude	46.5° N
	Longitude	6.6° E
	Elevation	396 m
Climate	Average temperature (winter)	4° C
	Average temperature (summer)	22° C
	Annual average precipitation	1250 mm
	Annual average sunshine hours	1907 hours
Annual solar irradiation	Average global horizontal irradiation	1176 kWh/m ²
	Average diffuse horizontal irradiation	255 kWh/m ²
Annual daylight flux	Average global illuminance	14719 lux
	Average diffuse illuminance	9253 lux
Window orientation		South
Surroundings	Placement	Concrete platform
	North	Car parks
	East	Field
	South	Field
	West	Test module
Ground reflectance	Platform A	20.2 ± 2 %
	Platform B	12.4 ± 2 %
	Ground 1	10.2 ± 3 %
	Ground 2	12.8 ± 3 %
Geometry		
Interior dimensions	Width	6.50 ± 0.01 m
	Length	3.00 ± 0.01 m
	Height	2.50 ± 0.01 m
Window dimensions	Width	3.00 ± 0.01 m
	Height	1.65 ± 0.01 m
Interior details		
Materials	North wall	Canvas (white)
	East wall	Satin (white)
	South wall	Painted metal (white)
	West wall	Satin (white)
	Ceiling	Satin (white)
	Floor	Fitted carpet (grey-green)
	Window frame	Painted metal (white)
	Window glazing	Double glazing (6/12/6-mm)
Photometry		
Reflectance	North wall	82.6 ± 3 %
	East wall	81.5 ± 3 %
	South wall	72.1 ± 3 %
	West wall	82.3 ± 3 %
	Ceiling	79.9 ± 3 %
	Floor	16.1 ± 3 %
	Window frame	72.1 ± 3 %
Transmittance	Double glazing window	80.5 ± 3 %

58

Chrominance CIE chromatic coordinates (x,y,z)	North wall	(0.32, 0.34, 0.34)
	East wall	(0.31, 0.33, 0.36)
	South wall	(0.32, 0.34, 0.34)
	West wall	(0.31, 0.33, 0.36)
	Ceiling	(0.32, 0.34, 0.34)
	Floor	(0.34, 0.36, 0.30)
	Window frame	(0.32, 0.34, 0.34)
	Fenestration details	Glazing window
	Laser cut panel	6mm single acrylic w / 4mm parallel cuts
	Prismatic film	3M Brand optical lighting film (90° micro-prisms)
Measuring devices	Outdoor illuminance	1 horizontal LMT/BAP30FCT 4 vertical Hagner ELV 641
	Sky luminance distribution	1 digital sky scanner
	Indoor illuminance	7 BEHA 96408 sensors
	Interior surface luminance	Luminance meter Minolta LS-110 HDR imaging technique

Table 3.9
Test module attributes (real building)



Fig. 3.44
External view of the scale model

3.2 The physical model

Daylighting scale models are commonly used for assessing the daylighting performance of buildings. The model's daylight quality should resemble as closely as possible that of the real building. To ensure this accuracy the model should be scaled appropriately; a general recommendation is shown in Table 3.10 (Robbins, 1987) (Schilder, 1989).

Scale of physical model

In this study, a scale model was carefully constructed in order to simulate the daylighting quality and details of the real building. To reduce the bias due to an inadequate mock up of the real building, its physical parameters, comprising geometrical and photometric features, were accurately reproduced at a scale of 1:10 and improved by iterations. The scale model had to be portable in order to be tested under both real and artificial sky conditions.

The 1:10 scale model (Fig. 3.44) was constructed using synthetic foam sandwich cardboard of an appropriate mechanical resistance. The different model elements were fixed using screws and glue; to avoid parasitic light the joints were sealed with black tape.

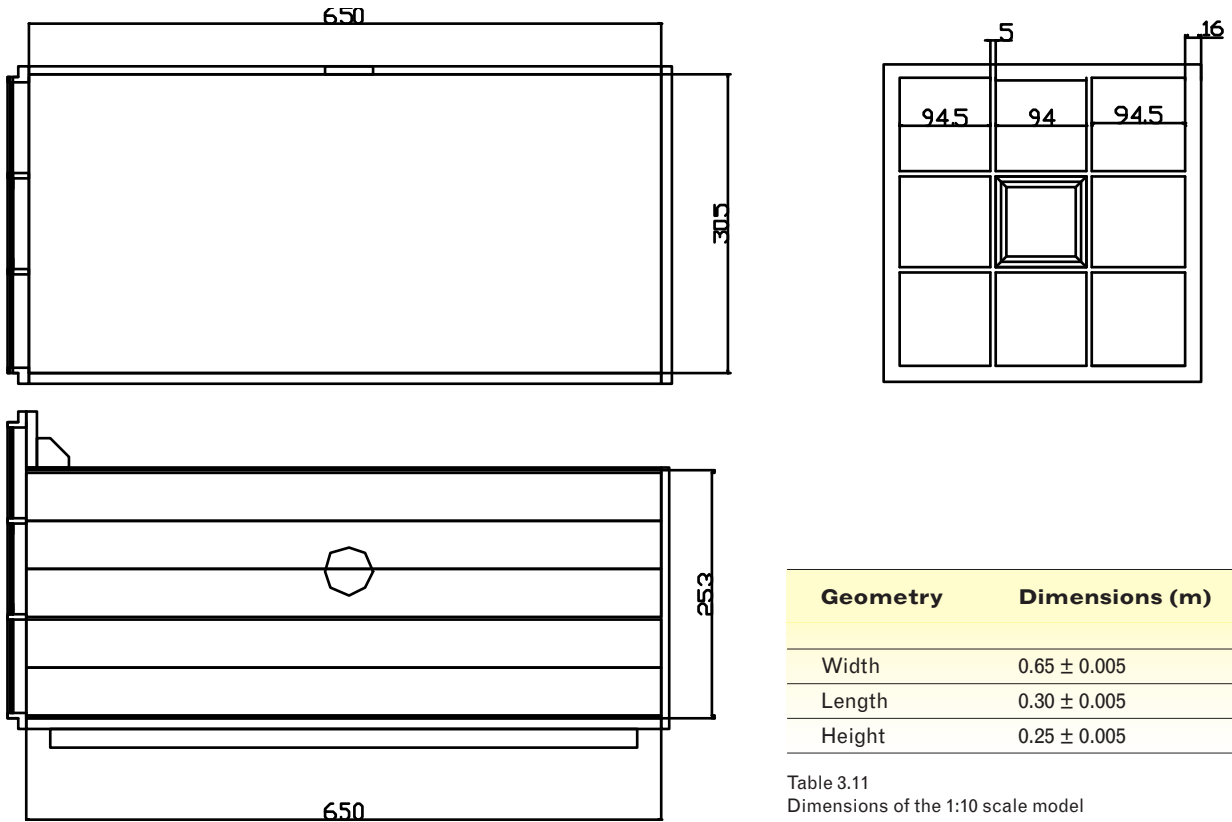
Table 3.10
Scale according to model type

Type	Purpose	Scale
Massing model	Shade and shadow analysis	1:400 - 1:50
Study model	Sun and sky light distribution (Observed from outside)	1:50 - 1:10
Detailed model	Sun and sky light distribution (Observed from inside)	1:10 - 1:1

Geometry and dimensions

60

To duplicate the real building the scale model has also a simple interior rectangular space as shown in the drawings of Fig. 3.45. The interior dimensions are shown in Table 3.11.



↑ Fig. 3.45
The scale model (unit: mm)

Geometry	Dimensions (m)
Width	0.65 ± 0.005
Length	0.30 ± 0.005
Height	0.25 ± 0.005

Table 3.11
Dimensions of the 1:10 scale model

The double glazing window of the real building was reproduced in the scale model using acrylic panels and filter films. The dimensions (interior) are shown in Table 3.12 .

Geometry	Dimensions (m)
Width	0.30 ± 0.005
Height	0.16± 0.005

Table 3.12
Dimensions of the window (scale model)

Interior features

Interior surface reflectances are very important for the daylight quality of buildings. It is important to reproduce the surface reflectance accurately in the scale model. An attempt to duplicate in the scale model the real building’s surface reflectance was done by comparing the interior surface reflectance (directional-hemispherical reflectance) which was carefully measured. However, the real materials could not be used in the model. The dissimilarity between the real materials and those of the scale model is responsible for significant errors in daylighting performance assessment.

Table 3.13 and Fig. 3.46 present the surface reflectance of the scale model compared with the real building reflectance. The internal scale model surfaces are made of matte white paper (walls and ceiling); the floor is covered with a grey-green paper; the furnishing materials used are shown in Table 3.14. Fig. 3.47 shows an indoor view of the room, with close-ups of the surfaces. The chromatic properties of the surfaces within the scale model monitored using the XYZ CIE Colour Space (i.e., (x,y,z) chromatic coordinates) are described in Table 3.15.

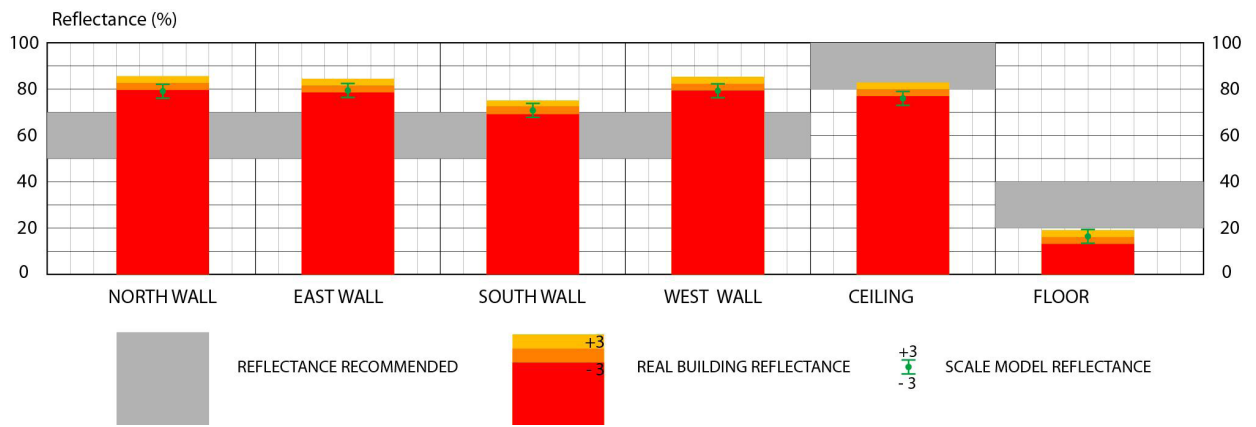


Fig. 3.46 Surface reflectance of the scale model compared with that of the real building

Surfaces	Reflectance of the real building (%)	Reflectance of the scale model (%)
North wall	82.6 ± 0.4	79.1 ± 0.1
East wall	81.5 ± 0.3	79.4 ± 0.1
South wall	72.1 ± 0.4	70.8 ± 0.1
West wall	82.3 ± 0.4	79.3 ± 0.1
Ceiling	79.9 ± 0.2	76.0 ± 0.1
Floor	16.1 ± 0.3	16.4 ± 0.1
Window frame	72.1 ± 0.4	70.8 ± 0.1

Table 3.13 Surface reflectance: real building and scale model

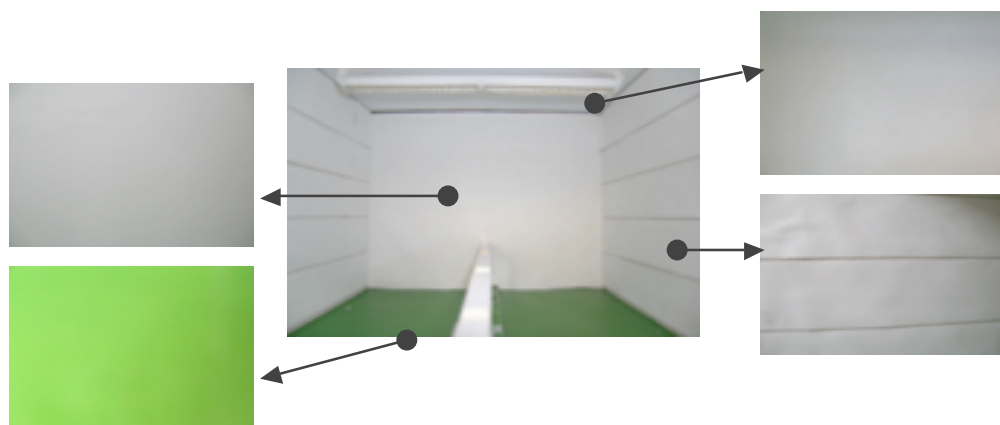


Fig. 3.47 Internal view of the scale model (walls, ceiling and floor)

Surfaces	Materials of the real building	Materials of the scale model
North wall	Canvas (white)	Paper (white)
East wall	Satin (white)	Paper (white)
South wall	Painted metal (white)	Paper (white)
West wall	Satin (white)	Paper (white)
Ceiling	Satin (white)	Paper (white)
Floor	Fitted carpet (grey-green)	Paper (grey-green)
Window frame	Painted metal (white)	Paper (white)

Table 3.14 Furnishing materials of the model's interior surface compared with those of the real building

Surfaces	CIE Chromatic coordinators
North wall	(0.32, 0.33, 0.35)
East wall	(0.31, 0.33, 0.36)
South wall	(0.31, 0.33, 0.36)
West wall	(0.31, 0.33, 0.36)
Ceiling	(0.31, 0.32, 0.37)
Floor	(0.32, 0.41, 0.27)
Window frame	(0.32, 0.33, 0.35)

Table 3.15 Chromatic properties of the surfaces monitored using the XYZ CIE Colour Space

62

Moreover, the specular properties of the paper and the real building's interior wall were also measured using a Minolta LS-110 luminance meter. A spotlight was shone at a 45 degree incident grazing angle to the normal onto the interior wall and onto paper in the same position (Fig. 3.48). The luminance was measured at 10 degree intervals between 0 and 90° to see the specular properties in each position. The specular properties of the paper and wall are comparable, as shown in Fig. 3.49.

The two rows of suspended luminaries (2 x 36W fluorescent, Zumtöbel Licht) were reproduced using a matte white paper, located respectively at 17 and 50 cm from the window façade (Fig. 3.50).

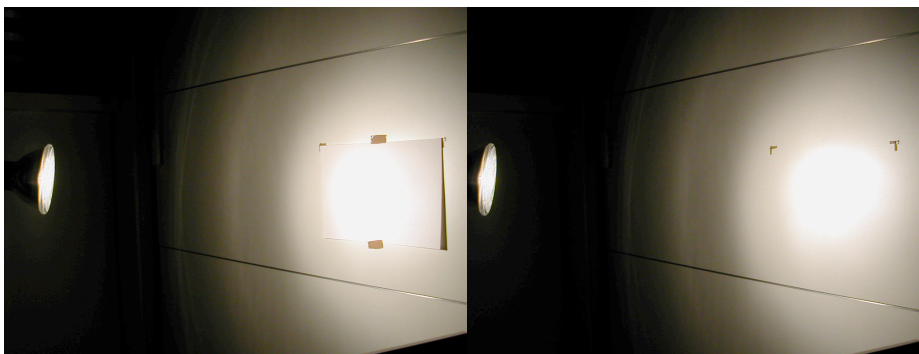


Fig. 3.48
Comparing the specular properties of wall and paper (photo)

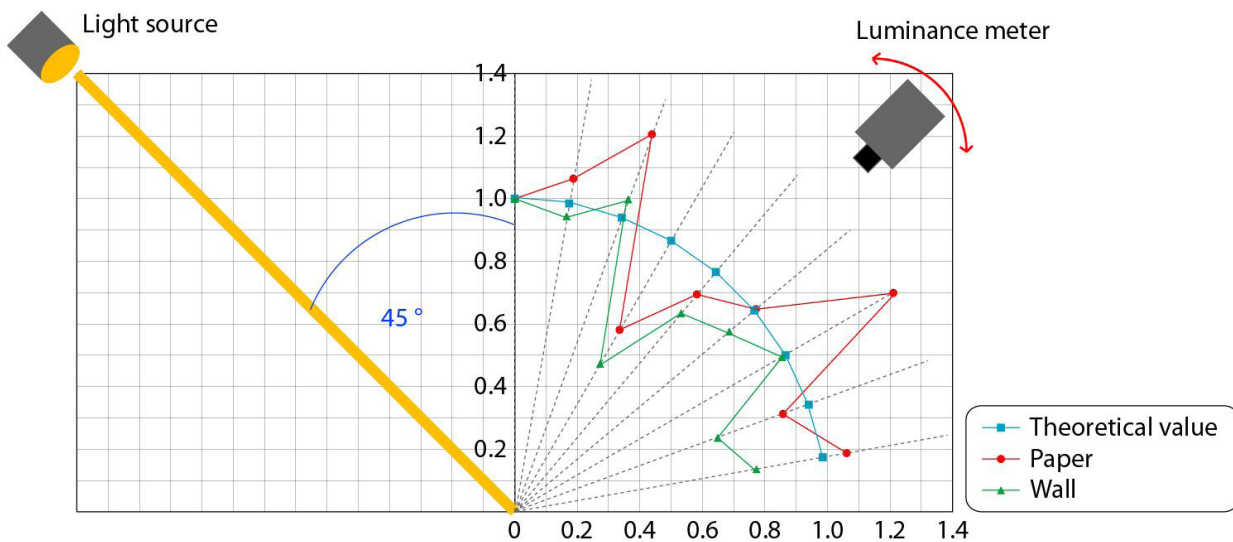


Fig. 3.49
Comparing the specular properties of wall and paper (graphically)

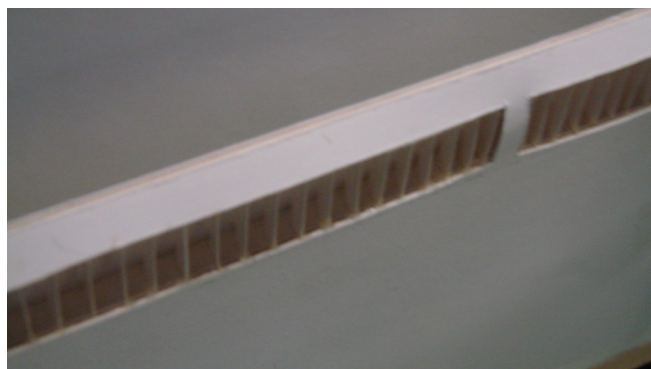


Fig. 3.50
Two rows of suspended luminaries were simulated using a matte white paper

Fenestration details

The double-glazed window was reproduced using a single 2mm-thick acrylic panel to which several sheets of neutral filter film were stuck. The transmittance property is shown in Table 3.16.

Table 3.16
Transmittance of the
model window's glazing
(acrylic panel combined
with filters)

Window	Transmittance (%)
Single 2 mm acrylic with neutral filter films	79.2 ± 3

Reproducing a CFS in a daylighting scale model is very difficult. The CFS used in this study - LCP and prismatic film - were not scaled down (details in Appendix B).

Fig. 3.51 shows the cross-section of the CFS attached to the window and Fig. 3.52 the scale model with the CFS attached. The CFS were attached on the outside of the window, not on the interior surface as in the test module. However, prior tests had shown no significant discrepancy was caused by this difference.

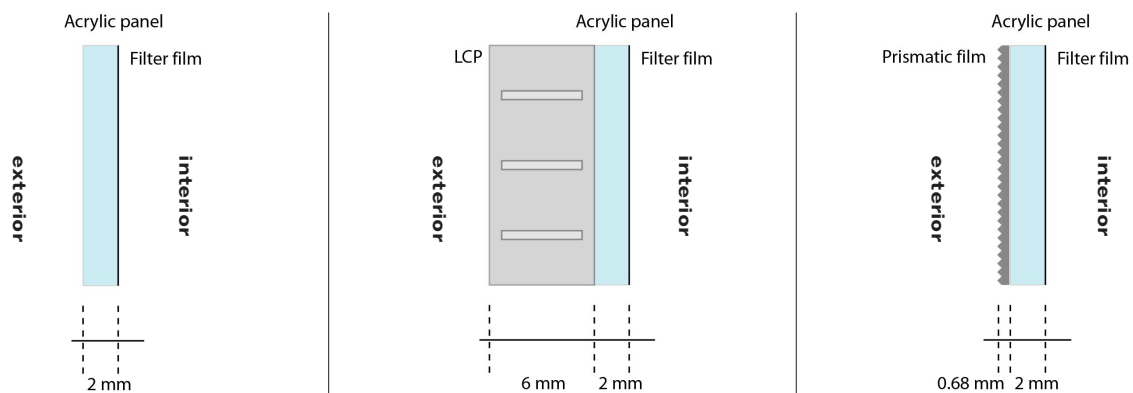


Fig. 3.51
Sections of the scale model's fenestration



Fig. 3.52
Double glazing, Laser-cut panel
and Prismatic film attached to the
scale model's window

The scale model under real sky conditions

64

Strictly identical positions of the scale model and the real building are impossible to achieve; this would mean placing the scale model in the test module and therefore affect the monitoring of the latter. So the scale model was placed in front of the adjacent module (Fig. 3.53), its open facade perfectly aligned with the facade of the real object. Shadowing effects of the blind fixtures were avoided by having the scale model jut out from the window at a distance of 10-20 centimetres. The ground reflectance of the scale model under real sky conditions is presented in Table 3.17 and Fig. 3.54.



Fig. 3.53
The scale model located in front of an adjacent test module

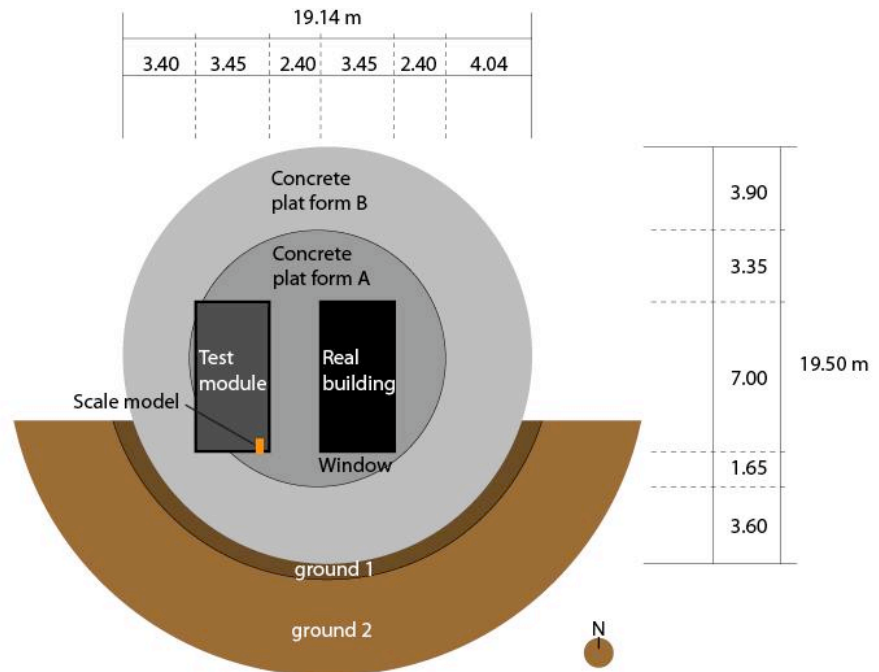


Fig. 3.54
Ground reflectance around scale model located in front of an adjacent test module

Ground surface	Ground reflectance (%)
Platform A (concrete)	20.2 ± 2
Platform B (concrete)	12.4 ± 2
Ground 1 (soil)	10.2 ± 3
Ground 2 (soil and grass)	12.8 ± 3

Table 3.17
Surface reflectance of platform around the scale model under real sky conditions

The scale model under simulated sky

The scale model was placed under a scanning sky simulator (Fig. 3.55) on a board coated with paper which corresponded to the real ground reflectance. The scanning sky simulator used in this study can produce both CIE standard skies and reproduce the real sky by the daylight coefficient method (Michel, 1995). The ground reflectances of the scale model under the scanning sky simulator are presented in Table 3.18 and Fig. 3.56.

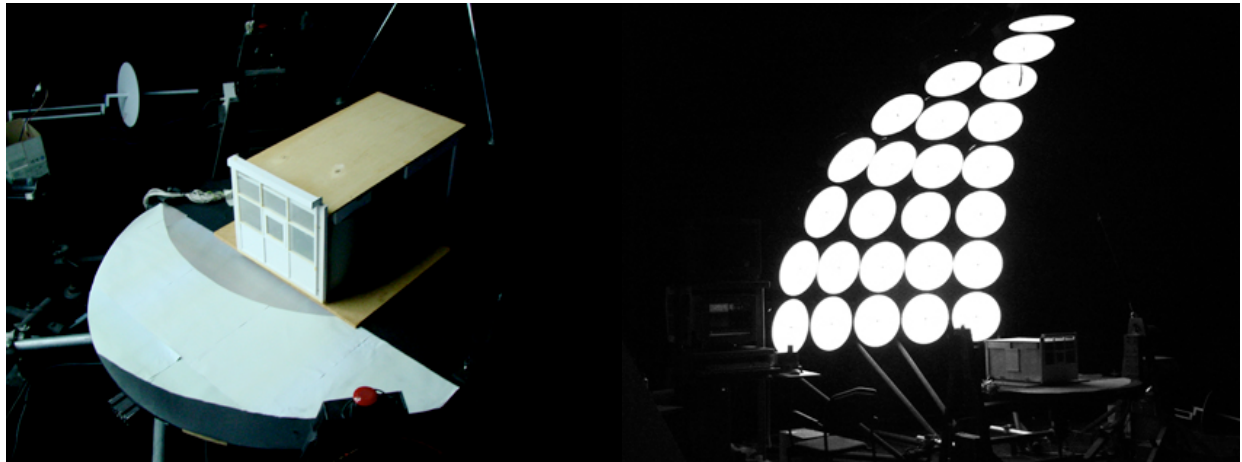
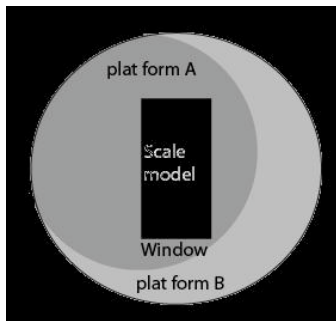


Fig. 3.55
The scale model under a sky simulator

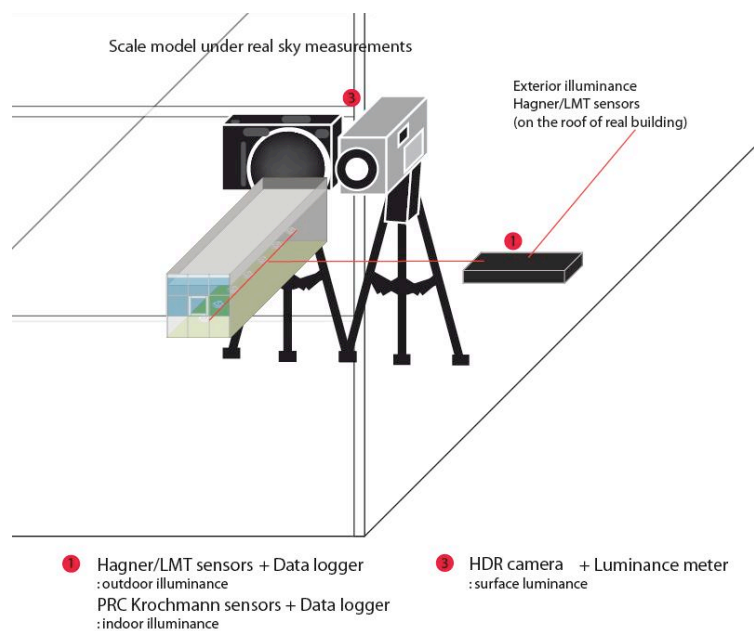


←
Fig. 3.56
Ground reflectance of the scale model under a sky simulator

Ground surface	Ground reflectance (%)
Platform A	20 ± 2
Platform B	12 ± 2

↑
Table 3.18
Surface reflectance of the model's platforms under the scanning sky simulator

→
Fig. 3.57
Experimental set-up used for the scale model's performance measured under real sky conditions



Equipment set-up

66

The scale model required several devices to provide both quantitative and qualitative data for daylighting evaluation. The equipment used in the scale model under real sky conditions is shown in the graphic in Fig. 3.57 and that under the scanning sky simulator is shown in Fig. 3.58.

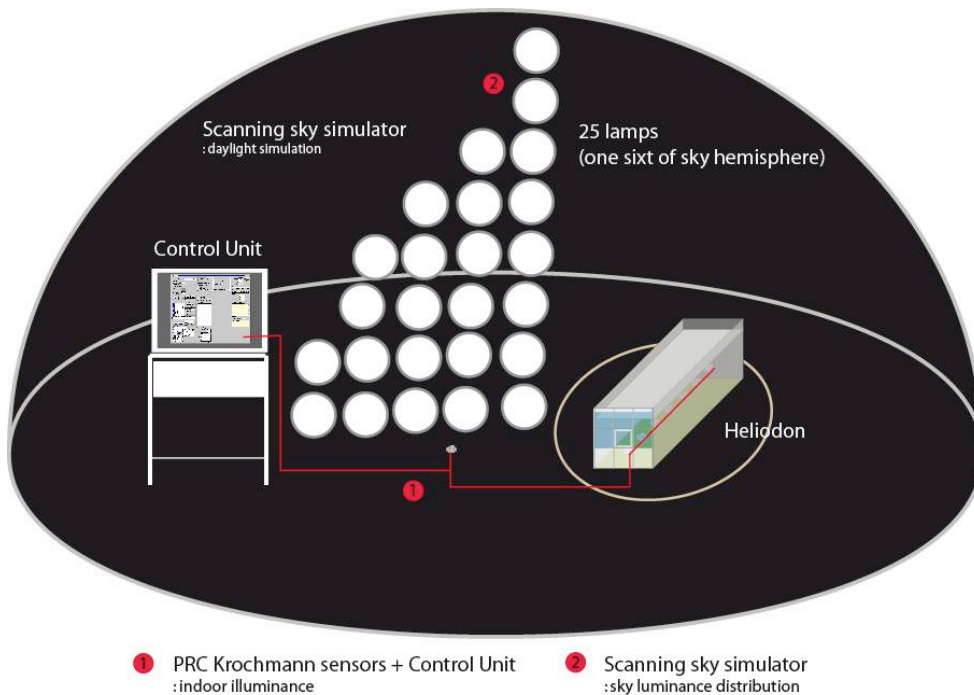


Fig. 3.58
Experimental set-up used for the scale model's performance measured under the scanning sky simulator

Illuminance meters

The scale model was equipped with 7 calibrated PRC Krochmann sensors (Fig. 3.59) for indoor illuminance monitoring under both real sky and simulated sky. One more PRC Krochmann sensor was used to measure the outdoor horizontal illuminance when the scale model was placed under the sky simulator (Fig. 3.60). To measure the scale model's outdoor illuminance monitoring under real sky conditions the same devices (1 horizontal LMT/BAP30FCT and 4 vertical Hagner ELV641 sensors) were used as for the real building.

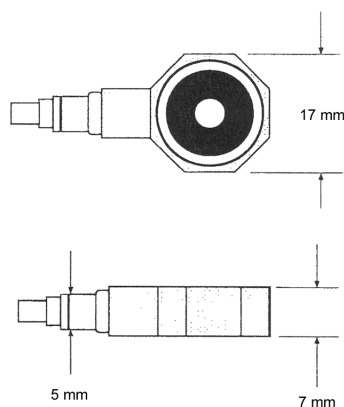


Fig. 3.59
Dimensions of the calibrated PRC Krochmann sensor used for indoor illuminance monitoring inside the scale model



Fig. 3.60
The calibrated PRC Krochmann sensor for exterior illuminance under the scanning sky simulator

The sensors were placed on a stable base laid along the middle of the model at 10 cm intervals which corresponds to the real building's layout (Fig. 3.61 and 3.62). The sensors were connected to a data logger, which also collected the illuminance value at one minute intervals. The indoor illuminance was used for daylight factor and illuminance ratio for comparison to the real building's values.

67

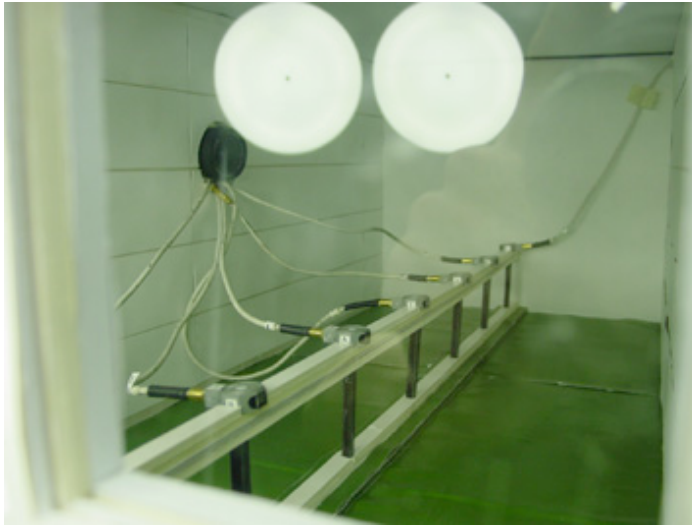


Figure 3.61
The calibrated PRC
Krochmann sensors used
for indoor illuminance
monitoring in place in the
scale model

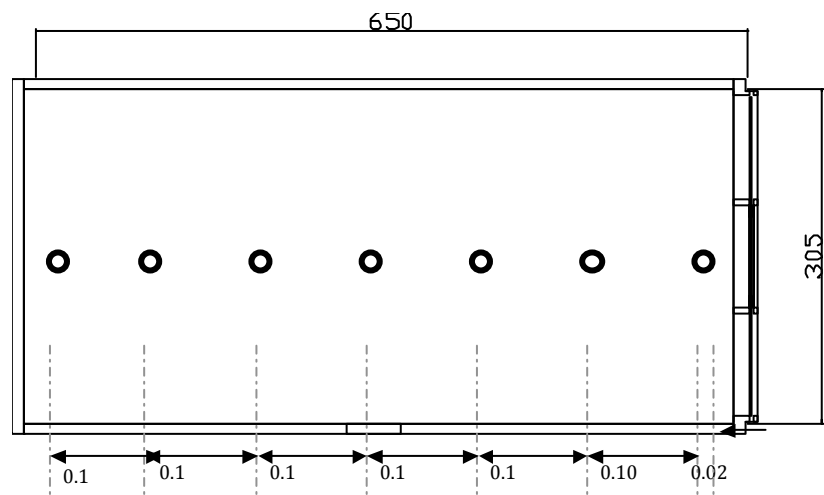


Figure 3.62
Layout of the calibrated
PRC Krochmann sensors
monitoring indoor
illuminance in the scale
model (unit: mm)

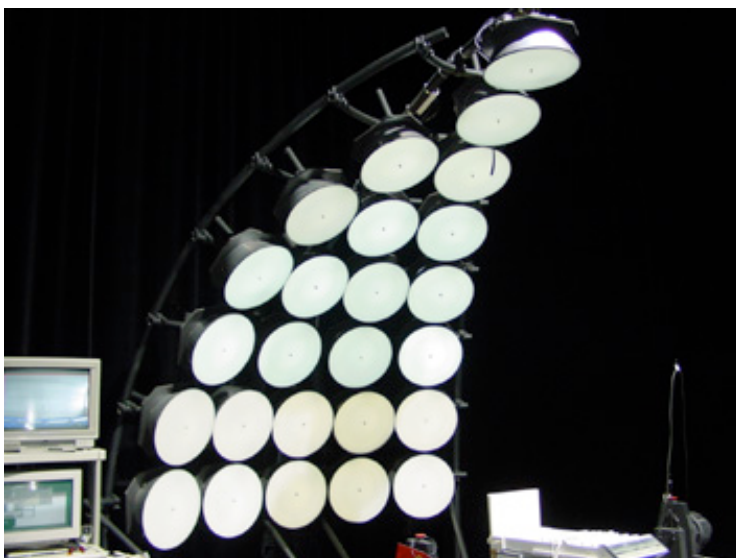


Figure 3.63
The scanning sky
simulator developed
at EPFL (Lausanne,
Switzerland)

68

Daylight simulation

Fig. 3.63 illustrates the scanning sky simulator which was developed at EPFL (Michel, 1995). It allows accurate reproduction of the luminance distributions of every type of sky (Fig. 3.64) with low construction, operating and maintenance costs. It can be used for diffuse daylight simulation within building scale models for any time of year and any location - a precious tool for testing innovative architectural solutions and daylighting systems.

The scanning sky simulator uses a specific computer process to rebuild the overall sky hemisphere by starting with a sixth of the sky vault constructed with 25 light sources. The whole hemisphere, based on Tregenza's model of 145 sky sectors (Fig. 3.65), is rebuilt in consequence. Quantitative (illuminance) and qualitative data (video digitised image) are added at the end of the process.

The scanning sky simulator has three main components:

- a) 25 light sources making up a sixth of the sky hemisphere (Fig. 3.63).
- b) An automated platform which rotates the scale model through a complete sky hemisphere (Fig. 3.66).
- c) A control unit incorporating a user-friendly interface (Fig. 3.67).

In this study, two sky simulation methods were used in order to analyse the causes of error in daylight simulation.

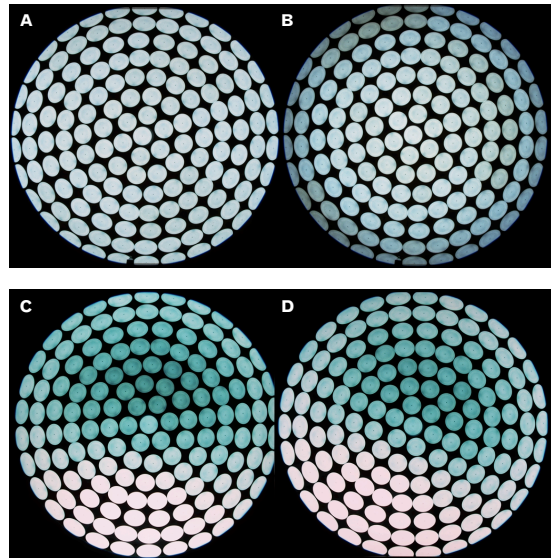


Figure 3.64 Sky luminance distribution simulated by the way of the EPFL scanning sky simulator: a) uniform sky, b) CIE overcast sky, c) CIE clear sky, d) CIE intermediate sky

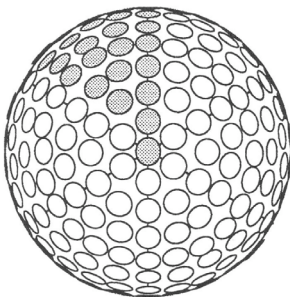


Figure 3.65 The 145 sky sectors of the scanning sky simulator defined according to Tregenza model

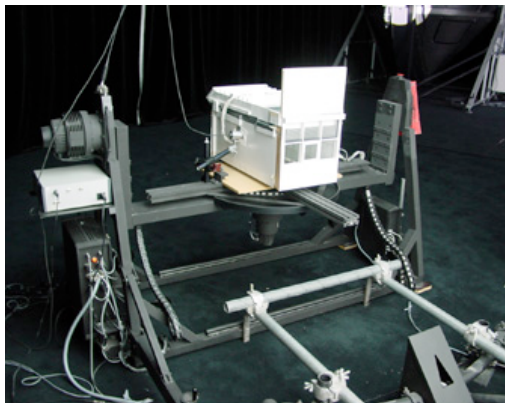


Figure 3.66 Automated movable platform (PC driven) used to rotate the scale model



Figure 3.67 PC control unit with interface

Standard sky models

Standard sky models (details in Appendix A) can easily be produced by the way of the scanning sky simulator. They can be selected using the computer interface, their luminance distribution being precisely reproduced by the 25 different light sources. Using six consecutive 60 ° angle rotations of the platform, the overall sky hemisphere luminance distribution is simulated around the scale model.

Partial daylight factor method

The partial daylight factor method was suggested by Michel (Michel, 2002), as an alternative method to reproduce real sky luminance distributions. For this the scale model is once again placed on the automatic platform which is rotated to achieve the measurement of partial daylight factors, each one being linked to a given light source of the sky dome. Fig. 3.68 illustrates the principal of the method.

A part of the illuminance (E_{ij}) being measured at a considered point on a given surface comes from the particular luminous zone j . When E_{ij} is the indoor partial illuminance at the point and E_{ej} is the partial illuminance measured at the exterior horizontal plane, the partial daylight factor (D_{ij}) is determined according to the following equation:

$$\text{Partial daylight factor } (D_{ij}) = E_{ij}/E_{ej} \quad (3.1)$$

The sky luminance distribution of a real sky (measured by the sky scanner) is introduced in the calculation in order to determine daylight factor and indoor illuminances.

Interior surface luminances

As with the real building, the interior surface luminances of the scale model were measured using a luminance meter and a HDR camera.

However, this measurement with the scale model was done only under real sky conditions due to the complexity of monitoring the scale model under the scanning sky simulator.

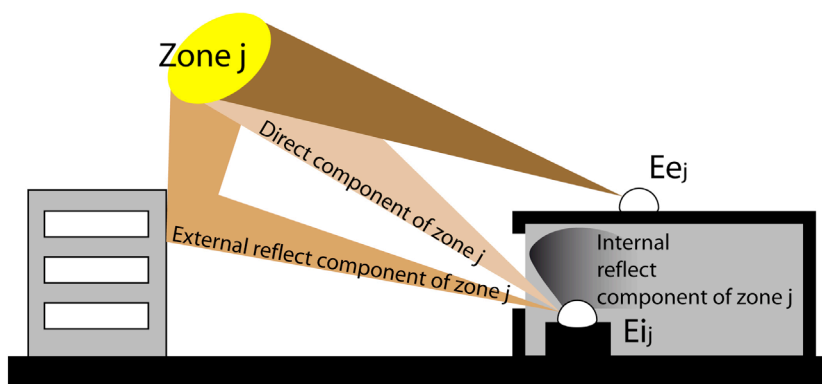


Figure 3.68
Illustrating the principles of the partial daylight factor method

Tables summarising the scale model's features**Scale model under real sky condition**

70

Placement	In front of the adjacent test module		
Sky type	Real sky		
Type of model	Detailed quality study		
Scale	1:10		
Location	Address	South car park EPFL Lausanne Switzerland	
	Latitude	46.5° N	
	Longitude	6.6 °E	
	Elevation	396 m	
Climate	Average temperature (winter)	3° C	
	Average temperature (summer)	22° C	
	Annual average precipitation	1250 mm	
	Annual average sunshine hours	1907 hours	
Annual solar irradiation	Average global horizontal irradiation	1176 kWh/m ²	
	Average diffuse horizontal irradiation	255 kWh/m ²	
Annual daylight flux	Average global illuminance	14719 lux	
	Average diffuse illuminance	9253 lux	
Window orientation	South		
Ground reflectance	Platform A	20.2 ± 2 %	
	Platform B	12.4 ± 2 %	
	Ground A	10.2 ± 3 %	
	Ground B	12.8 ± 3 %	
Geometry	Interior dimensions	Width	0.65 ± 0.005 m
		Length	0.30 ± 0.005 m
		Height	0.25 ± 0.005 m
	Window dimensions	Width	0.30 ± 0.005 m
		Height	0.16 ± 0.005 m
	Interior details	Materials	North wall
East wall			Paper (white)
South wall			Paper (white)
West wall			Paper (white)
Ceiling			Paper (white)
Floor			Paper (textured grey-green)
Window frame			Painted metal (white)
Glazing window			Single 2 mm acrylic with neutral filter films
Photometry	Reflectance	North wall	79.1 ± 3 %
		East wall	79.4 ± 3 %
		South wall	70.8 ± 3 %
		West wall	79.3 ± 3 %
		Ceiling	76.0 ± 3 %
		Floor	16.4 ± 3 %
		Window frame	70.8 ± 3 %
	Transmittance	Window glazing	79.2 ± 3 %

→

Chrominance		
Chromatic coordinates (x,y,z)	North wall	(0.32, 0.33, 0.35)
	East wall	(0.31, 0.33, 0.36)
	South wall	(0.31, 0.33, 0.36)
	West wall	(0.31, 0.33, 0.36)
	Ceiling	(0.31, 0.32, 0.37)
	Floor	(0.32, 0.41, 0.27)
	Window frame	(0.32, 0.33, 0.35)
Fenestration details		
	Glazing	Single 2 mm acrylic with neutral filter films
	Laser-cut panel	6mm single acrylic with 4mm parallel cuts
	Prismatic film	3M Brand optical lighting film (90° micro-prisms)
Measuring devices		
	Outdoor illuminance	1 horizontal LMT/BAP30FCT
	Indoor illuminance	4 vertical Hagner ELV 641
	Interior surface luminance	7 sensors PRC Krochmann Luminance meter HDR imaging technique

Table 3.19
Scale model attributes when under real sky
conditions

Scale model under scanning sky simulator

Placement	On an automated movable platform		
Sky type	Sky simulator		
Type of model	Detailed quality study		
Scale	1:10		
Window orientation	South		
Surroundings	Placement	Paper board	
	North	Dark room	
	East	Dark room	
	South	Dark room	
	West	Dark room	
Ground reflectance	Platform A	20 ± 3 %	
	Platform B	12 ± 3 %	
Geometry	Interior dimensions	Width	0.65 ± 0.005 m
		Length	0.30 ± 0.005 m
		Height	0.25 ± 0.005 m
	Window dimensions	Width	0.30 ± 0.005 m
		Height	0.16 ± 0.005 m
Interior details			
Materials	North wall	Paper (white)	
	East wall	Paper (white)	
	South wall	Paper (white)	
	West wall	Paper (white)	
	Ceiling	Paper (white)	
	Floor	Paper (textured grey-green)	
	Window frame	Painted metal (white)	
Window glazing	Single 2 mm acrylic with neutral filter films		

→

72

Photometry		
Reflectance	North wall	79.1 ± 3 %
	East wall	79.4 ± 3 %
	South wall	70.8 ± 3 %
	West wall	79.3 ± 3 %
	Ceiling	76.0 ± 3 %
	Floor	16.4 ± 3 %
	Window frame	70.8 ± 3 %
Transmittance	Glazing window	79.2 ± 3 %
Chrominance		
Chromatic coordinates (x,y,z)	North wall	(0.32, 0.33, 0.35)
	East wall	(0.31, 0.33, 0.36)
	South wall	(0.31, 0.33, 0.36)
	West wall	(0.31, 0.33, 0.36)
	Ceiling	(0.31, 0.32, 0.37)
	Floor	(0.32, 0.41, 0.27)
	Window frame	(0.32, 0.33, 0.35)
Fenestration details		
	Glazing	Single 2 mm acrylic with neutral filter films
	Laser-cut panel	6mm single acrylic with 4mm parallel cuts
	Prismatic film	3M Brand optical lighting film (90° micro-prisms)
Measuring devices		
	Illuminance	7 PRC Krochmann sensors

Table 3.20
Scale model attributes when under real sky
conditions

Comparison of geometry and photometry features between the real building (test module) and its scale model

73

Geometrical features	Scale model	Real building	Photometrical features	Scale model	Real building
Window Frame	✓	✓	Surface reflectances	✓	✓
Depth	✓	✓	Window frames	✓	✓
Slope	✓	✓	Door	✓	✓
Handle	N/A	✓	Wall	✓	✓
Dimension	✓	✓	Floor	✓	✓
Material	✓	✓	Ceiling	✓	✓
Hinges	N/A	✓	Furniture	✓	✓
Door	N/A	✓	Window transmittance	✓	✓
Doorknob	N/A	✓	Grazing incident angles	✓	✓
Frame (material and dimension)	N/A	✓	Dust and dirt	N/A	N/A
Door-panel	N/A	✓			
Hinges	N/A	✓	Photometric sensors	✓	✓
Wall	✓	✓	Calibration	✓	✓
Dimension	✓	✓	Cosine response	✓	✓
Material	✓	✓	Placement and levelling	✓	✓
Texture	✓	✓	Sensing aperture and shape	✓	✓
Floor	✓	✓			
Texture	✓	✓	Maintenance	✓	✓
Small pieces of scientific equipment	N/A	✓	Dirt on surfaces and windows	✓	✓
Moving track for lux-meter	✓	N/A	Dust in the air	N/A	✓
Ceiling	✓	✓			
Dimension	✓	✓			
Materials	✓	✓			
Texture (furrow)	N/A	✓			
Furniture	N/A	✓			
Cupboard and computer	N/A	✓			
Tripod and mount	N/A	✓			

✓ → Available

N/A → Not available

Table 3.21
List of potential sources of error caused by the scale model related to physical details



Fig. 3.69
External view of the virtual
model of the test module
(Radiance program)

3.3 The virtual model

Computer simulation program

This study employed the Radiance suite of programs for daylighting simulation of the real building (Fig. 3.69). The photometry and geometry of the test module were carefully reproduced. The surroundings and daylighting environment of the real building were also simulated. The digital sky scanner and bi-directional gonio-photometer were used to facilitate the acquisition of the sky luminance and the Bi-directional Transmission Distribution Function data (BTDF).

Surroundings

Not only the real building itself was reproduced in the virtual model, as shown in Table 3.22, but also the ground reflectance of the real building's surroundings was simulated. Fig. 3.70 shows the ground as simulated in the virtual model. The building's obstructions were not taken into account as they were lower than 10 degrees over the horizon.

Ground surface	Ground reflectance (%)
Platform A	20.19
Platform B	12.35
Ground 1	10.23
Ground 2	12.84

Table 3.22
Surface reflectance, used in the virtual model,
of the platform and ground of the real building

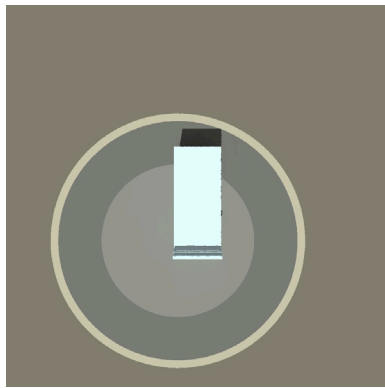


Fig. 3.70
Virtual model surroundings

Geometry and dimensions

The real building has a simple interior rectangular space as shown in the renderings of Fig. 3.71. The interior dimensions are shown in Tables 3.23 and 3.24.

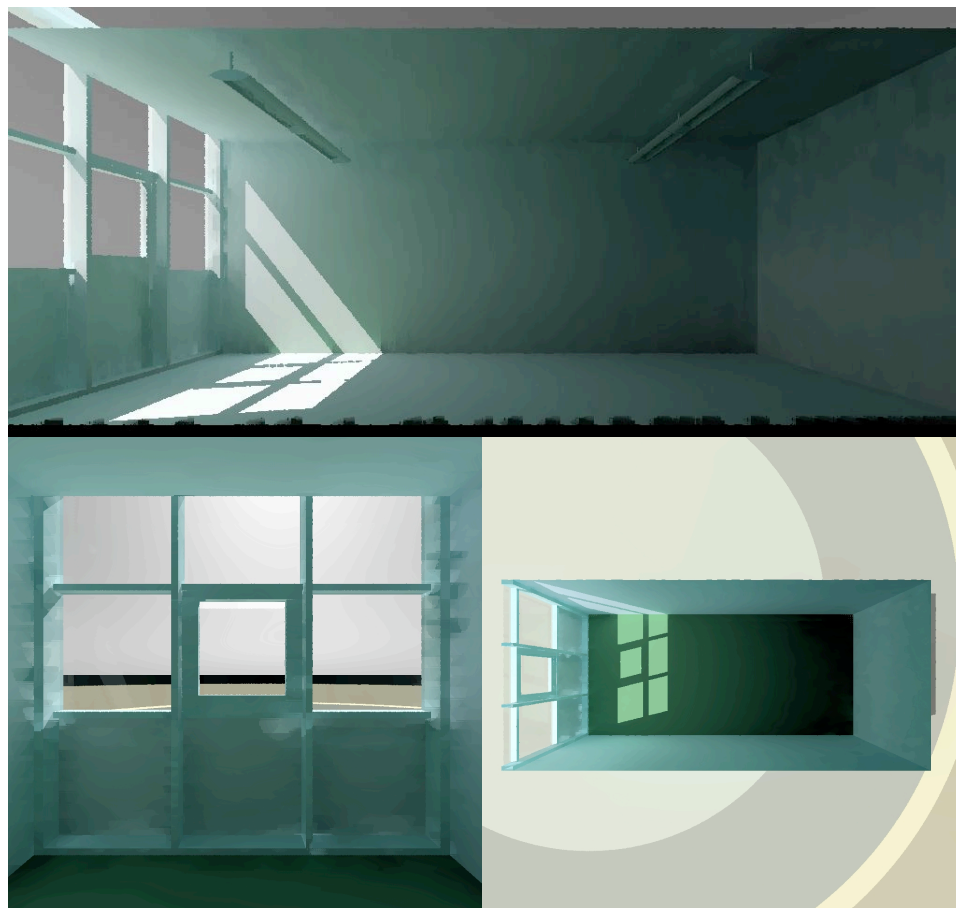


Fig. 3.71
Virtual model renderings

Geometry	Dimensions (m)
Width	6.5
Length	3.0
Height	2.5

Table 3.23
Dimensions of the virtual model

Geometry	Dimensions (m)
Width	3.0
Height	1.6

Table 3.24
Dimensions of the virtual model's window

Interior details

76

The interior surface reflectances of the real building were employed in the virtual model as presented in Table 3.25. Two rows of suspended luminaires (2 x 36W fluorescent, Zumtobel Licht) were also reproduced. However, the sensors and computer unit were not modelled in the virtual model; the virtual model's interior was empty (Fig. 3.71).

The chromatic properties of the surfaces monitored using the XYZ CIE Colour Space (i.e., (x,y,z) chromatic coordinates) (CIE, 1986), are described in Table 3.26.

Surfaces	Reflectance of the real building (%)	Reflectance of the virtual model (%)
North wall	82.6 ± 3	82.6
East wall	81.5 ± 3	81.5
South wall	72.1 ± 3	72.1
West wall	82.3 ± 3	82.3
Ceiling	79.9 ± 3	79.9
Floor	16.1 ± 3	16.1
Window frame	72.1 ± 3	72.1

Table 3.25
Surface reflectance of the virtual model compared to that of the real building

Surfaces	CIE Chromatic coordinates
North wall	(0.32, 0.34, 0.34)
East wall	(0.31, 0.33, 0.36)
South wall	(0.32, 0.34, 0.34)
West wall	(0.31, 0.33, 0.36)
Ceiling	(0.32, 0.34, 0.34)
Floor	(0.34, 0.36, 0.30)
Window frame	(0.32, 0.34, 0.34)

Table 3.26
Chromatic properties of the surfaces using the XYZ CIE Colour Space

Fenestration details

The double-glazed window of the virtual model was simulated by the window function of the Radiance program (Ward, 1998). The window transmittance of the real building was also employed in the virtual model as presented in Table 3.27. For the CFS properties, they were reproduced by the BTDF integration method (Kaempf, 2003). As presented in Fig. 3.72 and Table 3.28, BTDF data of the laser cut panel and prismatic film were acquired by the way of a bi-directional gonio-photometer.

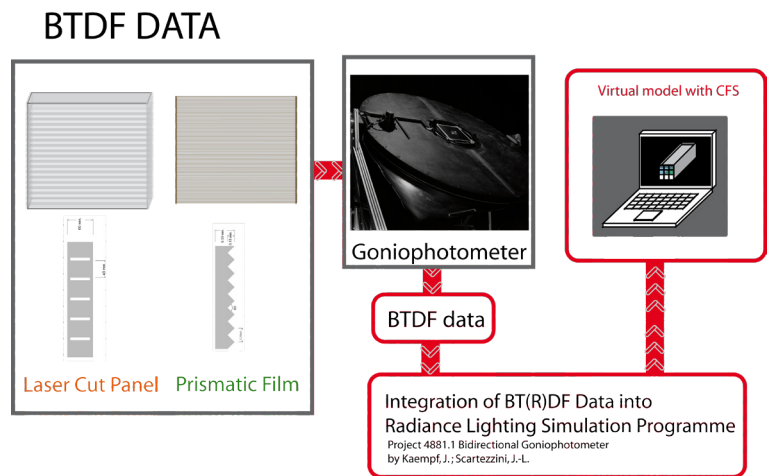
Table 3.27
Transmittance of the double glazing window

Window	Transmittance (%)
Double glazing	80.5

Fenestration materials	Real building	Scale model	Virtual model
Side Window	Double glazing	Single 2 mm acrylic with neutral filter films	Window function
Laser-cut Panel	6mm single acrylic with 4mm parallel cuts	6mm single acrylic with 4mm parallel cuts	BTDF Data
Prismatic film	3M Brand optical lighting film (90° micro-prisms)	3M Brand optical lighting film (90° micro-prisms)	BTDF Data

Table 3.28
Comparison of the fenestration details of the real building with its physical and virtual models

Fig. 3.72
Radiance simulation
technique for CFS using
BTDF data



77

Experimental set-up

Bi-directional Transmission Distribution Function (BTDF)

The novel BT(R)DF Goniophotometer (Fig. 3.73), developed at EPFL (Andersen, 2001), allows accurate measurements of directional light transmission (reflection) properties of Complex Fenestration Systems (CFS). The apparatus uses a video image capture device (CCD digital camera) and a powerful image analysis program to considerably reduce, in comparison to other existing devices, the scanning time of BT(R)DF data.

The device has three major components:

- a. a calibrated light source that provides a collimated and spectrally optimal light beam (close to sunlight),
- b. a movable mechanical support that allows one to modify the incident light beam on the fenestration sample in a continuous way for transmission measurements (BTDF assessment) and in a fixed way for reflection measurements (BRDF assessment),
- c. a computer-controlled device, linked to a CCD video camera, to detect transmitted (or reflected) light.

The Bidirectional Transmission (Reflection) Goniophotometer is a user-friendly device which facilitates data acquisition and treatment and offers diverse possibilities of BT(R)DF data visualisation (hemispherical representation, axonometric views of photometric solids, etc.). Reference (Andersen, 2001) gives a details description of this device.

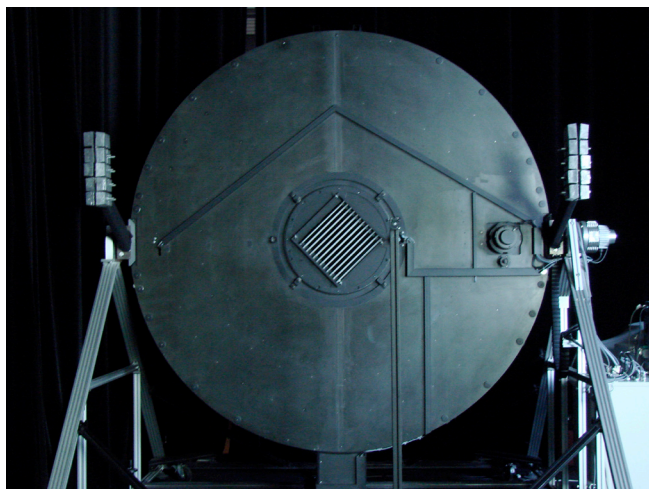


Fig. 3.73
Bi-directional goniophotometer based on
CCD imaging techniques for assessment of
BT(R)DF data

78

Daylight simulation

The daylight simulation of the virtual model was achieved using the Radiance program. Radiance is a suite of programs for lighting performance analysis and visualization developed at Lawrence Berkeley National Laboratory (LBNL) in California (Ward and Shakespeare, 1998). It is a powerful ray-tracing program used by the international lighting research community, capable of handling all geometries and materials. The parameters of the scene's geometry and sky conditions must be entered. The evaluations are reported by calculations of radiance, irradiance and glare indices, as well as being displayed in renderings and false colour images.

Two of the virtual model's sky simulation methods were used to analyse the causes of error of daylight simulation. However, the same important parameters of the Radiance program (shown in Table 3.29) were used for every computer simulation done in this study.

These parameters drive the following computer program features:

ab: ambient bounces – the maximum number of diffuse bounces computed by the indirect calculation.

aa: ambient accuracy – a value approximately equal to the error for indirect illuminance interpolation.

ad: ambient divisions - error in the Monte Carlo calculation of indirect illuminance.

ar: ambient resolution – a number determining the maximum density of ambient values used for the interpolation.

Radiance simulation parameters	
ab	9
aa	0.1
ad	26315
ar	128

Table 3.29
Radiance simulation parameters used throughout this thesis

Standard sky models

To reproduce the CIE standard skies (see appendix A) simulation, the virtual model used the Gensky function. The values of the sky and sun geometry were accurately entered into the program.

Partial daylight factor method

The partial daylight factor method was suggested by Michel (Michel, 1995), as an alternative method to reproduce real sky luminance distributions.

The sky luminance distribution of a real sky (measured by the sky scanner) is introduced in the calculation in order to determine daylight factor and indoor illuminances.

The contribution of each of Tregenza's sky model elements was computed for each measured point in the virtual model. Afterwards it computed the daylight factor or illuminance value using this fraction and the luminance distribution. This method is convenient and rapidly calculated.

Interior surface luminance

Interior surface luminance of the virtual model was simply assessed using the Photosphere program. Rendering of the virtual model created with Radiance was used as input for Photosphere and converted into luminance distribution.

Interior surface luminance values, measured by the Photosphere program, were input to Radiance and, converted to luminance distribution, rendered in the virtual model.

Tables summarising the virtual model's features

Virtual model under real sky condition

79

Computer simulation program			Radiance
Window orientation			South
Ground reflectance	Platform A		20.2 %
	Platform B		12.4 %
	Ground 1		10.2 %
	Ground 2		12.8 %
Geometry			
Interior dimensions	Width		6.5 m
	Length		3.0 m
	Height		2.5 m
Window dimensions	Width		3.0 m
	Height		1.6 m
Photometry			
Reflectance	North wall		82.6 %
	East wall		81.5 %
	South wall		72.1 %
	West wall		82.3 %
	Ceiling		79.9 %
	Floor		16.1 %
	Window frame		72.1 %
Transmittance	Window glazing		76.2 %
Chromatic properties (x,y,z)	North wall		(0.32, 0.34, 0.34)
	East wall		(0.31, 0.33, 0.36)
	South wall		(0.32, 0.34, 0.34)
	West wall		(0.31, 0.33, 0.36)
	Ceiling		(0.32, 0.34, 0.34)
	Floor		(0.34, 0.36, 0.30)
	Window frame		(0.32, 0.34, 0.34)
Fenestration details	Double glazing		"Window" function
	Laser-cut panel		BTDF data
	Prismatic film		BTDF data
Radiance simulation parameters			
	ab		9
	aa		0.1
	ad		26315
	ar		128

Table 3.30
Virtual model attributes for Radiance program

Comparison of geometry and photometry features between the real building (test module) and its virtual model

Geometrical features	Virtual model	Real building	Photometrical features	Virtual model	Real building
Window Frame	√	√	Surface reflectances	√	√
Depth	√	√	Window frames	√	√
Slope	√	√	Door	√	√
Handle	N/A	√	Wall	√	√
Dimension	√	√	Floor	√	√
Material	√	√	Ceiling	√	√
Hinges	N/A	√	Furniture	√	√
Door	N/A	√	Window transmittance	√	√
Doorknob	N/A	√	Grazing incident angles	√	√
Frame (material and dimension)	N/A	√	Dust and dirt	N/A	N/A
Door-panel	N/A	√			
Hinges	N/A	√	Photometric sensors	N/A	√
Wall	√	√	Calibration	N/A	√
Dimension	√	√	Cosine response	N/A	√
Material	√	√	Placement and levelling	N/A	√
Texture	N/A	√	Sensing aperture and shape	N/A	√
Floor	√	√			
Texture	N/A	√	Maintenance	N/A	√
Small pieces of scientific equipment	N/A	√	Dirt on surfaces and windows	N/A	√
Moving track for lux-meter	√	N/A	Dust in the air	N/A	√
Ceiling	√	√			
Dimension	√	√			
Materials	√	√			
Texture (furrow)	N/A	√			
Furniture	N/A	√			
Cupboard and computer	N/A	√			
Tripod and mount	N/A	√			

√ → Available

N/A → Not available

Table 3.31
List of potential sources of error caused by the virtual model related to physical details

3.4 Photometric variables

Lighting units

Light is a form of energy and can normally be quantified in units of power. However, to enumerate it in terms of visual sensibility (or how we see light), there are four important variables which can quantify the visual perception.

Luminous flux (lumen)

The luminous flux is the flow of light emitted from its source in all directions as shown in Fig. 3.74. Luminous flux has the lumen as its unit; for instance, a 100W incandescent lamp emits 1360 lumens.

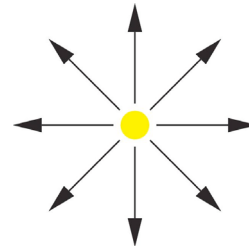


Fig. 3.74
Luminous flux of a point source: the light flowing directly from the source

Intensity (candela)

The intensity of light is the luminous flux (power emitted) in a particular cone-shaped direction, as shown in Fig. 3.75. The solid angle is normally measured in steradians.

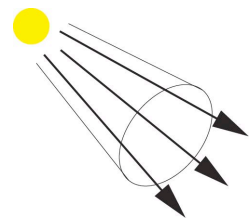


Fig. 3.75
Light intensity: the light flowing in a given direction

Illuminance (lux)

Illuminance is the density of the luminous flux incident on a surface as shown in Fig. 3.76.

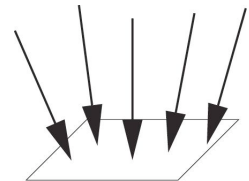


Fig. 3.76
Illuminance on a given surface (Average value): the density of the incident luminous flux

For instance, a winter overcast sky provides around 10000 lux to the ground. Illuminance is commonly used for evaluating a room's horizontal workplane lighting design properties; for example, in a common office the recommended illuminance for a workplane is about 500 lux.

Illuminance can also be described as lumens per square metre by the mathematical calculation shown below:

$$E = d\Phi / dA \text{ (lux)} \quad (3.2)$$

E = illuminance (lux)
 $d\Phi$ = luminous flux (lumen)
 dA = area (square metre)

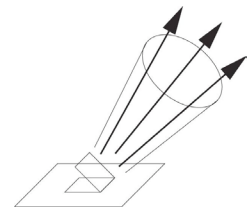


Fig. 3.77
Luminance of a given surface : the objective brightness of the surface

Luminance (candela / square meter)

Luminance is the physical property which describes the objective brightness of the surface; the light passing through or emitted from an area falling in a given solid angle. It depends on the intensity of light impinging the surface and the reflectance of the surface which reflects the light as shown in Fig. 3.77; the unit of luminance is candela per square metre. An average overcast sky has a luminance of 3000 cd / m². Luminance can be described by the following equation :

$$L = d^2 F / dA d\Omega \cos\theta \quad (3.3)$$

L = luminance (cd/m²)
 F = luminous flux (lumen)
 A = surface area (m²)
 Ω = solid angle (steradian)
 θ = angle between the surface normal and the specified direction.

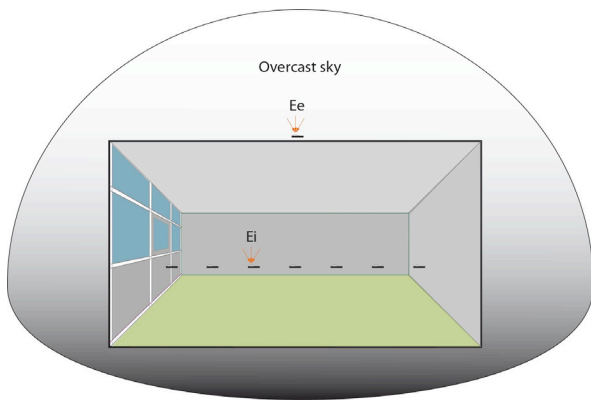


Fig. 3.78
Daylight factor: the proportion of overcast outdoor lighting arriving at a point indoors

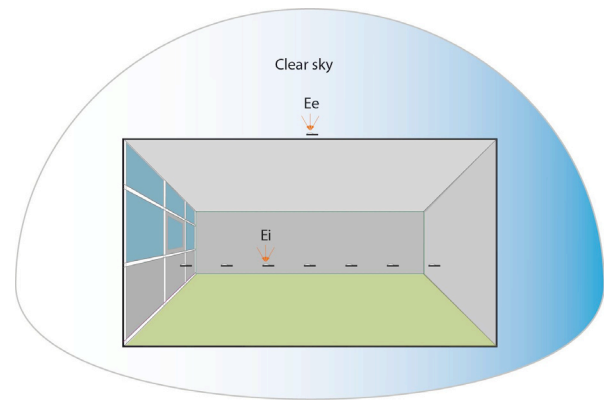


Fig. 3.79
Illuminance ratio: the proportion of clear-sky outdoor lighting arriving at a point indoors

Daylighting performance

To quantify the daylight properties of the interior space in this study so as to compare the different design tools, two calculation approaches were used.

Daylight factor

The daylight factor is the value used to characterize the quantity of daylight at the specific point of the interior space. It is defined as the ratio of indoor illuminance on a horizontal surface by the simultaneously available outdoor illuminance for an overcast sky (Fig. 3.78) (IES lighting handbook, 1984).

$$DF = (E_i/E_e) \times 100 (\%) \quad (3.4)$$

DF = daylight factor (%)

E_i = indoor illuminance on a horizontal surface (lux)

E_e = outdoor illuminance on a horizontal surface (lux)

Illuminance ratio

The illuminance ratio is defined as the ratio of the indoor illuminance on a horizontal surface and the simultaneously available outdoor illuminance for a clear sky (Fig. 3.79).

$$IR = (E_i/E_e) \times 100 (\%) \quad (3.5)$$

IR = Illuminance ratio (%)

E_i = indoor illuminance on a horizontal surface (lux)

E_e = outdoor illuminance on a horizontal surface (lux)

chapter

4

identification of potential sources of errors



Fig. 4.1
1:10 scale model placed under real sky conditions

To identify how and where assessment errors can occur, different types of model were studied using various daylight simulation methods and compared with measurements made of a real building. Once the potential sources of error had been broadly outlined a more detailed analysis was made to add precision.

4.1 Parameters of physical and virtual models under study

This study assessed daylighting performance of five different model cases, comparing their values to measurements made of a real building. Table 4.1 shows how the model types and daylight simulations of the five cases relate to the real building's assessment.

Simulations /real	Model type /real	Daylight source	Daylight source	Sky luminance distribution
Real	Real building	Real sky	1 (continuous sky)	Real sky
Case A	Scale model	Real sky (not simulated)	1 (continuous sky)	Real sky
Case B	Scale model	Sky simulator	145 circular sky patches ²	Simulated standard skies
Case C	Scale model	Sky simulator + PDF ¹	145 circular sky patches ²	Mapped real sky values
Case D	Virtual model	Virtual sky	1 (continuous sky)	Simulated standard sky
Case E	Virtual model	Virtual sky + PDF ¹	145 square sky patches ²	Mapped real sky values

¹ PDF : Partial daylight factor method : an alternative method to reproduce real sky luminance distribution using illuminance measurement at considered point on a given surface comes from the particular luminous zone (details in chapter 3).

² Distribution of sky patches follows the Tregenza IDMP (International daylight measurement program) protocole

Table 4.1
The real building and the five modelled cases

Case A

86

The 1:10 scale model was placed on site adjacent to the real building (Fig. 4.1). The illuminance measurements of the model were acquired at the same time as those of the real building and afterwards provided daylight factor (DF) and illuminance ratio (IR) values (Fig. 4.2).

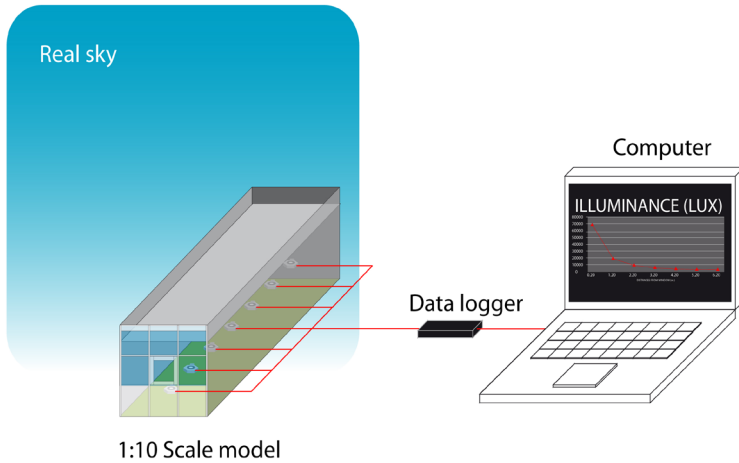


Fig. 4.2
Illuminance data acquisition:
1:10 scale model under real sky
conditions

Case B

The daylighting flux of this case was generated by a scanning sky simulator (Fig. 4.3) following selected standard sky conditions (CIE overcast sky, CIE clear sky). The 1:10 scale model was placed under the sky simulator; photometers collected illuminance measurements which provided the DF and IR (Fig. 4.4) by later calculation.

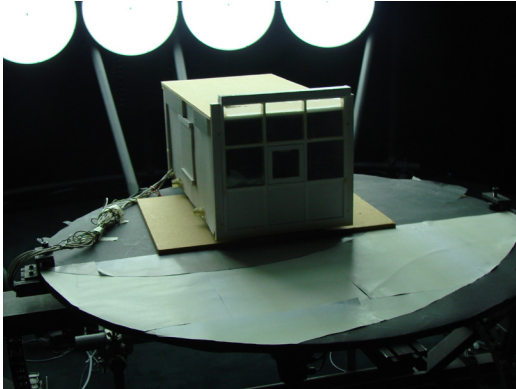


Fig. 4.3
1:10 scale model placed under the scanning sky simulator

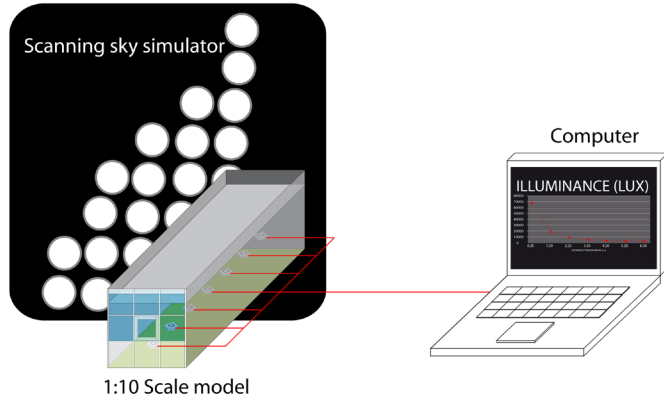


Fig. 4.4
Illuminance data acquisition: 1:10 scale model under
the scanning sky simulator

Case C

At the same time as Case A's measurements were made, a sky scanner logged real sky luminance values for each of the 145 Tregenza sectors. Whereas Case B used 'standard sky' values, Case C (Fig. 4.5) measured the PDF for each individual sky sector while the physical model was under the scanning sky simulator and then multiplied it by the sky scanner's corresponding 'real sky' value to give DF and IR.

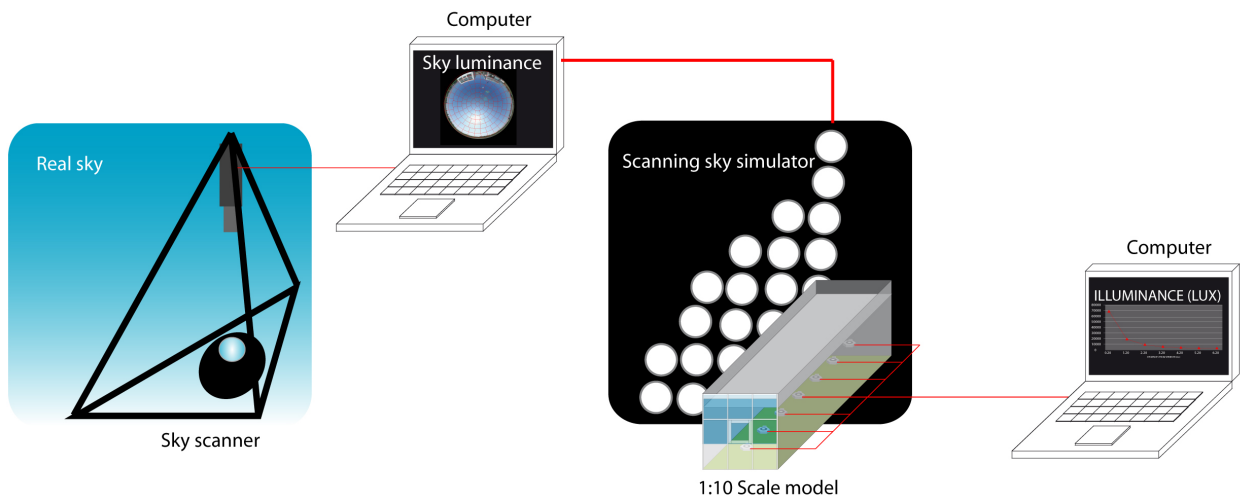


Fig. 4.5
Illuminance data acquisition: 1:10 scale model under the scanning sky simulator while using real sky luminance distribution (PDF method)

Case D

The virtual model was created using the Radiance program, the GenSky function (Ward, 1998) being used to produce the scene under CIE standard sky distribution (CIE standard skies Type 1 and Type 12). The illuminance was evaluated using Radiance scene calculation and afterwards converted into DF and IR (Fig. 4.6).

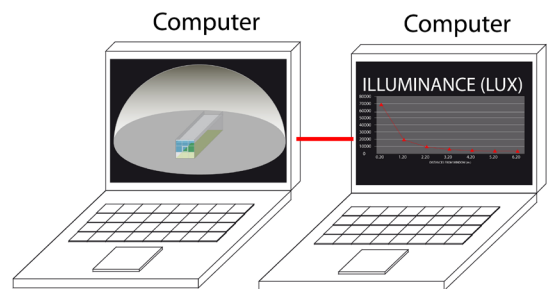


Fig. 4.6
Illuminance data acquisition for the virtual model

Case E

To map the real sky luminance distribution in the virtual model, the 145 Tregenza's sector and sky luminance distribution measured by the digital sky scanner (as in Case C) were reproduced in the Radiance scene using the PDF method. The illuminance was evaluated using Radiance scene calculation and afterwards converted into DF and IR (Fig. 4.7).

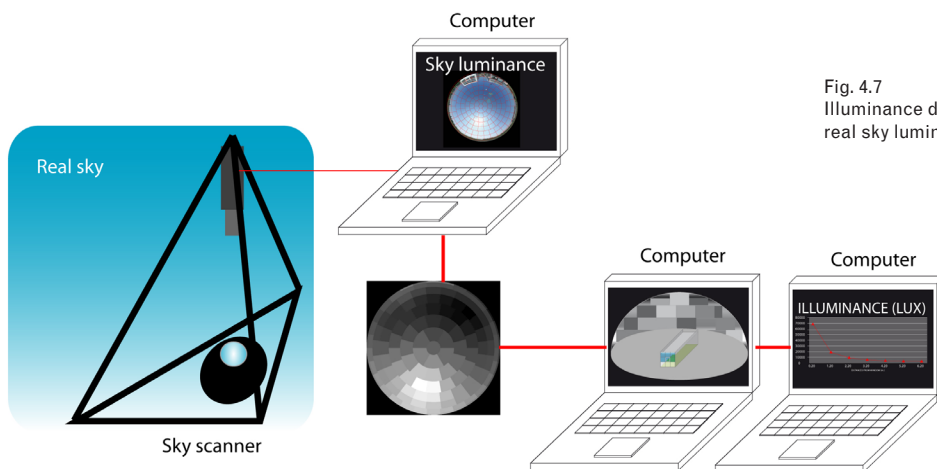


Fig. 4.7
Illuminance data acquisition: virtual model using real sky luminance distribution (PDF method)

4.2 Sky conditions used in the assessments

88

Overall procedure for identification of sky conditions

This study assessed daylighting performance under both overcast and clear sky conditions. To identify the sky's daylight conditions, the sky luminance distribution was monitored according to the procedure presented in Table 4.2 and Fig. 4.8.

The same procedure illustrated on Fig. 4.8 was followed when the real building and its 1:10 scale model were equipped with Laser-cut panel and Prismatic film respectively.

a.	Sky observation	<ul style="list-style-type: none"> The real sky condition was observed and the sky luminance distribution was measured point to point using a Minolta LS110 luminance meter.
b.	Sky luminance monitoring	<ul style="list-style-type: none"> A digital sky scanner monitored the sky luminance distribution (as 145 Tregenza sectors) at the same time as illuminance was measured. Case A evaluated the real building together with its 1:10 scale model (both with double glazing window).
c.	Comparison of measured sky luminance distribution with that of standard sky by graphical methods	<ul style="list-style-type: none"> The measured sky luminance distribution was compared with 15 CIE standard skies to identify which one most resembled the monitored real sky. The graph of the distribution of sky luminance of each CIE standard sky was compared with that of the real sky during the particular measurements.
d.	Comparison of measured sky luminance distribution with that of standard sky by calculation of divergences	<ul style="list-style-type: none"> The 145 Tregenza sectors of the real sky were re-examined, comparing them with the standard skies. The value of each individual sky sector of standard skies was numerically compared with the corresponding real measurement. For each of the 145 sky sector the difference between the standard sky value and the real one was evaluated. To simplify the evaluation the R-square (quadratic residues) of the 145 sky sectors was analysed. The range of the difference between the measured and standard sky was also calculated.
e.	Identification of the standard sky which most resembled the reality	<ul style="list-style-type: none"> The CIE standard sky which most resembled the reality (the 'best fit') was identified for daylight simulation. This 'best fit' standard sky was used to simulate daylight for the evaluation of Case B (the physical 1:10 scale model) and Case D (the virtual model). The measured sky luminance distribution was used to simulate daylight for the evaluation of Case C (physical model) and Case E (virtual model).

Table 4.2
The procedure of selecting a specific CIE standard sky by comparison with measured values

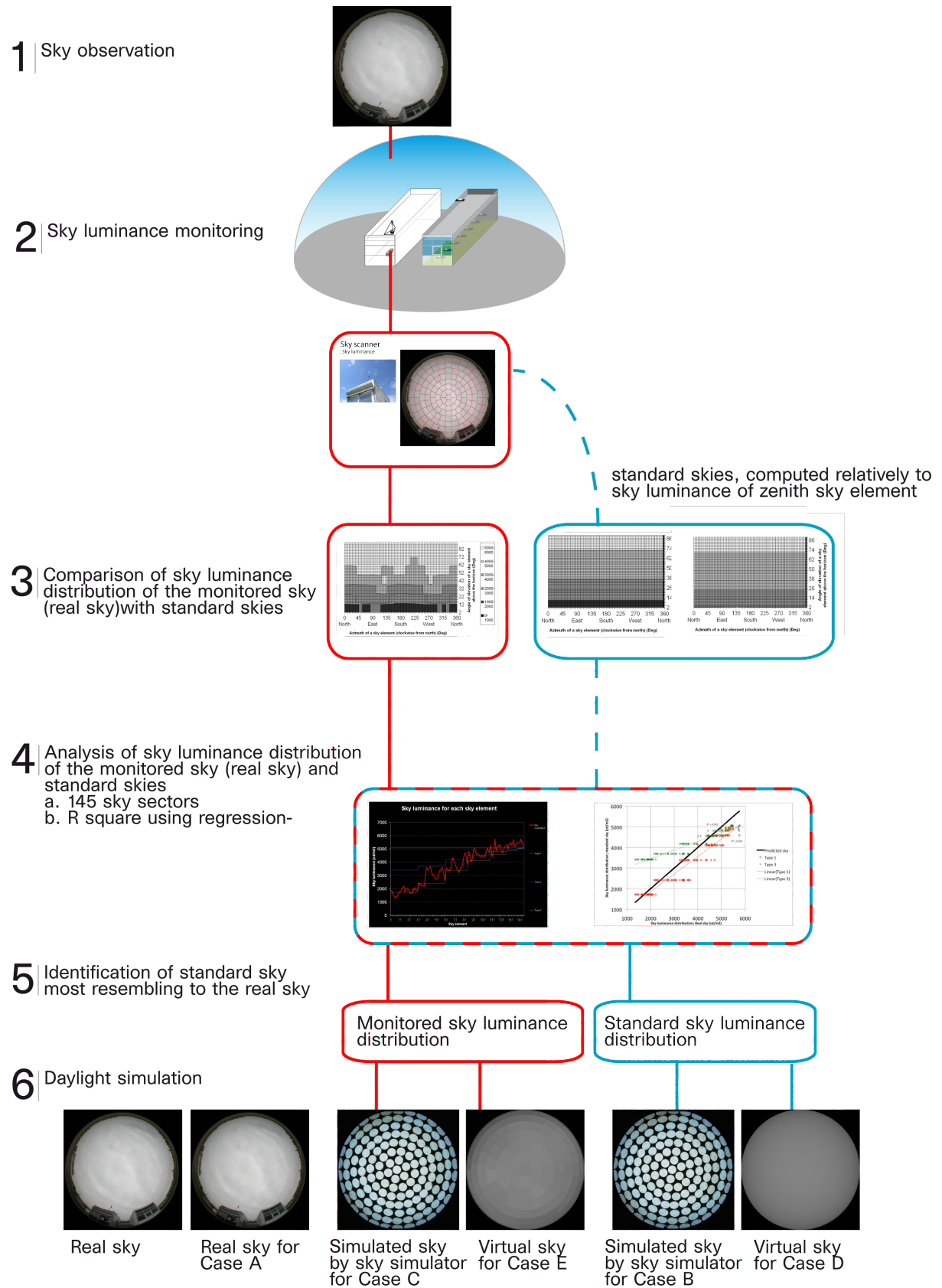


Fig. 4.8 Procedure of selection of a specific CIE standard sky by comparison with monitored (measured) sky luminance distribution

Overcast sky

90

Daylighting assessment of complex fenestration systems (CFS) for overcast skies

Daylighting performance assessments of the double glazing window, Laser-cut panel and Prismatic film were made on three separate occasions when the sky was overcast. All the measurements were taken on the EPFL campus in Lausanne, Switzerland (46.31° N, 6.33° E). The results are presented in Table 4.3 and Fig. 4.9.

	Overcast sky#A	Overcast sky#B	Overcast sky#C
Fenestration system	Double glazing	Laser Cut Panel (LCP)	Prismatic Film
Sky condition	Overcast	Overcast	Overcast
Date	28 August 2006	5 April 2007	28 August 2006
Day of year (-)	240	95	240
Local time (hh:mm)	11:17	9:13	13:11
Solar time (hh:mm)	9:42	7:38	11:36
Solar altitude angle (°)	52.56	26.72	50.67
Solar azimuth angle (°)	162.41	111.32	208.25
Sun zenith (°)	37.44	63.28	39.33

Table 4.3
General information about daylighting performance assessments made on overcast days

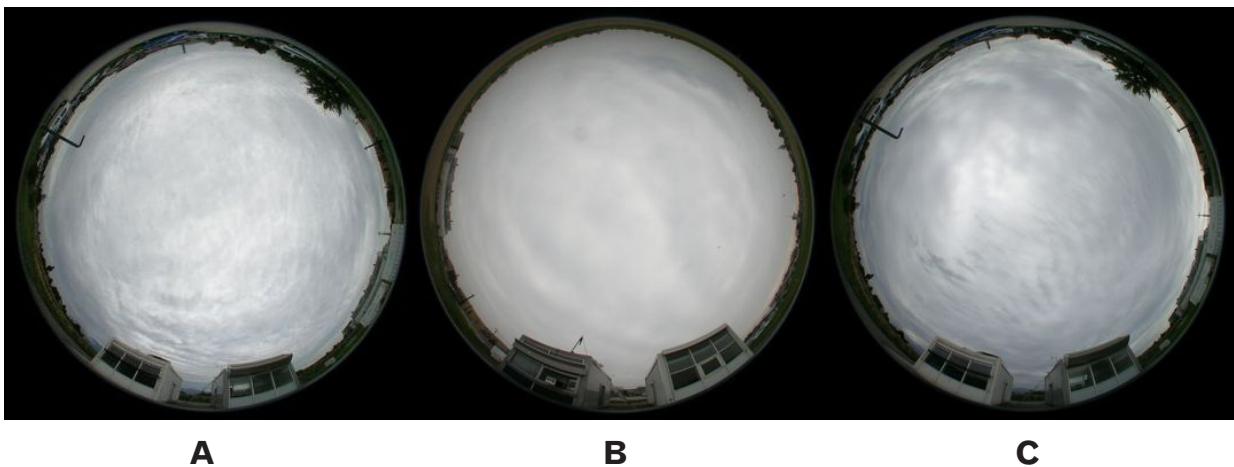


Fig. 4.9
Real sky conditions during daylight performance assessment of Case A (the real building and its 1:10 scale model) equipped with:
a) Double glazing, b) LCP and c) Prismatic film

Sky luminance distribution

On each occasion the luminance distribution of the real sky was monitored using a digital sky scanner: the luminance of each sky sector is shown graphically in Fig. 4.10. The three monitored overcast sky luminance distributions were compared with CIE standard skies. Fig. 4.11, 4.12 and 4.13 present graphically for double glazing window, LCP and Prismatic film respectively, the luminance distribution of the measured sky luminance distribution together with that of CIE standard skies.

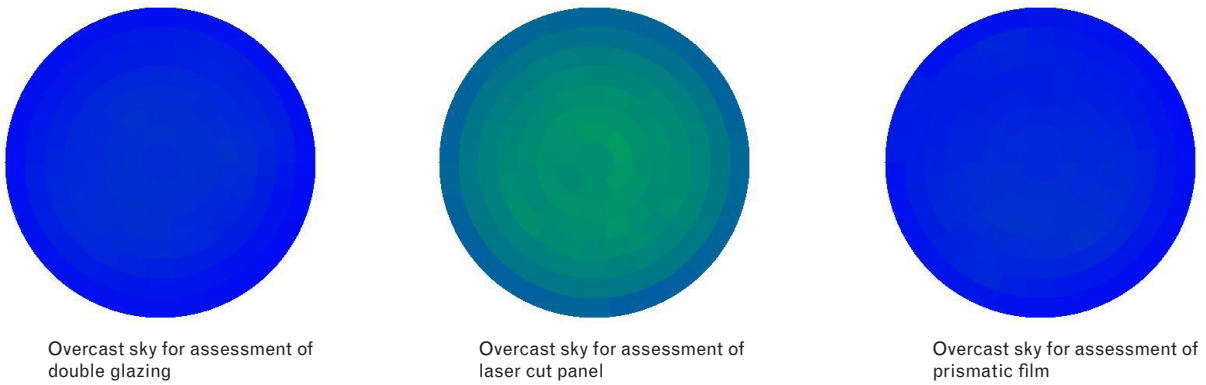


Fig. 4.10 Luminance distribution of the real sky monitored using a digital sky scanner (luminance of each sky sector)

SKY LUMINANCE

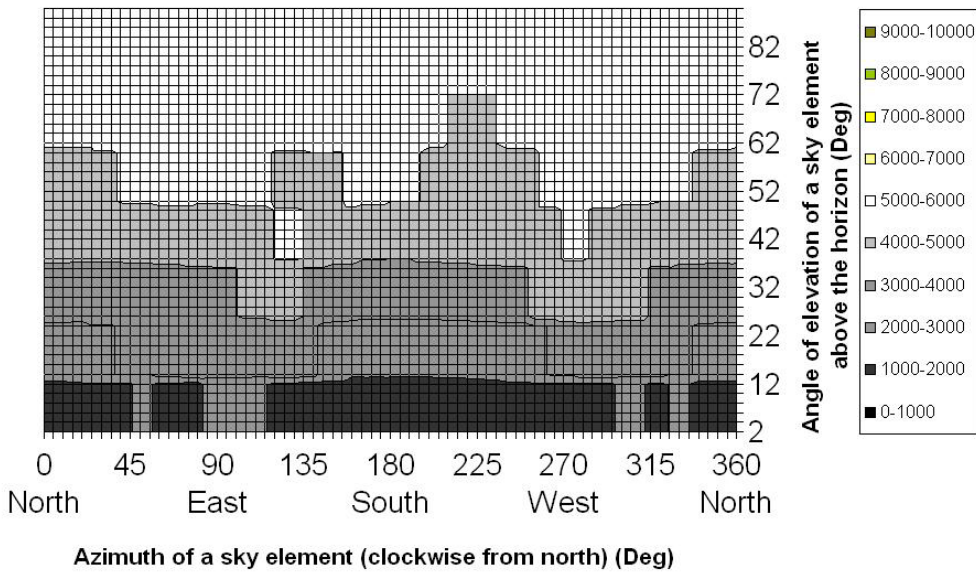
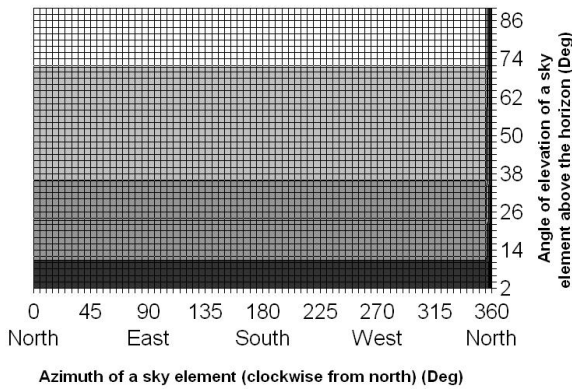
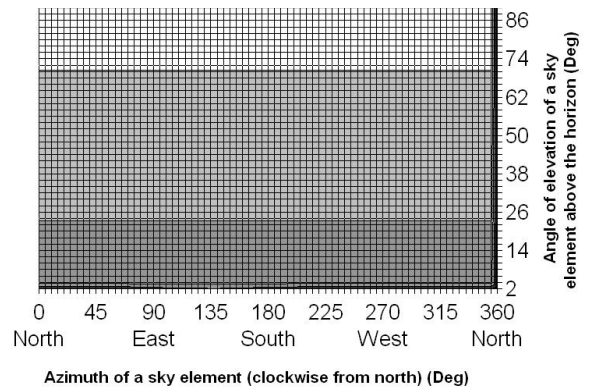


Fig. 4.11 Graphic comparison of real sky luminance observed for the double glazing with CIE standard skies

Type 1 CIE STANDARD OVERCAST SKY

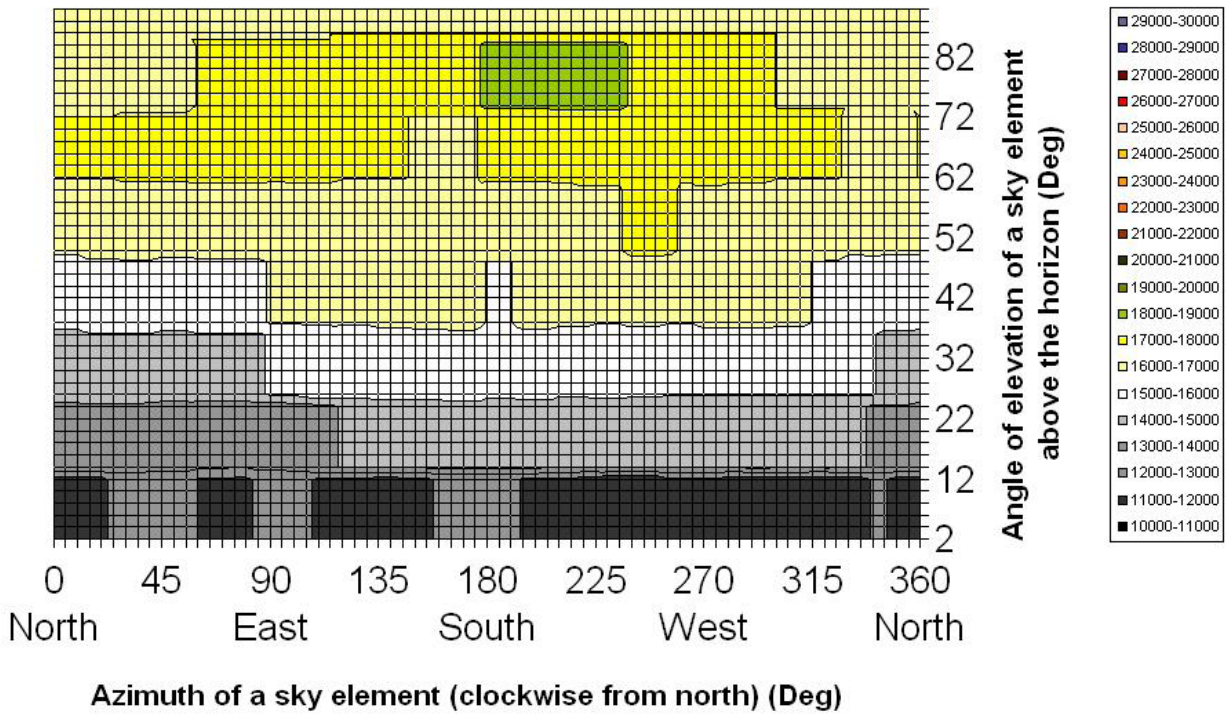


Type 3 OVERCAST, MODERATELY GRADED WITH AZIMUTHAL UNIFORMITY

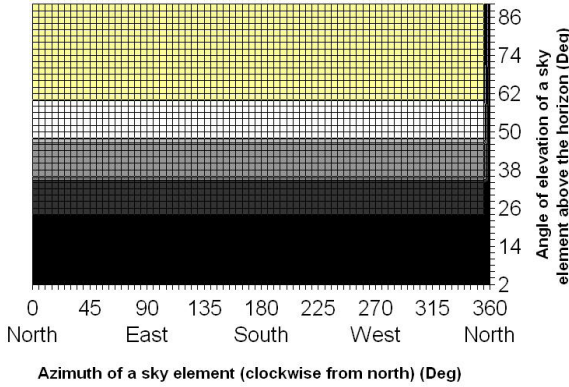


SKY LUMINANCE

92



**Type 1 CIE
STANDARD OVERCAST SKY**



**Type 3 OVERCAST, MODERATELY GRADED
WITH AZIMUTHAL UNIFORMITY**

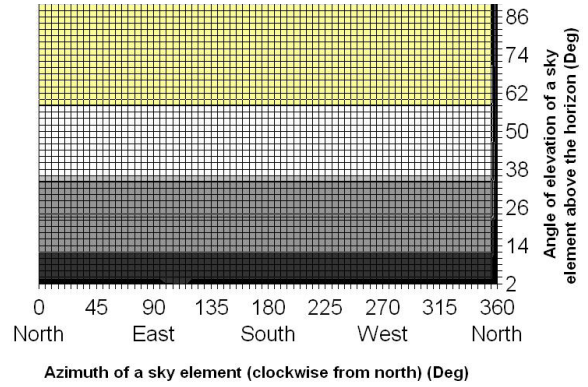
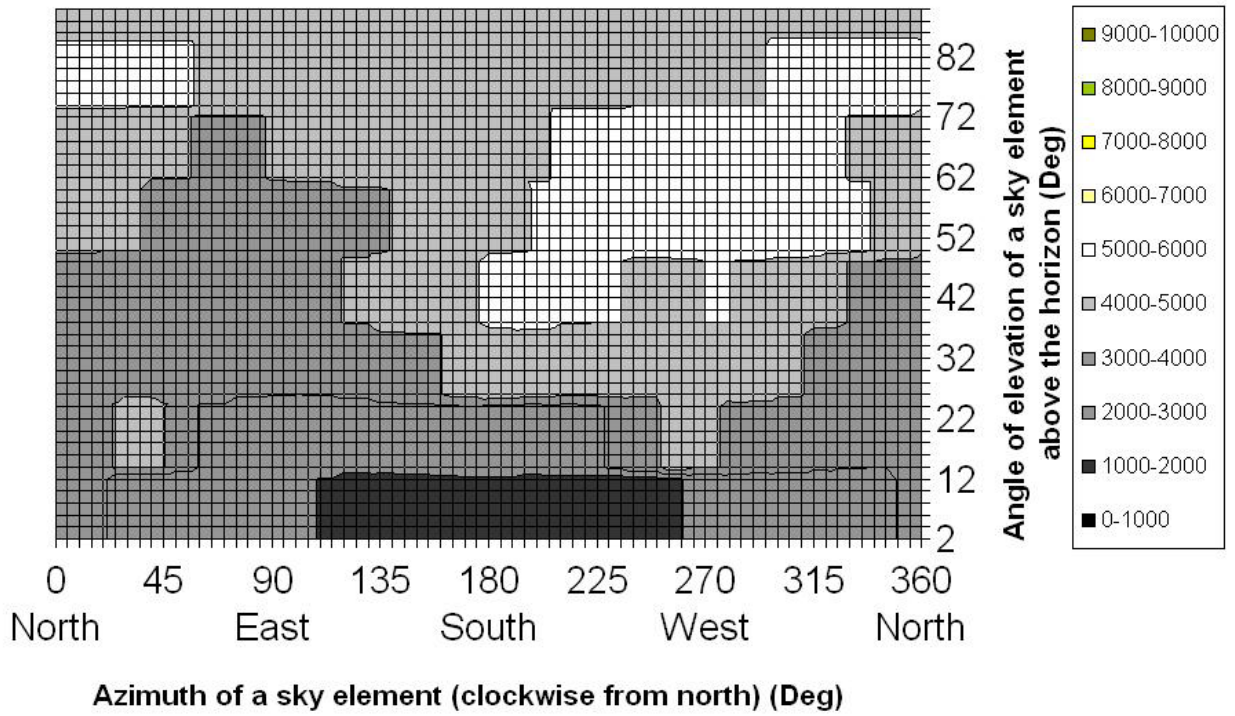
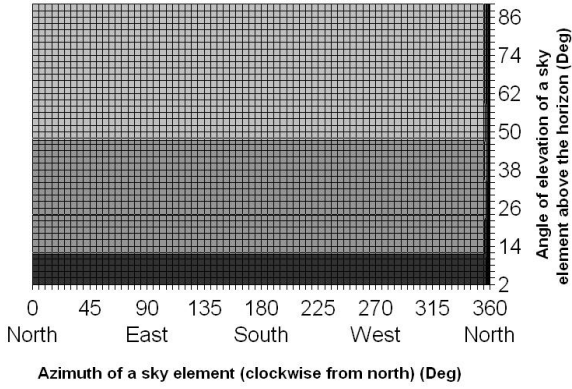


Fig. 4.12
Graphic comparison of real sky
luminance observed for the laser cut
panel (LCP) with CIE standard skies

SKY LUMINANCE



**Type 1 CIE
STANDARD OVERCAST SKY**



**Type 3 OVERCAST, MODERATELY GRADED
WITH AZIMUTHAL UNIFORMITY**

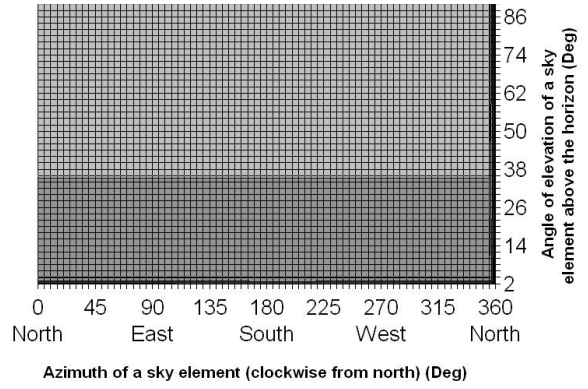


Fig. 4.13
Graphic comparison of real sky
luminance observed for the prismatic
film with CIE standard skies

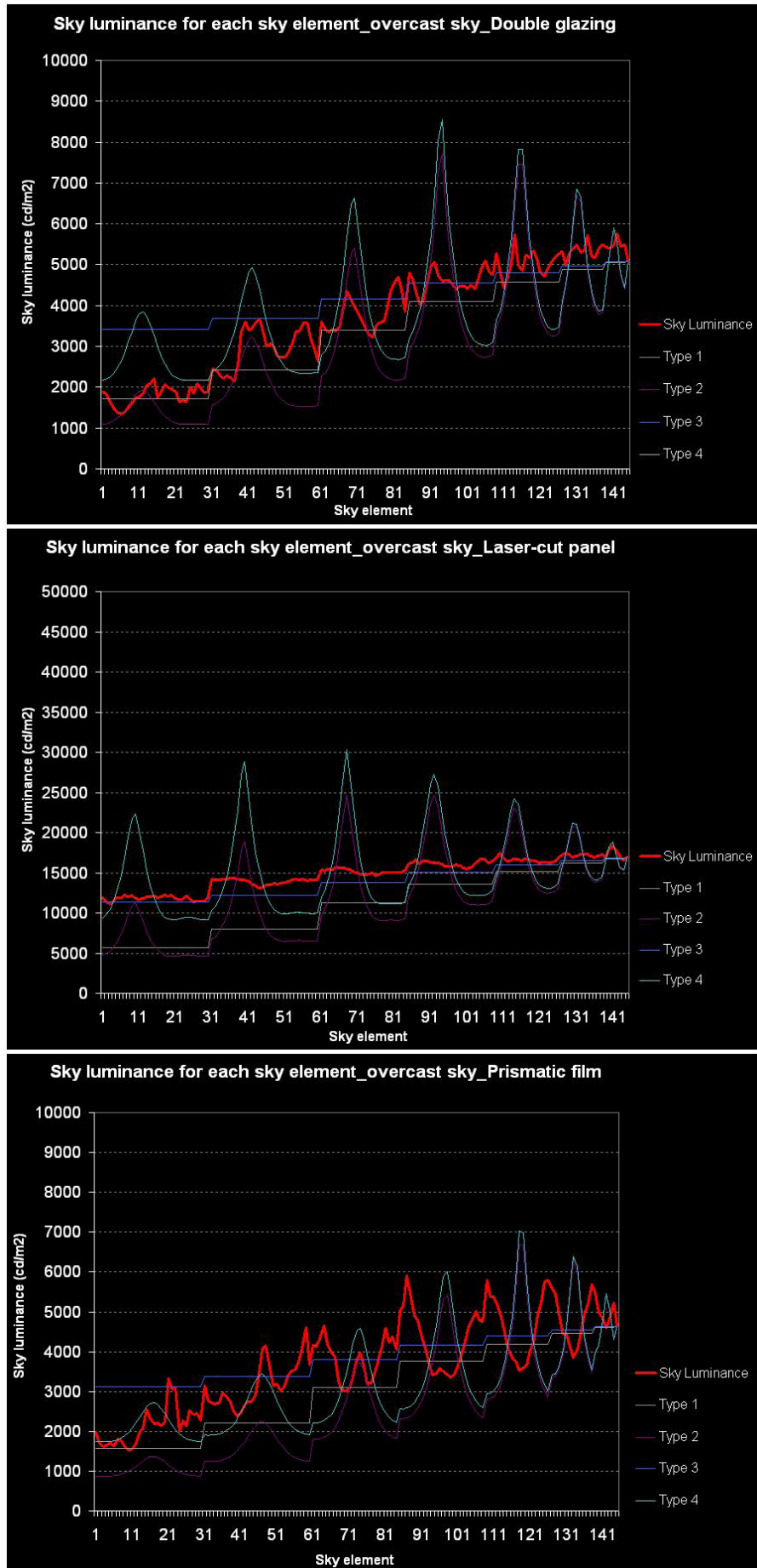


Fig. 4.14
 Diagrams comparing the 145 sky sectors of measured skies to the corresponding CIE standard skies

Comparison of real skies with CIE standard skies

As shown in Fig. 4.14, the sky luminance distribution of the 145 sky sectors of two CIE standard skies was compared to the monitored values using the three fenestration systems. Table 4.4 presents for each standard sky the range of differences between real and standard skies for each system, as well as the average difference.

Standard sky		Double glazing	LCP	Prismatic film
Type 1	Range of the differences between real and standard sky (cd/m ²)	0.36 - 1316.36	221.65 - 6528.54	3.50 - 2400.54
	Average difference between real and standard sky (cd/m ²)	435.94	3828.17	710.86
Type 3	Range of the differences between real and standard sky (cd/m ²)	13.75 - 2075.17	6.56 - 2099.74	2.08 - 1742.16
	Average difference between real and standard sky (cd/m ²)	690.11	995.19	646.66

Range of the difference = Minimal to Maximal differences

$$\text{Discrepancies of the measured sky and standard sky} = \frac{\text{Sky luminance}_1 + \text{Sky luminance}_2 + \dots + \text{Sky luminance}_{145}}{145}$$

Table 4.4

The range of differences between the measured 145 sky sectors and standard sky, together with the average of the differences

In addition, the R-square regression method was used to analyse the real skies. Fig. 4.15 presents the scattering diagrams which show how each real sky compared to CIE standard skies (Types 1 and 3).

From these measured sky luminance values it became apparent that CIE overcast sky Type1 was the closest to reality for the double glazing system and prismatic film, while CIE Type 3 sky (overcast, moderately graded with azimuthal uniformity) was the 'best fit' for the Laser cut panel.

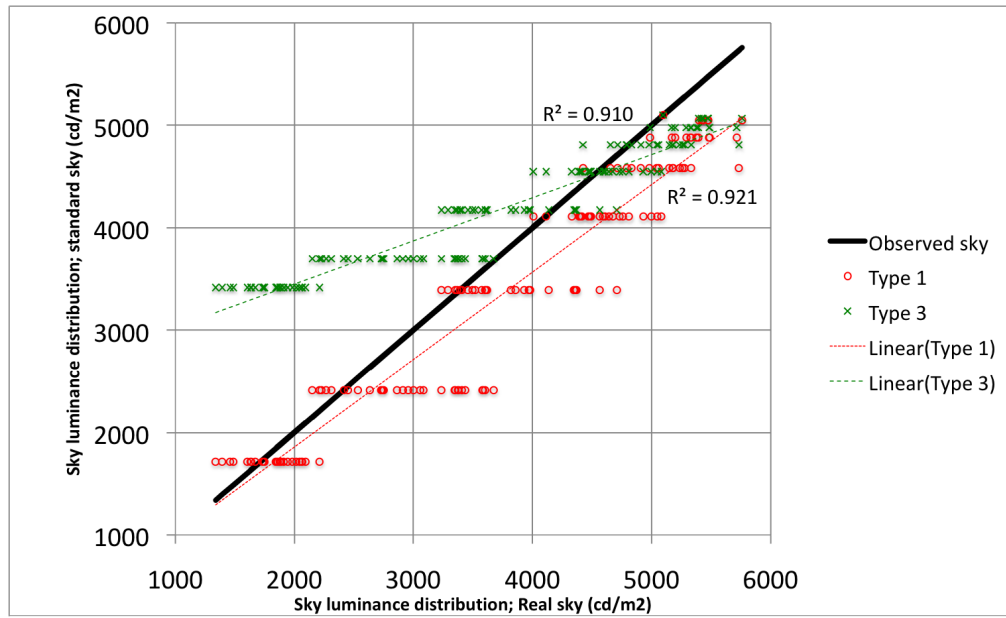
	Overcast sky#A	Overcast sky#B	Overcast sky#C
Fenestration system	Double glazing	Laser Cut Panel (LCP)	Prismatic Film
Most similar CIE standard sky	Type 1: CIE standard overcast sky	Type 3: Overcast, moderately graded with azimuthal uniformity	Type 1: CIE standard overcast sky

Table 4.5

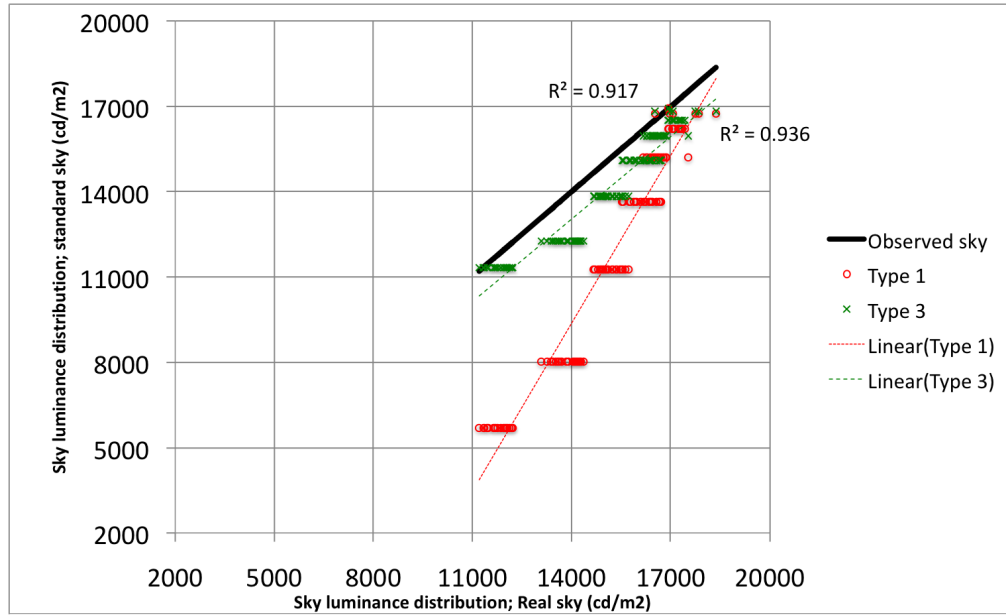
The standard skies that best resembled the real overcast skies

96

Overcast sky#A



Overcast sky#B



Overcast sky#C

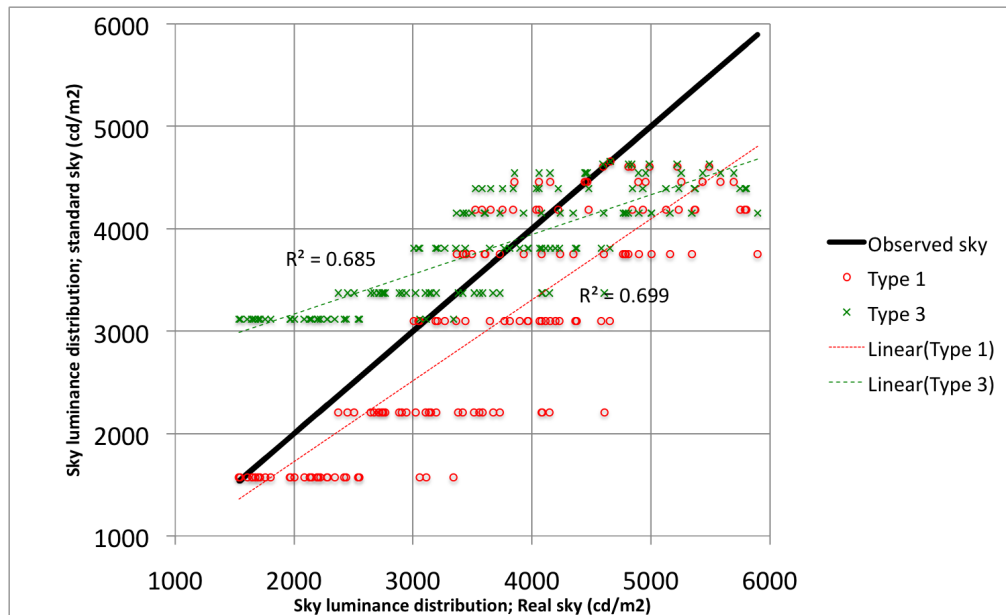


Fig. 4.15
Scattering diagram
for comparison of
luminance distribution.

Daylighting simulation for overcast sky

Daylighting simulations of overcast sky for Cases B, D and E are presented in the Table 4.6.

97

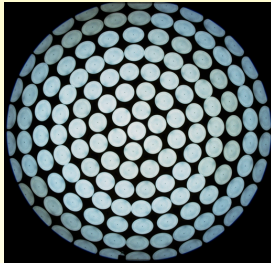
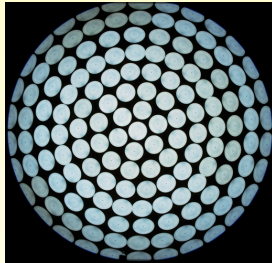
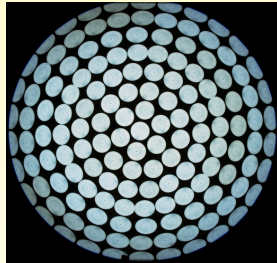

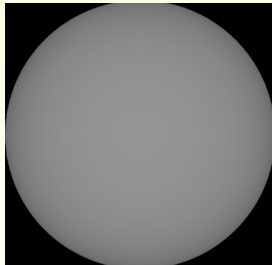

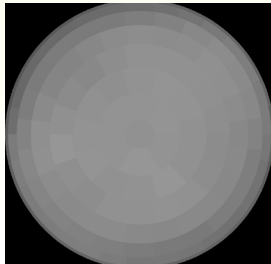
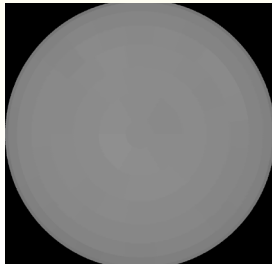
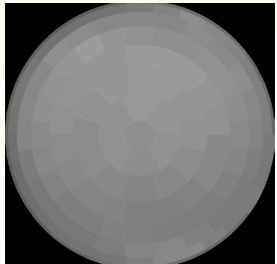
	Double glazing	Laser Cut Panel (LCP)	Prismatic Film
Scanning sky simulator CIE standard sky Type 1 (Case B)			
Radiance CIE standard sky (Case D)			
Radiance+Partial day- light factor method (Case E)			

Table 4.6
Daylight simulations of Cases B, D and E (overcast sky)

In Case B (1:10 scale model under scanning sky simulator), only the CIE standard sky Type 1 (overcast sky) could be used, the scanning sky simulator being unfortunately unable to simulate other overcast sky models (current limitation of the device). However comparison of computer simulations involving Type 1 and 3 overcast skies has shown no significant difference between them (details in Appendix C).

The daylighting simulations of Case C (1:10 scale model using scanning sky simulator and the PDF method) cannot be presented graphically, simulations being done by the way of calculations.

The daylighting simulations of Cases D and E (virtual model using the GenSky Radiance program) were based on the CIE standard overcast sky (Type 1) for all fenestration systems in order to facilitate the simulations.

Clear sky

98

Daylighting assessment of complex fenestration systems for clear sky (morning, midday and afternoon clear skies)

Daylighting performance assessments of the double glazing, the Laser-cut panel and the Prismatic film were made on three separate occasions when the sky was perfectly clear.

Once again a digital sky scanner monitored the sky luminance distribution (as 145 Tregenza sectors) while illuminance was simultaneously measured. The real building together with its 1:10 scale model (both with double glazing window) were considered simultaneously for case A. The skies were analysed and evaluated at morning, midday and the afternoon (Fig. 4.16, 4.17 and 4.18).

All the measurements were taken on the EPFL campus in Lausanne, Switzerland (46.31° N, 6.33° E). The results are presented in Tables 4.7, 4.8 and 4.9.

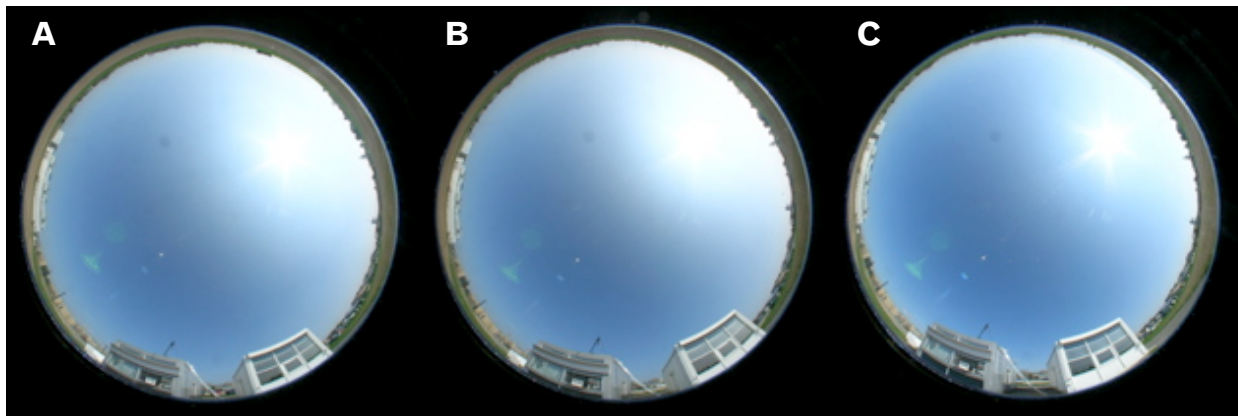


Fig. 4.16 Real sky conditions (morning, clear sky) during daylight performance assessment of Case A (the real building and its 1:10 scale model) equipped with: a) Double glazing, b) LCP and c) Prismatic film

	Morning clear sky#A	Morning clear sky#B	Morning clear sky#C
Fenestration system	Double glazing	Laser Cut Panel (LCP)	Prismatic Film
Sky condition	Clear	Clear	Clear
Date	11 April 2007	9 April 2007	10 April 2007
Day of year (-)	101	99	100
Local time (hh:mm)	10:01	10.01	10.01
Solar time (hh:mm)	8:26	8.26	8.26
Solar altitude angle (°)	30.57	30.01	30.29
Solar azimuth angle (°)	112.55	113.10	112.82
Sun zenith (°)	59.43	59.99	59.71

Table 4.7

General information about daylighting performance assessments made in the morning underneath clear skies

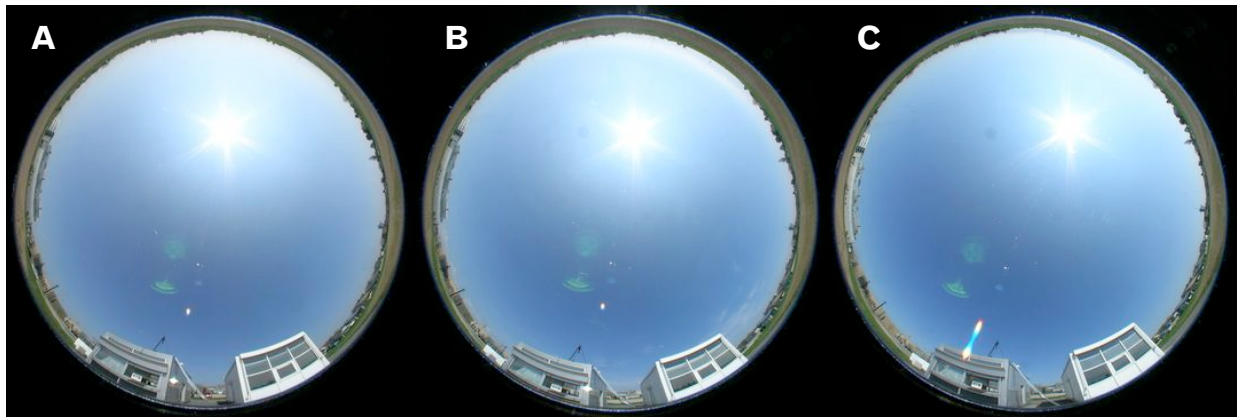


Fig. 4.17
Real sky conditions (midday, clear sky) during daylight performance assessment of Case A (the real building and its 1:10 scale model) equipped with: a) Double glazing, b) LCP and c) Prismatic film

Table 4.8
General information about daylighting performance assessments made at midday underneath clear skies

	Midday clear sky#A	Midday clear sky#B	Midday clear sky#C
Fenestration system	Double glazing	Laser Cut Panel (LCP)	Prismatic Film
Sky condition	Clear	Clear	Clear
Date	11 April 2007	9 April 2007	10 April 2007
Day of year (-)	101	99	100
Local time (hh:mm)	13:01	13.01	13.01
Solar time (hh:mm)	11:26	11.26	11.26
Solar altitude angle (°)	51.05	50.32	50.69
Solar azimuth angle (°)	166.66	166.85	166.76
Sun zenith (°)	38.95	39.68	39.31

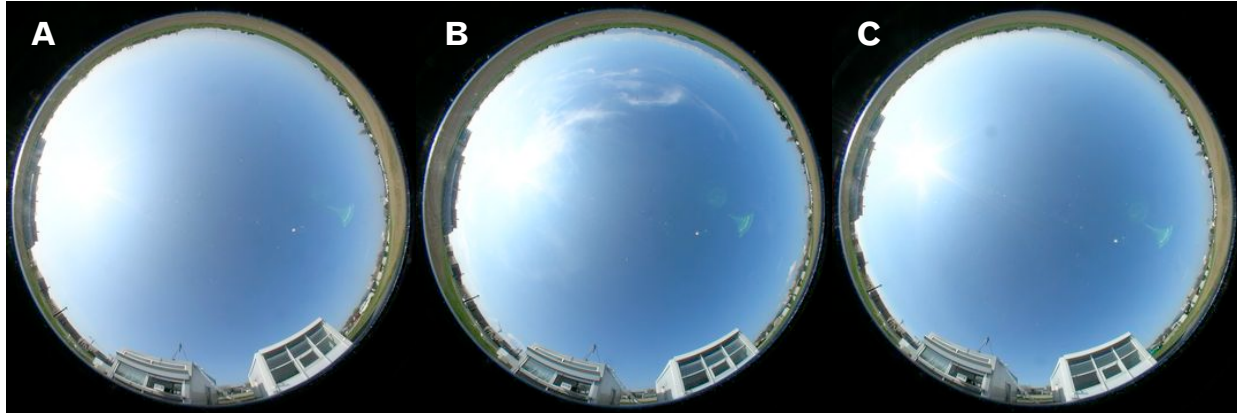
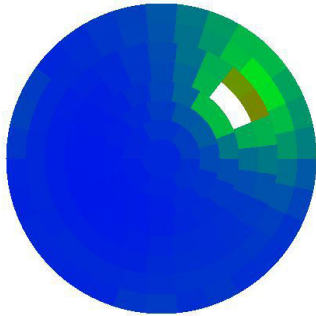


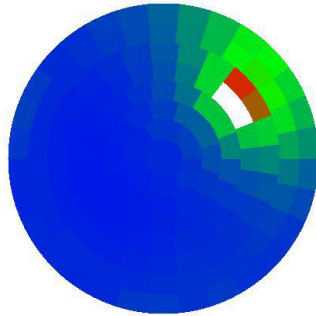
Fig. 4.18
Real sky conditions (afternoon, clear sky) during daylight performance assessment of Case A (the real building and its 1:10 scale model) equipped with: a) Double glazing, b) LCP and c) Prismatic film

Table 4.9
General information about daylighting performance assessments made in the afternoon underneath clear skies

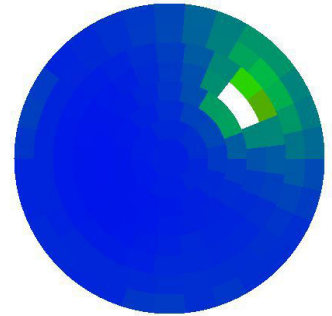
	Afternoon clear sky#A	Afternoon clear sky#B	Afternoon clear sky#C
Fenestration system	Double glazing	Laser Cut Panel (LCP)	Prismatic Film
Sky condition	Clear	Clear	Clear
Date	11 April 2007	9 April 2007	10 April 2007
Day of year (-)	101	99	100
Local time (hh:mm)	17.01	17.01	17.01
Solar time (hh:mm)	15.26	15.26	15.26
Solar altitude angle (°)	31.74	31.01	31.46
Solar azimuth angle (°)	245.82	245.49	245.54
Sun zenith (°)	58.26	58.99	58.54



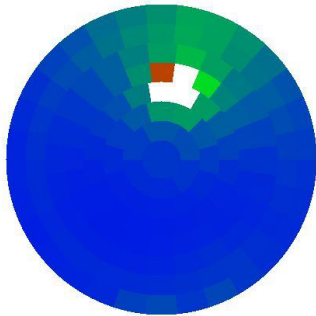
Morning clear sky for assessment of double glazing



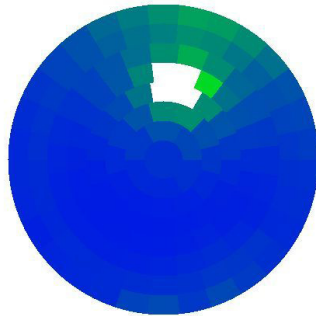
Morning clear sky for assessment of laser cut panel



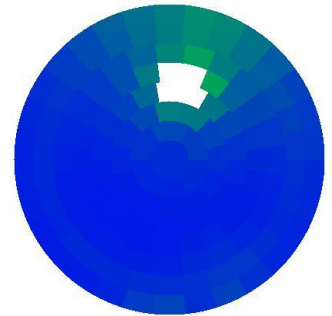
Morning clear sky for assessment of prismatic film



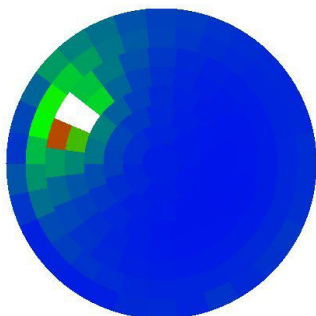
Midday clear sky for assessment of double glazing



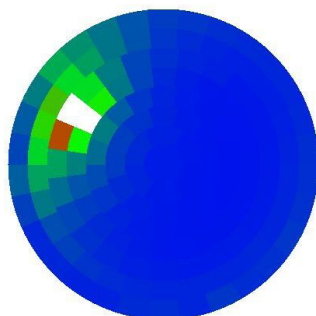
Midday clear sky for assessment of laser cut panel



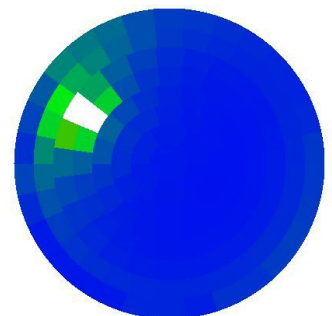
Midday clear sky for assessment of prismatic film



Afternoon clear sky for assessment of double glazing



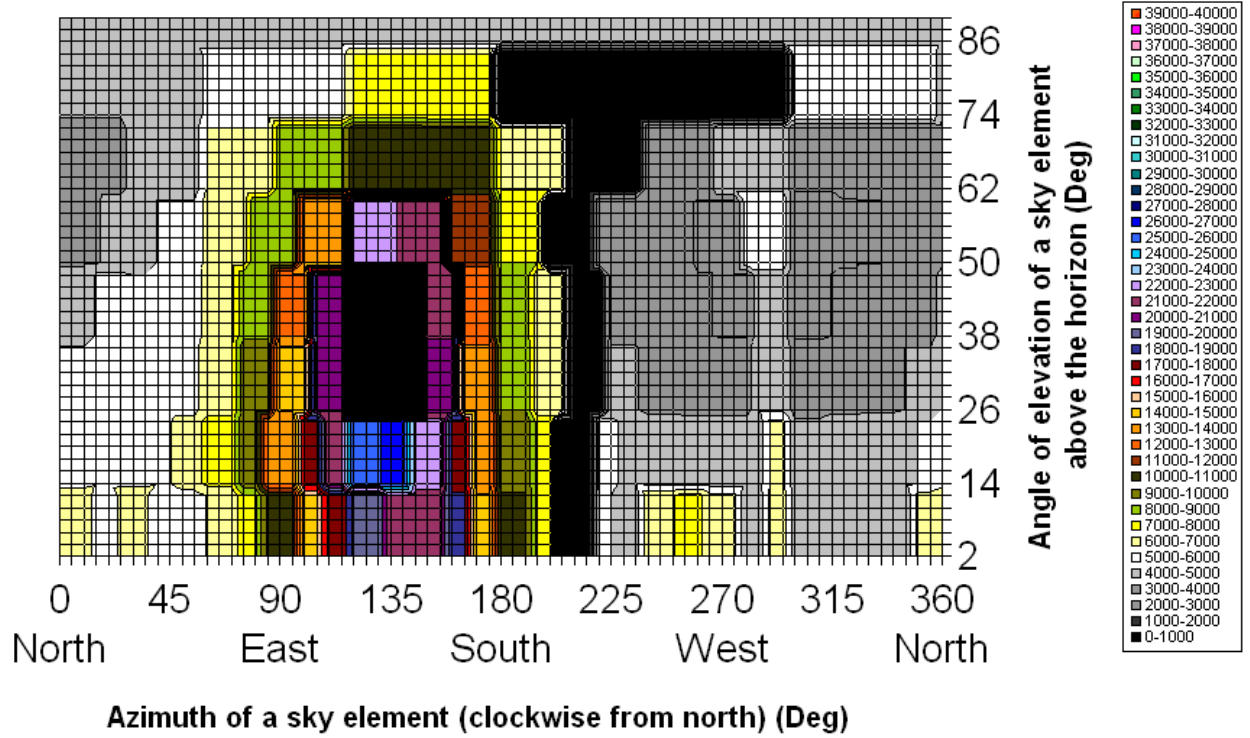
Afternoon clear sky for assessment of laser cut panel



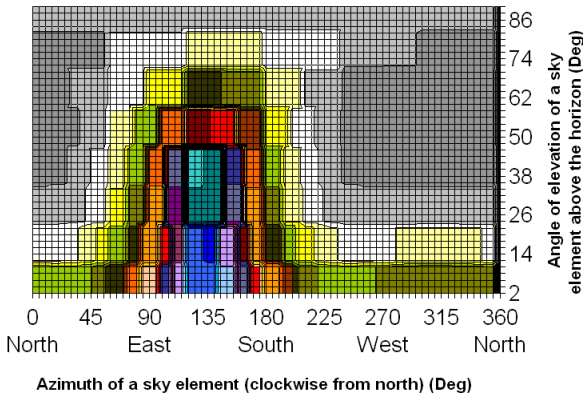
Afternoon clear sky for assessment of prismatic film

Fig. 4.19 Luminance distribution of the real sky monitored using a digital sky scanner

SKY LUMINANCE



Type 12 CIE STANDARD CLEAR SKY, LOW LUMINANCE TURBIDITY



CIE STANDARD CLEAR SKY, POLLUTED ATMOSPHERE

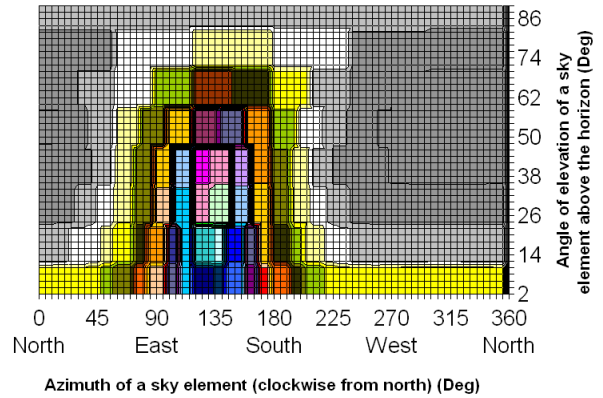
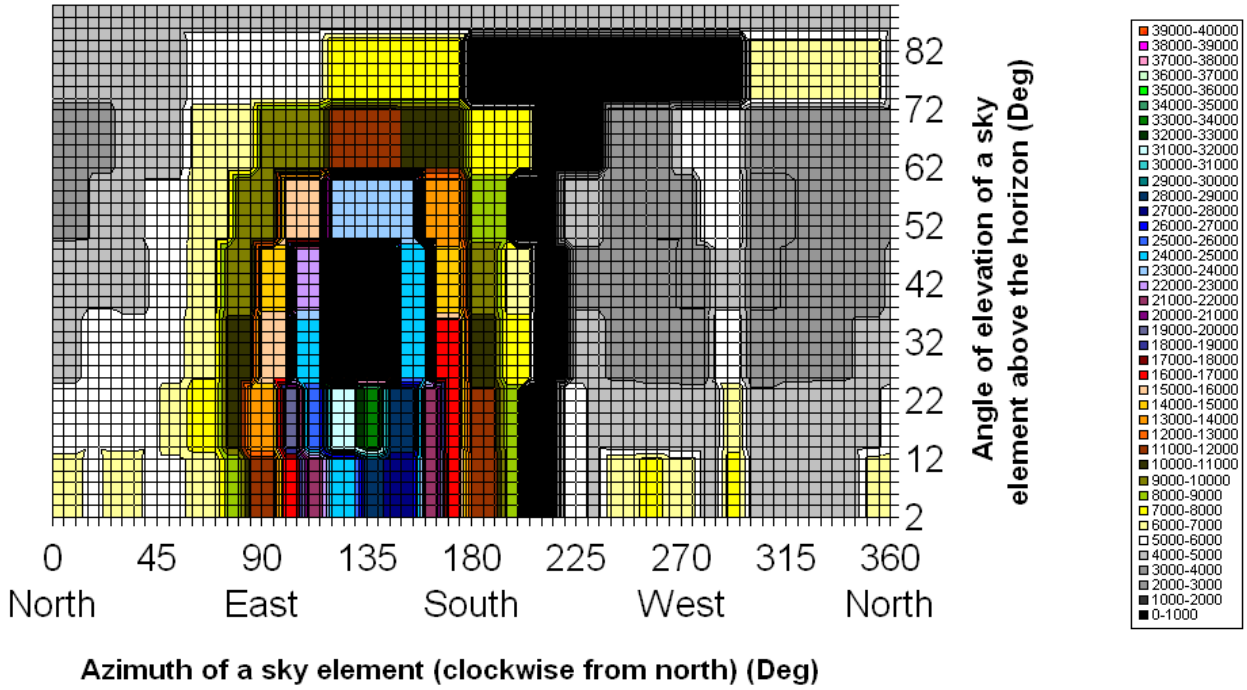


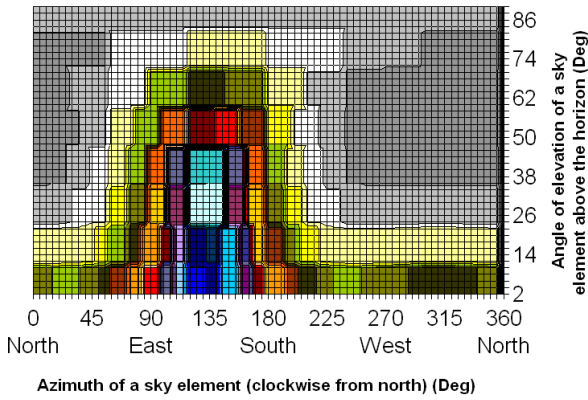
Fig. 4.20
Graphic comparison of real sky luminance observed for the double glazing (morning clear sky) with CIE standard skies

SKY LUMINANCE

102



Type 12 CIE STANDARD CLEAR SKY, LOW LUMINANCE TURBIDITY



CIE STANDARD CLEAR SKY, POLLUTED ATMOSPHERE

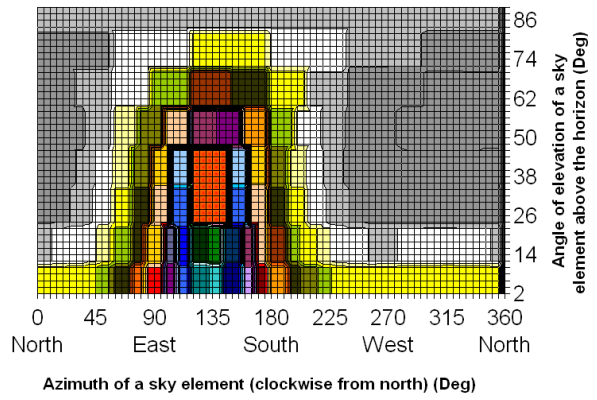
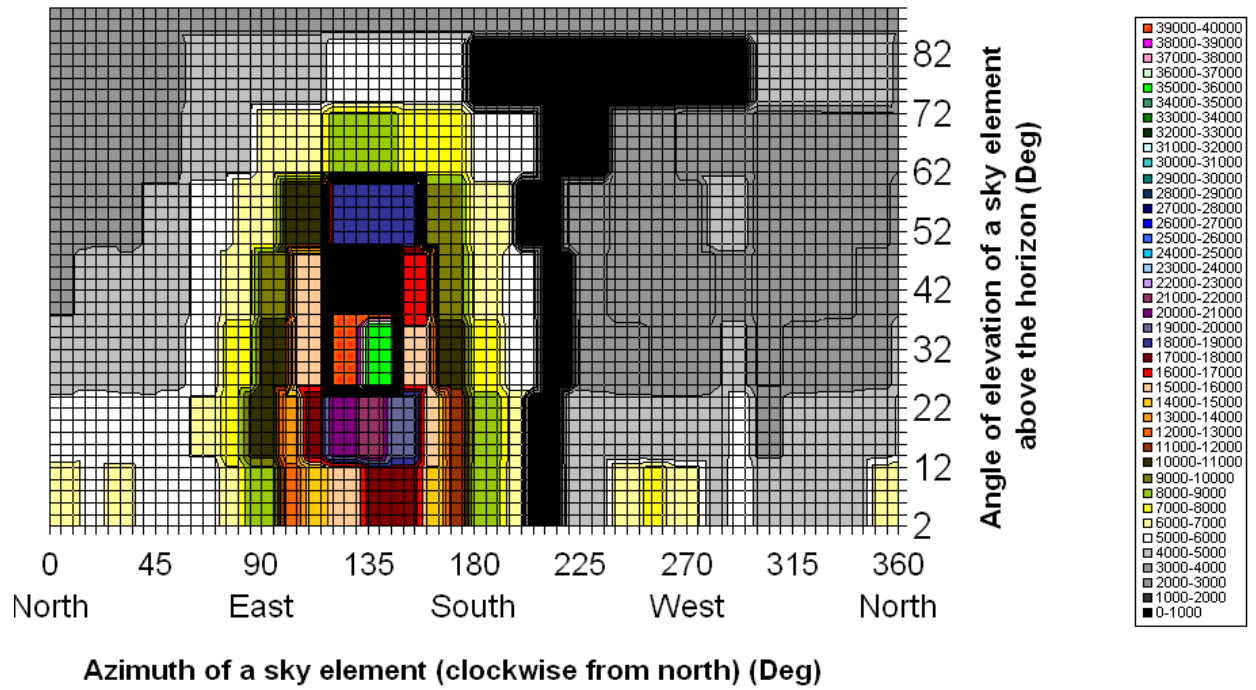
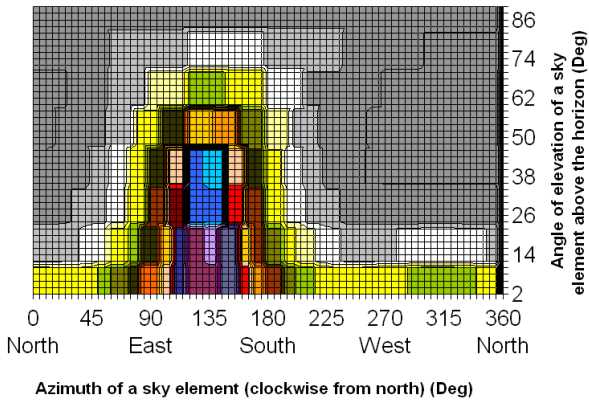


Fig. 4.21
Graphic comparison of real sky luminance observed for the Laser-cut panel (morning clear sky) with CIE standard skies

SKY LUMINANCE



Type 12 CIE STANDARD CLEAR SKY, LOW LUMINANCE TURBIDITY



CIE STANDARD CLEAR SKY, POLLUTED ATMOSPHERE

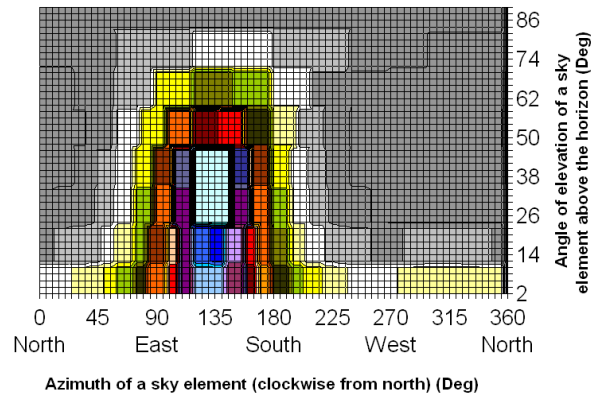


Fig. 4.22
Graphic comparison of real sky luminance observed for the Prismatic film (morning clear sky) with CIE standard skies

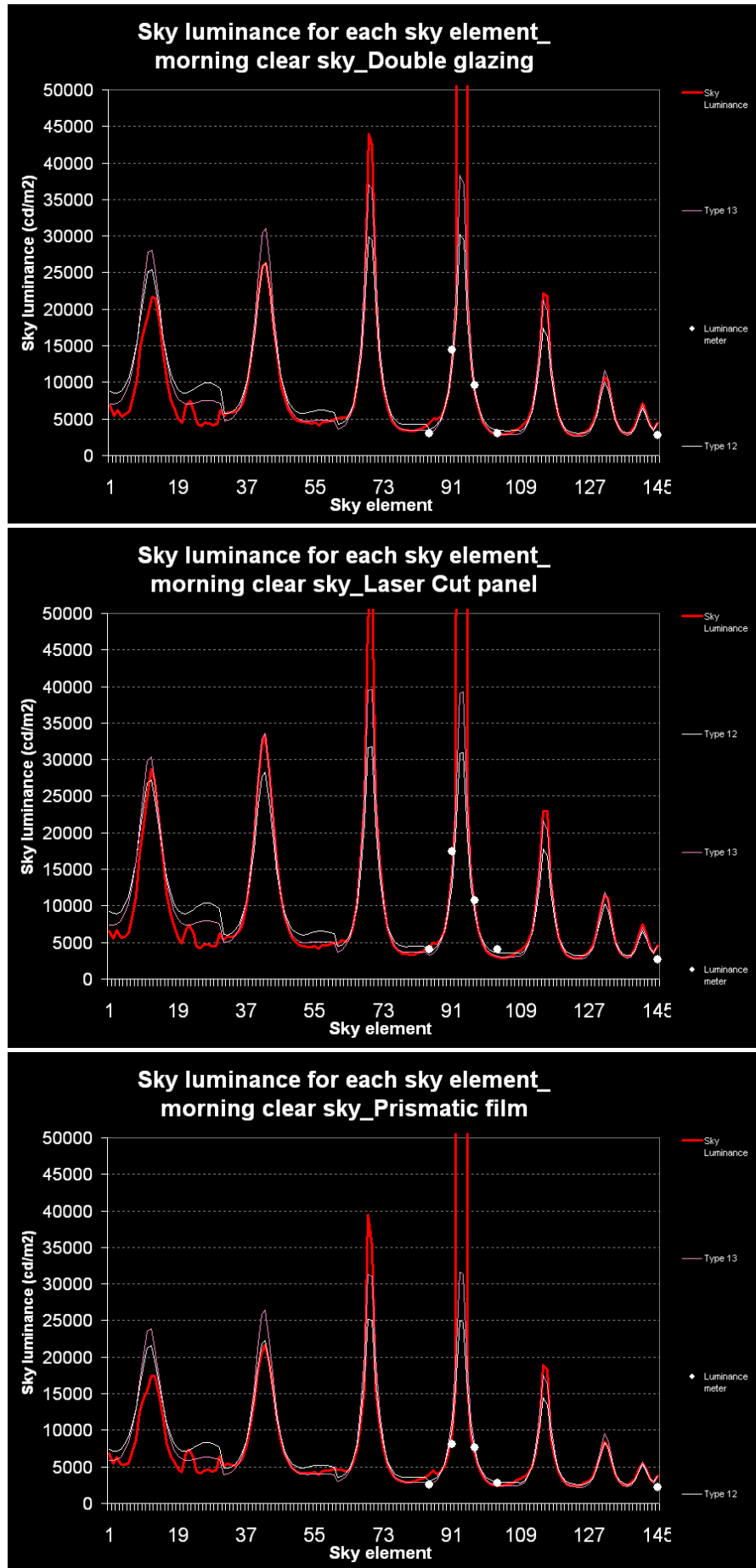
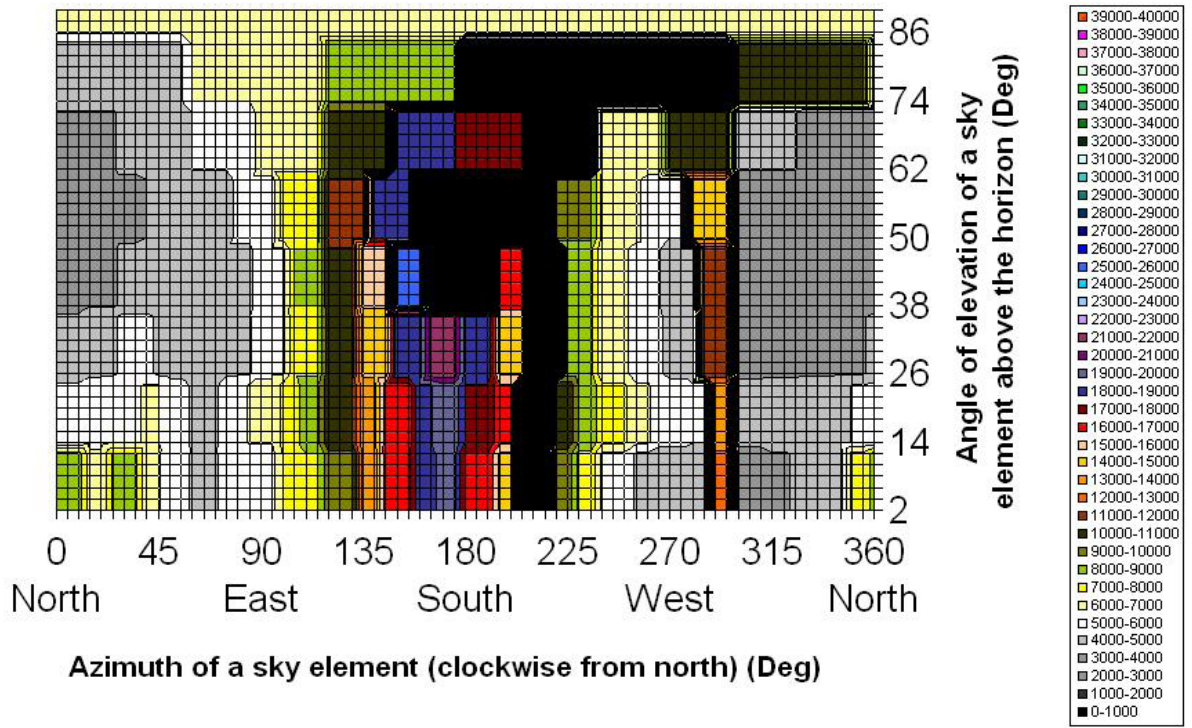
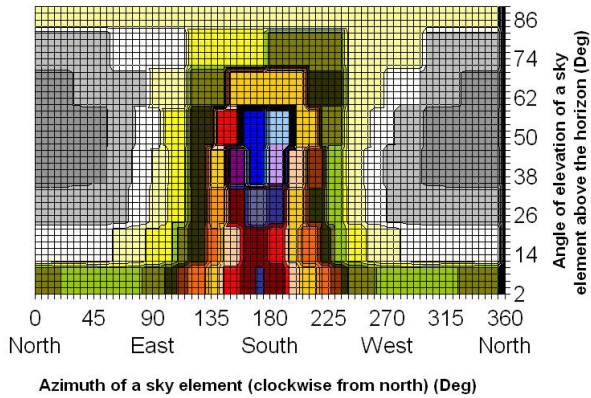


Fig. 4.23
Diagrams comparing the 145 sky sectors of measured skies to the corresponding CIE standard sky (morning clear sky)

SKY LUMINANCE



Type 12 CIE STANDARD CLEAR SKY, LOW LUMINANCE TURBIDITY



CIE STANDARD CLEAR SKY, POLLUTED ATMOSPHERE

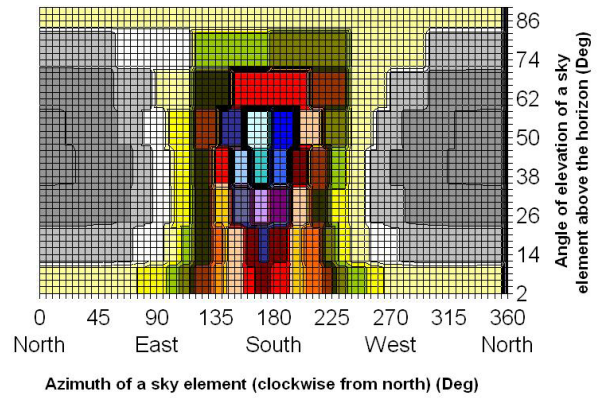
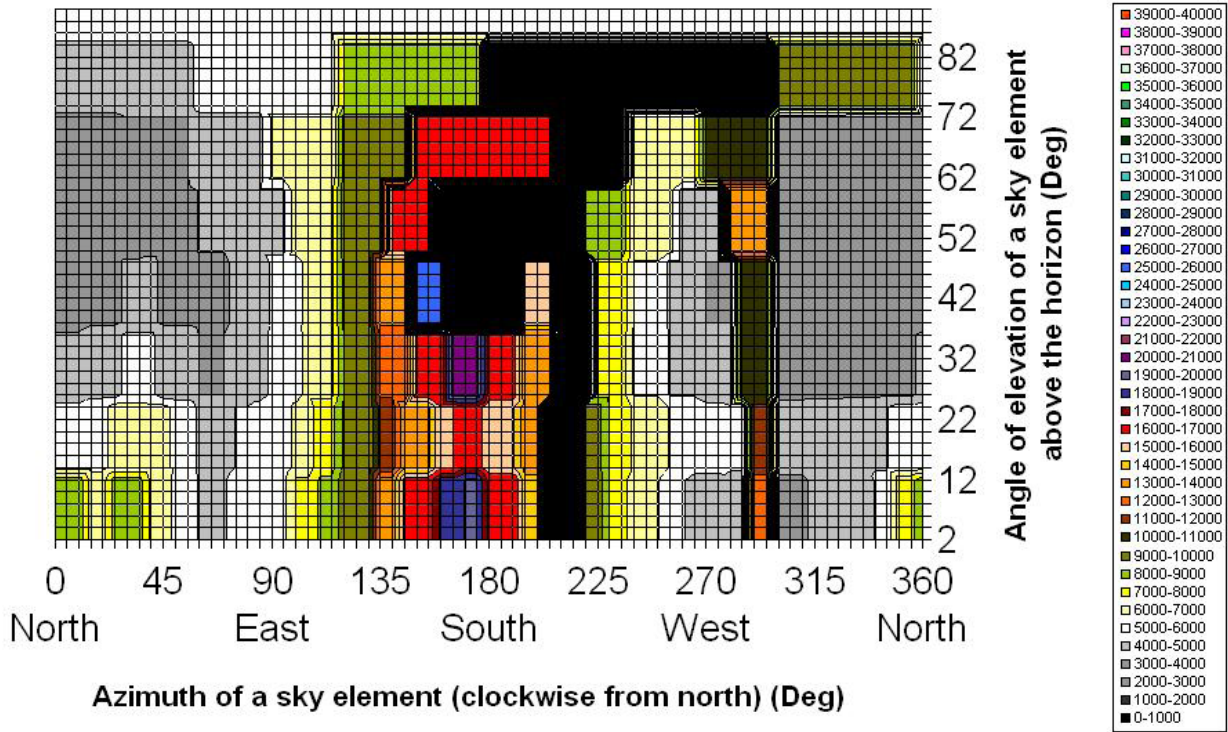


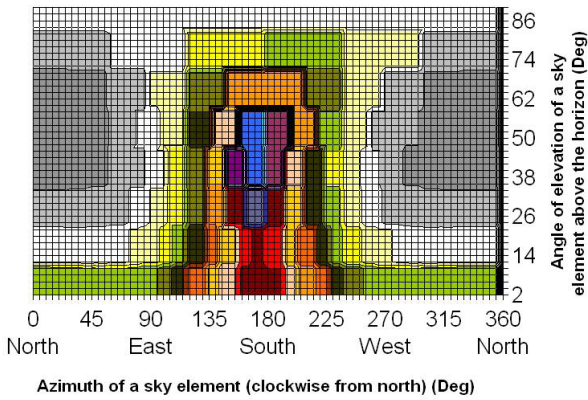
Fig. 4.24
Graphic comparison of real sky luminance observed for the double glazing (midday clear sky) with CIE standard skie

SKY LUMINANCE

106



Type 12 CIE STANDARD CLEAR SKY, LOW LUMINANCE TURBIDITY



CIE STANDARD CLEAR SKY, POLLUTED ATMOSPHERE

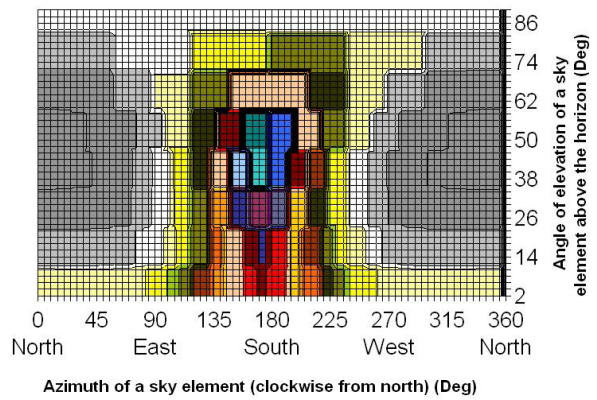
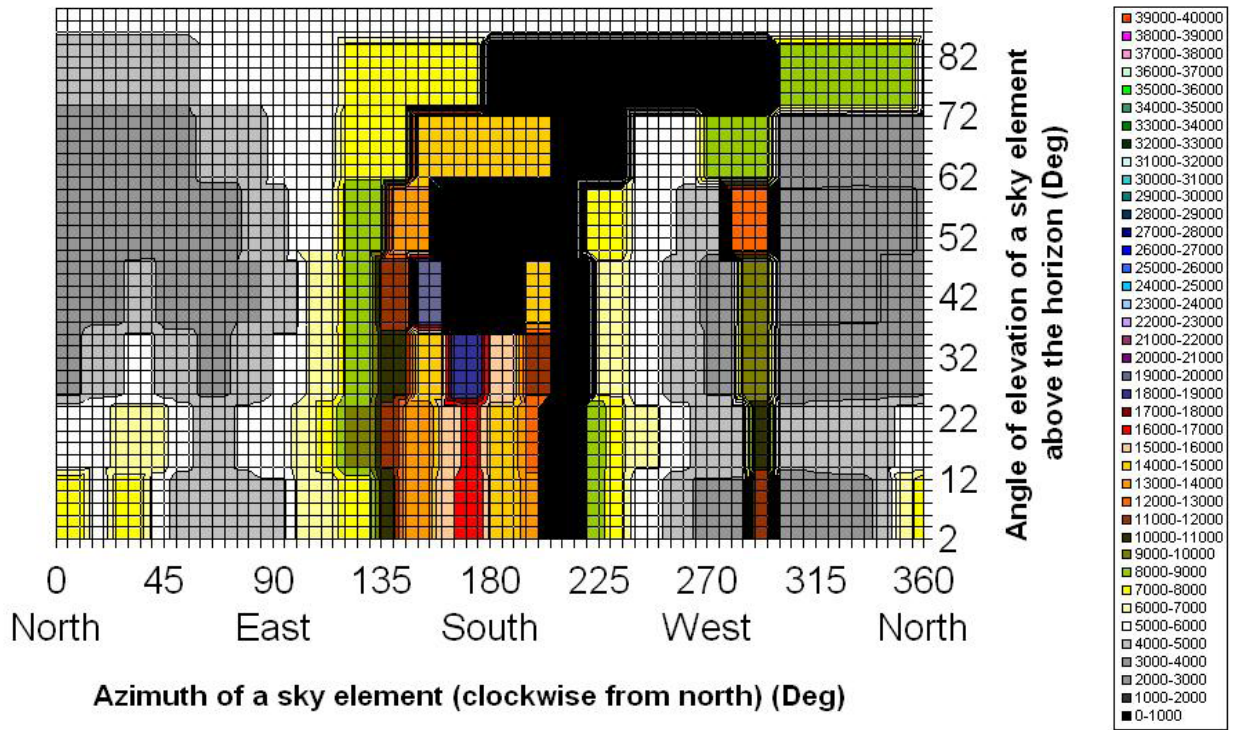
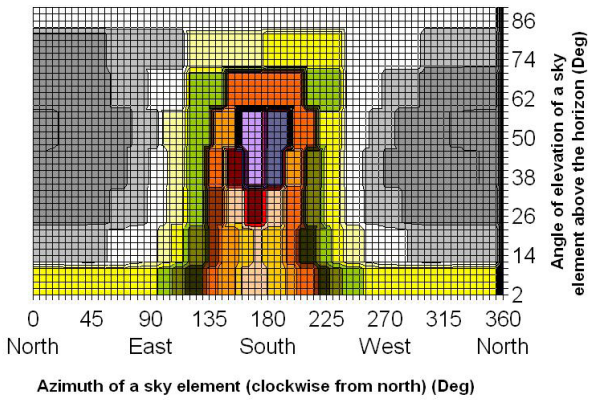


Fig. 4.25
Graphic comparison of real sky luminance observed for the Laser-cut panel (midday clear sky) with CIE standard skies

SKY LUMINANCE



Type 12 CIE STANDARD CLEAR SKY, LOW LUMINANCE TURBIDITY



CIE STANDARD CLEAR SKY, POLLUTED ATMOSPHERE

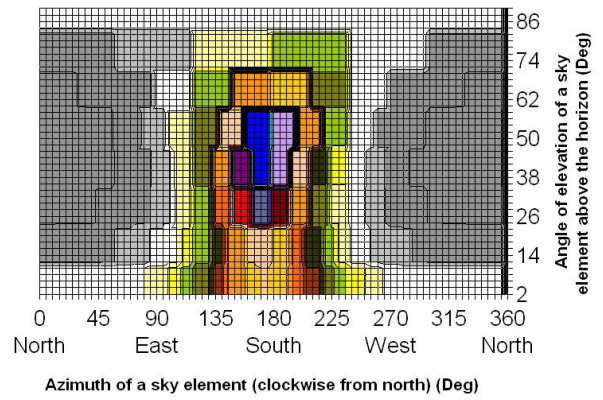


Fig. 4.26
Graphic comparison of real sky luminance observed for the Prismatic film (midday clear sky) with CIE standard skies

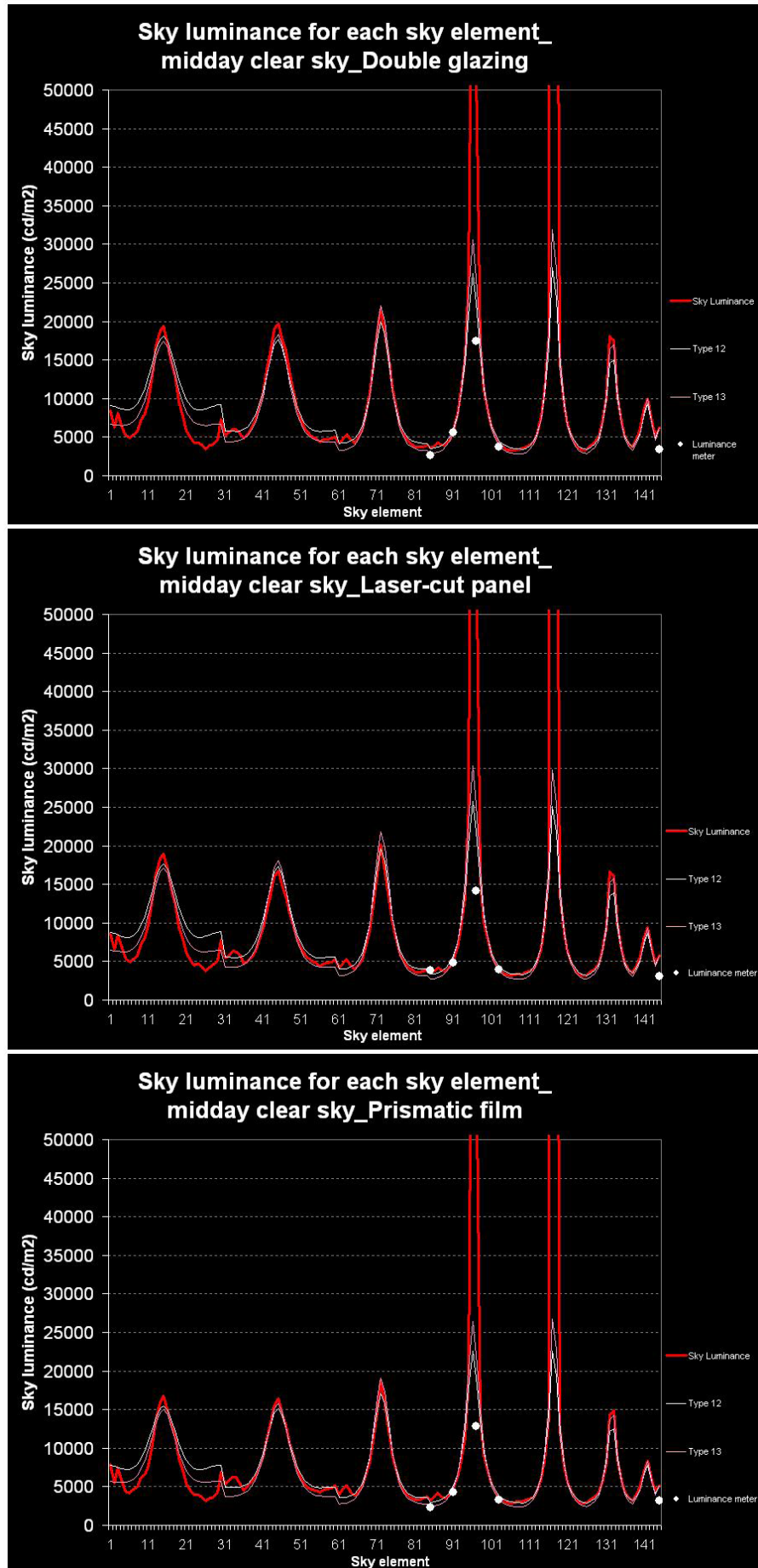
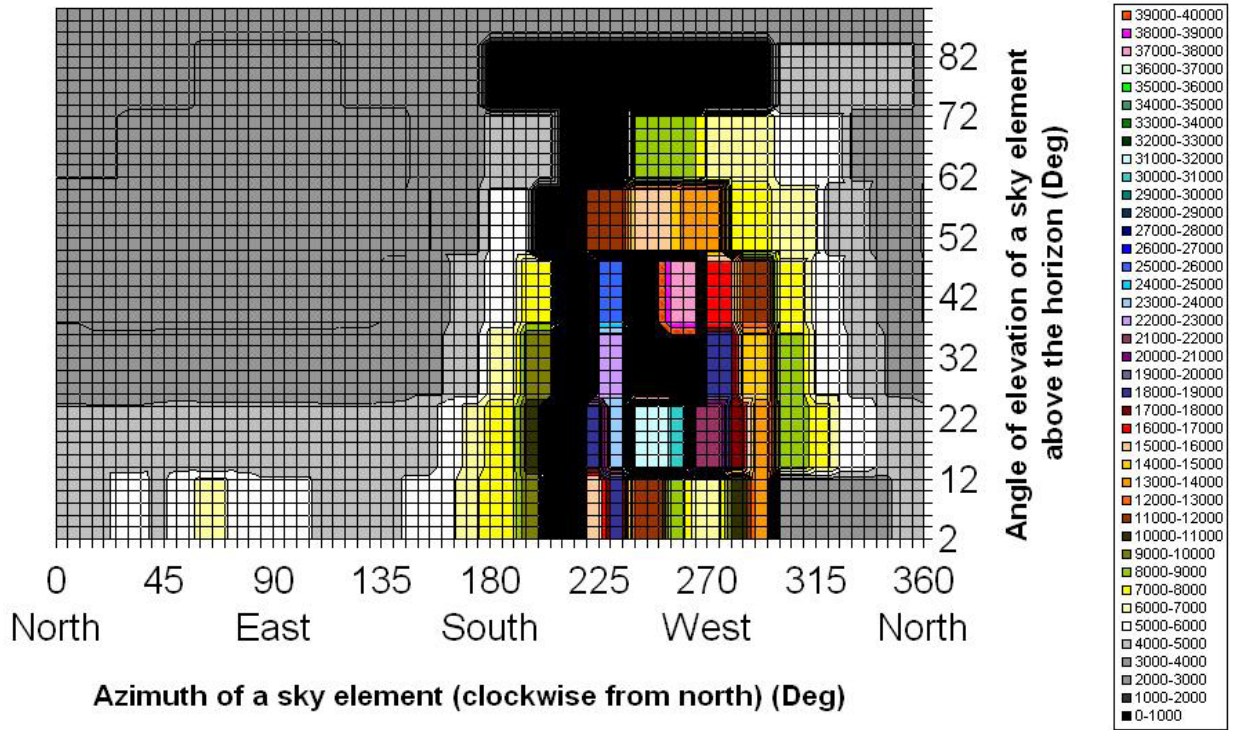
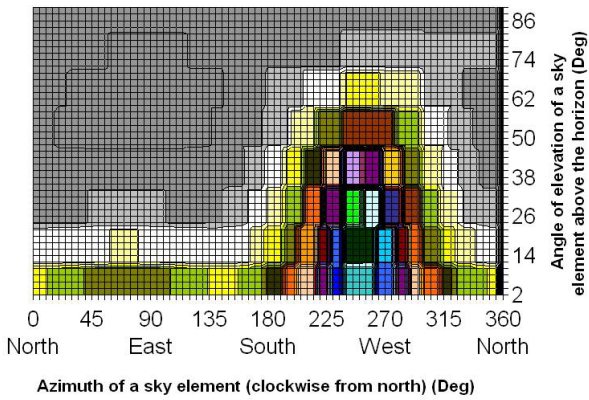


Fig. 4.27
Diagrams comparing the 145 sky sectors of measured skies to the corresponding CIE standard sky (midday clear sky)

SKY LUMINANCE



Type 12 CIE STANDARD CLEAR SKY, LOW LUMINANCE TURBIDITY



CIE STANDARD CLEAR SKY, POLLUTED ATMOSPHERE

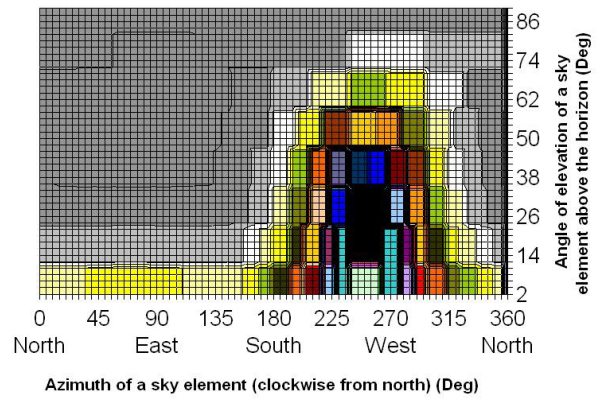
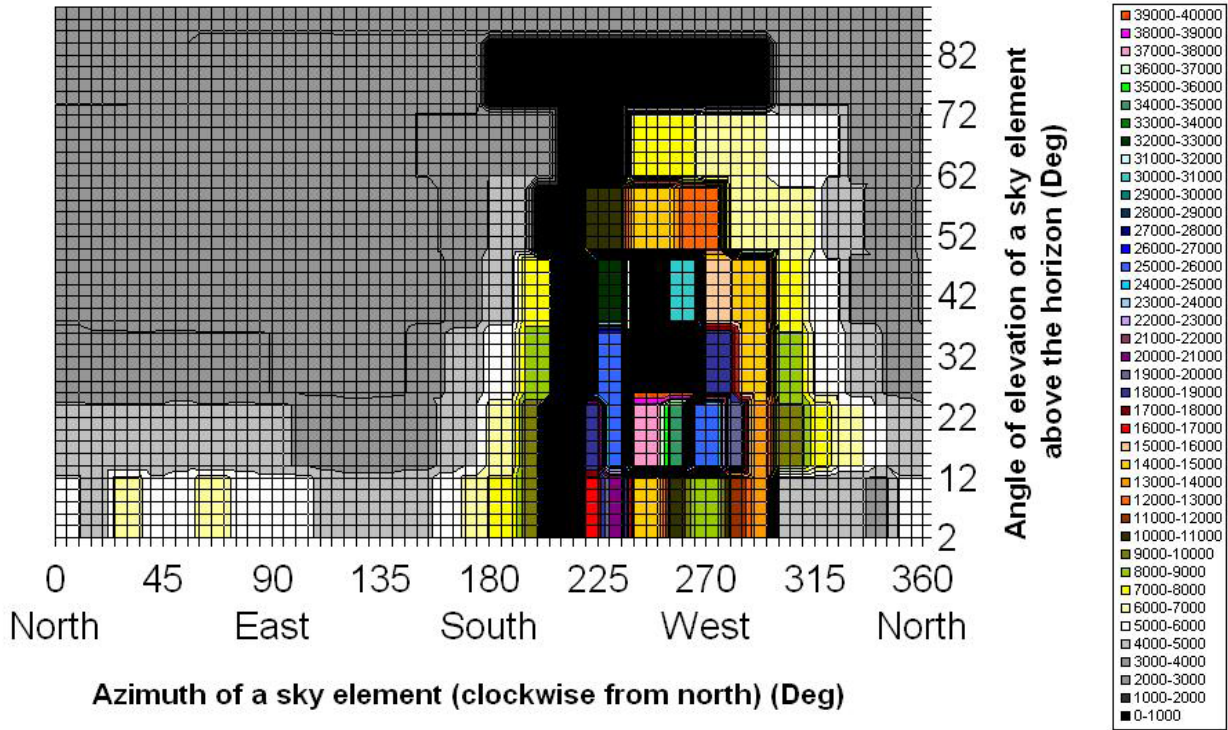


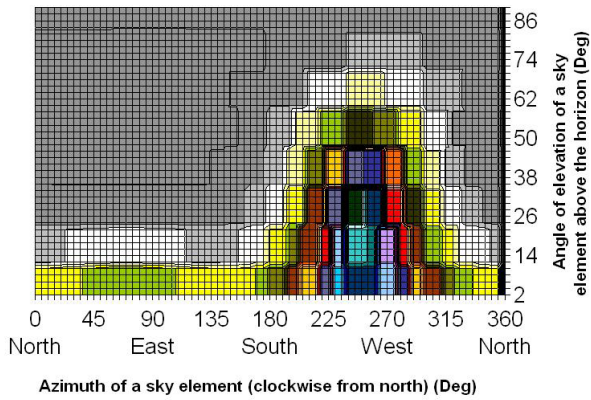
Fig. 4.28
Graphic comparison of real sky luminance observed for the double glazing (afternoon clear sky) with CIE standard skies

SKY LUMINANCE

110



Type 12 CIE STANDARD CLEAR SKY, LOW LUMINANCE TURBIDITY



CIE STANDARD CLEAR SKY, POLLUTED ATMOSPHERE

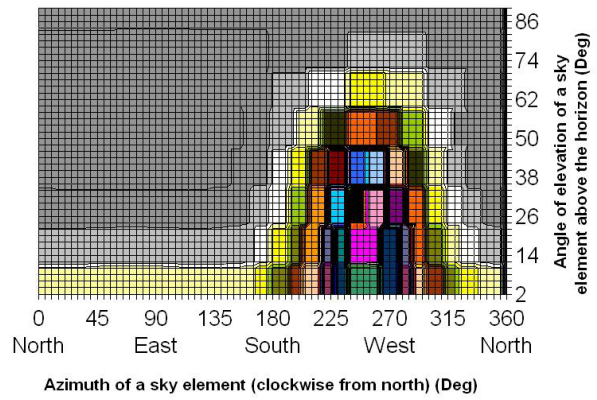
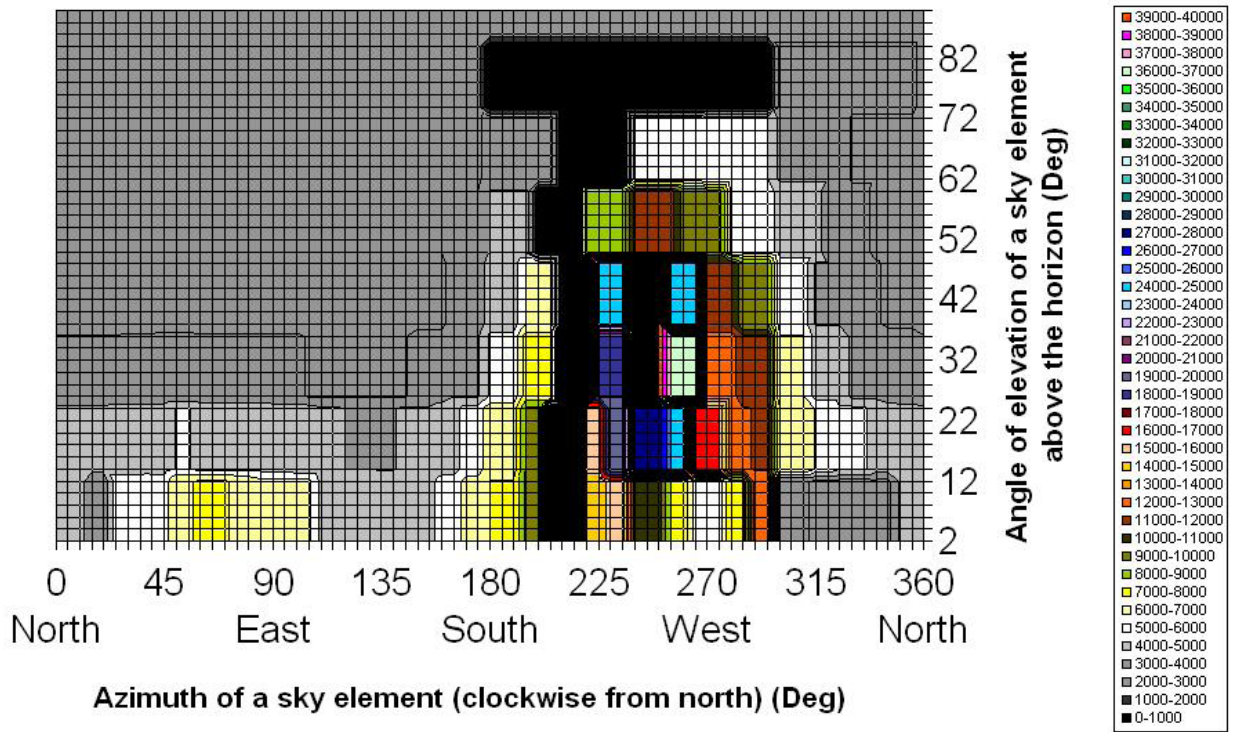
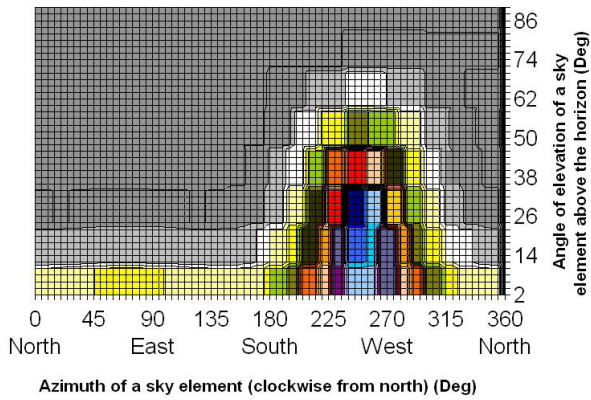


Fig. 4.29
Graphic comparison of real sky luminance observed for the Laser-cut panel (afternoon clear sky) with CIE standard skies

SKY LUMINANCE



Type 12 CIE STANDARD CLEAR SKY, LOW LUMINANCE TURBIDITY



CIE STANDARD CLEAR SKY, POLLUTED ATMOSPHERE

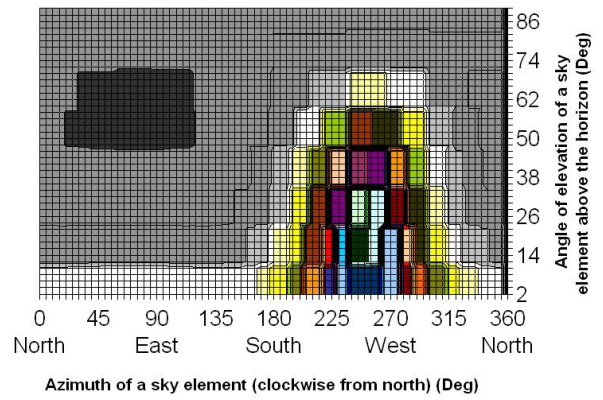


Fig. 4.30
Graphic comparison of real sky luminance observed for the Prismatic film (afternoon clear sky) with CIE standard skies

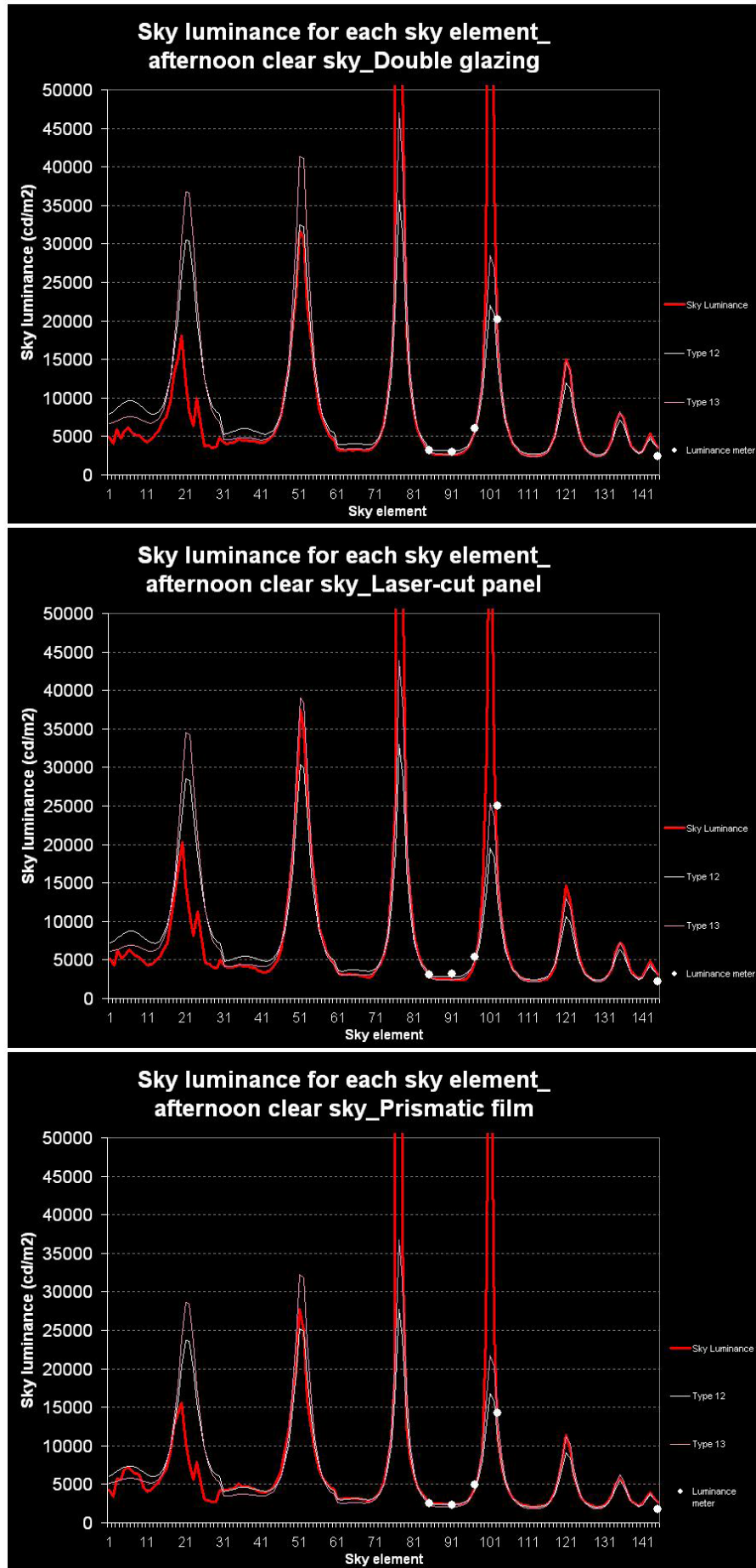


Fig. 4.31
Diagrams comparing the 145 sky sectors of measured skies to the corresponding CIE standard sky (afternoon clear sky)

Sky luminance distribution

On each occasion the sky luminance distribution of the sky vault was monitored using the digital sky scanner. This was to ensure the daylighting simulation of the following step would be as close to reality as possible. The sky luminance distributions are shown in Figure 4.19.

Comparison of real skies with CIE standard skies

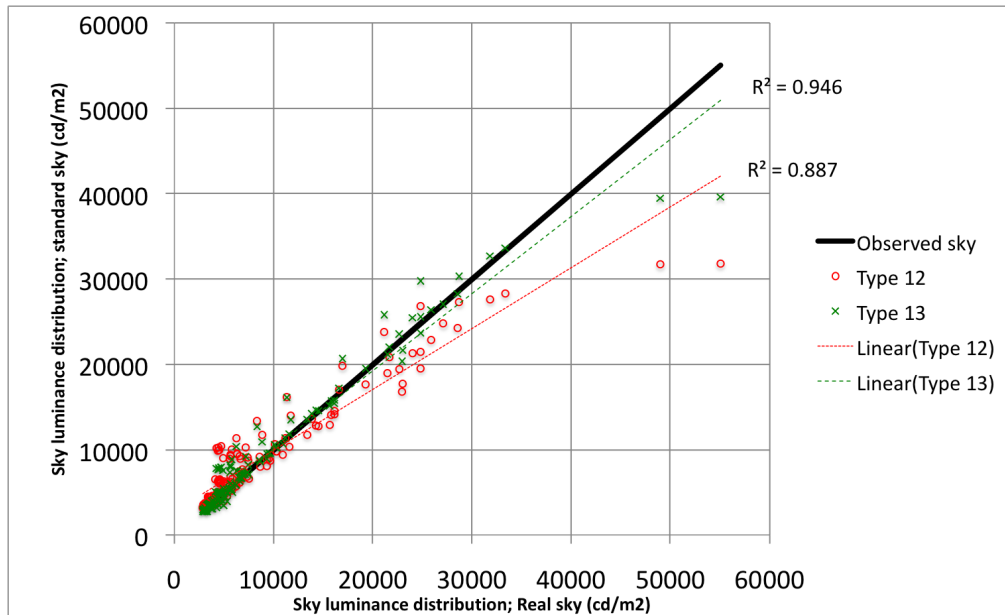
After comparison (Fig. 4.20 - 4.31), a CIE standard sky Type 12 (clear sky, low luminance turbidity) and a CIE standard sky Type 13 (clear sky, polluted atmosphere) were found to be the closest to the observed real sky. The R-square regression method was used to analyse the real skies with more details. Fig. 4.32, 4.33 and 4.34 present the scattering diagrams which show how each real sky compared to CIE standard skies (Types 12 and 13).

From these measured sky luminances it became apparent that Type 13 (clear sky, polluted atmosphere) was the closest to reality for all systems.

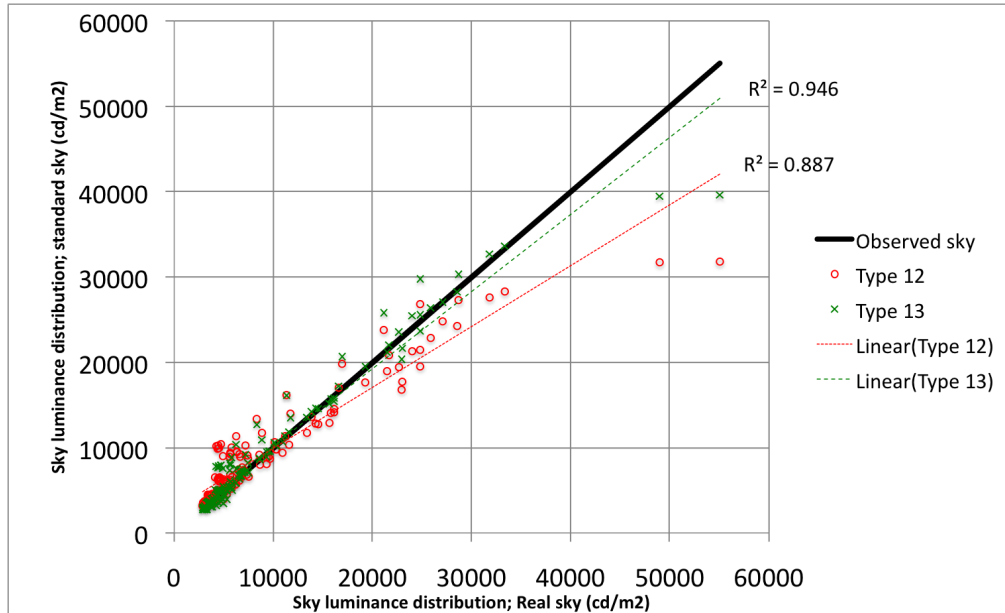
	Morning clear sky			Midday clear sky			Afternoon clear sky		
	Double glazing	LCP	Prismatic film	Double glazing	LCP	Prismatic film	Double glazing	LCP	Prismatic film
Most similar standard sky	Type 13 (clear sky, polluted atmosphere)								

Table 4.11
The CIE standard skies that were most similar to the real clear skies

A
Morning
clear
sky#A



B
Morning
clear
sky#B



C
Morning
clear
sky#C

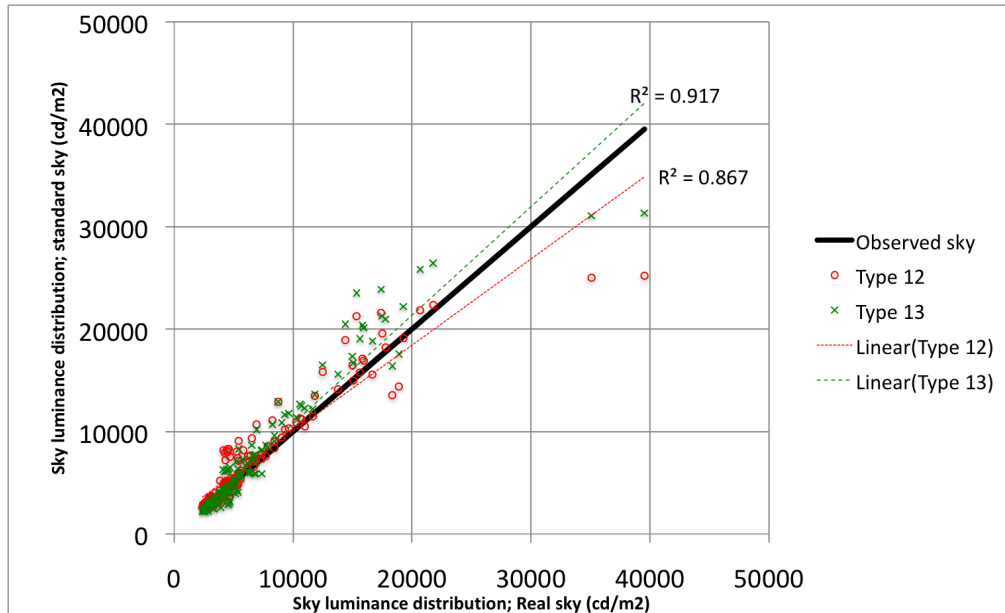


Fig. 4.32
Scattering diagram
for comparison of
luminance distribution
of morning clear
sky#A, #B and #C

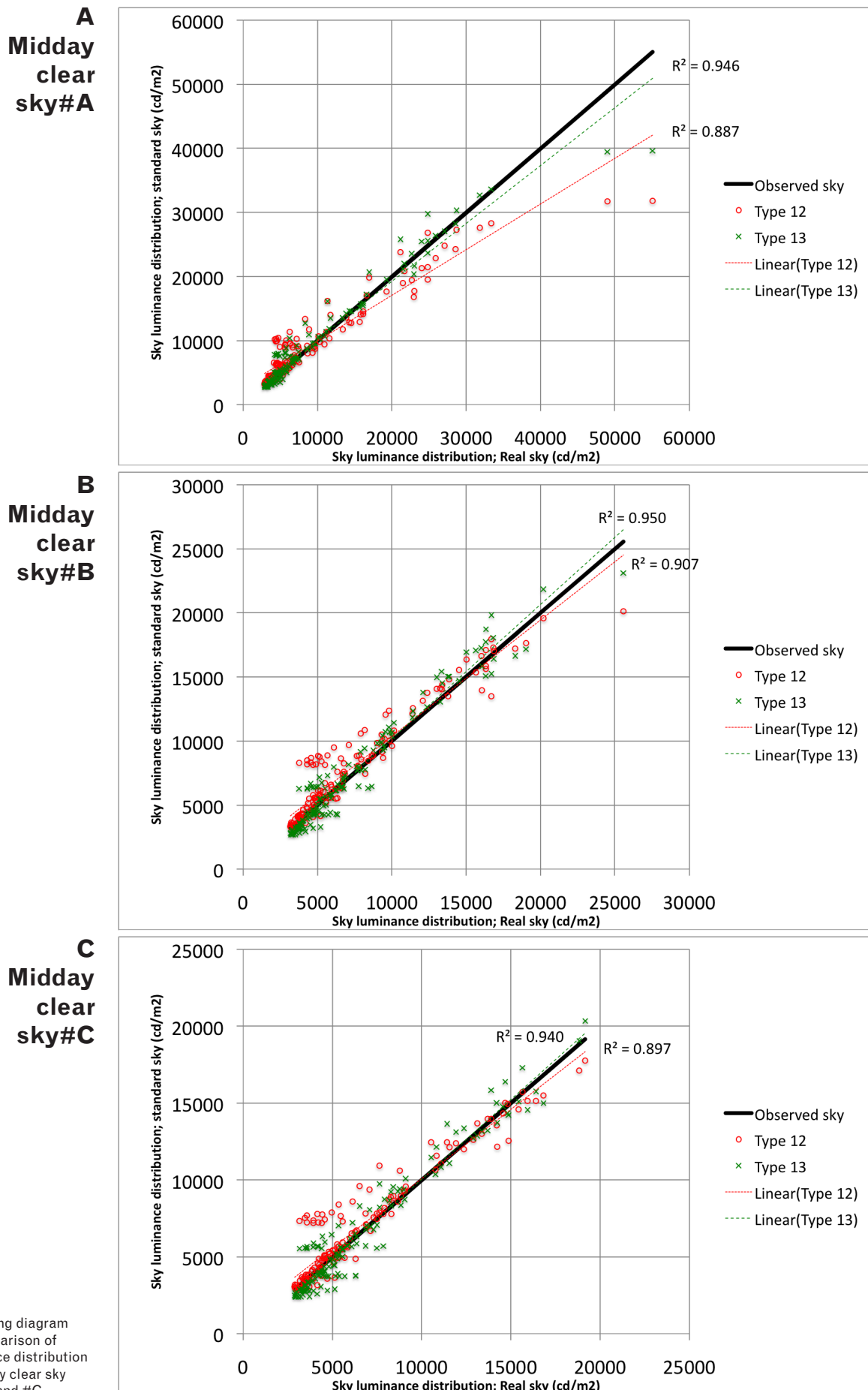
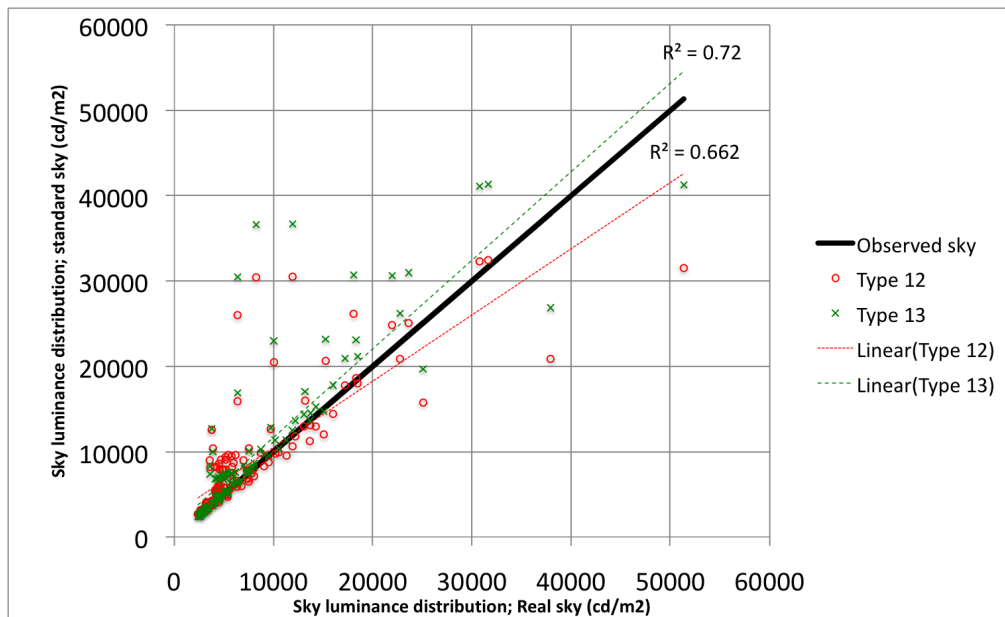
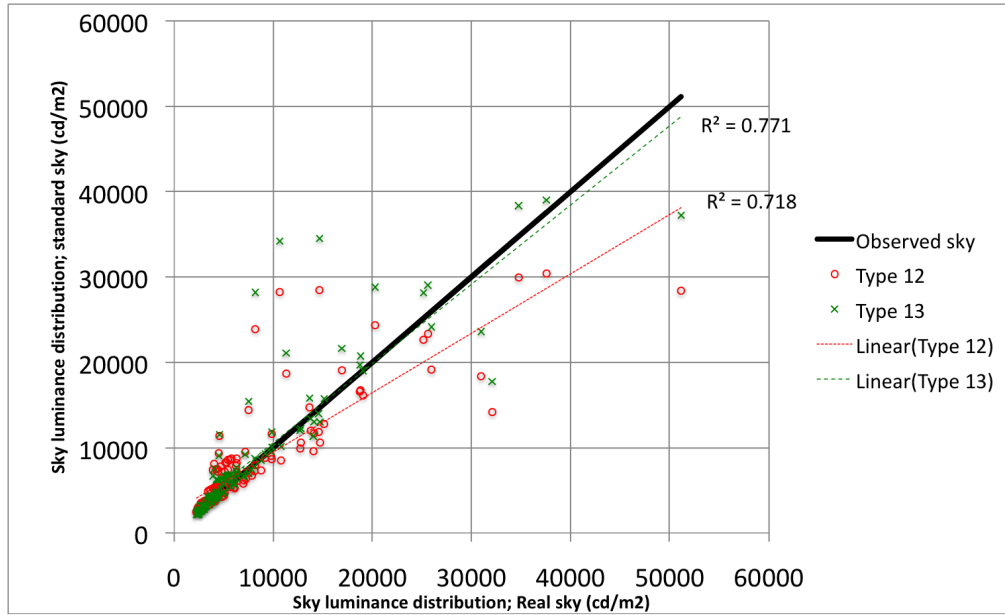


Fig. 4.33
Scattering diagram for comparison of luminance distribution of midday clear sky #A, #B and #C

A
Afternoon
clear
sky#A



B
Afternoon
clear
sky#B



C
Afternoon
clear
sky#C

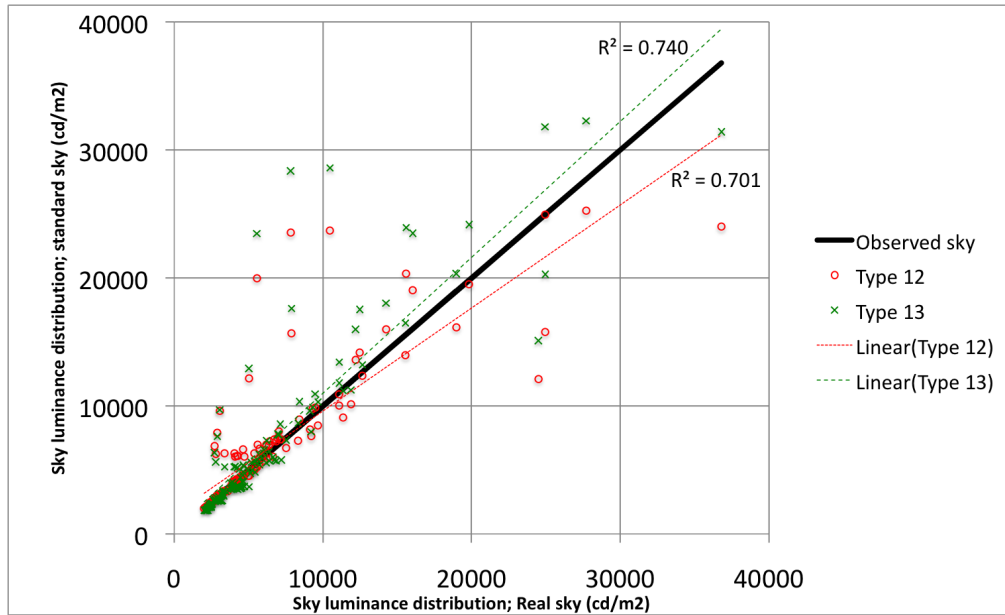


Fig. 4.34
Scattering diagram
for comparison of
luminance distribution
of afternoon clear sky
#A, #B and #C

Daylighting simulation for clear sky

Daylighting simulations of clear sky in the morning, at midday and in the afternoon for Cases B, D and E are presented in Tables 4.12, 4.13 and 4.14 respectively.

Morning clear sky

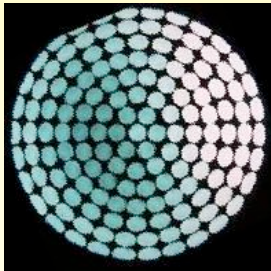
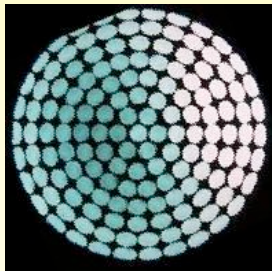
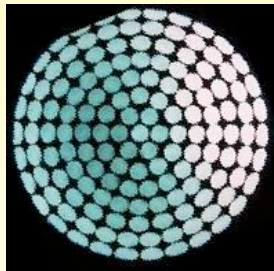
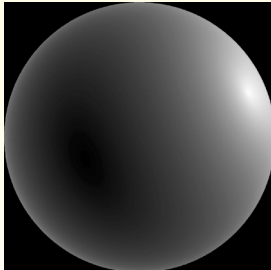
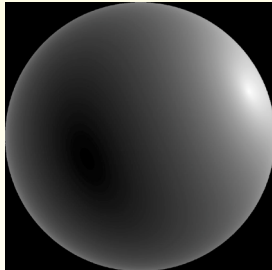
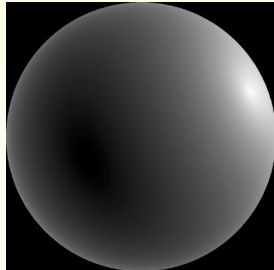
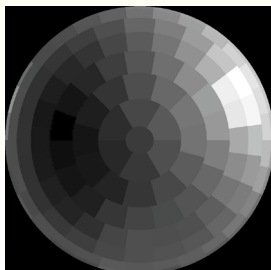
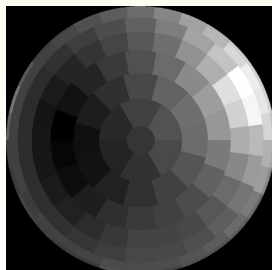
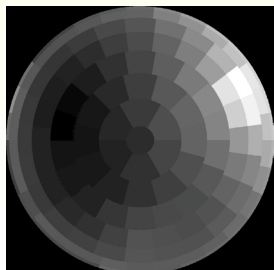
	Double glazing	Laser Cut Panel (LCP)	Prismatic Film
Scanning sky simulator CIE standard sky (Case B)			
Radiance CIE standard sky (Case D)			
Radiance+Partial daylight factor method (Case E)			

Table 4.12
Daylight simulations of Cases B, D and E (morning clear sky)

Midday clear sky

118

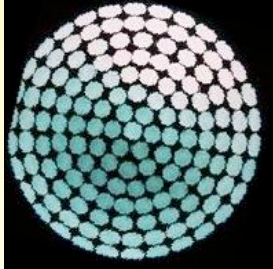
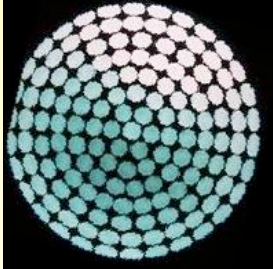
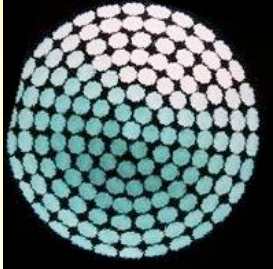
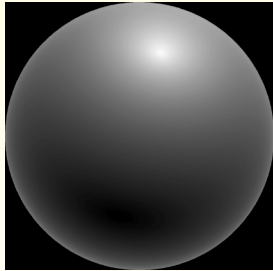
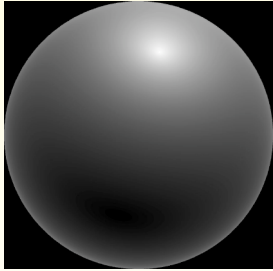
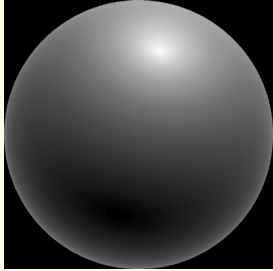
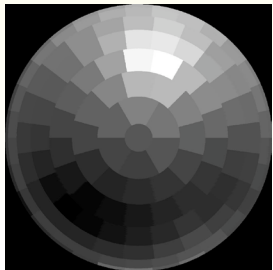
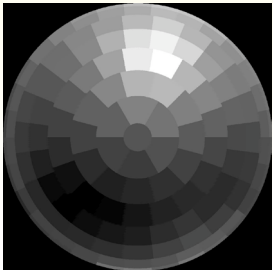
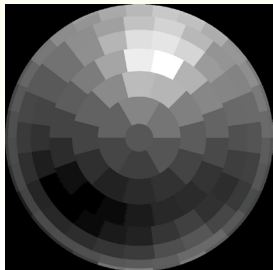
	Double glazing	Laser Cut Panel (LCP)	Prismatic Film
Scanning sky simulator CIE standard sky (Case B)			
Radiance CIE standard sky (Case D)			
Radiance+Partial daylight factor method (Case E)			

Table 4.13
Daylight simulations of Cases B, D and E (midday clear sky)

Afternoon clear sky

119

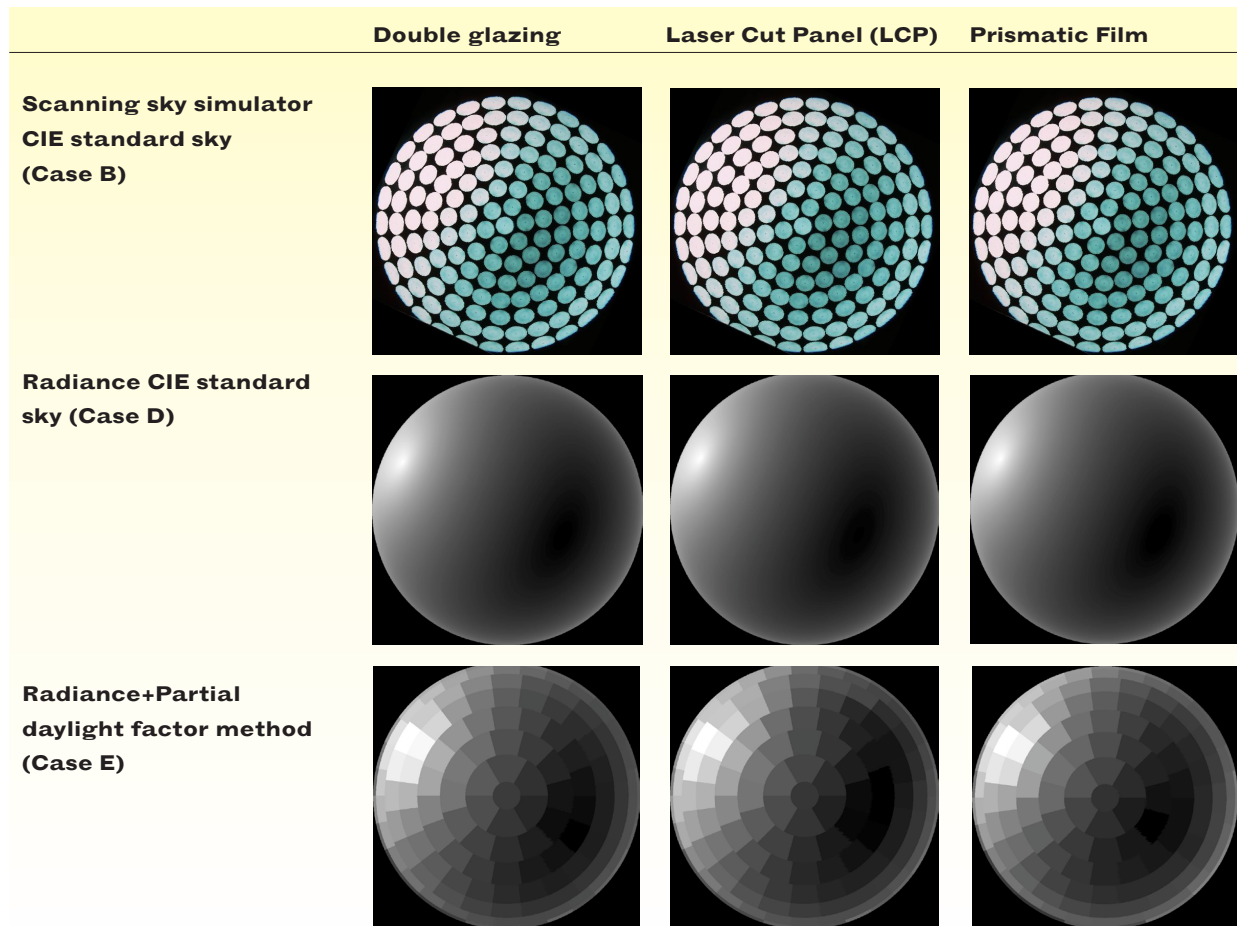


Table 4.14
Daylight simulations of Cases B, D and E (afternoon clear sky)

In Case B (1:10 scale model under scanning sky simulator), the CIE standard sky Type 13 (clear sky, polluted atmosphere) was used. However comparison by computer simulation with Type 12 and 13 skies has shown there is no significant difference between them (details in Appendix C).

The daylighting simulations of Case C (1:10 scale model using scanning sky simulator and the PDF method) cannot be presented graphically simulations, being done by the way of calculations.

The daylighting simulations of Cases D and E (virtual model using the Radiance GenSky program) were based on the CIE standard clear sky (Type 12) for all fenestration systems in order to facilitate the simulations. However comparison by computer simulation with sky Types 11, 12 and 13 has shown there is no significant difference between them (details in Appendix C).

4.3 Discrepancies in daylight factor (DF) or illuminance ratio (IR)

Inexact modelling and an injudicious choice of daylighting simulation can be primary sources of errors in daylighting performance assessment. To identify other sources of error, measurements of the real building, necessarily the most precise case, were compared with those of the models. Differences in daylight factor (DF) and illuminance ratio (IR) were analysed and afterwards used to identify error sources in daylighting performance assessment.

As described above, the comparisons were made under both overcast and clear sky conditions. Three fenestration systems were used for the evaluations.

	Sky condition	Window system
1.	Overcast sky	Double glazing
2.	Overcast sky	Laser cut panel
3.	Overcast sky	Prismatic film
4.	Morning clear sky	Double glazing
5.	Morning clear sky	Laser cut panel
6.	Morning clear sky	Prismatic film
7.	Midday clear sky	Double glazing
8.	Midday clear sky	Laser cut panel
9.	Midday clear sky	Prismatic film
10.	Afternoon clear sky	Double glazing
11.	Afternoon clear sky	Laser cut panel
12.	Afternoon clear sky	Prismatic film

Table 4.15
List of all assessments
made in the study

In this study the discrepancies that were found during assessment are given as relative divergence, calculated by :

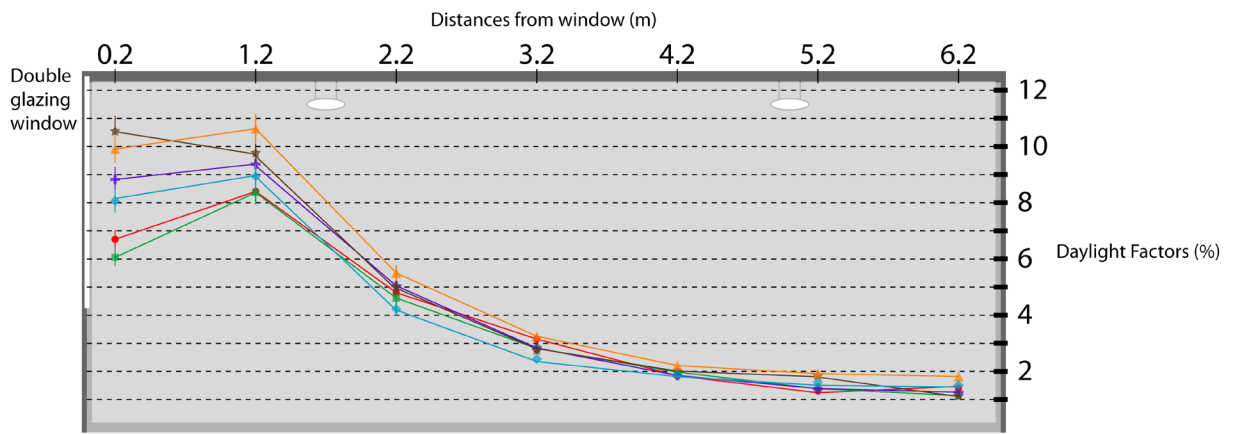
$$R = \frac{\text{Difference of DF or IR between real building and model} \times 100 (\%)}{\text{DF or IR of the real building}}$$

Where R is the relative divergences given in percentage.

Comparison of the daylight factor (DF) of the real building and its models under overcast sky conditions

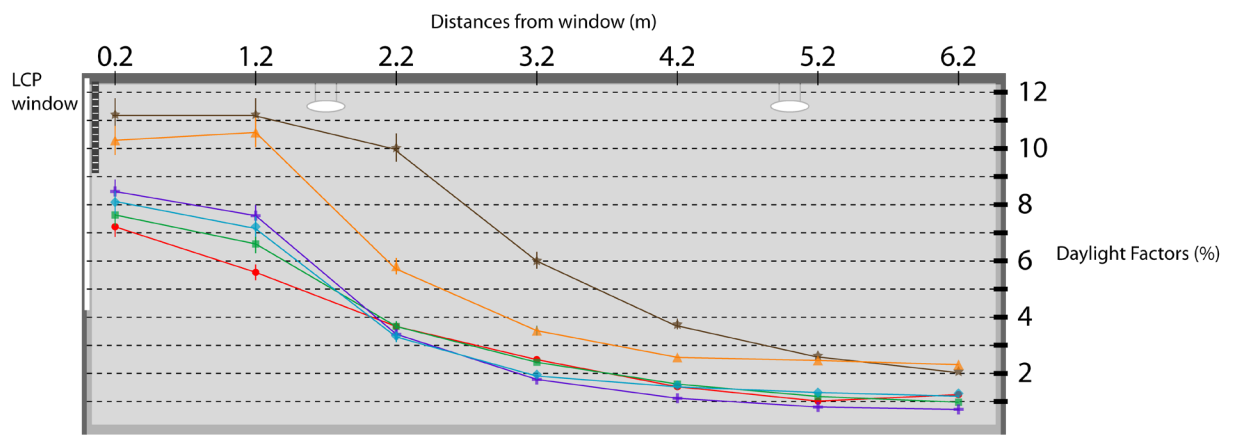
Fig. 4.35, 4.36 and 4.37 present the DF assessment under overcast sky conditions of the models when equipped with double glazing, Laser cut panel and Prismatic film respectively.

Fig. 4.38 and 4.39 present the relative divergences of each model when compared with the daylight factor of the real building.



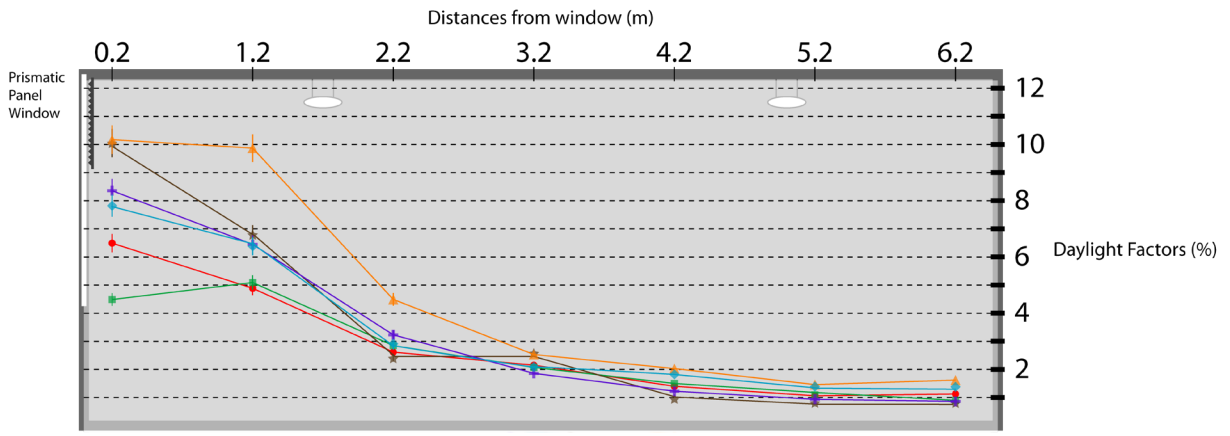
	0.2	1.2	2.2	3.2	4.2	5.2	6.2	
Real Building	6.68	8.41	4.80	3.15	1.84	1.31	1.40	Real Building
Case A	6.06	8.36	4.61	2.82	1.98	1.39	1.14	Case A
Case B	8.06	8.94	4.22	2.44	1.89	1.61	1.51	Case B
Case C	9.91	10.63	5.50	3.25	2.21	1.92	1.82	Case C
Case D	8.83	9.37	5.05	2.83	1.86	1.39	1.26	Case D
Case E	10.56	9.79	5.05	2.76	2.02	1.86	1.14	Case E

Fig. 4.35 Daylight factor (DF) assessment of the models equipped with double glazing under overcast sky conditions



	0.2	1.2	2.2	3.2	4.2	5.2	6.2	
Real Building	7.21	5.60	3.67	2.49	1.52	1.15	1.24	Real Building
Case A	7.64	6.60	3.67	2.39	1.62	1.18	0.98	Case A
Case B	8.09	7.22	3.33	1.96	1.58	1.32	1.29	Case B
Case C	10.29	10.57	5.81	3.52	2.57	2.46	2.31	Case C
Case D	8.47	7.61	3.40	1.79	1.12	0.80	0.72	Case D
Case E	11.23	11.23	10.03	6.03	3.76	2.65	2.08	Case E

Fig. 4.36 Daylight factor (DF) assessment of the models equipped with Laser cut panel under overcast sky conditions



	Daylight Factors (%)							
◆	6.49	4.88	2.61	2.15	1.40	1.06	1.13	Real Building
■	4.49	5.09	2.85	2.07	1.50	1.09	0.90	Case A
▲	7.82	6.38	2.91	2.09	1.82	1.39	1.38	Case B
▲	10.17	9.87	4.49	2.53	2.03	1.46	1.62	Case C
✕	8.35	6.45	3.23	1.86	1.23	0.93	0.87	Case D
✕	10.05	6.79	2.40	2.57	0.96	0.81	0.81	Case E

Fig. 4.37 Daylight factor (DF) assessment of the models equipped with prismatic film under overcast sky conditions

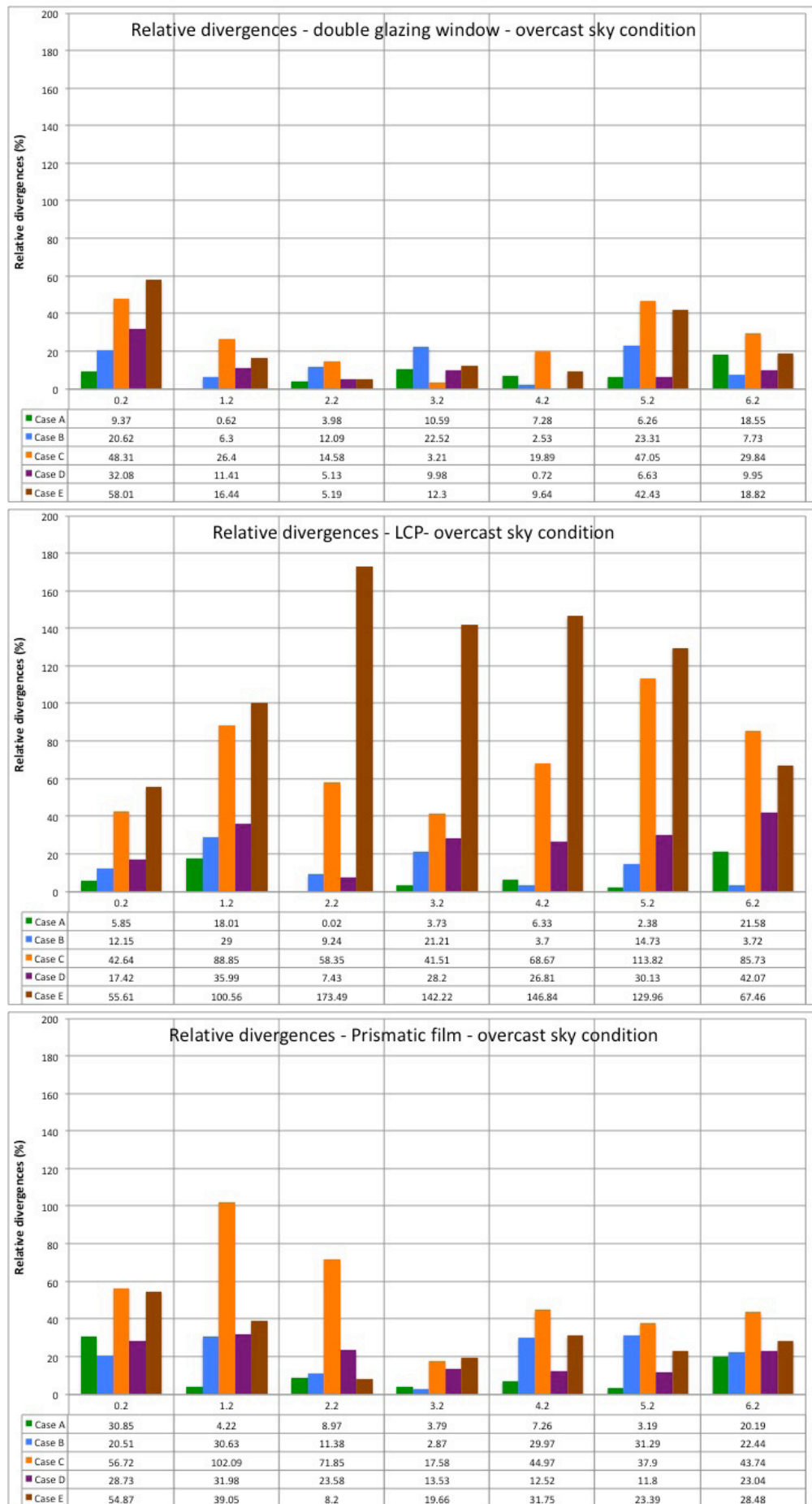


Fig. 4.38 Relative divergences of the models when compared with the DF of the real building under overcast sky conditions

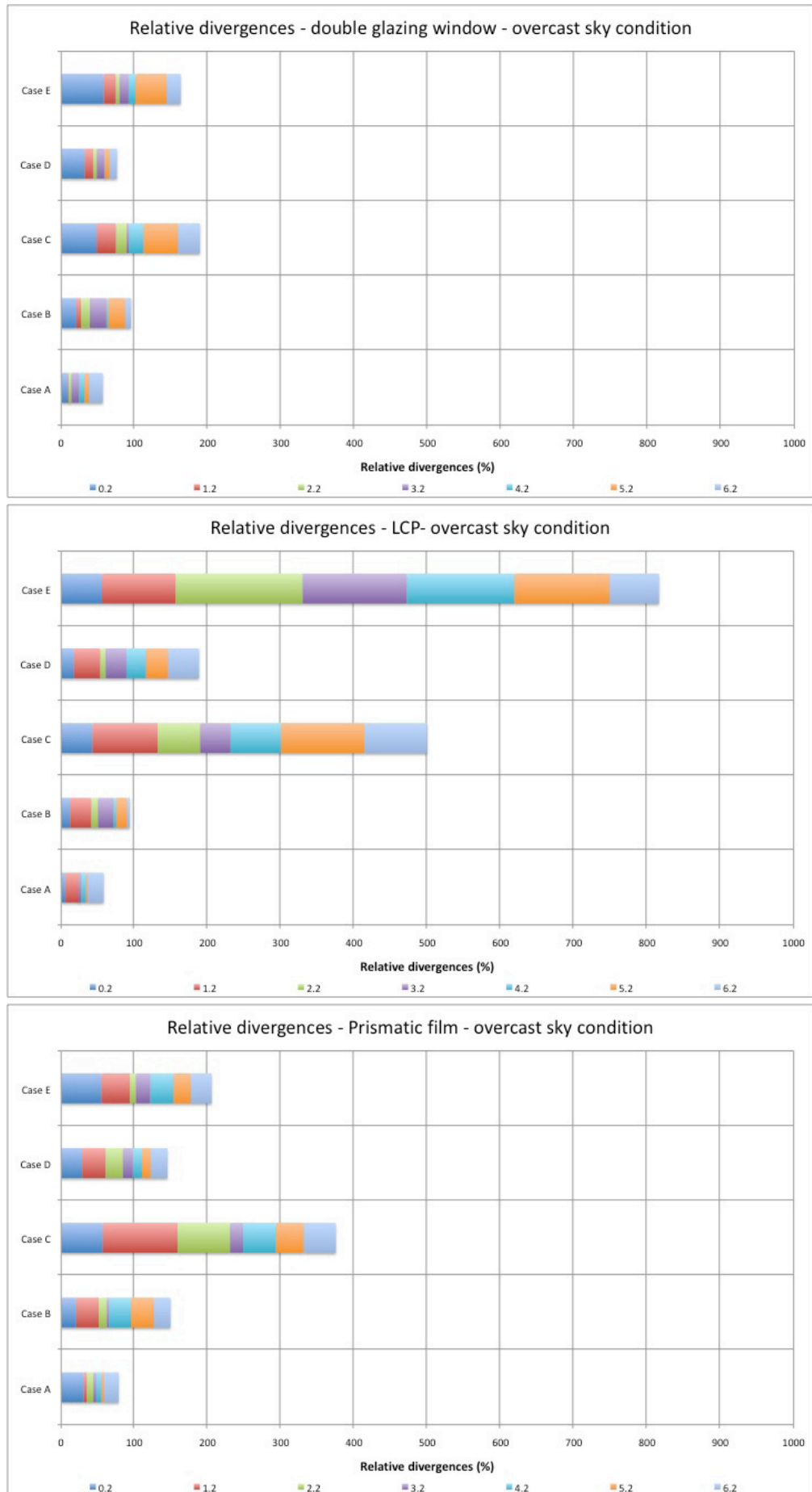


Fig. 4.39 Overall relative divergences of the models when compared with the DF of the real building under overcast sky conditions

Daylight factors and relative divergences of the models : Cases A, B, C, D and E

- The DF of **Case A** (1:10 scale model, real sky) was the closest to reality. Most of the relative divergences of this case were lower than 20 % (Fig. 4.38); the sum of the relative divergences was less than 80 % (Fig. 4.39). The larger error at the measured point near the window is due to an error of detail in the scale model, while the error in the deeper part of the room is probably due to surface reflectance.

- Daylight evaluation in **Case B** (scale model, sky simulator) showed overestimation for the double glazing window, but underestimation for the CFS when the measured points were located away from the window (Fig. 4.35, 4.36 and 4.37). 'Overestimation' here means the model suggested more daylight would fall in the interior than was actually observed in the real building. Relative divergences were less than 30 % at most points (Fig. 4.38); the sum of the divergences was less than 150 % (Fig. 4.39). Errors over and above those of Case A can be explained by the difference between the real sky luminance distribution and that of the CIE standard sky used in the sky simulator or the computer models.

- **Case C** (scale model, sky simulator, partial daylight factor method) presented the greatest overestimation - up to 120 % - particularly in CFS evaluation (Fig. 4.38). These errors can be attributed to the PDF method using the average sky luminance distribution. When the corresponding values were introduced into the scanning sky simulator to outline this fact, this made the sky elements appear brighter. The sum of the divergences was as large as 180 to 500% (Fig. 4.39).

- **Case D** (virtual model, simulated standard sky) was similar to Case B. The main errors were due to the CFS simulation technique and the standard sky used differing from the real sky. Relative divergences were less than 45% (Fig. 4.38) and total relative divergences less than 190% (Fig. 4.39).

- **Case E** (virtual model, simulated standard sky, partial daylight factor method) performed very like Case C as it used the same sky data and procedure from the sky scanner. However, the evaluation of the CFS - especially LCP - gave greater errors due to the CFS simulation technique. Relative divergences were below 60% when assessing double glazing and prismatic film and less than 180% for LCP (Fig. 4.38). The total relative divergences fell in the range of 160 to 820 % (Fig. 4.39).

Potential sources of error in daylighting performance assessment under overcast sky conditions

Looking at the above daylight factor profiles for the three fenestration systems, one sees that those involving the double glazing window are all fairly similar (Fig. 4.35). The divergences of each case compared with the real building measured less than 60%. It shows that for an uncomplicated window system such as double glazing the daylight performance assessment under overcast sky conditions is easier to achieve. An accurate simulation can be made, particularly if a comparable overcast real sky is available. In other double glazing situations the daylight simulation of a CIE standard sky condition (using the Radiance GenSky function or a scanning sky simulator) is relatively accurate.

Fig. 4.40 compares a single, sky element under an overcast sky. The sky images (Fig. 4.40a) show that even on an individual sky element inexactitude in its luminous property can have great impact on the daylight evaluation. The scanning sky simulator (Fig. 4.40b) can only simulate a uniform sector for this sky element; **both Radiance simulations (Fig. 4.40c and 4.40d) present luminous properties differing from those of the real sky.** However, in two last cases the differences cannot easily be seen because adjacent sky elements have very similar luminance values.

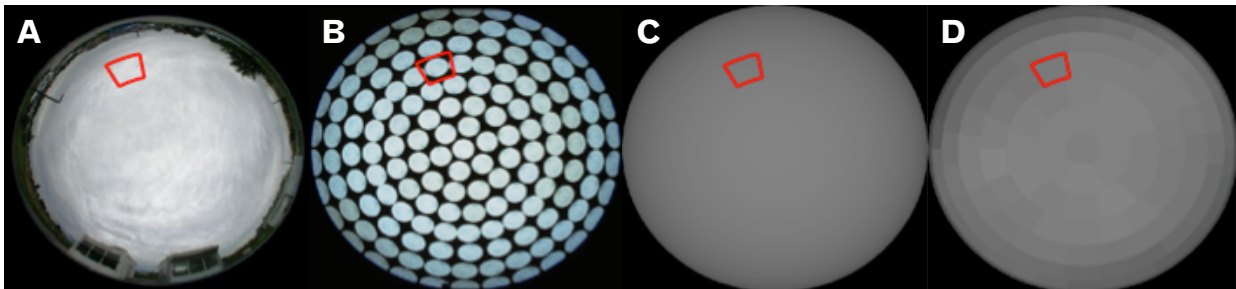


Fig. 4.40 Sky luminance distribution of a single sky element under different sky simulations differs slightly from that of the real overcast sky:
 (a) The considered example element of the real sky shows non-uniform luminance.
 (b) The circular sky sector of the scanning sky simulator has a uniform luminance.
 (c) The continuous luminance distribution of the CIE standard sky in the GenSky function is non-uniform, it has a constant gradient from the horizon (border of the sky vault) to the zenith (center of the sky vault).
 (d) The virtual model using the PDF method generates uniform luminance for the sky element by using the average luminance value measured by the sky scanner

Moreover, the partial daylight factor method (Fig. 4.40d) which, used together with the sky scanner to simulate the luminance distribution of real sky conditions, increases errors because of inexactitude created when averaging the luminance of each sky element (according to Tregenza model). This method appears not to be necessary for either virtual or physical models, if the sky conditions match any of the CIE standard skies which GenSky or a sky simulator can produce, though it is useful when non-standard sky conditions must be used.

When assessing CFS, the complexity of the window system generally brought greater errors. When the assessments were made under real sky, the tendency of the errors was not significantly different for the LCP and only a little more incorrect for prismatic film. This shows that the non-optimal scale at which the CFS is modelled (it cannot be scale down to the 1:10 model scale) is not significant in this case.

As shown in Fig. 4.41b, the effect of the real sky sector (round dashed circle) does not create major errors in the assessment using scale model for the CFS and the double glazing.

The errors were greater for CFS than for double glazing, when the sky simulator was used in the assessment. This can be explained by the fact that when the real sky is used the light flux penetrates the room with a steady gradient; the sky simulator separates the sky vault into 145 discontinuous cir-

cular patches. As seen in Fig. 4.41b, this is sufficiently accurate when simulating a simple window; for CFS any small details impacting on the light redirection can lead to the sensors noting very different daylighting conditions in the room. Fig. 4.41c illustrates the point, which can be particularly significant in the deeper part of the room where additional errors appear if the surface reflectance is relatively different (surface reflectance has an impact because reflected light plays an important role in the deeper parts of the room).

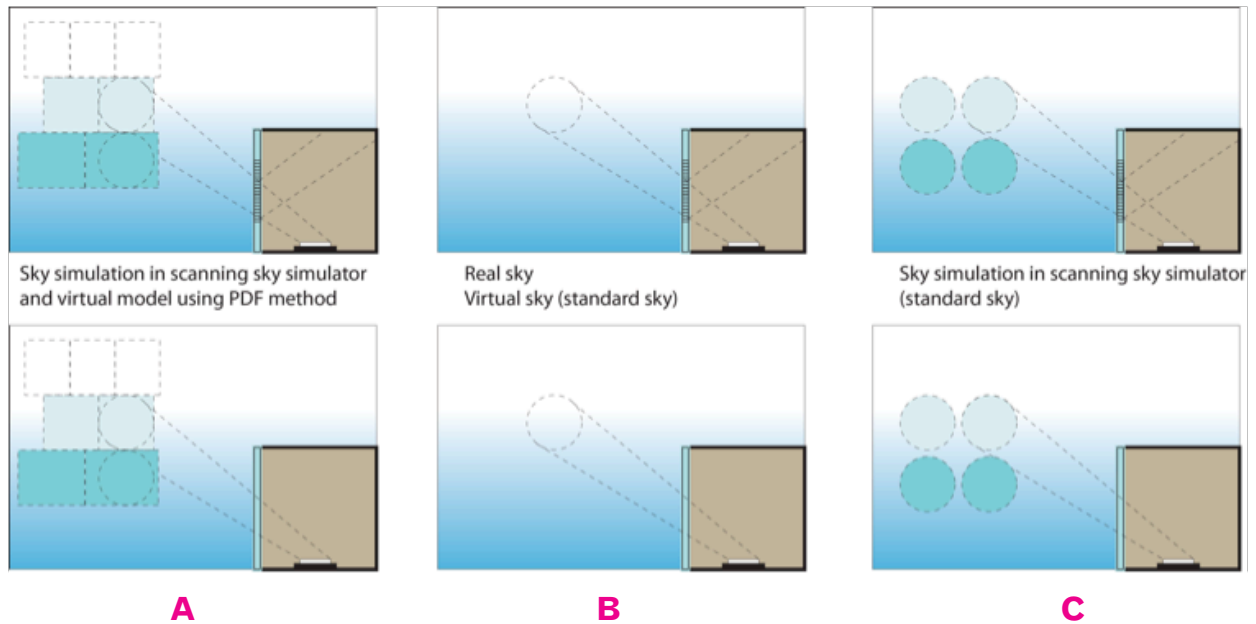


Fig. 4.41 Different daylighting simulations can cause divergent lighting measurements when using a photometric sensor, particularly for CFS systems (upper), less so for simple window (below):

- When attempting to simulate a continuous overcast sky in scale or virtual models using the PDF method (the real sky luminance, measured by the sky scanner and averaged for each sky element, present nonconformant luminous properties).
- Daylight simulation using real sky or a virtual standard sky (continuous sky luminance distribution).
- The scanning sky simulator, reproducing a CIE standard sky, does not reproduce the same sky luminance as measured under the real sky.

An even greater impact was noted when the PDF method was used. Because the sky scanner initially averaged the real sky luminance element (as shown in Fig. 4.41a and 4.40d) and introduced discontinuities in the sky simulator or in Radiance, the errors are greater than with the CIE standard sky produced by the sky simulator or the GenSky function alone. This result can be most clearly seen in the comparison of the scene renderings of the virtual model using a CIE standard sky (GenSky) and the real sky using the PDF method (Fig. 4.42). The PDF method suggests a slightly reduced daylight flux in the deeper parts of the room.

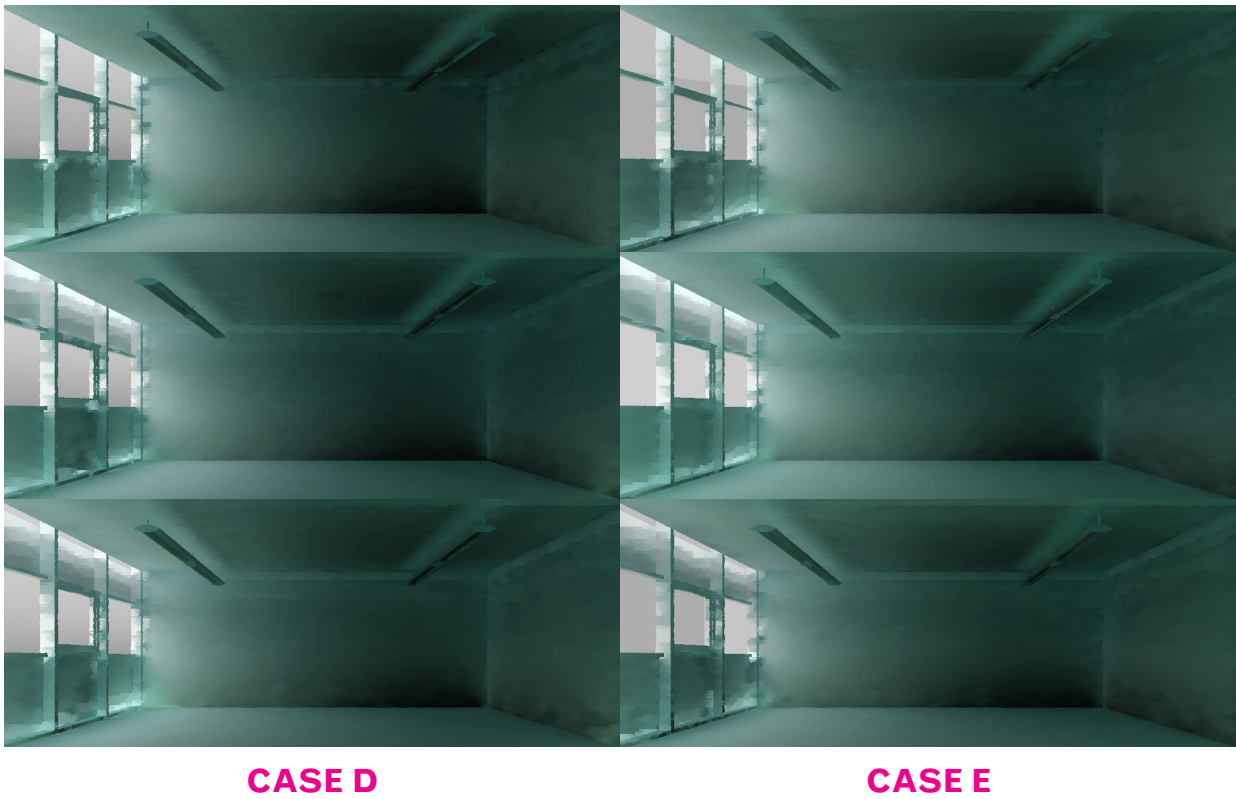


Fig. 4.42 Virtual models created by Radiance to assess double glazing window (upper), Laser cut panel (centre) and prismatic film (below) under overcast sky conditions: (a) Case D (continuous standard sky) and (b) Case E (using PDF on 145 sky zones)

Table 4.16 summarises the potential sources of error that can occur in the assessments for each case.

Potential sources of error			
	Double glazing	Laser cut panel	Prismatic film
Case A	Photometric sensors + model geometry and photometry	Photometric sensors + model geometry and photometry	Photometric sensors + model geometry and photometry
Cases B, C, D, E	Photometric sensors + model geometry and photometry + sky simulation	Photometric sensors + model geometry and photometry + sky simulation + CFS reproduction	Photometric sensors + model geometry and photometry + sky simulation + CFS reproduction

Table 4.16 Potential sources of error in daylighting performance assessment under overcast sky condition

Comparison of the illuminance ratio (IR) of the real building and its models under clear sky conditions

Illuminance ratio were measured under clear sky consitions, comparing the models with the real building, for the 5 study cases, three types of glazing and at three times of day. The results are presented in the following paragraph:

Clear sky conditions	IR Double glazing	IR Laser Cut Panel	IR Prismatic film	IR - relative divergences - all glazing types	Sum of relative divergences - all glazing types
Morning	Fig. 4.43	Fig. 4.46	Fig. 4.49	Fig. 4.52	Fig. 4.55
Midday	Fig. 4.44	Fig. 4.47	Fig. 4.50	Fig. 4.53	Fig. 4.56
Afternoon	Fig. 4.45	Fig. 4.48	Fig. 4.51	Fig. 4.54	Fig. 4.57

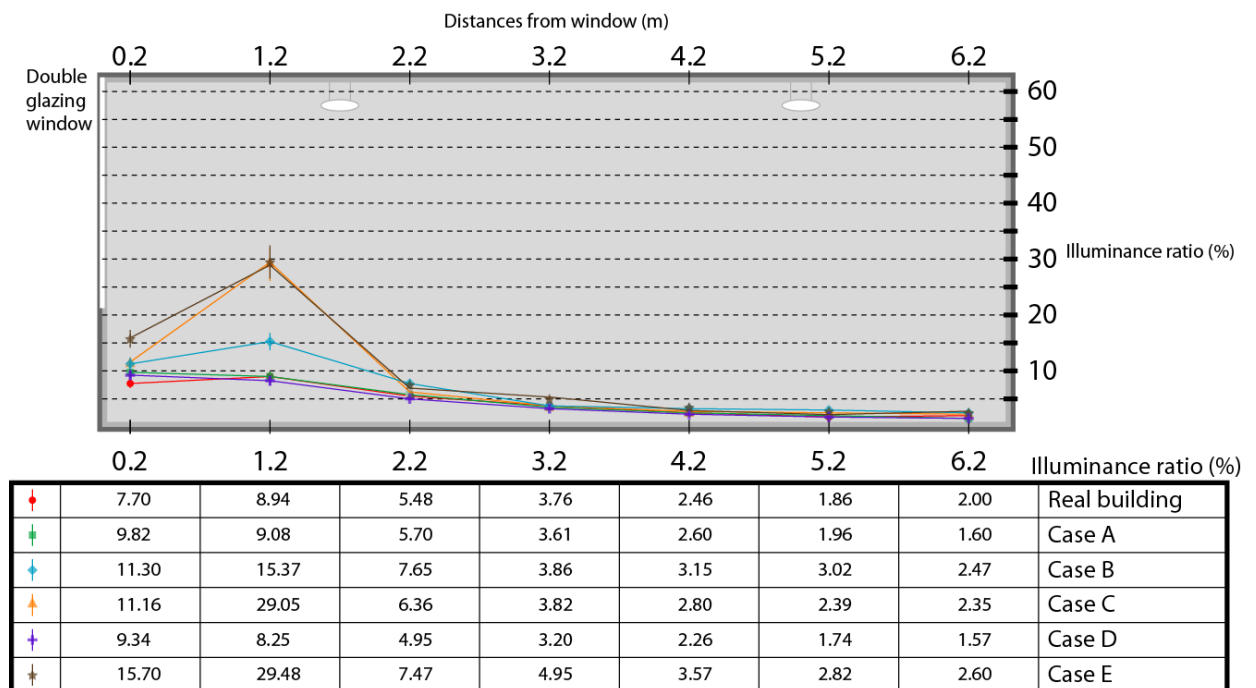


Fig. 4.43 Illuminance ratio (IR) assessment of the models equipped with double glazing window under morning clear sky conditions

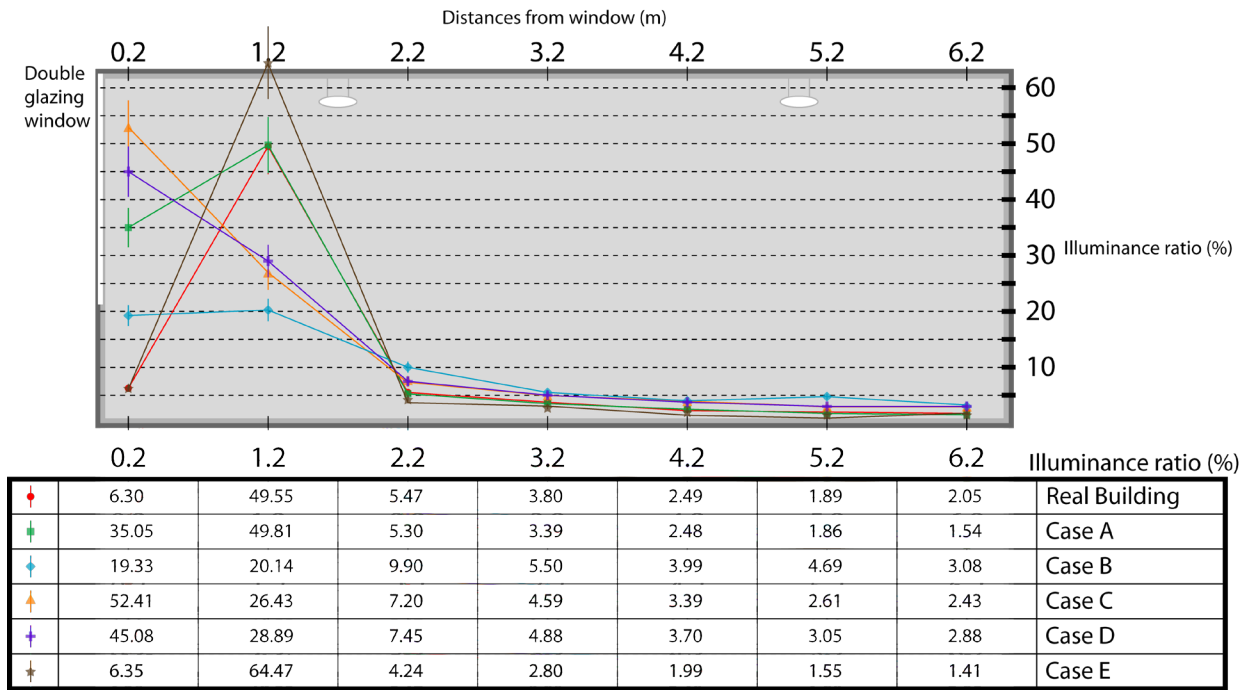


Fig. 4.44 Illuminance ratio (IR) assessment of the models equipped with double glazing window under midday clear sky conditions

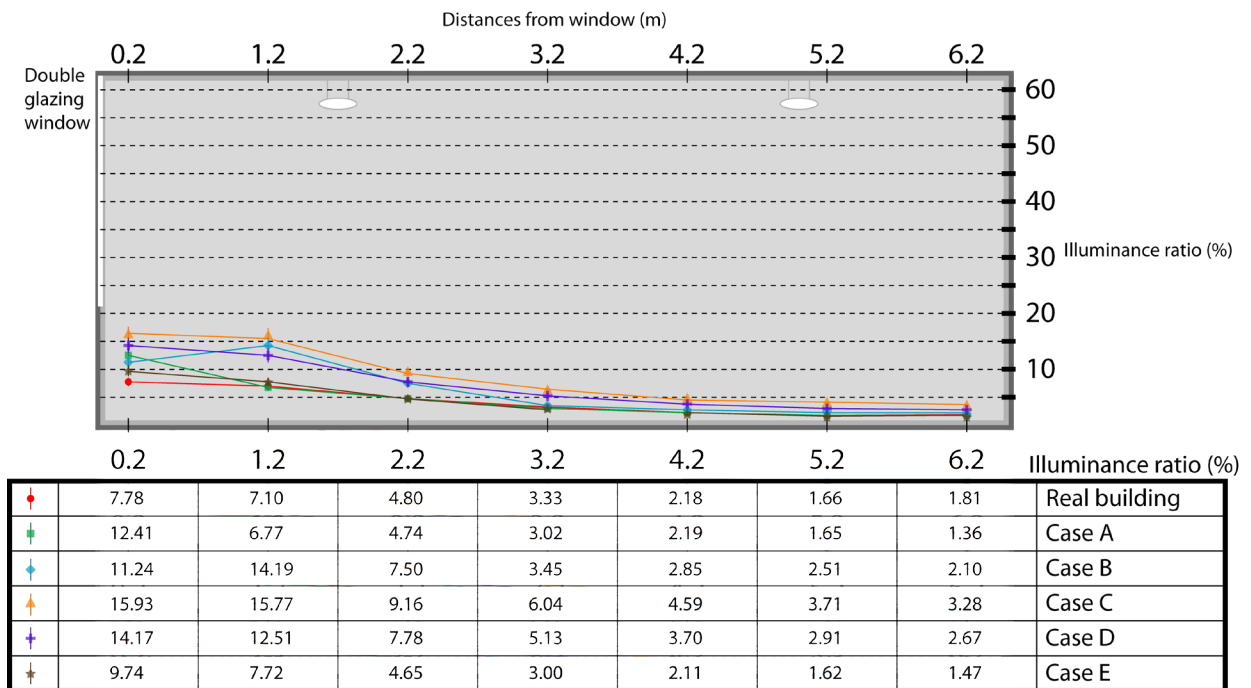


Fig. 4.45 Illuminance ratio (IR) assessment of the models equipped with double glazing window under afternoon clear sky conditions

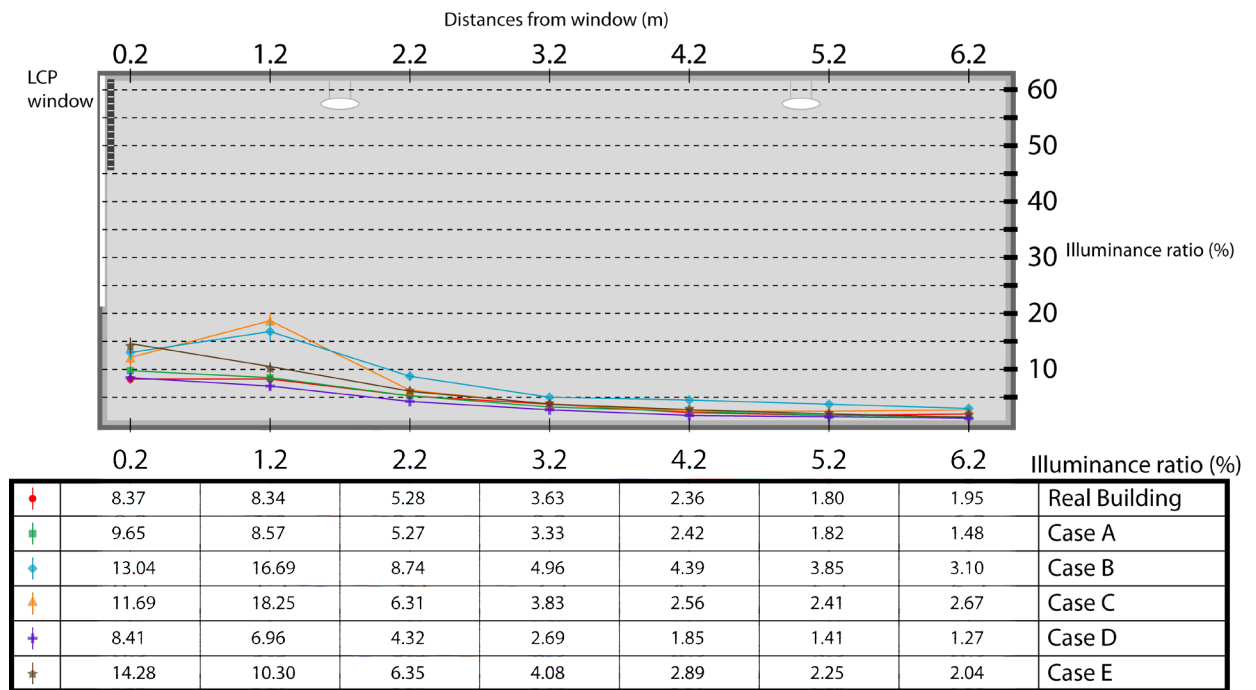


Fig. 4.46 Illuminance ratio (IR) assessment of the models equipped with LCP under morning clear sky conditions

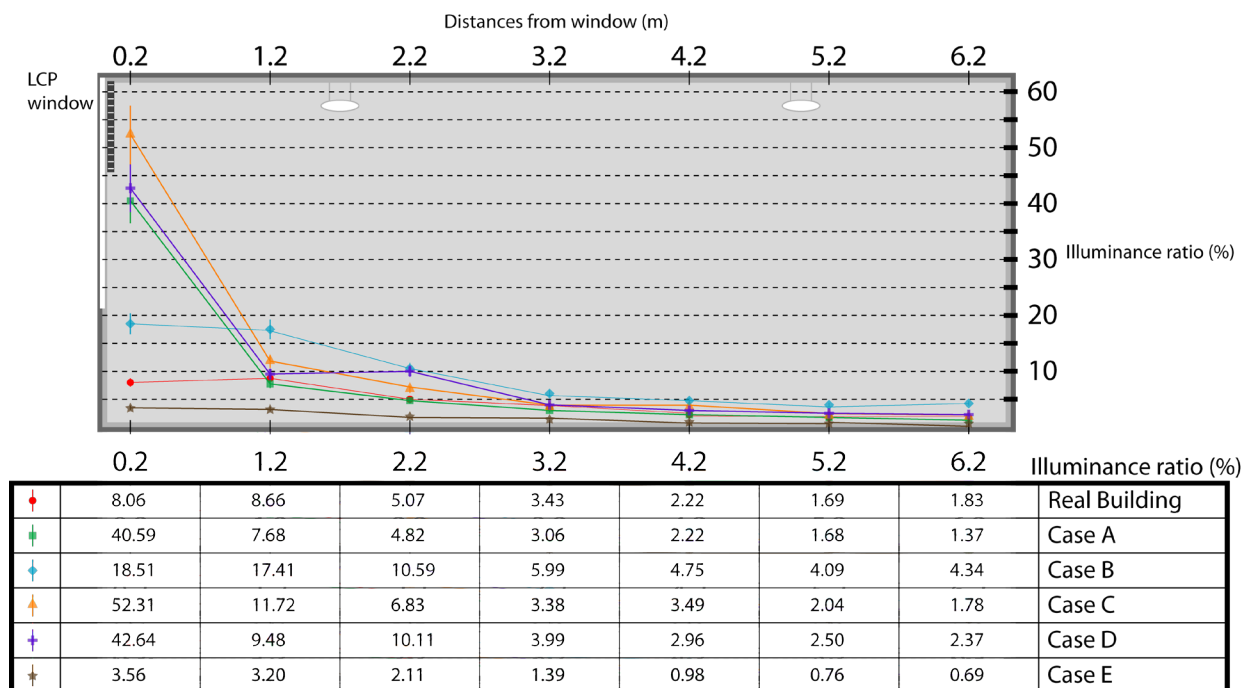


Fig. 4.47 Illuminance ratio (IR) assessment of the models equipped with LCP under midday clear sky condition

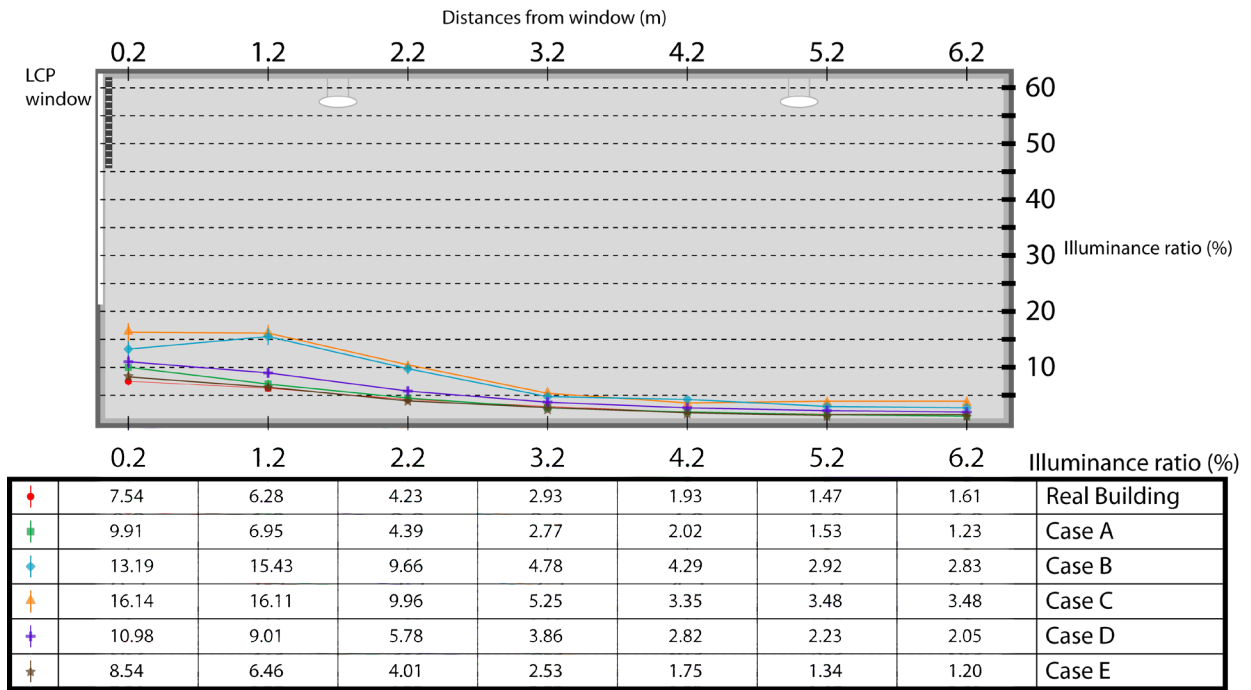


Fig. 4.48
Illuminance ratio (IR) assessment of the models equipped with LCP under afternoon clear sky conditions

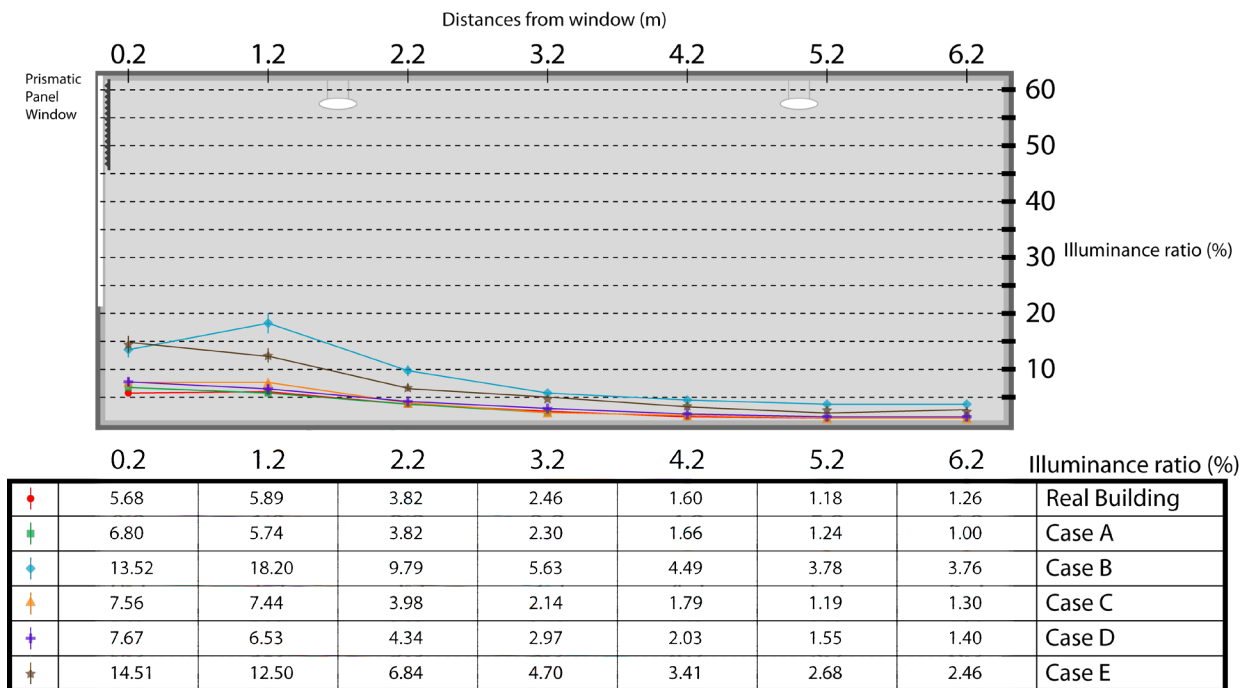


Fig. 4.49
Illuminance ratio (IR) assessment of the models equipped with Prismatic film under morning clear sky conditions

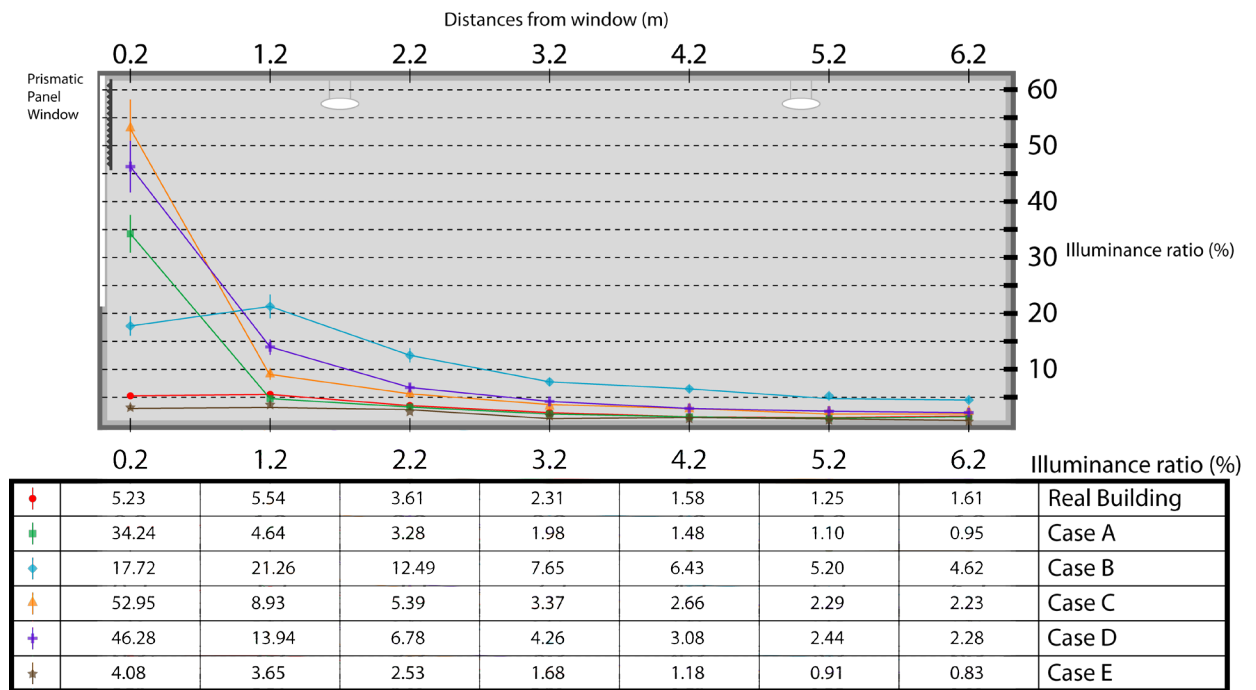


Fig. 4.50 Illuminance ratio (IR) assessment of the models equipped with Prismatic film under midday clear sky conditions

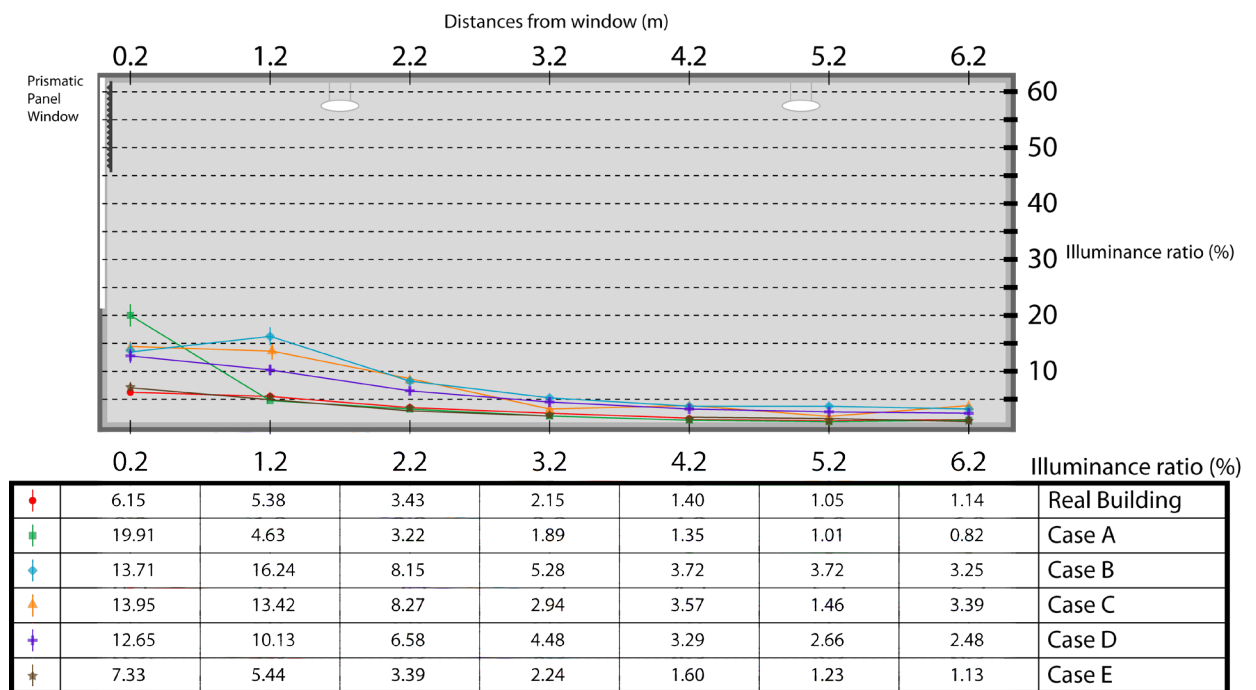


Fig. 4.51 Illuminance ratio (IR) assessment of the models equipped with Prismatic film under afternoon clear sky conditions

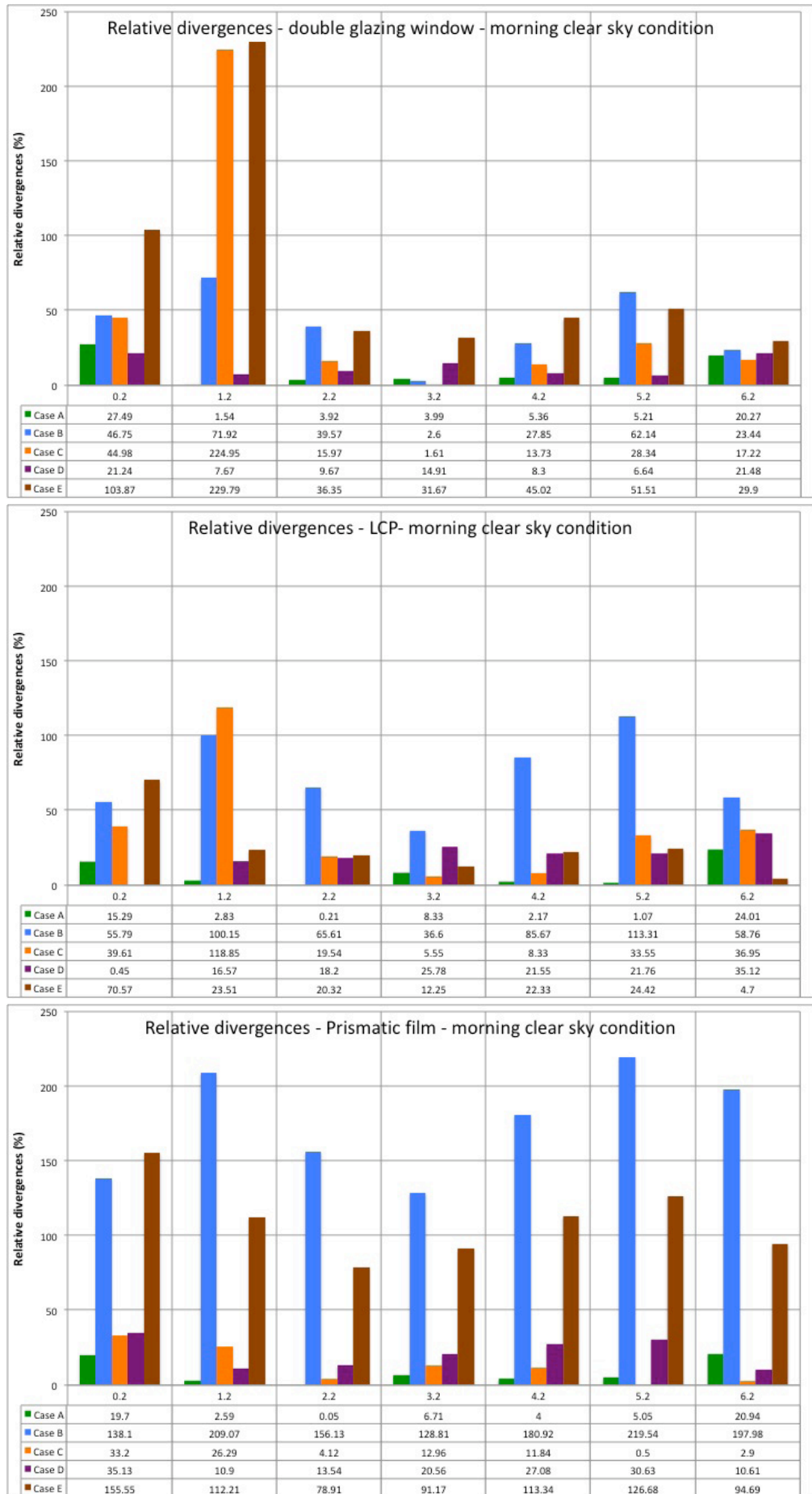


Fig. 4.52 Relative divergences of the IR assessment of all model cases compared with the real building under morning clear sky conditions

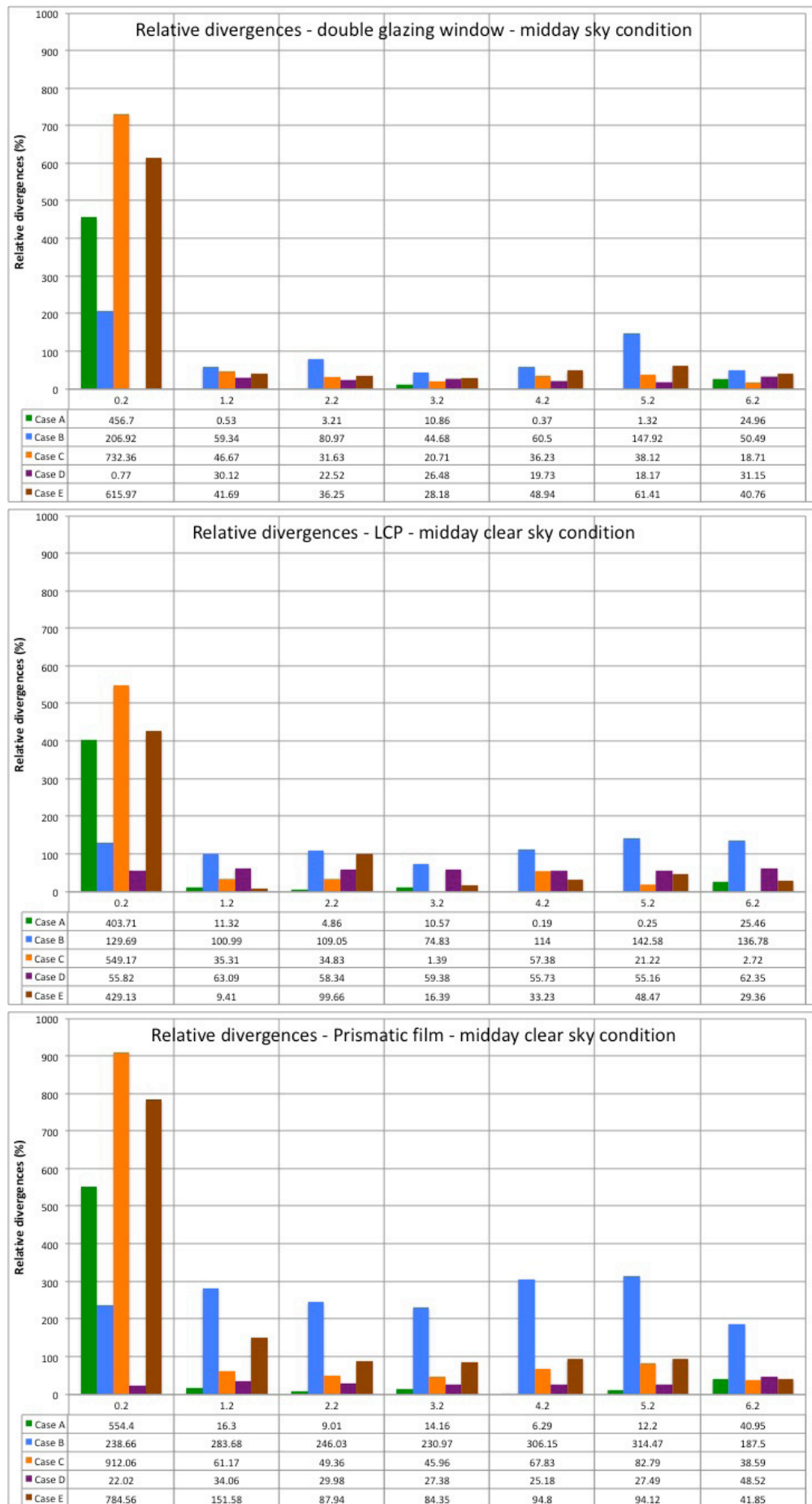


Fig. 4.53 Relative divergences of the IR assessment of all model cases compared with the real building under midday clear sky conditions

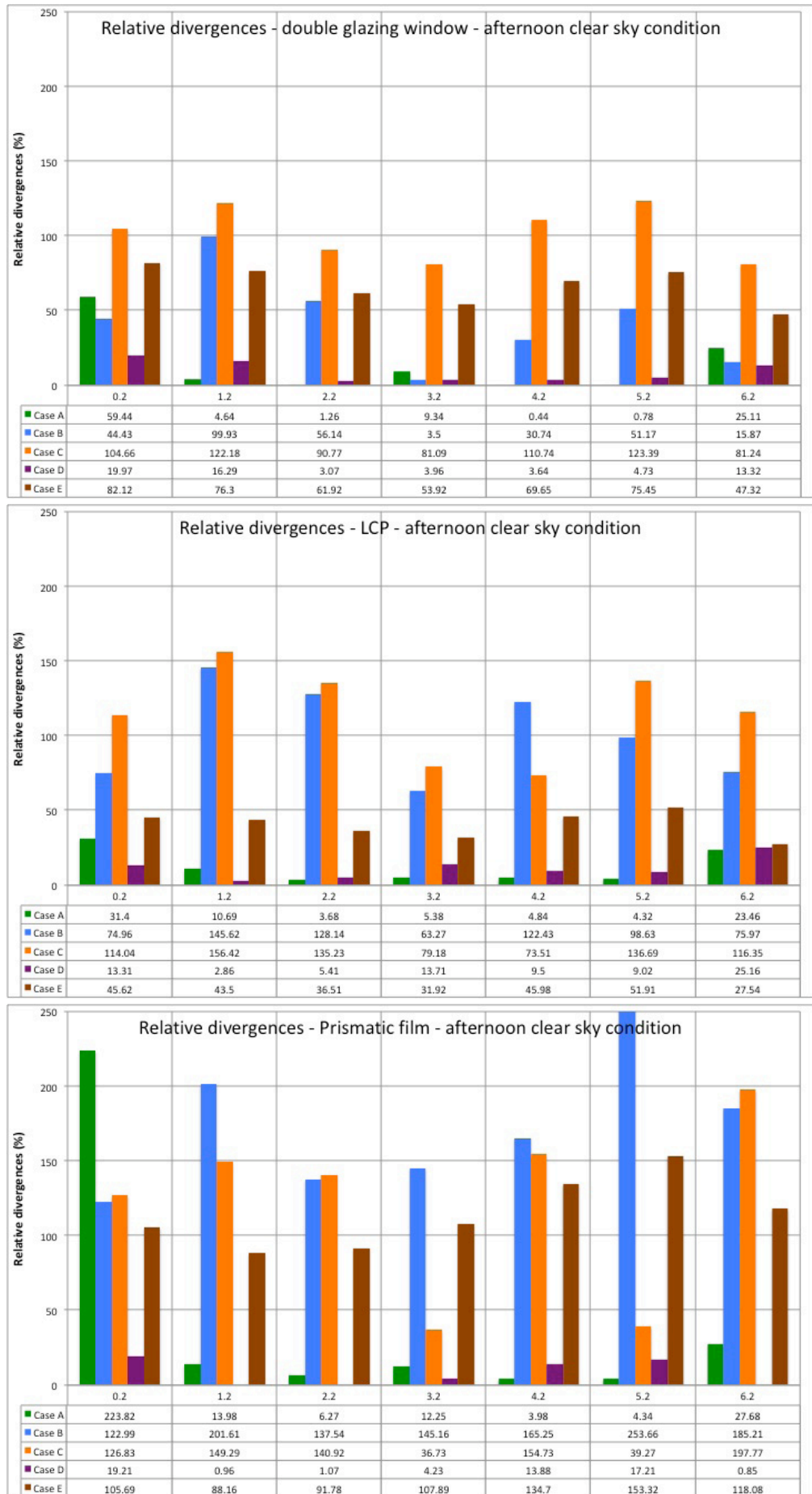


Fig. 4.54 Relative divergences of the IR assessment of all model cases compared with the real building under afternoon clear sky conditions

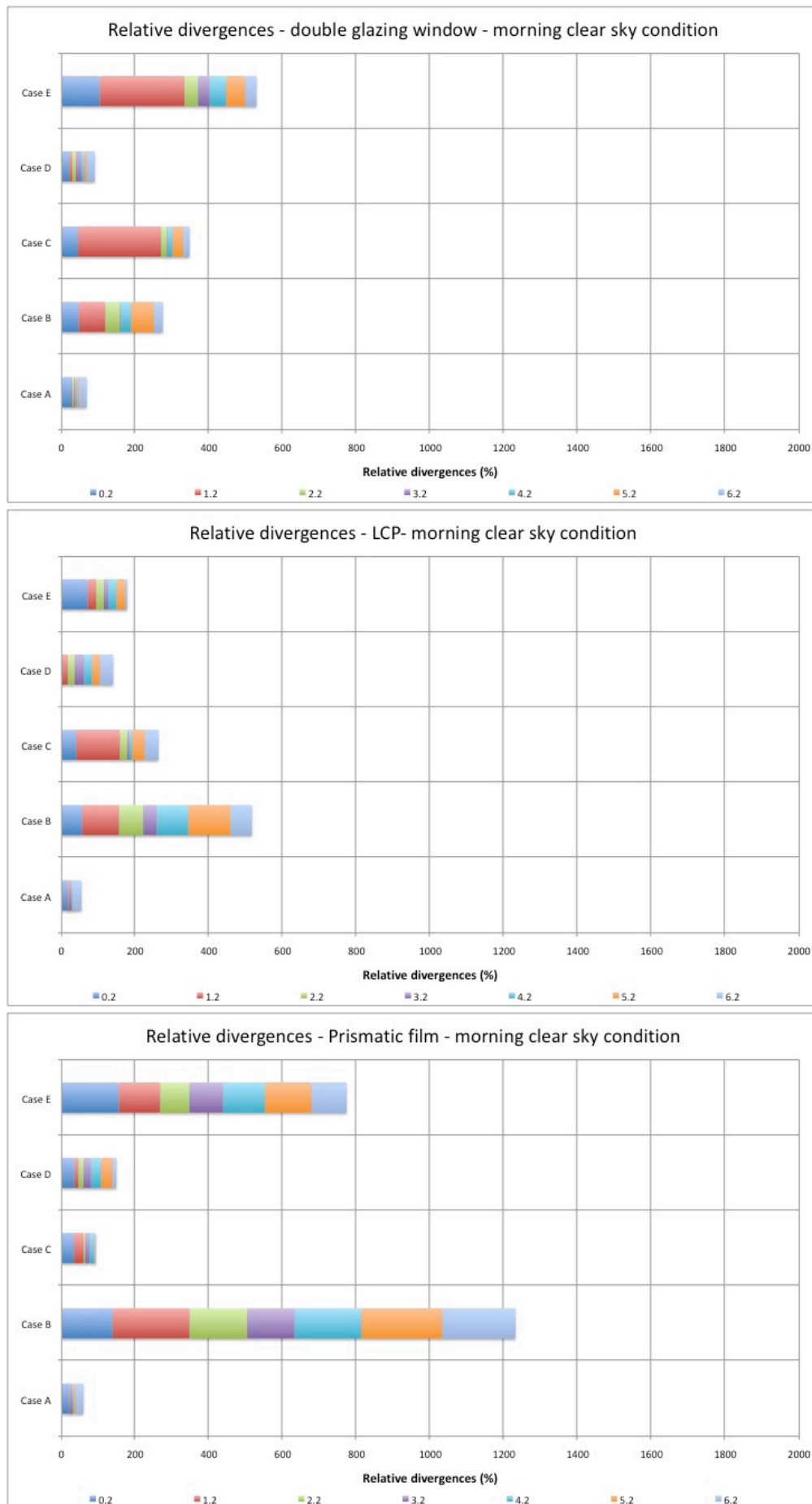


Fig. 4.55 Overall relative divergences of the IR assessment of all model cases compared with the real building under morning clear sky conditions

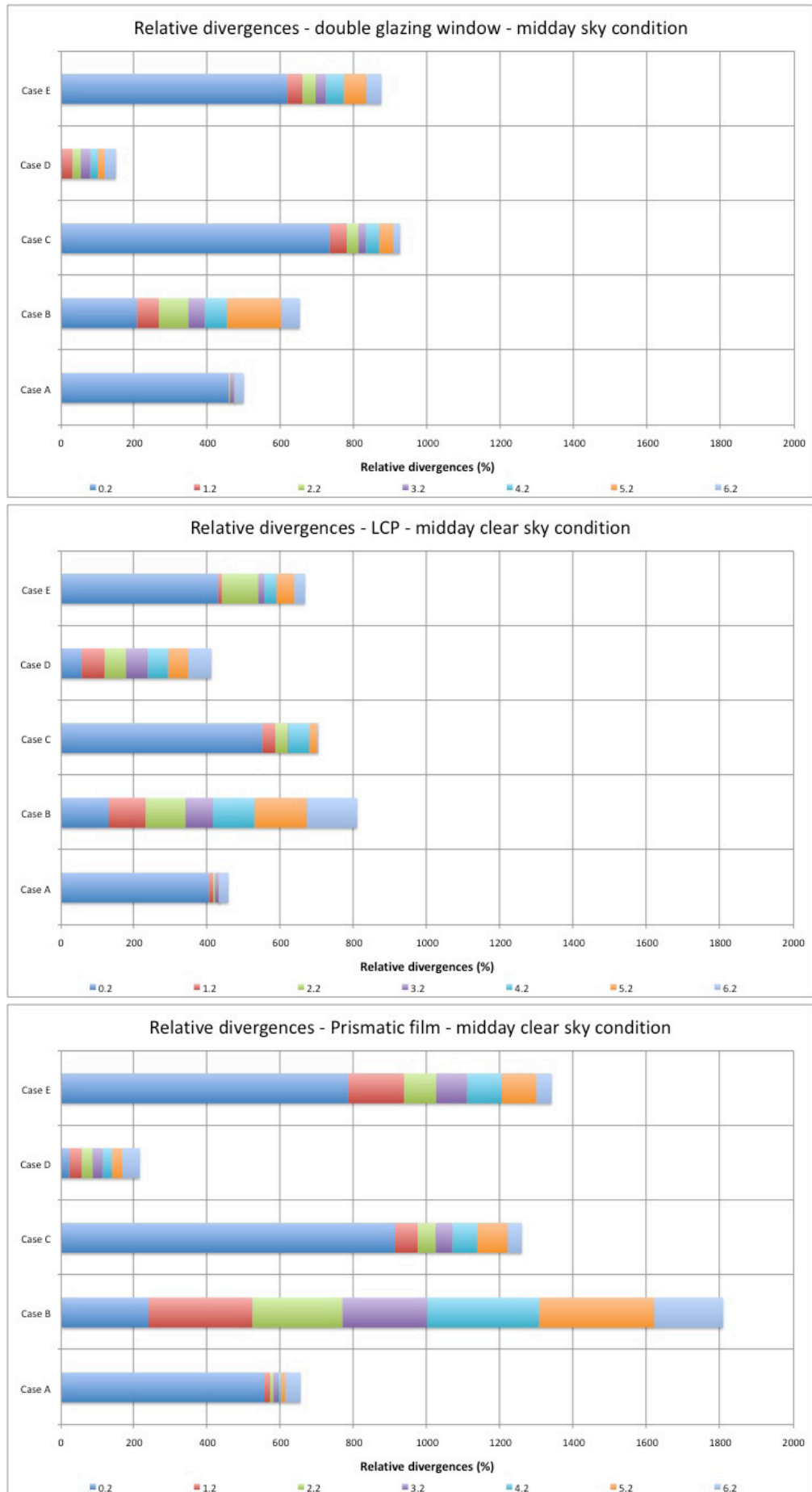


Fig. 4.56 Overall relative divergences of the IR assessment of all model cases compared with the real building under midday clear sky conditions

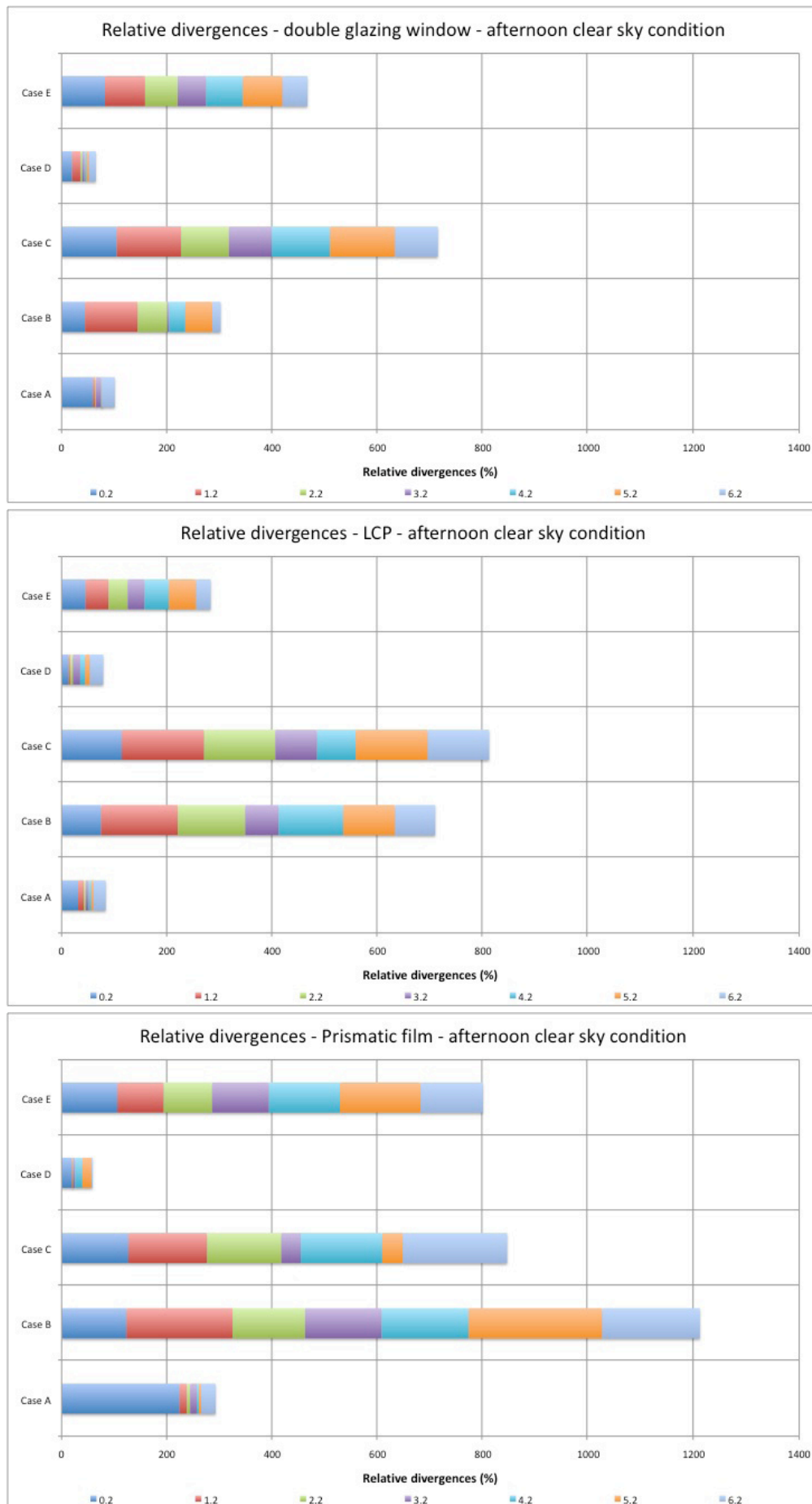


Fig. 4.57 Overall relative divergences of the IR assessment of all model cases compared with the real building under afternoon clear sky conditions

Illumination ratio and relative divergences of the daylighting performance assessment of double glazing under clear sky conditions

- The illuminance ratio (IR) of **Case A** (1:10 scale model, real sky) resembled the reality closely; relative divergences were mostly less than 10 % apart from the one at 0.2 m from the model's window in the afternoon and midday and the deeper part of the room which are about 25% . However the IR measurements were mostly too high at all times of day. The total relative divergence was less than 110 % for both the morning and afternoon assessments, and up to 500 % at midday indicating probably difference of shadow of direct sunlight in the scale model compared to reality.

- In **Case B** (scale model, sky simulator), in addition to Case A's error sources, the impact of the sky simulator produced daylighting assessment errors. The difference between real and CIE standard sky luminance distributions gave rise to a small error, which was especially significant near the window (0.2 or 1.2 m from the model's window). The relative divergences were mostly less than 100% except for some of the points at midday. The total divergences were between 300 and 650%.

- Like Case A and B, the errors in **Case C** (scale model, sky simulator, partial daylight factor method) can be attributed first to the model's reflectance, transmittance and detailed construction; as with Case B, the supplementary error is due to the sky simulation using the sky simulator. Apart from those sources, the errors of the digital sky scanner's sky luminance distribution monitoring had a great impact on the assessment. The relative divergences of this case are on average less than 50% in the morning and at midday except for the points near the window (0.2 or 1.2m from the model's window). However, greater overestimations appeared in the afternoon values where the relative divergences lead from 80 to 125%, the total divergences are from 340 to 1000%.

- **Case D** (virtual model, simulated standard sky) resembles that of the real building closely. The error on the daylighting assessment was especially found near the window (0.2 or 1.2 m from the model's window), where the effect of the shade and shadow can easily count. The relative divergences are mostly less than 30% while the total relative divergences are between 60 and 150%.

- **Case E** (virtual model, simulated standard sky, partial daylight factor method) suffered from the impact of the PDF method, just as in case C. Case E, differences were compounded by the digital sky scanner's sky luminance distribution monitoring. The greatest overestimation appeared in the afternoon measurements when relative divergences ranged from 80 to 615%. The total divergences were from 450 to 900%.

Illumination ratio and relative divergences of the daylighting performance assessment of Laser cut panel under clear sky conditions

- When equipped with LCP, the scale model of **Case A** was, again at all times of day, the nearest to reality; LCP gave errors as low as those of the double glazing window. Most of the relative divergences are less than 10%, the point nearest the real window giving the most discrepancies whilst the point farthest from the window (6.2m) giving about 25% relative divergences. The total divergences of this case were less than 35% except at midday when around 400% was measured.
- The greatest overestimation of IR occurred with the scale model of **Case B**, the sky simulator and the sky luminance distribution provoking the errors. They can likely be explained by the interaction of light redirection angle of the LCP and the light sources of the scanning sky simulator. Most of the relative divergences were greater than 100%, except in the morning when even so the majority were above 50%. The total relative divergences are from 500 to 810%.
- **Case C** was generally better than Case B because the values monitored by the digital sky scanner have sounded the sky luminance distribution. The afternoon relative divergences were the greatest - over 100%; the total relative divergences were from 220 to 820%.
- **Case D** performed close to reality, a situation observed for all fenestration systems, a strong argument in favour of computer modelling. Because the LCP reflected the daylight flux to the end of the room (6.2m), errors near the window were less than with simple double glazing. The relative divergences of this case were rather even; in the morning and afternoon they were less than 25%, greater at midday although still less than 60% then. The sum of the relative divergences were between 70 and 410%
- **Case E** presented an overestimation of illuminance ratio. The values monitored by the digital sky scanner modified the sky luminance distribution, thus creating assessment errors for the PDF method. The relative divergences of the case varied, however most of them were less than 100%. The total relative divergences were from 170 to 670%.

Illumination ratio and relative divergences of the daylighting performance assessment of prismatic film under clear sky conditions

- Once again **Case A**, this time with prismatic film, presented one of the most precise result when compared with the real situation (especially for the morning clear sky situation). The critical parts were, as before, the points near the window (0.2m) and the deeper part of the room (6.2m). Most of the relative divergences were less than 15%; less than 40% relative divergence was measured at the point farthest from the window (6.2m) whilst that near the window (at 0.2m) gave the most discrepancies. The sum of the divergences of this case were between 60 and 700%.

- For **Case B**, the scale model presented the greatest overestimation of IR at all times of day, the causes being very likely the interaction of the light sources of the scanning sky simulator, the sky luminance distribution and the light redirection angle of the prismatic film. The relative divergences varied from 120 to 315%; the total divergences were from 60 to 700%.

- **Case C** gave sound IR results compared with reality in the morning; at midday and in the afternoon greater errors were noted. This can be attributed to the scanning sky simulator itself and to errors in the sky luminance distribution, which was adjusted according to values measured by the digital sky scanner. The relative divergences were less than 35% in the morning and varied from 40 to 900% later in the day. The total divergences of the case were from 90 to 1260%.

- IR results of **Case D** based on the virtual model equipped with prismatic film, were as close to reality as Case A. The prismatic film reflected the daylight to the end of the room; the errors near the window were less than when double glazing was simulated. The relative divergences of Case D varied though were less than 50%; the total relative divergences were from 55 to 215%

- The adjustments made to the sky luminance distribution according to the partial daylight factor (PDF) method created errors in the daylighting evaluation of **Case E**. The relative divergences of this case varied; most were above 80%. The sums of the relative divergences were from 750 to 1400%

Potential sources of error in daylighting performance assessment under clear sky conditions

For clear sky conditions, looking at the graphs concerning illuminance ratio (Fig. 4.43 - 4.51) makes it immediately clear that the greatest discrepancy is at points near the window, particularly at midday. Even Case A' s scale model, which was very accurate under overcast sky, presented up to 450% divergence for double glazing assessment at midday. This proves that large errors can be derived purely from the model itself when there is no error source from sky simulation. However, this error is very likely due to the window transmittance, model detail construction or sensor details producing a different lighting profile in the room space. This is particularly true near the window which is the critical point where sunlight can penetrate into the space and is particularly sensible to masking and/or shadowing effect. The example presented in the next figure (Fig. 4.58) shows that slight differences in light penetration can provoke inaccurate measurements.

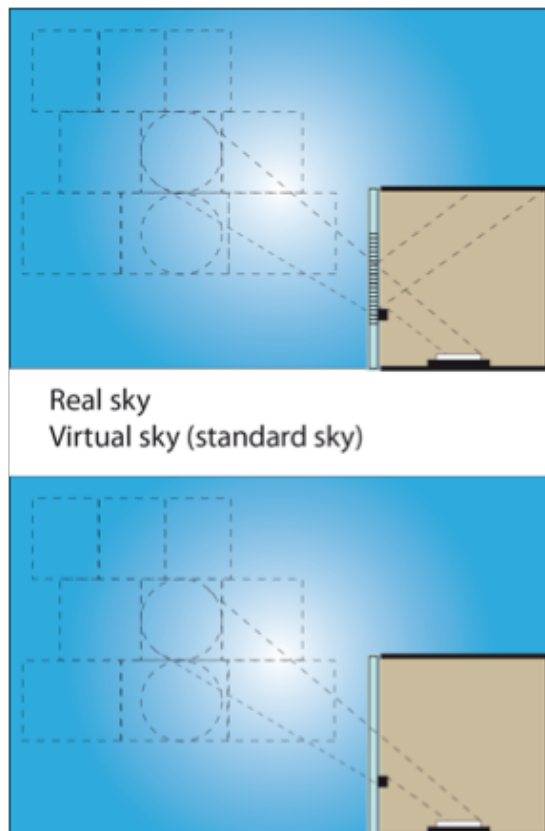


Fig. 4.58
A small error in critical detail can create divergence close to the window side in the IR evaluation for all types of daylight simulation; real sky, scanning sky simulator (circular patch) or PDF method (rectangular) for both CFS (upper) and simple windows (below).

In addition, errors can be induced in the CFS evaluation by not scaling-down the CFS. The impact of the much higher luminance of some sky elements under clear skies than in overcast ones is that more light is redirected into the room, leading to greater errors and compounds the effects of surface reflectance. As presented in Fig. 4.59, taking the same sky element under different sky simulation procedures produces different lighting properties. Real sky has a continuous gradient (Fig. 4.59a), while the scanning sky simulator (Fig. 4.59b) and the virtual model using PDF (Fig. 4.59d) both work with discontinuous elements of averaged sky luminance. Although the virtual model using GenSky (Fig. 4.59c) has a sky of continuous gradient, the distribution of the sky luminance (CIS standard clear sky) differing from that of the real sky caused a significant error.

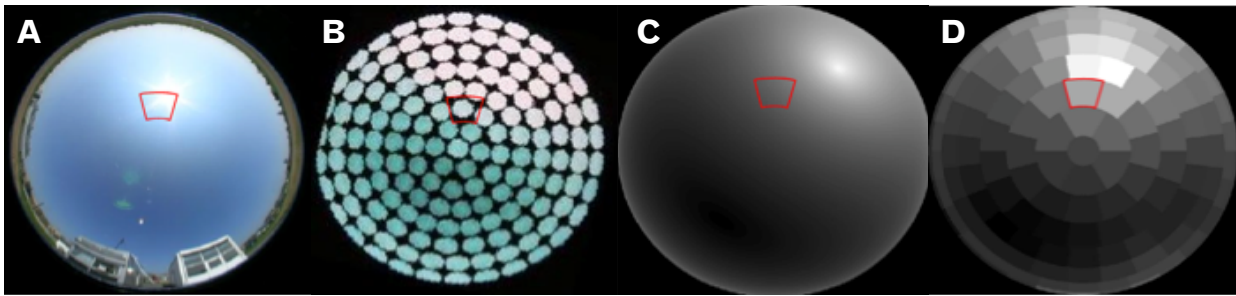


Fig. 4.59 The sky luminance distribution of the same sky element in different sky simulation procedures is obviously different under clear skies

- The luminance property of the considered sky element of the real sky shows non-uniform luminance.
- The circular sky sector of a scanning sky simulator has a uniform light luminance.
- The continuous sky element of the standard sky in the virtual model (GenSky) has a non-uniform property but the gradient of the light is different from the one of the real sky.
- The sky element in the virtual model using PDF method has a uniform luminance given by the average value measured by the sky scanner.

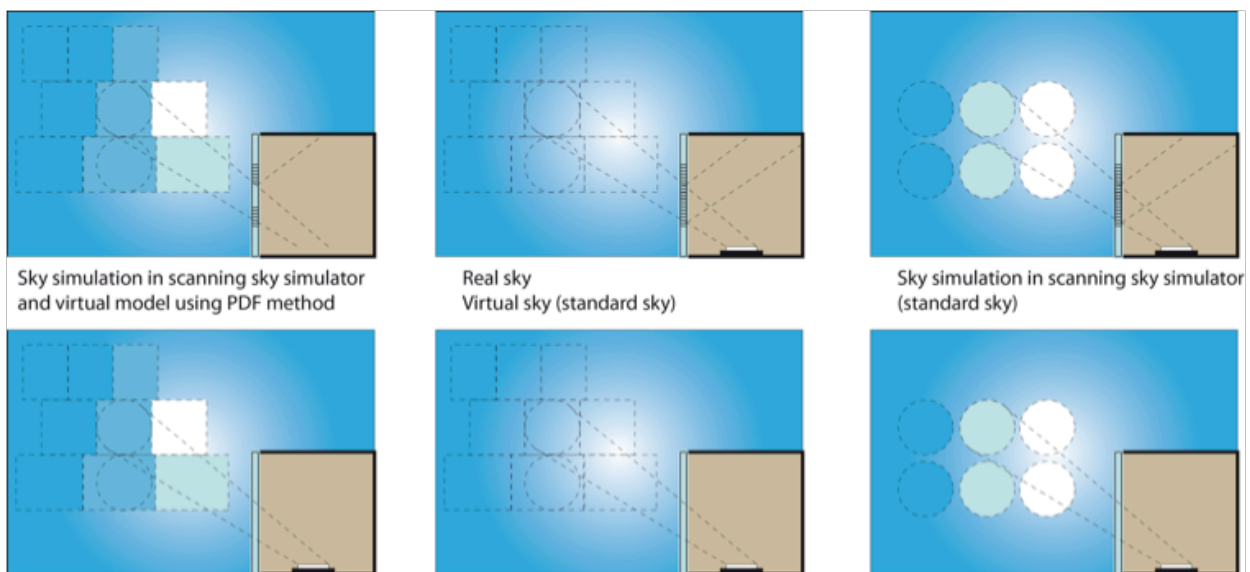


Fig. 4.60 The different daylight simulation procedures can create divergences in the monitoring of illuminance using a photometric sensor, particularly for CFS systems (upper row);

- When attempting to simulate a continuous clear sky in scale or virtual models using the PDF method (the real sky luminance, measured by the sky scanner and averaged for each sky element, presents nonconformant luminance properties).
- Daylight simulation using real sky or a virtual CIE standard sky.
- The scanning sky simulator, simulating standard sky, does not project the exactly same sky luminance as measured under the real sky.

One can see that the scale model Cases B and C give larger errors, particularly for CFS assessment. Sources of error are very likely the window transmittance, model construction details and dimension as mentioned earlier. The sky simulation using the scanning sky simulator can provoke additional errors, multiplying the error created by the lighting condition of the different daylight source elements. As presented in Fig. 4.60c, the luminance distribution using a scanning sky simulator is reasonably accurate for simple fenestration systems, like double glazing. However, when the CFS were attached, the initially small lighting property divergences brought about larger ones, particularly when the daylight flux was redirected by CFS to the deeper parts of the room.

Case D, the virtual model using CIE standard sky (GenSky), was in general the most accurate assessment, particularly for CFS. It confirmed the importance of having a continuous varying sky luminance distribution in the daylight simulation. The sky simulations using discrete sky elements, as in Fig. 4.60a and 4.60c, produced generally larger errors than a continuous clear sky, such as GenSky's standard sky (Fig. 4.60b).

The greatest impact was observed in the cases using the PDF method. Because the sky scanner initially averaged for each element the real sky luminance, as shown in Fig. 4.59d and 4.60a, the errors are consequently greater than with a standard sky generated by the sky simulator or the GenSky function. The most obvious results can be seen in the comparison of the scene renderings of the virtual model using CIE standard sky simulation (GenSky) and real sky simulation using PDF method in Fig. 4.61, 4.62 and 4.63. The images show the double glazing, LCP and prismatic film daylight properties of the virtual model (Cases D and E: without and with PDF values respectively). The virtual models were created using the Radiance program to simulate the daylight distribution in the space. The scene shown in Case E's scene is blurred due to the non-continuous luminance element of the sky luminance distribution when using the PDF method: this explains the case's additional errors.

A summary of the sources of errors that can occur in the assessments for each case is given here in (see also Table 4.17):

- The 1:10 scale model under real sky (**Case A**) presented the greatest similarity to the real daylighting performance. However most values are slightly overestimated, the model reporting IR values that were greater than those measured in the real building. The causes of error are due to the model's detailed construction, as well as its surface reflectance and window transmittance. The fact that the luxmeters used in the real building and its model were different can also explain the remaining discrepancy.
- **Case B** (scale model, sky simulator) presented greater overestimation than Case A at all measured points, especially when equipped with CFS. One cause of error (in addition to those of Case A) comes from the scanning sky simulator itself; the light sources influenced the redirection angle of the CFS and the uniform luminance shape of the sources. Another cause could be the slight difference of the CIE standard sky do not fit to the reality sky when compared to the real sky conditions.
- **Case C** (scale model, sky simulator, partial daylight factor method) presented rather large discrepancies, excepting under morning skies. However, it overestimated more when CFS were equipped. Errors additional to those of Cases A and B, came from the inexact positioning of the brighter sky elements in the afternoon sky.
- **Case D** (virtual model, simulated standard sky) came very close to the real performance in most situations, small errors coming from the modelling details and differences in sky simulation. Simulation of CFS (LCP and Prismatic film) did give reasonably small errors, pointing out the apparent superiority of computer simulation of CFS when compared to physical modelling.
- **Case E** (virtual model, simulated standard sky, partial daylight factor method) gave again higher IR values than reality in most situations. The comparison with the very favourable case D indicates that the PDF method is responsible for this situation.

Potential sources of error			
	Double glazing	Laser cut panel	Prismatic film
Case A	Photometric sensors and model geometry and photometry	Photometric sensors and model geometry and photometry + CFS reproduction	Photometric sensors and model geometry and photometry + CFS reproduction
Cases B, C, D, E	Photometric sensors and model geometry and photometry + sky simulation	Photometric sensors and model geometry and photometry + sky simulation + CFS reproduction	Photometric sensors and model geometry and photometry + sky simulation + CFS reproduction

Table 4.17
Potential sources of error in daylighting performance assessment under clear sky conditions

146

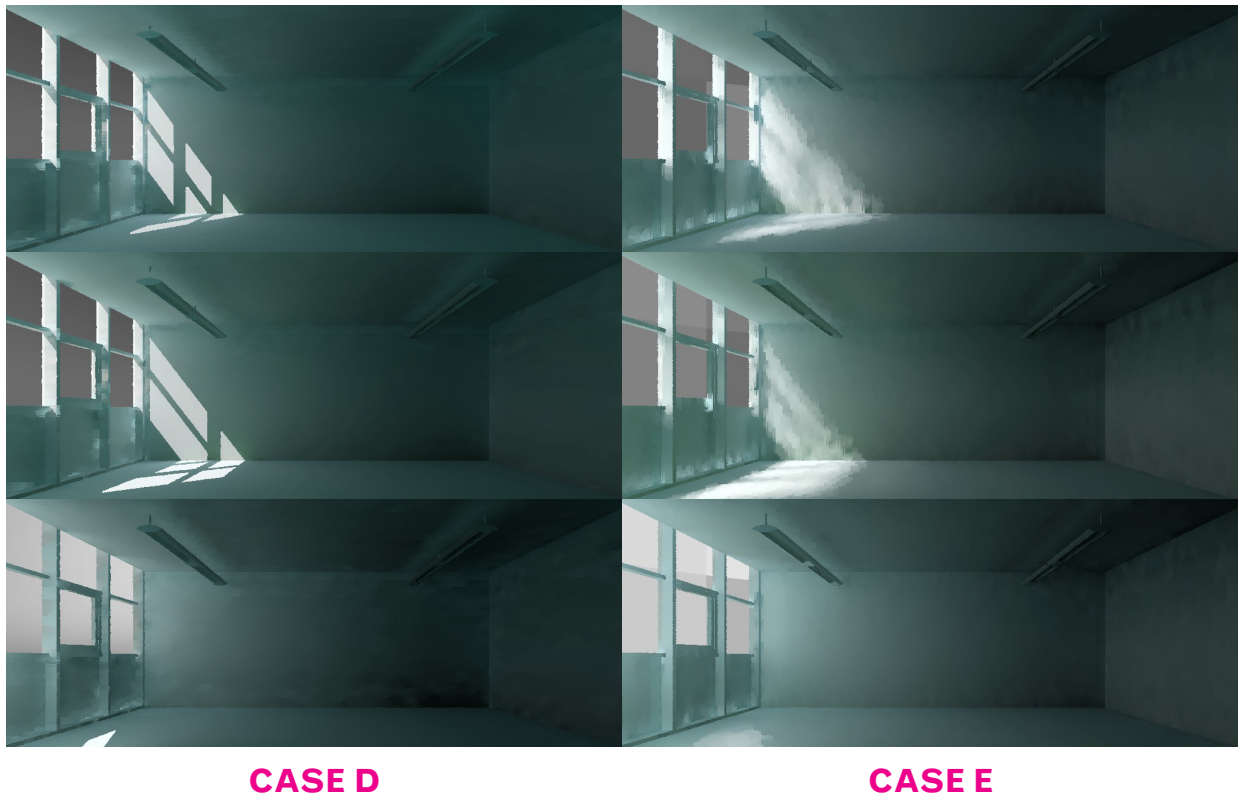


Fig. 4.61
Virtual model cases D and E created by Radiance for assessment of double glazing window under clear sky: morning (upper), midday (centre) and afternoon (lower)

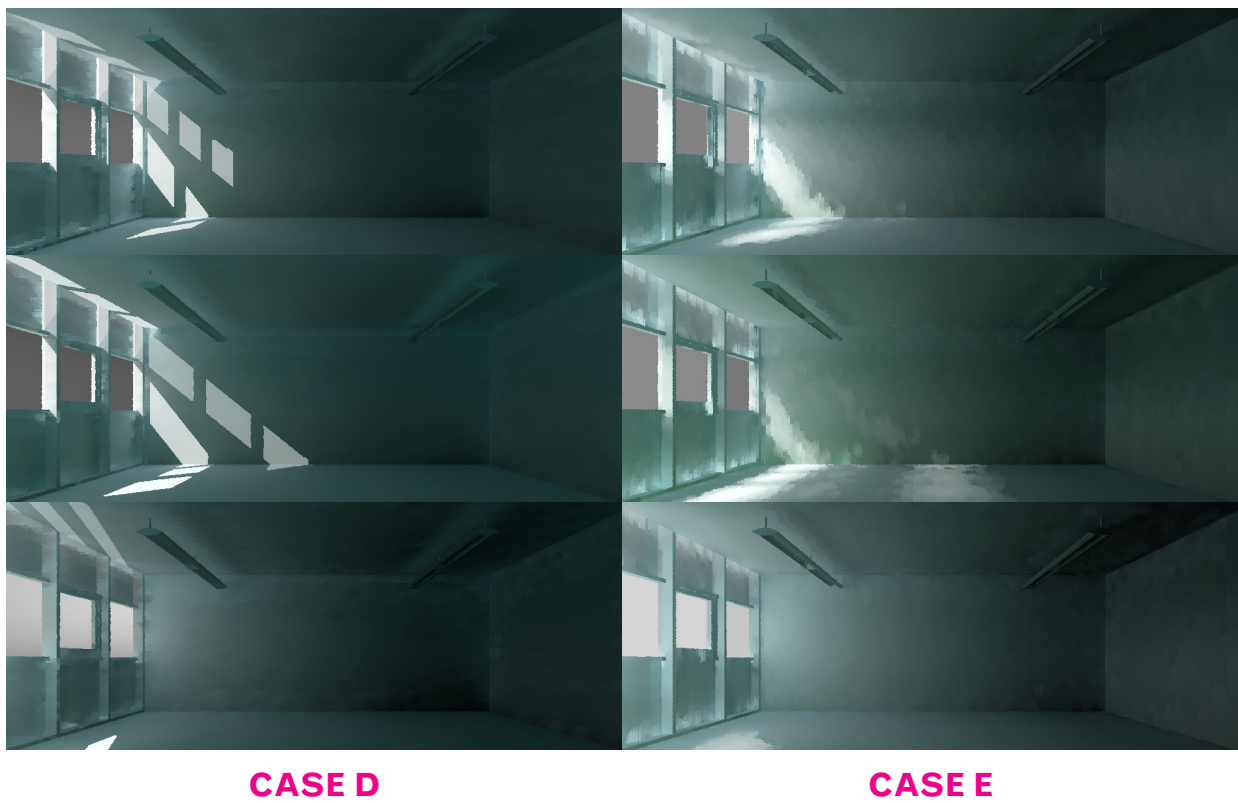


Fig. 4.62
Virtual model cases D and E created by Radiance for assessment of LCP under clear sky: morning (upper), midday (centre) and afternoon (lower)

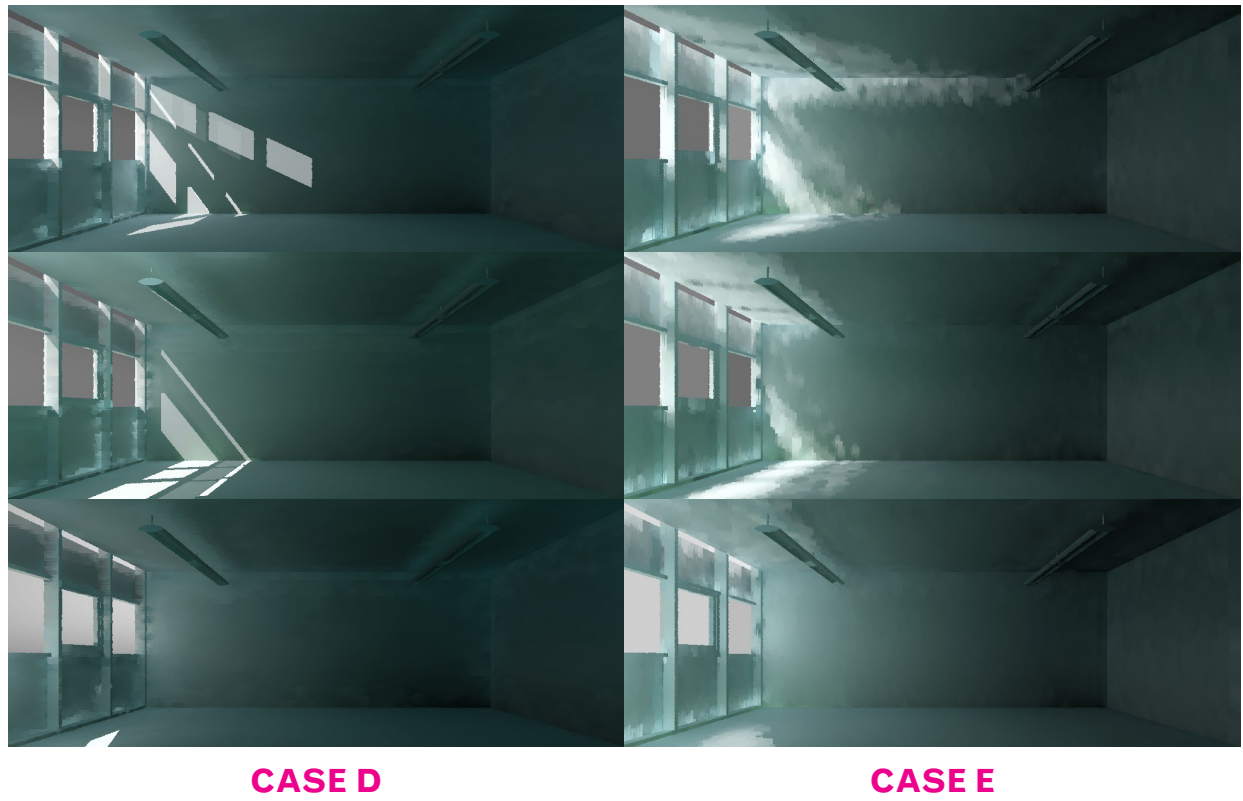


Fig. 4.63
Virtual model cases D and E created by Radiance for assessment of prismatic film under clear sky: morning (upper), midday (centre) and afternoon (lower)

4.4 Luminance measurement of the interior surfaces

Daylighting performance can also be assessed using interior luminance measurement, commonly used for visual comfort analysis. To identify potential sources of error this study additionally evaluated the luminance in the real building, scale model Case A (1:10 scale model, real sky condition) and virtual model Case D (Virtual model, simulated standard sky). The luminance could not be measured for scale model (Cases B and C) because of the limitation of the rotating sky section of the scanning sky simulator. Virtual model (Case E) could not be evaluated because the discontinuous light sources of the sky luminance distribution rendered the scene blurred.

These assessments were carried out under clear sky at midday (the sky details presented in Table 4.8). As there was only one digital camera and one luminance meter the measurements were not made simultaneously. However, they were done within a 45 minute period under similar sky conditions. The luminance evaluations for these 3 cases were made using the methods described below:

- Real building

The interior luminance was measured using a luminance meter (details in Chapter 2) and the HDR imaging technique. While the HDR images were being taken using two different objectives (a fisheye lens and a 24mm lens) the luminance meter was used to measure the surface luminance at 15 points as presented in Fig. 4.64. The HDR images were later combined using the Photosphere software, the fifteen corresponding point of luminance measurement being examined using the same program.

- Physical model

HDR images, using both the fisheye lens and the 24mm one, were taken afterwards in the scale model (Case A, located in the adjacent test module). The luminance meter measurements were made immediately after the images were taken within a 15 minute period; 14 corresponding points were measured, the point 7 not being considered due to the small size of the model. As with the real building the HDR photographs were later on combined using Photosphere software, the 14 corresponding point of luminance measurement being examined using the same program.

- Virtual model

The luminance in the virtual model was determined using the scene rendering by Radiance, the images being calculated for CIE standard clear sky conditions (GenSky function). The sky data corresponded to the midday clear sky as presented in Table 4.8. The corresponding points of luminance monitored in the real case were also examined using the Radiance rendering scenes.

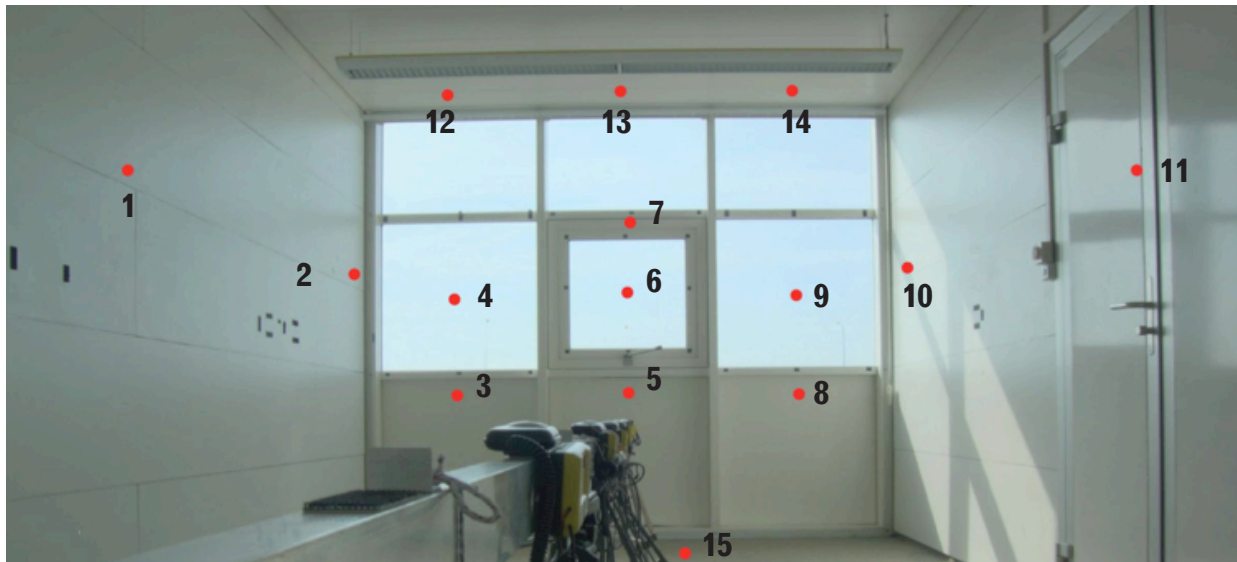


Fig. 4.64
The fifteen points of interior surfaces where luminance was measured with a luminance meter

The virtual model's rendering compared with HDR images of the real building and its scale model

By means of HDR images showing the daylight properties of the real building the evaluation of the models can be undertaken with accuracy. Clearly seen, for all three window systems, the scale model can simulate rather well the daylighting properties, shade and shadow. However, the inaccurate specular reflectance property of the scale model floor material brought different light reflections to the model's scene. Moreover, the images often show that different details of the scale model, such as the sensor track or the hole (on the right of the Fig. 4.65 centre) used for scale model maintenance, or the photography itself can lead to an inaccurate daylight qualitative evaluation.

The virtual model is another alternative for qualitative analysis because of its flexibility and convenience. As an example, the virtual model created with Radiance (presented in Fig. 4.65) has an open scene without obstacles. This virtual model can be used effectively in a conventional daylight analysis; however, in some complex analyses such as with prismatic film, the virtual model provides a different image from the real and scale model cases. The dissimilarity can be produced by a different simulation of the daylighting sources (mainly the sky luminance distribution), the CFS simulation or even the virtual model details compared with the reality (such as the lack of the sensor track shown on the same Figure).

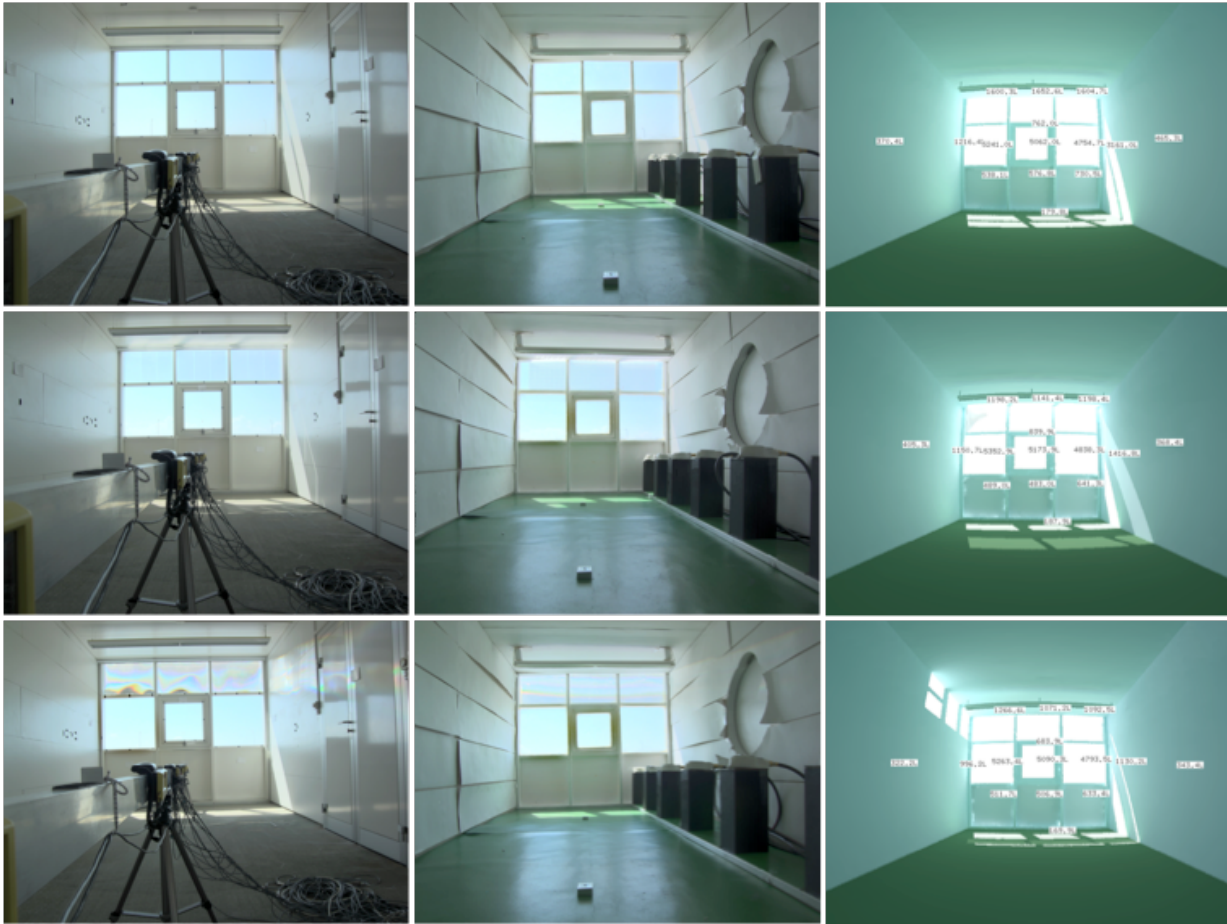


Fig. 4.65 HDR images of the real building (left) and scale model (centre), together with the rendering of the virtual model (right), used to assess double glazing window (top), LCP (centre) and prismatic film (bottom)

Comparison of luminance measurements

Observing the raw values presented in Table 4.18 as well as Fig. 4.66 for the luminance of the opaque interior surfaces (walls, ceiling and floor) and Fig. 4.67 for the transparent surfaces (glazing window), one notices that the most accurate luminance measurement observed was that of the scale model using the luminance meter, the same measuring instrument was however used under the same sky conditions as for the real building. Moreover, luminance measurements of opaque materials were closer to those of the real case than measurements on the glazing window, where variations were due to the dynamic nature of the exterior on lighting environment.

The HDR imaging technique, as expected, introduced higher errors in luminance evaluation due to the dissimilarity of the assessment compared with the real case. It gave a better evaluation for the real building than for the scale model, both with the fisheye and with the 24mm lens.

The least accurate case in this experiment was the luminance evaluation using the virtual model. The errors incurring in this case can be attributed to the fact that the sky luminance distribution, as well as the absolute luminance values, used in this case differed from the real sky. However, the measurement points in this study were mostly close to the window which is commonly the critical area, particularly when CFS is simulated; the errors of CFS simulation had a great impact on this evaluation.

To compare the reliability of the luminance measurements under the different lighting conditions (the measurements were non-simultaneous the sky being not exactly similar), the luminance ratio (LR) was used for comparison. It is defined as the luminance value of the given point divided by the luminance value of the centre of the image (the outdoor pointing sky luminance measured through the window glazing). Table 4.19 presents the LR value observed for the different measurement methods.

One notices the LR is a relatively accurate measurement, always following the same tendency. The most inaccurate evaluation occurred at points 12, 13 and 14 on the ceiling, especially when the CFS were attached. It can be explained by the fact that the light redirected by the CFS in the models (particularly the virtual one) differs from those of the daylighting assessments. This confirms that accurate modelling of the CFS is critical for the assessment: a slight difference of the CFS model compared with the real case can create a great difference in luminance evaluation.

However the scattering diagram of each method (Fig. 4.68) compared with the real building's luminance values given with a regression analysis shows the R-square is sound, confirming that every method gives an acceptable luminance evaluation when the luminance ratio is used for assessment.

Double glazing assessment

	Luminance meter		Luminance measurement using HDRI				Virtual model
	Real building	Scale model	Real building		Scale model		
			Fish-eye	24 mm	Fish-eye	24 mm	
1	1054	1063	1111	1274	1184	1473	370
2	2763	2228	3553	4364	2916	3681	1216
3	995	752	1097	1296	917	1085	538
4	16000	14730	22389	28340	22143	24330	5241
5	1086	812	1149	1422	870	1186	577
6	14340	14010	18470	24569	20197	21897	5062
7	1278		1731	1809			762
8	1710	1973	2041	2300	1457	1885	731
9	12700	12950	15536	19424	18238	18277	4755
10	7962	3633	10066	11589	5782	5685	3161
11	3111	1501	1449	1784	1447	1623	465
12	2071	1373	2386	2832	1800	2245	1600
13	2161	1344	2328	2869	1771	2171	1653
14	2235	1370	2554	3047	1920	2376	1605
15	488	813	704	670	1409	902	180

LCP assessment

	Luminance meter		Luminance measurement using HDRI				Virtual model
	Real building	Scale model	Real building		Scale model		
			Fish-eye	24 mm	Fish-eye	24 mm	
1	993	1017	1072	1195	1355	1084	405
2	2846	2130	3640	4458	3502	3122	1151
3	975	734	1028	1255	908	809	489
4	16875	13910	23043	28953	22101	20104	5353
5	1009	722	1007	1348	954	771	483
6	14710	13350	19039	23522	20538	18176	5174
7	1455		1998	2136			840
8	1588	1095	1770	2240	1313	1081	641
9	14130	11990	15274	18799	17233	15841	4838
10	4797	2848	6352	6321	5353	6521	1417
11	2594	1270	1239	1420	1456	1214	368
12	6818	2068	7224	9469	2685	2221	1198
13	6854	3031	7992	7457	2593	2216	1141
14	5384	1502	6192	4406	2623	2266	1198
15	560	648	637	698	1171	932	188

Prismatic film assessment

	Luminance meter		Luminance measurement using HDRI				Virtual model
	Real building	Scale model	Real building		Scale model		
			Fish-eye	24 mm	Fish-eye	24 mm	
1	608	602	615	770	651	772	322
2	2373	1592	2977	3671	2275	2657	996
3	763	522	832	855	656	710	512
4	14750	12800	19901	23021	19409	21398	5263
5	798	536	826	1060	601	713	507
6	13065	12130	16645	21686	17843	19965	5090
7	883		2746	1239			684
8	1339	815	1553	1789	1029	1219	633
9	11610	11100	14023	18005	16107	17115	4794
10	3887	1252	4662	5727	2876	3276	1130
11	2976	713	944	1133	741	894	343
12	1660	1075	2339	2288	1638	1837	1267
13	1528	1075	2109	2485	1547	1888	1071
14	1778	1048	2205	2356	1440	1884	1093
15	360	651	498	560	1042	784	170

Table 4.18
The raw luminance values using different luminance measurement methods

Double glazing assessment

	LR : Luminance meter		LR : Luminance measurement using HDRI				LR : Virtual model
	Real building	Scale model	Real building		Scale model		
			Fish-eye	24 mm	Fish-eye	24 mm	
1	0.07	0.08	0.06	0.05	0.06	0.07	0.07
2	0.19	0.16	0.19	0.18	0.14	0.17	0.24
3	0.07	0.05	0.06	0.05	0.05	0.05	0.11
4	1.12	1.05	1.21	1.15	1.10	1.11	1.04
5	0.08	0.06	0.06	0.06	0.04	0.05	0.11
6	1.00	1.00	1.00	1.00	1.00	1.00	1.00
7	0.09	0.00	0.09	0.07	0.00	0.00	0.15
8	0.12	0.14	0.11	0.09	0.07	0.09	0.14
9	0.89	0.92	0.84	0.79	0.90	0.83	0.94
10	0.56	0.26	0.55	0.47	0.29	0.26	0.62
11	0.22	0.11	0.08	0.07	0.07	0.07	0.09
12	0.14	0.10	0.13	0.12	0.09	0.10	0.32
13	0.15	0.10	0.13	0.12	0.09	0.10	0.33
14	0.16	0.10	0.14	0.12	0.10	0.11	0.32
15	0.03	0.06	0.04	0.03	0.07	0.04	0.04

LCP assessment

	LR : Luminance meter		LR : Luminance measurement using HDRI				LR : Virtual model
	Real building	Scale model	Real building		Scale model		
			Fish-eye	24 mm	Fish-eye	24 mm	
1	0.07	0.08	0.06	0.05	0.07	0.06	0.08
2	0.19	0.16	0.19	0.19	0.17	0.17	0.22
3	0.07	0.05	0.05	0.05	0.04	0.04	0.09
4	1.15	1.04	1.21	1.23	1.08	1.11	1.03
5	0.07	0.05	0.05	0.06	0.05	0.04	0.09
6	1.00	1.00	1.00	1.00	1.00	1.00	1.00
7	0.10	0.00	0.10	0.09	0.00	0.00	0.16
8	0.11	0.08	0.09	0.10	0.06	0.06	0.12
9	0.96	0.90	0.80	0.80	0.84	0.87	0.94
10	0.33	0.21	0.33	0.27	0.26	0.36	0.27
11	0.18	0.10	0.07	0.06	0.07	0.07	0.07
12	0.46	0.15	0.38	0.40	0.13	0.12	0.23
13	0.47	0.23	0.42	0.32	0.13	0.12	0.22
14	0.37	0.11	0.33	0.19	0.13	0.12	0.23
15	0.04	0.05	0.03	0.03	0.06	0.05	0.04

Prismatic film assessment

	LR : Luminance meter		LR : Luminance measurement using HDRI				LR : Virtual model
	Real building	Scale model	Real building		Scale model		
			Fish-eye	24 mm	Fish-eye	24 mm	
1	0.05	0.05	0.04	0.04	0.04	0.04	0.06
2	0.18	0.13	0.18	0.17	0.13	0.13	0.20
3	0.06	0.04	0.05	0.04	0.04	0.04	0.10
4	1.13	1.06	1.20	1.06	1.09	1.07	1.03
5	0.06	0.04	0.05	0.05	0.03	0.04	0.10
6	1.00	1.00	1.00	1.00	1.00	1.00	1.00
7	0.07	0.00	0.16	0.06	0.00	0.00	0.13
8	0.10	0.07	0.09	0.08	0.06	0.06	0.12
9	0.89	0.92	0.84	0.83	0.90	0.86	0.94
10	0.30	0.10	0.28	0.26	0.16	0.16	0.22
11	0.23	0.06	0.06	0.05	0.04	0.04	0.07
12	0.13	0.09	0.14	0.11	0.09	0.09	0.25
13	0.12	0.09	0.13	0.11	0.09	0.09	0.21
14	0.14	0.09	0.13	0.11	0.08	0.09	0.21
15	0.03	0.05	0.03	0.03	0.06	0.04	0.03

Table 4.19

Luminance ratio (LR) given by the different luminance measurement methods. The LR is the ratio of the luminance value at a point divided by the value at the centre of the image (in this study, the luminance value of point 6)

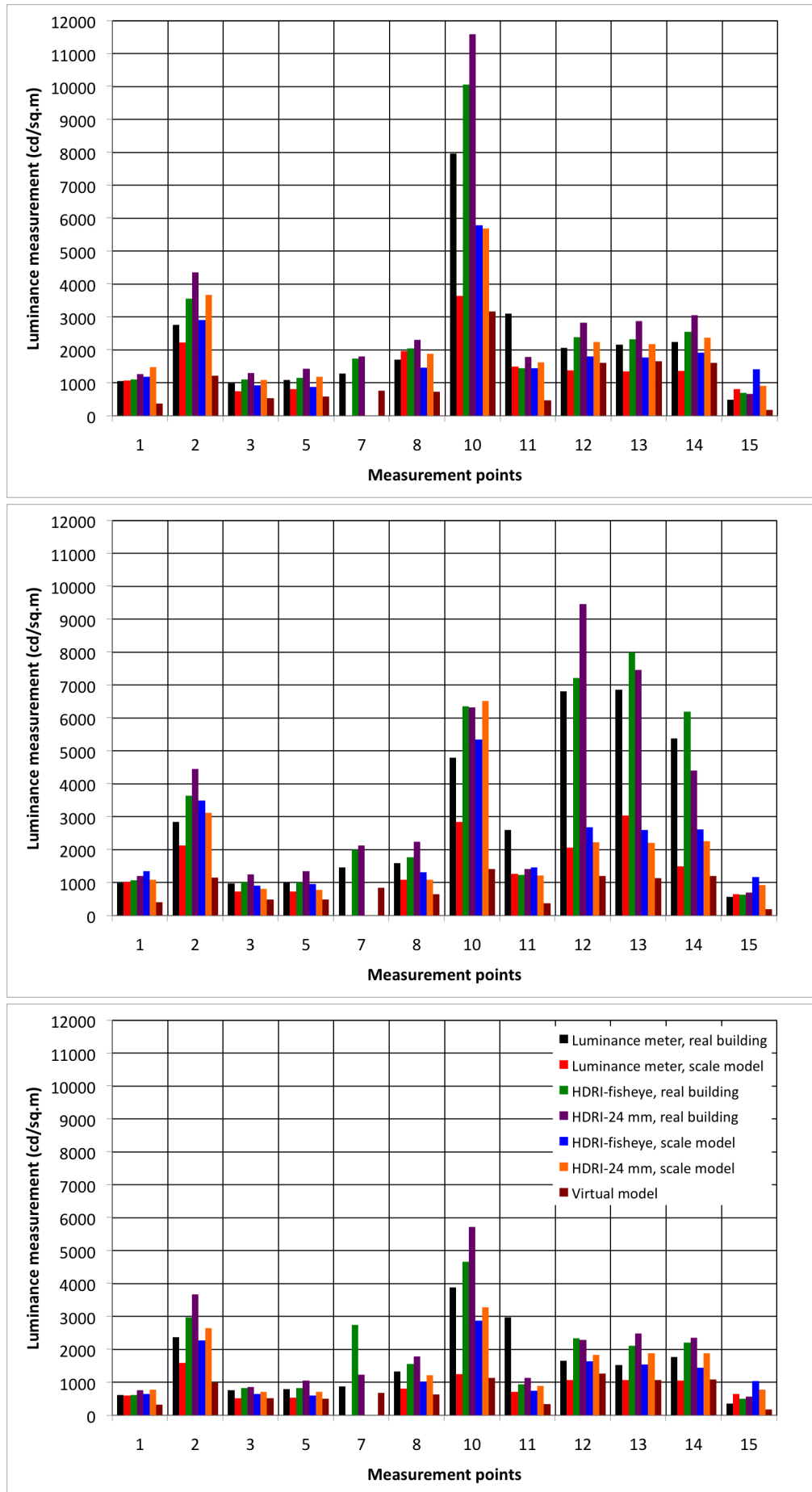


Fig. 4.66 Comparison of luminance values using different luminance measurement methods; assessments of opaque surfaces for double glazing (top), LCP (centre) and prismatic film (bottom)

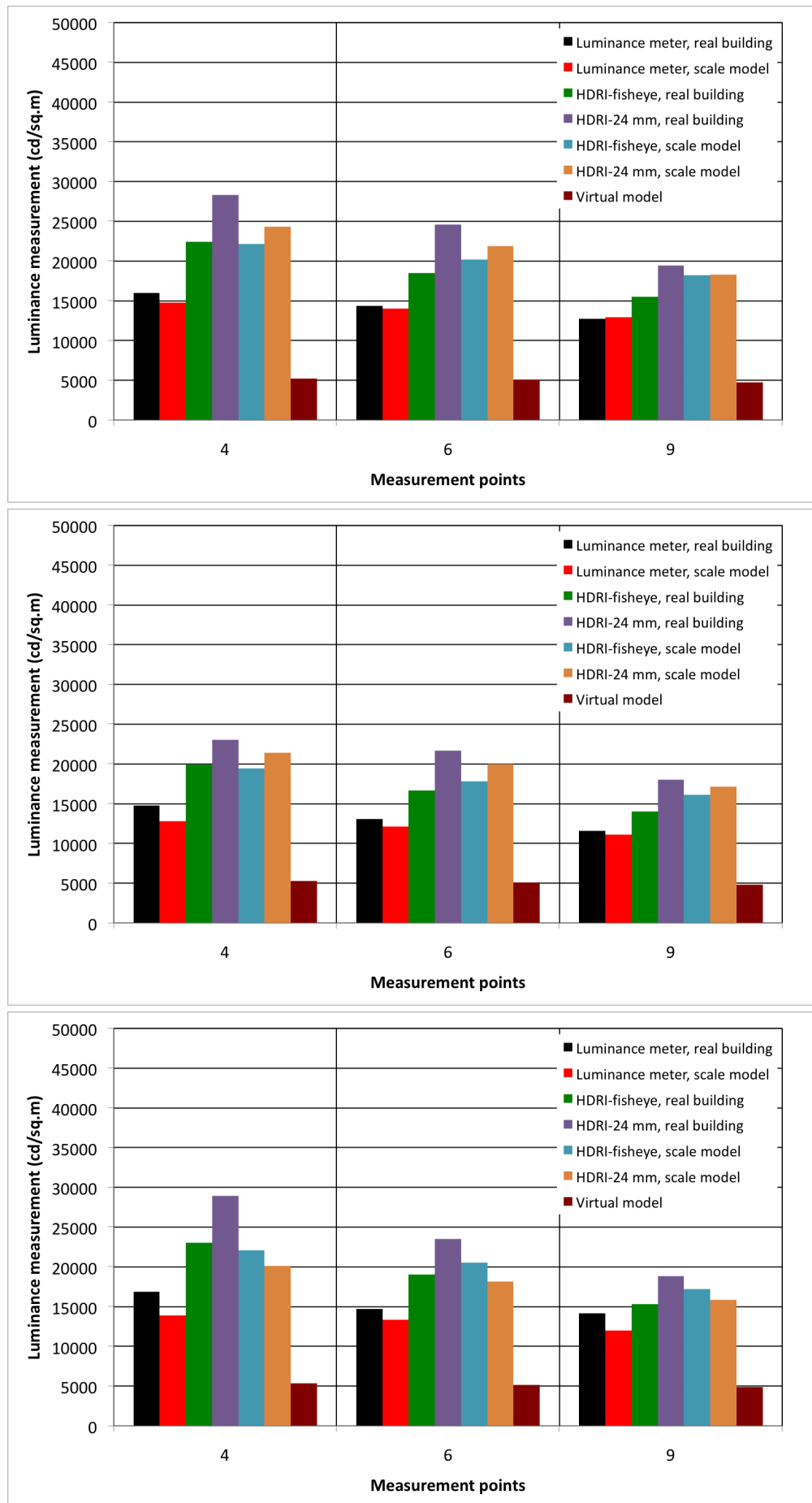


Fig. 4.67 Comparison of luminance values using different luminance measurement methods; assessments of transparent window for double glazing (top), LCP (centre) and prismatic film (bottom)

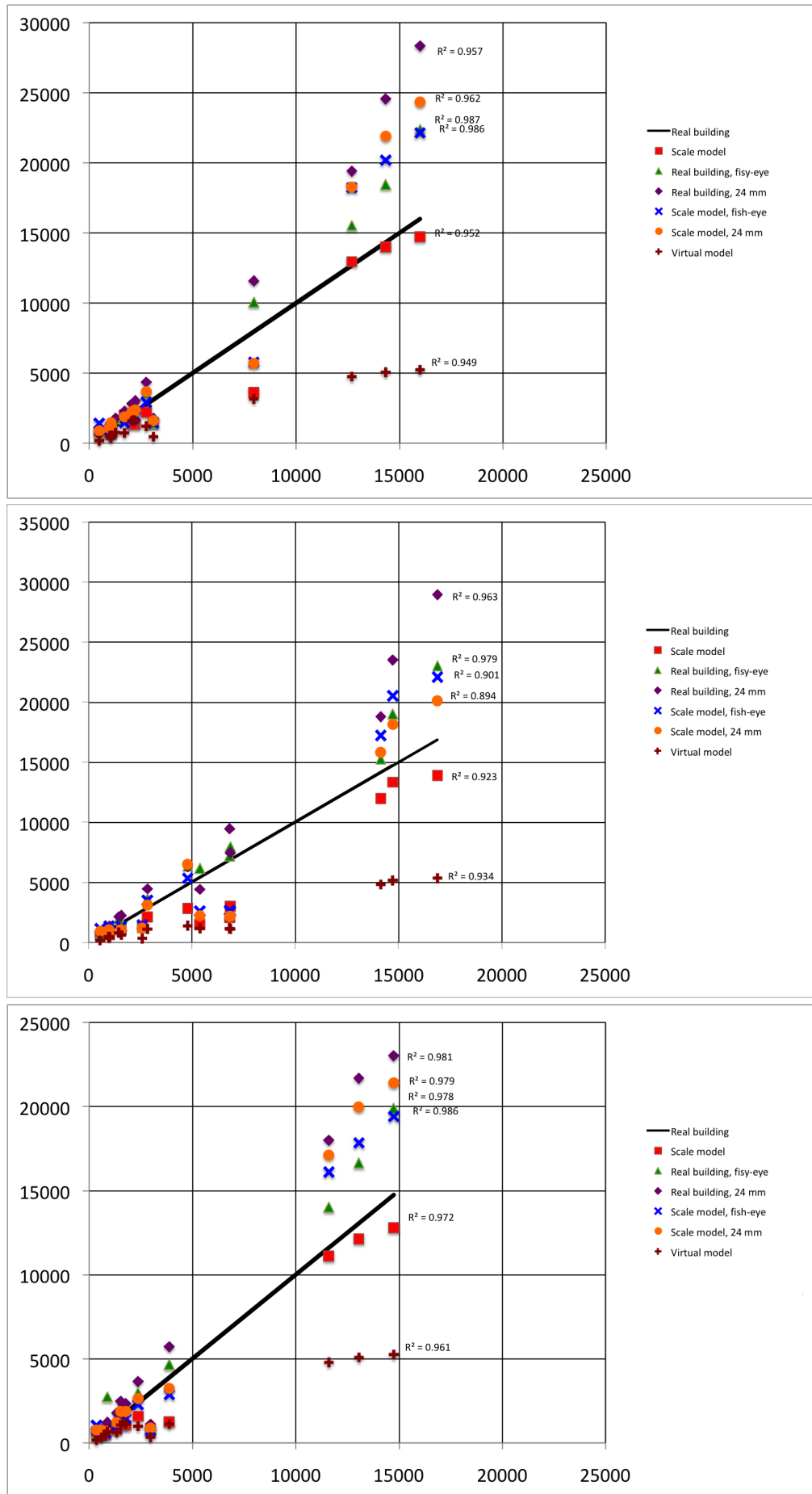


Fig. 4.68 Scattering diagram of the luminance measurement; assessments for double glazing (top), LCP (centre) and prismatic film (bottom)

4.5 Dissimilarity between models and real building

Physical and virtual models are very useful daylighting design tools but their accuracy and reliability for daylighting performance assessment really depends on the parameters of the model.

In this study the main causes of error in daylighting performance assessments of building are focused on the model properties: how the models compared with the real building is laid out in Table 4.20. The study of the main causes of difference are presented in the next chapter, some general considerations being that:

- Differences in the model geometry were observed when measuring the dimensions of both the real building and its physical model; the dimensions of a virtual model can be precisely indicated.
- Small details in physical and virtual models could not be constructed because they were too difficult or complicated. This was true, for instance, of the texture of the materials which was impossible to reproduce.
- Because real materials are difficult to use in a physical model (and cannot be used in a virtual model) the photometric properties of materials also differed from the real case. The models' surface reflectance, ground reflectance and window transmittance in general differed from the real situation. Moreover, dust and dirt in the real and physical model were also a cause of error in the assessment.
- Even though the photometric sensors are not the part of the models themselves, they have different properties and are the instruments of measurement; their sensitive area and positioning may be a cause of additional measurement error.

Some parameters are more important than others. Experiments were made with different modelling situations to understand the significance of each of the potential causes of error. The next chapter describes the amplitude of these discrepancies during daylighting performance assessment

	Real case	Case A	Case B	Case C	Case D	Case E
Geometry measurement						
Dimensions	± 0.01 m	± 0.005 m	± 0.005 m	± 0.005 m	N/A	N/A
Difference in dimensions compared to real building		< 0.12 m	< 0.12 m	< 0.12 m	N/A	N/A
Details						
Window	√	√	√	√	√	√
Door	√	none	none	none	none	none
Wall	√	√	√	√	√	√
Floor	√	√	√	√	√	√
Ceiling	√	√	√	√	√	√
Texture	√	textured paper	textured paper	textured paper	N/A	N/A
Furniture	none	none	none	none	none	none
Cupboard and computer	√	none	none	none	none	none
Luminaire	√	√	√	√	√	√
Scientific equipment	√	none	none	none	none	none
Lux-meter	√	√	√	√	N/A	N/A
Track for lux-meter	√	√	√	√	N/A	N/A
Tripod and mount	√	none	none	none	none	none
Photometry measurement						
Surface reflectance (reflectometer)	± 3 %	± 3 %	± 3 %	± 3 %	N/A	N/A
Window transmittance (luminance meter)	± 3 %	± 3 %	± 3 %	± 3 %	N/A	N/A
Dust and Dirt	√	√	√	√	N/A	N/A
Ground reflectance	± 3 %	± 3 %	± 3 %	± 3 %	N/A	N/A
Differences of surface and ground reflectance compared to real building		< 10%	< 10%	< 10%	< 6%	< 6%
Differences of window transmittance compared to real building		< 10%	< 10%	< 10%	< 6%	< 6%
Photometric sensors						
Precision (details in Appendix B)	± 10 %	± 10 %	± 10 %	± 10 %	N/A	N/A
Sensitivity area	6 cm	4 mm	5 mm	6 mm	Point measurement	Point measurement
Position	± 0.01 m	± 0.005 m	± 0.005 m	± 0.005 m	N/A	N/A
Differences of positioning area compared to real building		< 0.12 m	< 0.12 m	< 0.12 m	N/A	N/A

N/A = Not available

Table 4.20
Accuracy of the different parameters in the real building and the models used in the assessment

chapter

5

reliability and accuracy of daylighting models

5.1 Sets of parameters

To understand how important the precision of the models is to reliable daylighting performance assessment, several sets of potential sources of error were analysed. The sensitivity of models to the following five main sources of error was studied;

- 1. Geometrical measurements**
 - a. Main elements
 - Window dimensions
 - Model dimensions
- 2. Geometrical details**
 - a. Critical design features
 - Window frame
 - Luminaires (lighting fixtures)
- 3. Photometric measurements**
 - a. Surface reflectance
 - b. Ground reflectance
 - c. Window transmittance
- 4. Photometric sensors**
 - a. Sensitive area
 - b. Positioning
 - Horizontal plane
 - Tilting
- 5. Surrounding**
 - a. Ground reflected component
 - b. Sky view factors

Physical model

The physical model considered in this study is a 1:10 scale model of the real building used under real sky conditions which was presented in Chapter 3. It was considered under a clear real sky and photographs were taken for comparison purposes. A detailed sensitivity analysis will be found at the end of this chapter.

Virtual model

The virtual model was generated by the Radiance program as described in detail in Chapter 3. It was designed to match the geometric and photometric features of the test module exactly. For this reason external sources of error regarding the computer simulation were not expected. The virtual model accurately simulated both CIE standard overcast sky and CIE standard clear sky. The daylight factor (DF) and illuminance ratio (IR) profiles inside the model was analysed at 7 points placed 1 m apart, however only three of the measured points are evaluated in detail in this thesis. The one 0.2 m away from the window represents the space near the building's opening, the one 3.2 m from the window equates to the intermediate area and that 6.2 m from the window represents the room's deeper parts.

To identify the causes of the model inaccuracy, the DF and IR discrepancies between the 'base case' virtual model (whose parameters are presented in Table 5.1) and other variants were assessed and compared. The relative divergences were used to quantify the impact of sources of error on the model accuracy.

Base case	Parameters	Description
DF or IR calculation	Radiance parameters ¹	ab = 9 aa = 0.1 ad = 26315 ar = 128
	Sky model	CIE standard sky (created using GenSky)
	Sky condition	CIE standard overcast sky, CIE standard clear sky (16CEST) ²
Scene rendering	Radiance parameters	ab = 9 aa = 0.1 ad = 1536 ar = 45
	Sky model	CIE standard sky (created using GenSky)
	Sky condition	CIE standard overcase sky, CIE standard clear sky (16CEST) ²

Table 5.1
Base case virtual model properties

¹ The Radiance parameters used for the assessment were analysed using the RMSE (Root Mean Squared Error) among the combination of different parameters, as presented below, to obtain the most reliable parameters for accuracy and timing:

ab : 5, 6, 7, 8, 9
aa : 0.1, 0.2, 0.3
ad : 1681, 3455 8374, 26315
ar : 8, 64, 128, 256

² CIE standard skies created using the Radiance GenSky function presenting the least discrepancy as presented in Chapter 4

The afore-mentioned error sources were analysed, Table 5.2 presents several sets of related parameters considered in the sensitivity analysis.

Data set	Parameters in Radiance
Set 1: Window dimension	H = Window height (m)
Set 2: Model dimension	D = Model depth (m) Inclusion
Set 3: Model details	Disappearance of luminaires and window opening
Set 4: Surface photometry	ρ_s = Model surfaces reflectance
Set 5: Ground photometry	ρ_g = Ground reflectance
Set 6: Window photometry	τ = Window transmittance
Set 7: Sensor's sensitive area	Measured points
Set 8: Sensor placement (x coordinator, parallel to window)	P_s = Sensor position in model
Set 9: Sensor placement (y coordinator, perpendicular to window)	P_s = Sensor position in model
Set 10: Sensor positioning; tilting angle (x coordinator, parallel to window)	A_s = Sensor tilting angle and horizontal plane in model
Set 11: Sensor positioning; tilting angle (y coordinator, perpendicular to window)	A_s = Sensor tilting angle and horizontal plane in model

Table 5.2
Summary of sets of parameters for Radiance-generated virtual models

5.2 Geometric measurement

The simulations were done from two approaches; first for window dimensions and secondly for model dimensions.

Window dimensions

The analysis of the impact of inaccurate window dimensions was carried out through a sensitivity analysis, testing how sensitive daylighting was to window height. By progressively reducing the window height - the sill was raised - by 1 to 10 cm (Fig. 5.1), the relative divergences in comparison with the 'Base case' (Fig. 5.2 and 5.3) lead to the relative divergences induced by inaccurate window dimension.

Table 5.3 details the cases considered in the window dimension inaccuracy study. The simulations were carried out for models having a double glazing window as well as for different CFS. The window height, including the height of the CFS if it was attached to the upper part of the window, was decreased. Its impact was evaluated by comparing the relative divergence of DF (or IR) from that of the base case.

Data set	Parameters in Radiance
Set 1: Window dimensions	H = Window height (m)
	$H_{\text{base case}} = 1.60 \text{ m}$
	$H_{\text{base case}} - 0.01 \text{ m} = 1.59 \text{ m}$
	$H_{\text{base case}} - 0.02 \text{ m} = 1.58 \text{ m}$
	$H_{\text{base case}} - 0.03 \text{ m} = 1.57 \text{ m}$
	$H_{\text{base case}} - 0.04 \text{ m} = 1.56 \text{ m}$
	$H_{\text{base case}} - 0.05 \text{ m} = 1.55 \text{ m}$
	$H_{\text{base case}} - 0.06 \text{ m} = 1.54 \text{ m}$
	$H_{\text{base case}} - 0.07 \text{ m} = 1.53 \text{ m}$
	$H_{\text{base case}} - 0.08 \text{ m} = 1.52 \text{ m}$
	$H_{\text{base case}} - 0.09 \text{ m} = 1.51 \text{ m}$
	$H_{\text{base case}} - 0.10 \text{ m} = 1.50 \text{ m}$

Table 5.3
Set of comparative data used to outline the effect of inaccurate window dimension on daylighting performance assessment

Fig. 5.2 presents the impact of window dimension inaccuracy for CIE standard overcast sky conditions, Fig. 5.3 its impact under CIE standard clear sky.

The relative divergence of daylight factors under CIE overcast sky were, at 0.2m from the window and for all fenestration systems, on average equal to 10% when the window dimension error was less than 5 cm; it reaches a maximal value of 16.8% for the greatest error (10cm). Divergences are greater for positions near the window, indicating that the direct component of daylight contributes in a significant way to the daylight factor for these positions. The impact of the window dimension error can be considered using images which indicate by false colours the lighting threshold of DF or IR from 1% to 19% and more. Comparing the Base case model's images with the others variants shows where significant discrepancies of daylight quality occurred.

Under a CIE standard clear sky, the relative divergences are on average lower than with a CIE standard overcast sky, it reaches however, 12.9% for a prismatic film when the window of the full size model was too small by 10 cm - corresponding to an error of only 1 cm in a 1:10 scale model. The false colour images confirm this by showing significant daylighting flux modification between the 'Base case' and 1 cm or 10 cm errors.

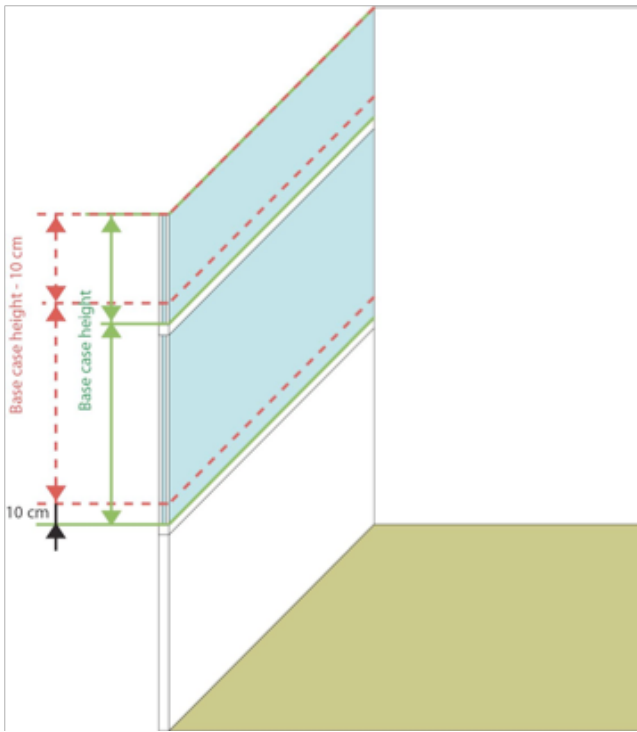
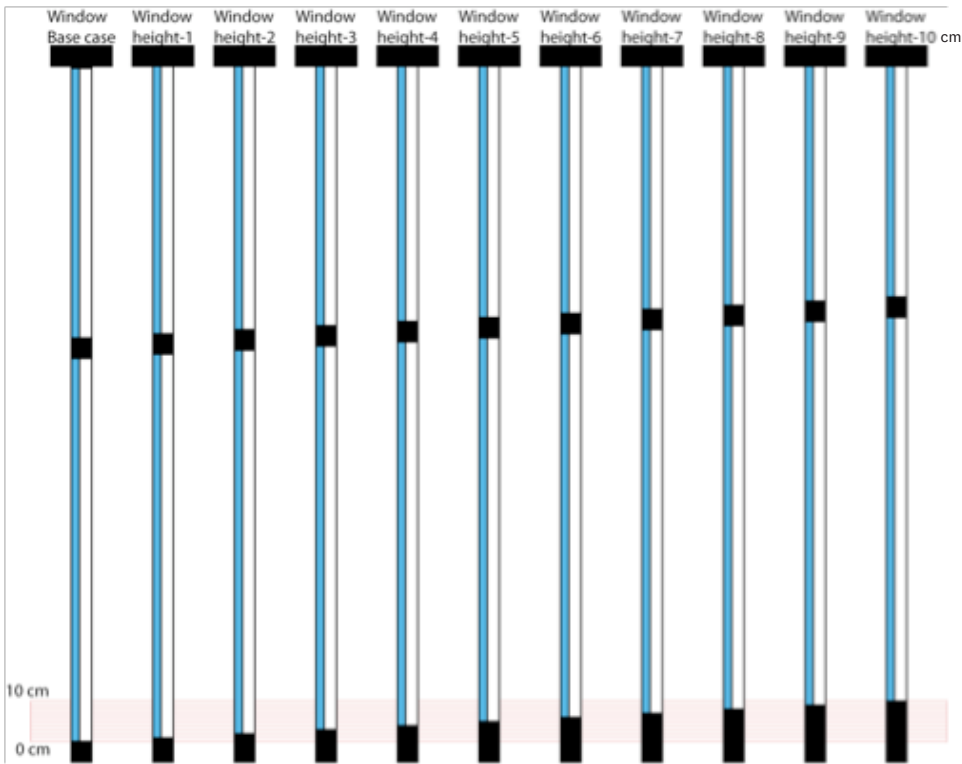


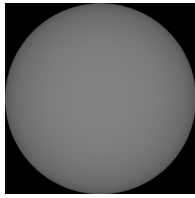
Fig. 5.1 Comparative data used to outline the effect of inaccurate window dimension on daylighting performance assessment.



As shown in Fig. 5.2 and 5.3, daylighting assessment accuracy became less as dimensional errors rose. This cause of error had greater effect under overcast sky conditions, particularly at the measured points closest to the window.

One concludes that a small error in window size has a significant effect on the lighting evaluation because less light can enter; 10 cm less height caused about 5.5% less window glazing area through which daylight could penetrate into the studied building.

Window dimensions
CIE standard overcast sky



Measured points

- + 6.2 m from window
- o 3.2 m from window
- 0.2 m from window

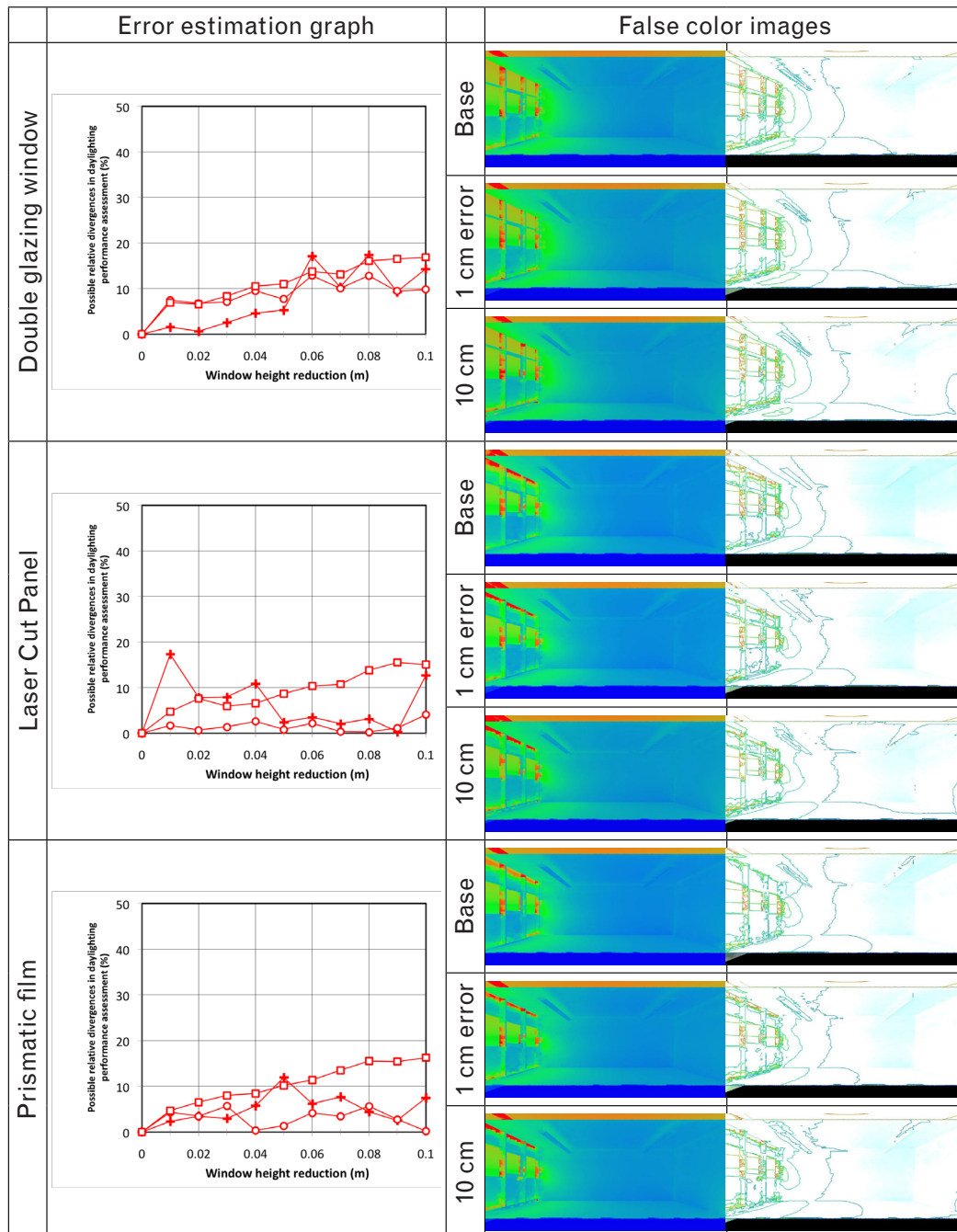
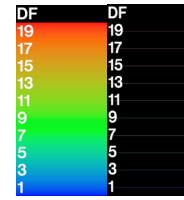


Fig. 5.2 CIE overcast sky; relative divergence (left) on daylight factors caused by inaccurate window dimension. Comparative false-colour images (right) present the daylight daylight factor profiles in the room.

Window dimensions
CIE standard clear sky

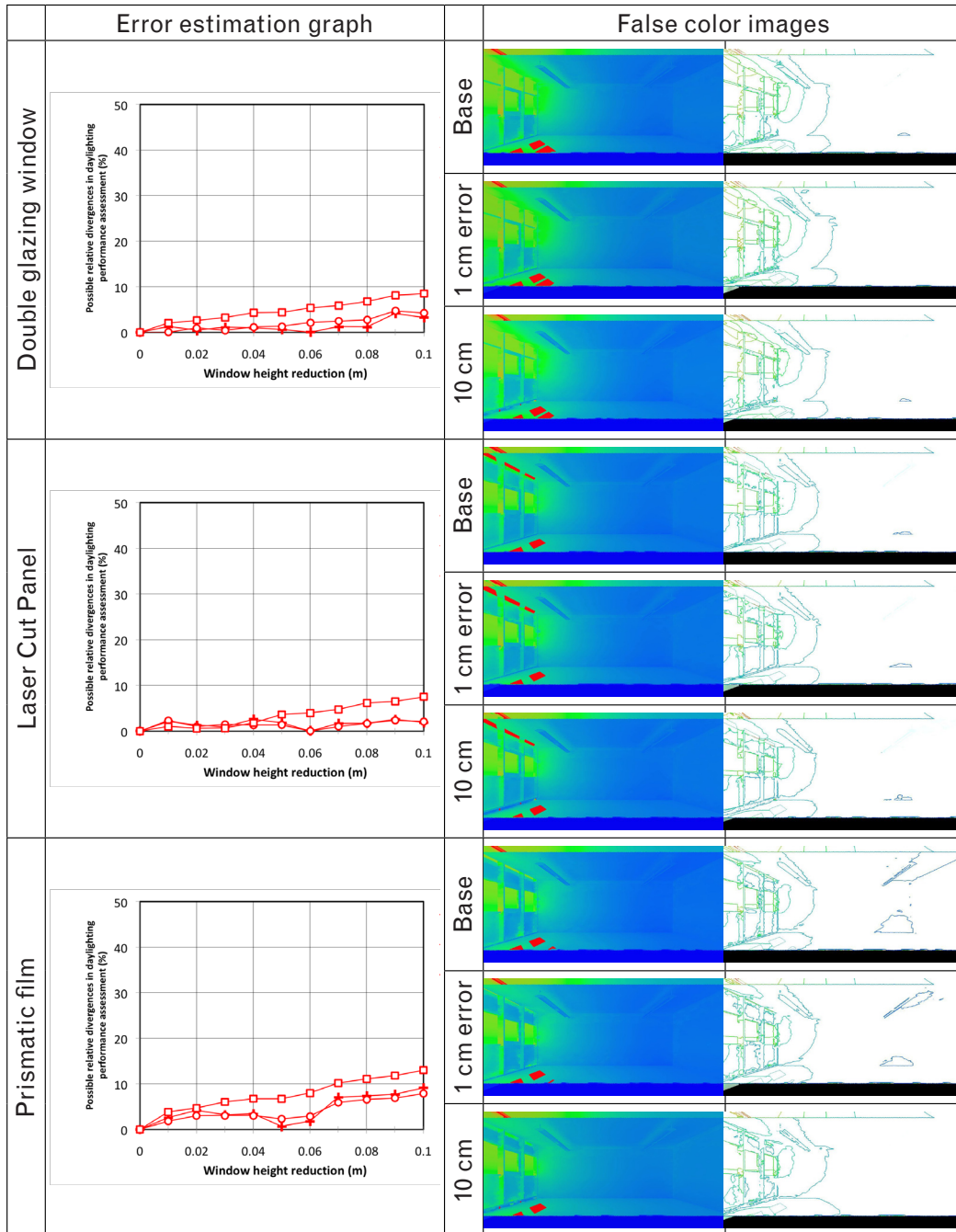
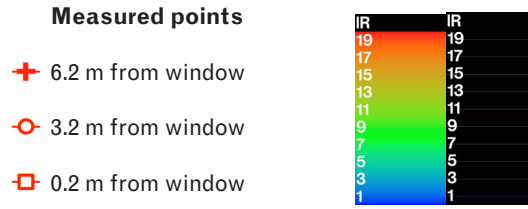
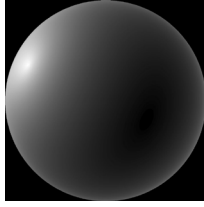


Fig. 5.3 CIE overcast sky: relative divergence (left) on illuminance ratios caused by inaccurate window dimension. Comparative false-colour images (right) present the daylight illuminance ratio profiles in the room.

Model dimensions

Similar simulations of the virtual model were made to determine the effect on daylighting performance of imprecise room depth. The real depth was 6.50 m; a sensitivity analysis (described in Table 5.5 and Fig. 5.4) were performed with virtual rooms shorter of 1cm to 10cm. The photometrically measured points were stationary in relation to the wall furthest from the window; it was the window that progressively approached the virtual sensors. Fig. 5.5 and 5.6 respectively show the relative divergence between DF under CIE overcast sky conditions and IR under CIE clear sky conditions, observed in at equal distances from the window side.

Data set	Parameters in Radiance
Set 2: Model dimensions	D = Model depth (m)
	$D_{\text{base case}} = 6.5 \text{ m}$
	$D_{\text{base case}} - 0.01 \text{ m} = 6.49 \text{ m}$
	$D_{\text{base case}} - 0.02 \text{ m} = 6.48 \text{ m}$
	$D_{\text{base case}} - 0.03 \text{ m} = 6.47 \text{ m}$
	$D_{\text{base case}} - 0.04 \text{ m} = 6.46 \text{ m}$
	$D_{\text{base case}} - 0.05 \text{ m} = 6.45 \text{ m}$
	$D_{\text{base case}} - 0.06 \text{ m} = 6.44 \text{ m}$
	$D_{\text{base case}} - 0.07 \text{ m} = 6.43 \text{ m}$
	$D_{\text{base case}} - 0.08 \text{ m} = 6.42 \text{ m}$
	$D_{\text{base case}} - 0.09 \text{ m} = 6.41 \text{ m}$
	$D_{\text{base case}} - 0.10 \text{ m} = 6.40 \text{ m}$

Table 5.4
Set of comparative data used to outline the effect of inaccurate model dimensions on daylighting performance assessment

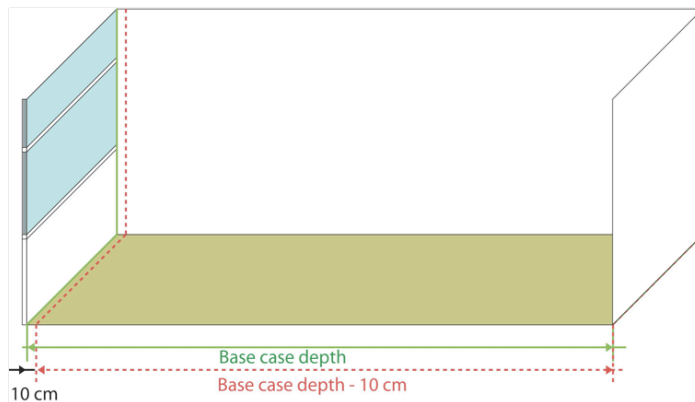


Fig. 5.4
How the room was shortened to test the effect of inaccurate model dimension on daylighting performance assessment.

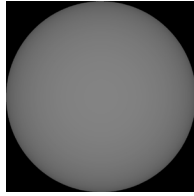
Significant divergences illustrated on Fig. 5.5 were observed for the simulations under an overcast sky; they reached a maximum of 30.5% for a prismatic film at a 20cm distance (originally) from the window and a model 10cm too short. This confirms that dimensional accuracy is very important in physical models – a 10cm error considered here in the real building to a 1cm in a 1:10 physical scale model.

For the models under clear sky conditions (Figure 5.6), errors provoked by imprecise model dimensions are less than under the overcast conditions. However, at the point nearest the window (0.2m away originally), where the greatest relative divergences were noted, especially for prismatic film, it reached 18.6%.

The false-colour images show the comparative differences in each case. Slight errors in model dimensions can lead to significant errors in the daylighting assessment, especially as the imprecision becomes greater.

The critical measured positions were those near the window, particularly under overcast sky. This can be explained by the fact that when the room depth was decreased, measured points in the building became closer to the window, so providing a greater light flux to the sensors and hence an overestimated assessment.

Model dimensions
CIE standard overcast sky



Measured points

- + 6.2 m from window
- 3.2 m from window
- 0.2 m from window

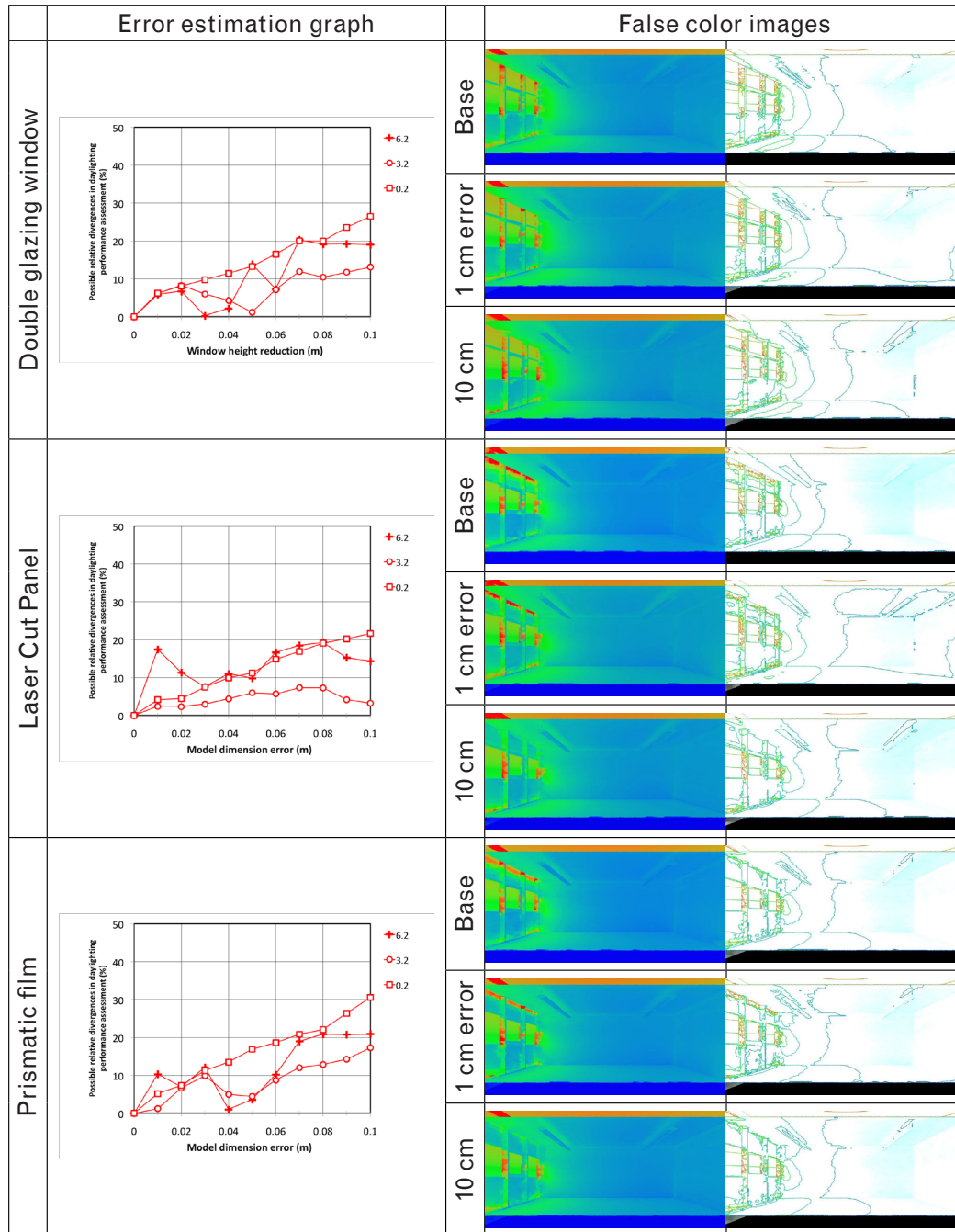
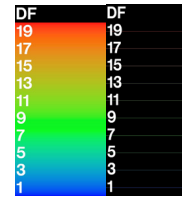
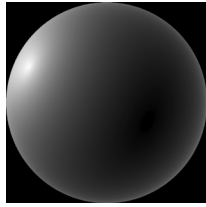


Fig. 5.5 CIE overcast sky; relative divergence (left) on daylight factors caused by model dimension imprecisions. Comparative false-colour images (right) present the daylight daylight factor profiles in the room.

Model dimensions
CIE standard clear sky



- Measured points**
- + 6.2 m from window
 - 3.2 m from window
 - 0.2 m from window

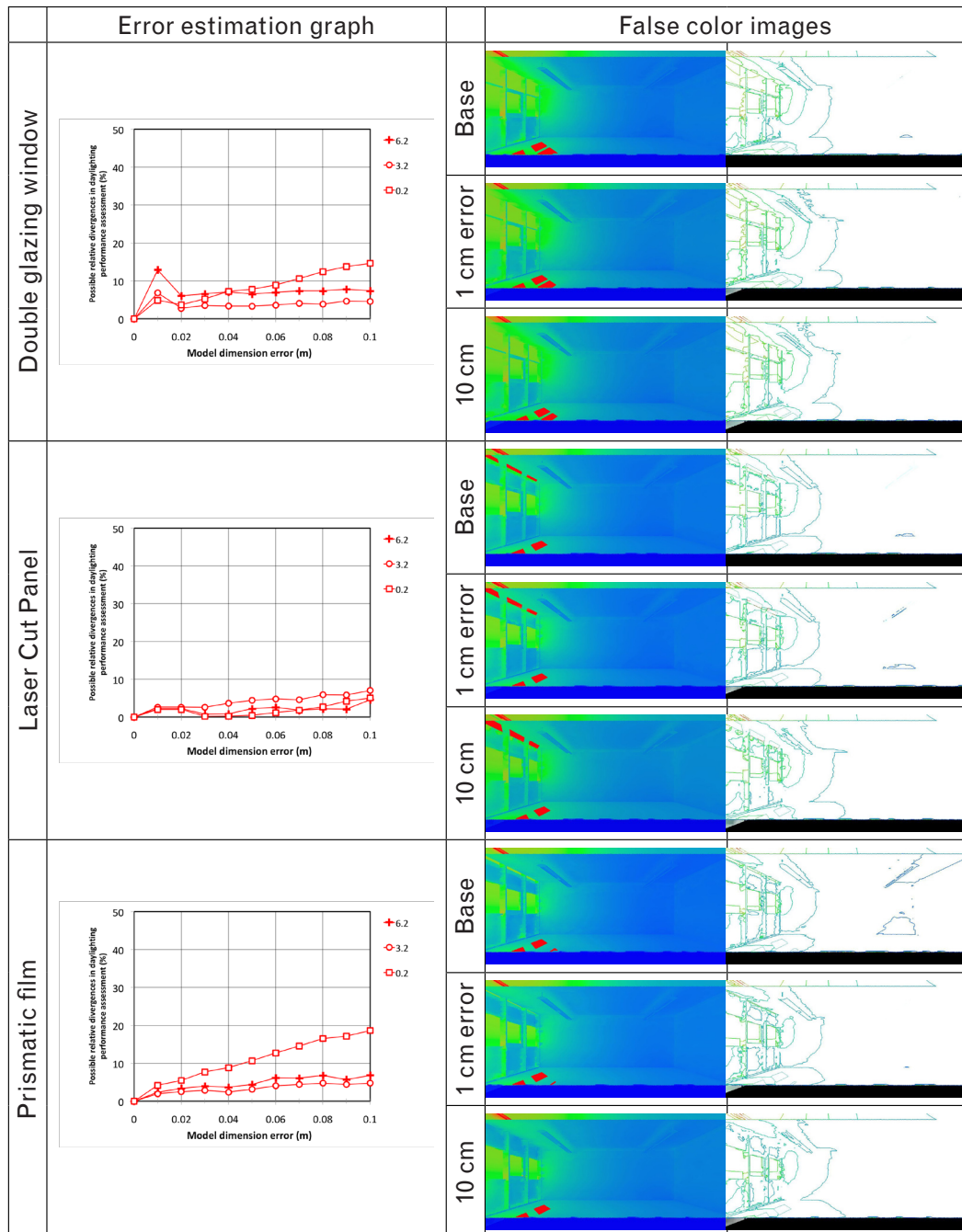
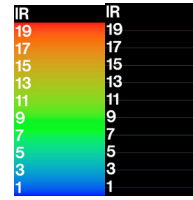


Fig. 5.6 CIE clear sky: graphs (left) present the tendency of assessment errors caused by model dimension imprecisions. The comparative false-colour images (right) present the daylight properties (illuminance ratio profile) of the interior space.

5.3 Geometric details

170

The real building used in this study as well as its models had as only few interior details in order to avoid further sources of error. However, the real building had lighting fixtures on the ceiling; the central section of the side window had a frame that allowed it to open (see Fig. 3.4 and 3.14). The simulations on modelling details were done for two critical features, firstly for luminaires (lighting fixtures) and secondly for window frame details. Table 5.5 describes the analysis of errors caused by inaccurate details.

Data set	Parameters in Radiance
Set 3: Model details	The 'Base case' model includes luminaires and window opening.
	Model without lighting fixtures
	Without window opening frame
	Without window opening frame and panels

Table 5.5
Set of comparisons used to outline the effect of inaccurate design details on daylighting performance assessment

Lighting fixtures

An analysis of lighting fixture detail was carried out for models including a double window as well as two different CFS. The model without lighting fixtures (Fig. 5.7) was compared of the 'Base case' model on the basis of DF and IR.

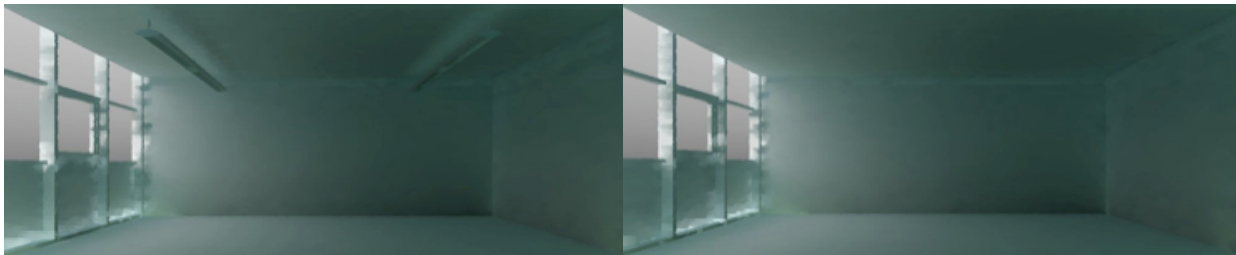


Fig. 5.7
Virtual model with lighting fixtures (left) and without lighting fixtures (right)

Window details

A similar analysis was carried out concerning the window details (the central window frame and panels) as illustrated in Fig. 5.8. The two CFS as well as the double glazing were considered.



Fig. 5.8
Virtual models with both window frame and panel (left), only with window frame (centre) and without window frame nor window (right)

Fig. 5.9 and 5.10 show the average relative divergence between DF under CIE overcast sky conditions and IR under CIE clear sky conditions, observed at equal window distances.

The impact of model details was vary by importance particularly for a CFS were considered under overcast sky conditions. The errors attributable to leaving out the lighting fixtures observed for the LCP under overcast sky were up to 14.4%; they reached an additional 17.6% and 11.2% relative divergences when the window details were ignored. This again confirms that window modelling accuracy has a very strong impact on daylighting assessment. Nevertheless, under clear sky conditions with LCP, the relative divergence was 4.4% if the lighting fixtures were missed out and more than 17.4% if the window details (frame and panel) were not included.

The impact of these errors of detail can be examined using false-colour images. The comparison of the 'Base case' model images and the others shows significant discrepancies among them, particularly when window details were ignored.

The relative errors presented in the study confirm that significant errors can occur when even small model details are left out during model construction.

Fig. 5.9 and 5.10 show that, the absence of lighting fixtures causes visible errors, even more when a CFS was employed. The latter normally contributes to redirect daylight to the deeper part of the room using the reflection of the light on the side walls and ceiling. When details at ceiling level are inaccurate, it can seriously impact on the reflected light.

Inaccurate window details lead to errors since daylight penetration is of critical importance. The absence of the window panel and frame provoke consequently large errors because a greater light flux could penetrate the building.

Model details

CIE standard overcast sky

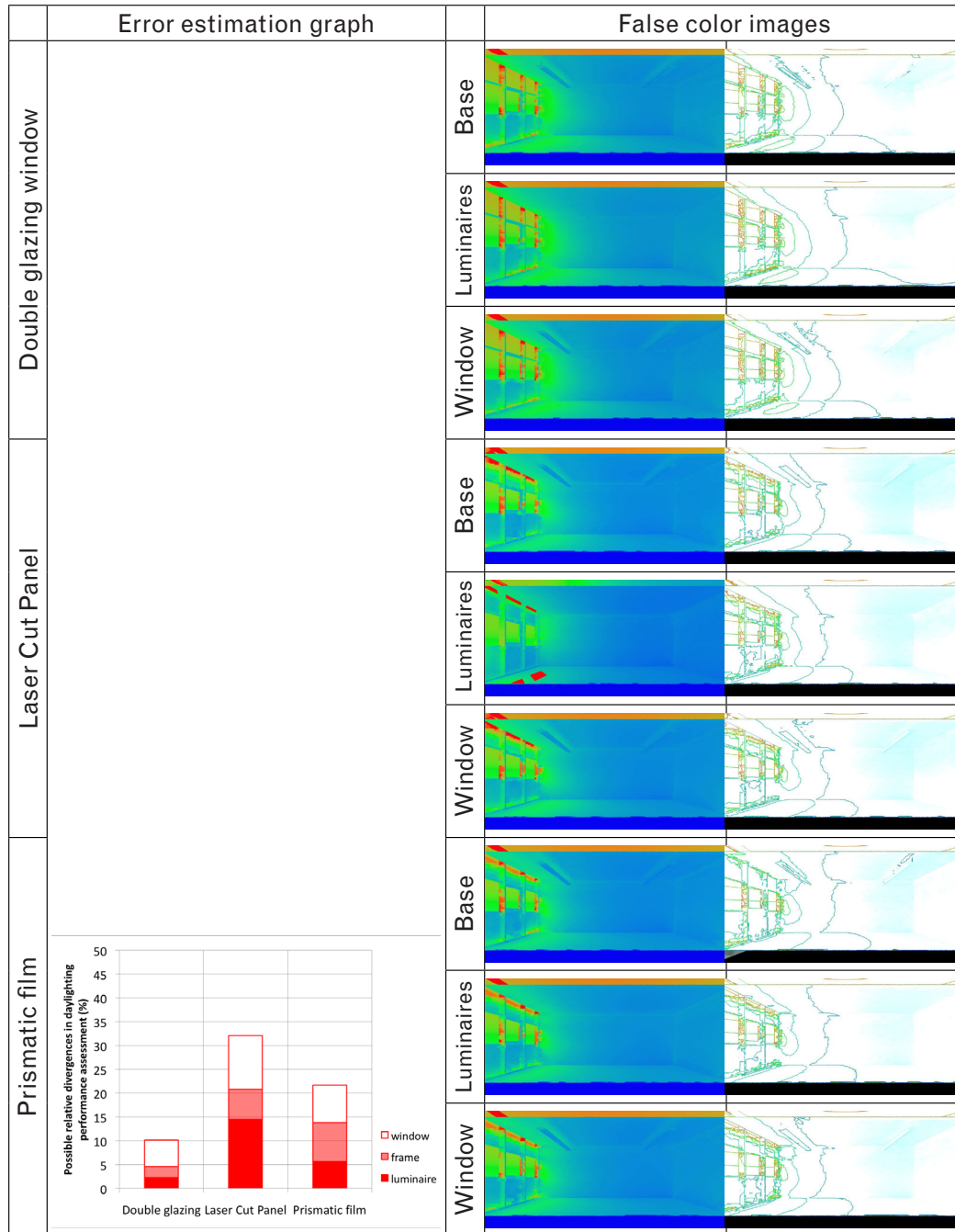
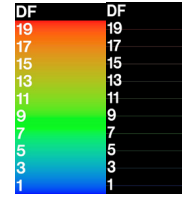
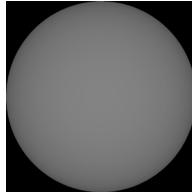


Fig. 5.9 CIE overcast sky; relative divergence (left) on daylight factors caused by leaving details out of the model. Comparative false-colour images (right) present the daylight daylight factor profiles in the room.

Model details
CIE standard clear sky

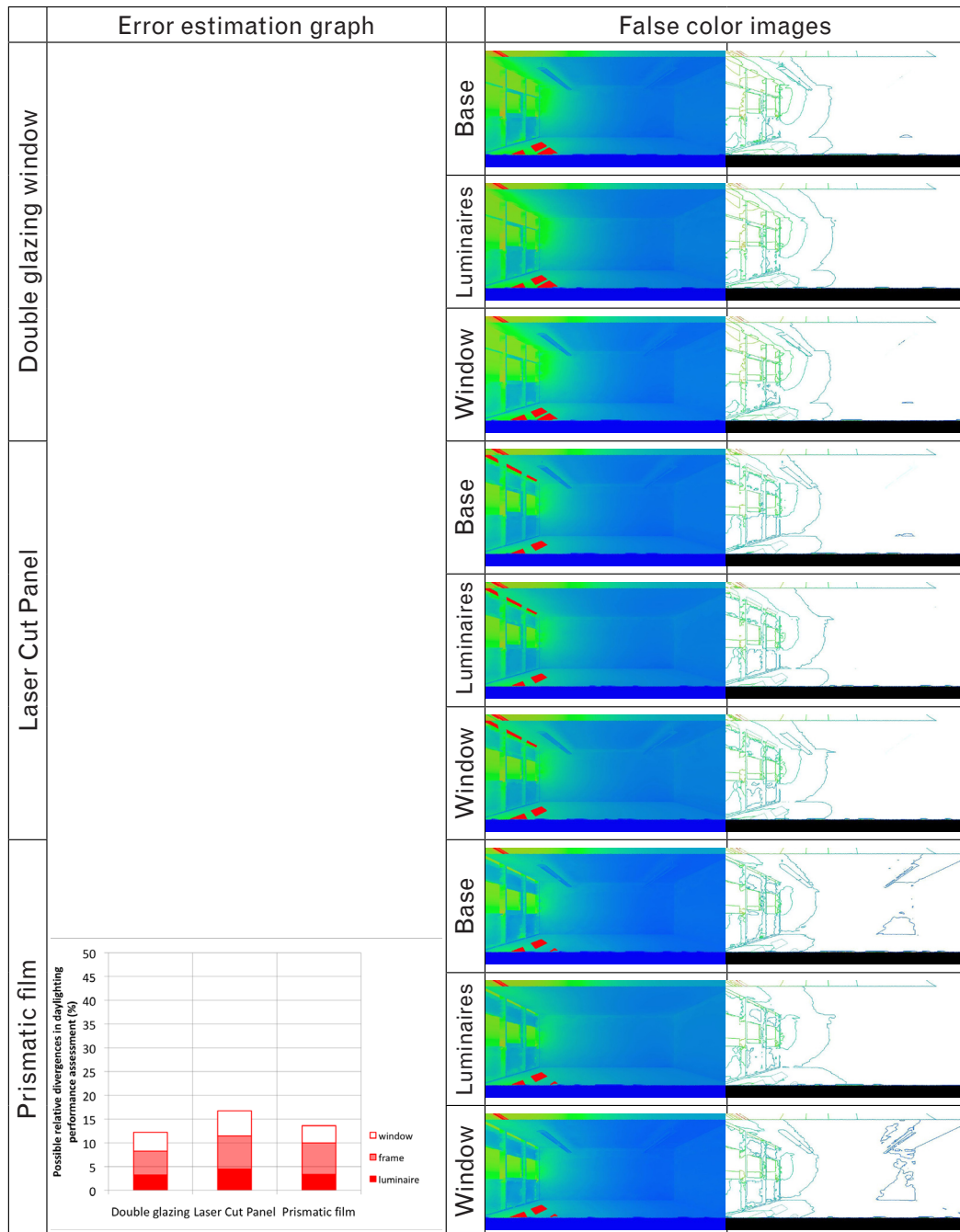
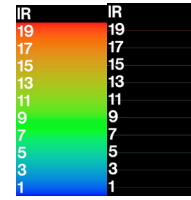
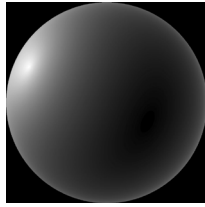


Fig. 5.10

CIE clear sky: graphs (left) present the level of assessment errors caused by leaving details out of the model. The comparative false-colour images (right) present the daylight properties (daylight factor profile) of the interior space.

5.4 Photometric measurement

174

Using virtual models, simulations concerning the effect of measurement errors were carried out for three important photometric values: interior surface reflectance, ground reflectance and window transmittance.

Interior surface reflectance

The effect of imprecise surface reflectance was analysed using computer simulation. They were carefully designed to exactly match the geometric and photometric features of the real building (details in Chapter 3). External sources of error regarding the computer simulation parameters were not expected for this reason. Both CIE standard overcast sky and CIE standard clear sky were considered during this study.

A sensitivity analysis of interior surface reflectance was carried out for models including a double glazing window as well as different CFS. Surface reflectance values ranging from $0.1 \times \rho_{\text{base case}}$ to $1.5 \times \rho_{\text{base case}}$ were considered for the floor; for the walls and ceiling the 'Base case' multiplier range was 0.1 to 1.1. Daylight factor and illuminance ratio profiles, observed in the models at 7 different locations at 1m intervals, were compared. The relative divergence observed between these figures were used to quantify the impact of surface reflectance on model accuracy.

The sensitivity analysis, performed by assuming surface reflectance up to 90% lower and 50% higher than the real 'base case' values, showed large relative divergences (wall and ceiling values were only up to 10% higher). The analysis is presented in detail in Table 5.6.

Data set	Parameters in Radiance
Set 4: Surface photometry	ρ_s = Model surface reflectances
	ρ_s base case x 0.1
	ρ_s base case x 0.2
	ρ_s base case x 0.3
	ρ_s base case x 0.4
	ρ_s base case x 0.5
	ρ_s base case x 0.6
	ρ_s base case x 0.7
	ρ_s base case x 0.8
	ρ_s base case x 0.9
	ρ_s base case x 1.1
	ρ_s base case x 1.2*
	ρ_s base case x 1.3*
	ρ_s base case x 1.4*
	ρ_s base case x 1.5*
* only floor surface reflectance was overestimated, other values reaching 100% reflectance.	

Table 5.6
Set of comparative data used to outline the effect of inaccurate interior surface reflectance on daylighting performance assessment

Fig. 5.11 and 5.13 shows the relative divergence of the DF profiles under CIE overcast sky conditions observed at the equal window distances. For the virtual model with a double glazing window, the relative discrepancy was 22.9% for a 10% reduction of surface reflectance at 6.2 m from the window and 32.4 - 65.3% for a 10% overestimation of surface reflectance at the same distance.

For the virtual model with Laser Cut Panel, the discrepancy was 8.2 - 21.3% for a 10% reflectance reduction and 30.7 - 89.2% when overestimating reflectance by 10%. Similar figures were observed for the prismatic film, compared to the 'Base case'; the discrepancy reached 5% for a 10% reflectance reduction and 90% for a 90% reduction.

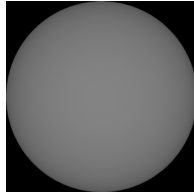
Under a CIE clear sky the "Base case" (Fig. 5.12 and 5.14), equipped with a double glazing window, led to the same tendency of the relative divergence as found under overcast sky conditions. The relative divergence of the illuminance ratio was 5.8 - 16.3% for a 10% reduction of surface reflectance and 42.5 - 78.2% for a 10% overestimation of surface reflectance. With a laser cut panel attached to the window the discrepancy reached 6.2-16.1% for a 10% reflectance reduction and 39.8-771.7% for a 10% reflectance overestimation. Similar figures were also observed for the prismatic film when compared to the 'Base case', the discrepancy reaching 6.1-16.6% for a 10% reflectance reduction.

Surface reflectance can be seen as an important parameter regarding the virtual model's accuracy, particularly for positions deeper in the room where internally reflectance tends to dominate. However, the complexity of light propagation through CFS, taken into account by the integration of monitored BTDF data into the Radiance program, discrepancies remain reasonable for CFS.

The errors caused by inaccurate reflectance is greater in the deeper part of the room because of inter reflections on the interior surfaces. It was also noted that errors increase more for overestimation of the reflectance than for underestimation: this has to deal with the non-linear relation existing in between the daylight flux entering deep into the room versus the incoming light flux at the window side (infinite number of inter-reflection).

The impact of these errors can be seen on false-colour images. Comparing the 'Base case' model images with the others shows significant discrepancies, particularly when CFS were attached to the window.

Surface reflectance over-estimation
CIE standard overcast sky



Measured points

- + 6.2 m from window
- o 3.2 m from window
- 0.2 m from window

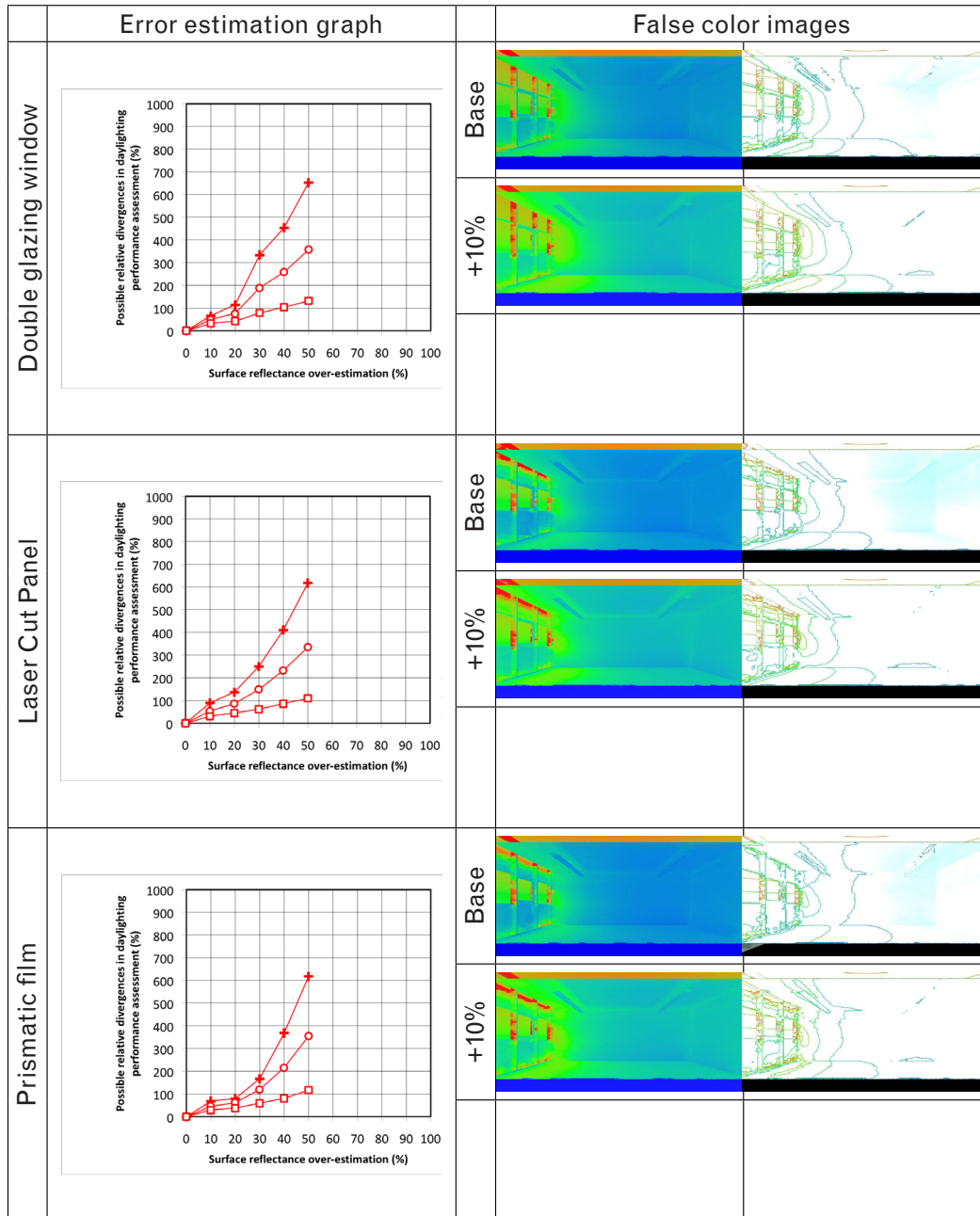
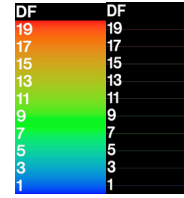
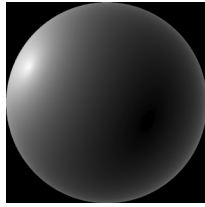


Fig. 5.11 CIE overcast sky; relative divergence (left) on daylight factors caused by overestimating interior surface reflectance. Comparative false-colour images (right) present the daylight daylight factor profiles in the room.

Surface reflectance over-estimation
CIE standard clear sky



- Measured points**
- + 6.2 m from window
 - 3.2 m from window
 - 0.2 m from window

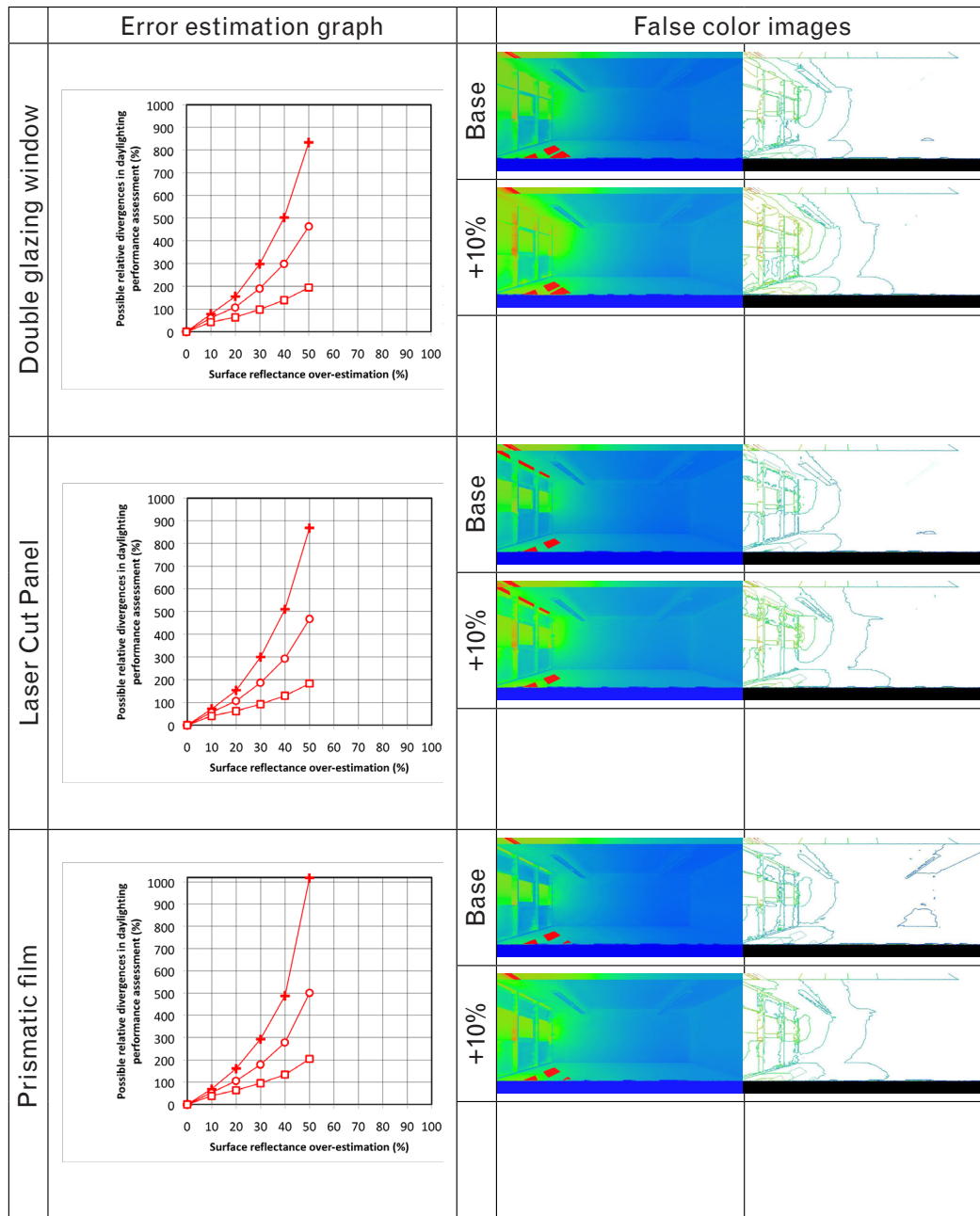
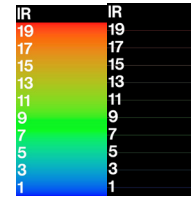
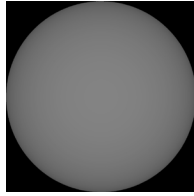


Fig. 5.12

CIE clear sky: graphs (left) present the level of assessment errors caused by overestimating interior surface reflectance. The comparative false-colour images (right) present the daylight properties (daylight factor profile) of the interior space.

Surface reflectance under-estimation
CIE standard overcast sky



Measured points

- + 6.2 m from window
- o 3.2 m from window
- 0.2 m from window

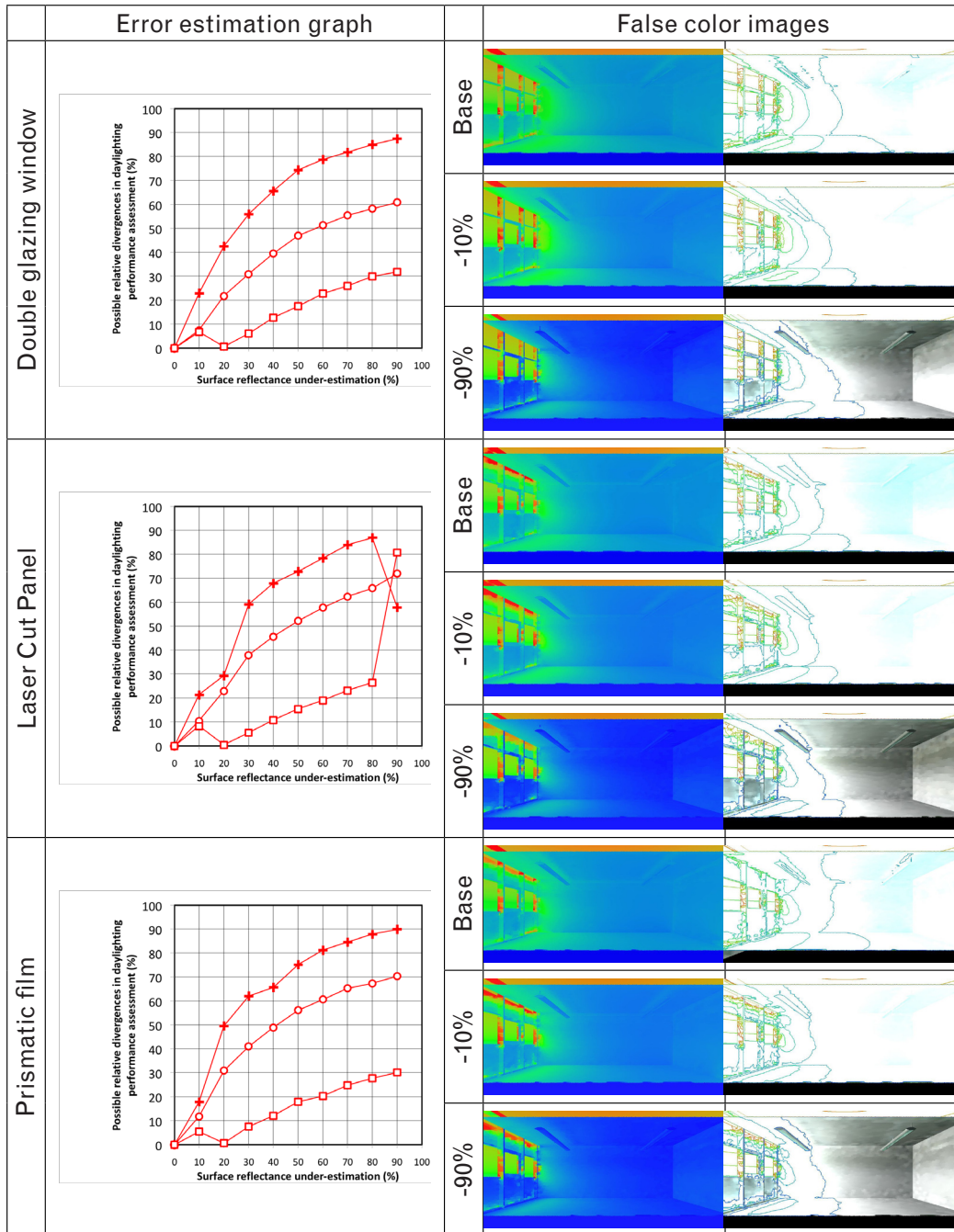
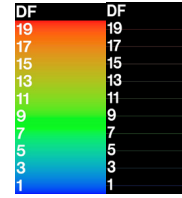
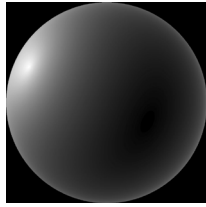


Fig. 5.13 CIE overcast sky; relative divergence (left) on daylight factors caused by underestimating interior surface reflectance. Comparative false-colour images (right) present the daylight daylight factor profiles in the room.

Surface reflectance under-estimation
CIE standard clear sky



- Measured points**
- + 6.2 m from window
 - 3.2 m from window
 - 0.2 m from window

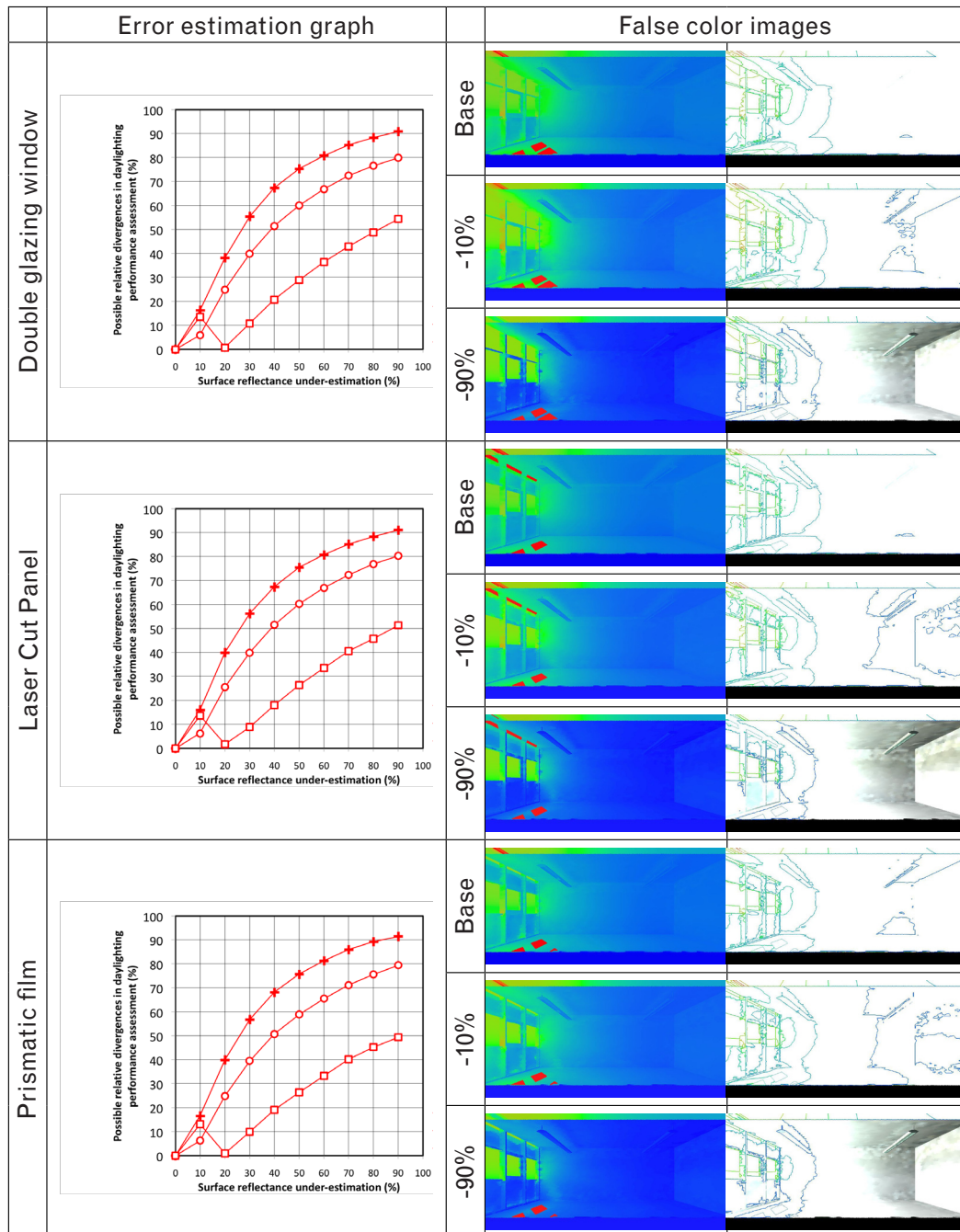
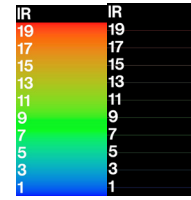


Fig. 5.14

CIE clear sky: graphs (left) present the level of assessment errors caused by underestimating interior surface reflectance. The comparative false-colour images (right) present the daylight properties (daylight factor profile) of the interior space.

Ground reflectance

180

Imprecise ground reflectance modelling can also be a source of assessment error. In this study its effect was analysed using virtual models which were carefully designed to exactly match the geometric and photometric features of the ground reflectance of the real building (details in chapter 2). The virtual models accurately simulated both CIE standard overcast sky and CIE standard clear sky.

A sensitivity analysis of ground reflectance was carried out for models including a double glazing window, as well as different CFS; ground reflectance values were considered ranging from 0.1 to 1.5 times those of the real building. Daylight factor and illuminance ratio profiles, observed in the models at 7 different locations at 1m intervals, were compared. The relative divergence observed between these figures were used to quantify the impact of ground reflectance on model accuracy.

The sensitivity analysis, performed by assuming ground reflectance up to 90% lower and 50% higher than the real 'Base case' values, showed large relative divergences. The analysis is presented in detail in Table 5.7.

Data set	Parameters in Radiance
Set 5: Ground photometry	$\rho_g =$ Ground reflectances
	$\rho_{g \text{ base case}} \times 0.1$
	$\rho_{g \text{ base case}} \times 0.2$
	$\rho_{g \text{ base case}} \times 0.3$
	$\rho_{g \text{ base case}} \times 0.4$
	$\rho_{g \text{ base case}} \times 0.5$
	$\rho_{g \text{ base case}} \times 0.6$
	$\rho_{g \text{ base case}} \times 0.7$
	$\rho_{g \text{ base case}} \times 0.8$
	$\rho_{g \text{ base case}} \times 0.9$
	$\rho_{g \text{ base case}} \times 1.1$
	$\rho_{g \text{ base case}} \times 1.2$
	$\rho_{g \text{ base case}} \times 1.3$
	$\rho_{g \text{ base case}} \times 1.4$
$\rho_{g \text{ base case}} \times 1.5$	

Table 5.7
Set of comparative data used to outline the effect of inaccurate ground reflectance on daylighting performance assessment

Results are presented on Fig. 5.15 to 5.18. For a model including a double glazing window, the discrepancy was less than 5.4% for a 10% reduction of ground reflectance under both overcast and clear sky, they were less than 6.5% when overestimating ground reflectance by 10%.

For the a model with Laser Cut Panel under clear sky conditions the discrepancy was 5.3% for a 10% reflectance overestimation at 6.2 m from the window. Larger figures were observed for a 10% overestimation under overcast sky conditions, showing an 8.8% discrepancy. For the prismatic film compared to the 'Base case', the discrepancy was less than 5.8 % for a 10% ground reflectance reduction and 13.2% for a 10 % overestimation of the ground reflectance.

Thus, as with interior surface reflectance, ground reflectance is shown to be an important parameter regarding the accuracy of virtual models, particularly for positions deeper within the room where internal reflection tends to dominate. The overall relative discrepancies created by imprecise ground reflectance were less than 10% when the ground reflectance was underestimated by less than 50% and less than 20% when the ground reflectance was less than 20% overestimated. The greater the ground reflectance error, the more inaccurate the daylight assessment becomes, particularly under overcast sky conditions : the errors however remain lower than those induced by inaccurate wall surface reflectance.

The false-colour images presented show a clear difference between 'Base case' and a 10% overestimation or underestimation of the ground reflectance under overcast sky conditions (particularly in the deeper part of the room) : its impact however remains lower than those of wall surface reflectance.

Ground reflectance over-estimation
CIE standard overcast sky

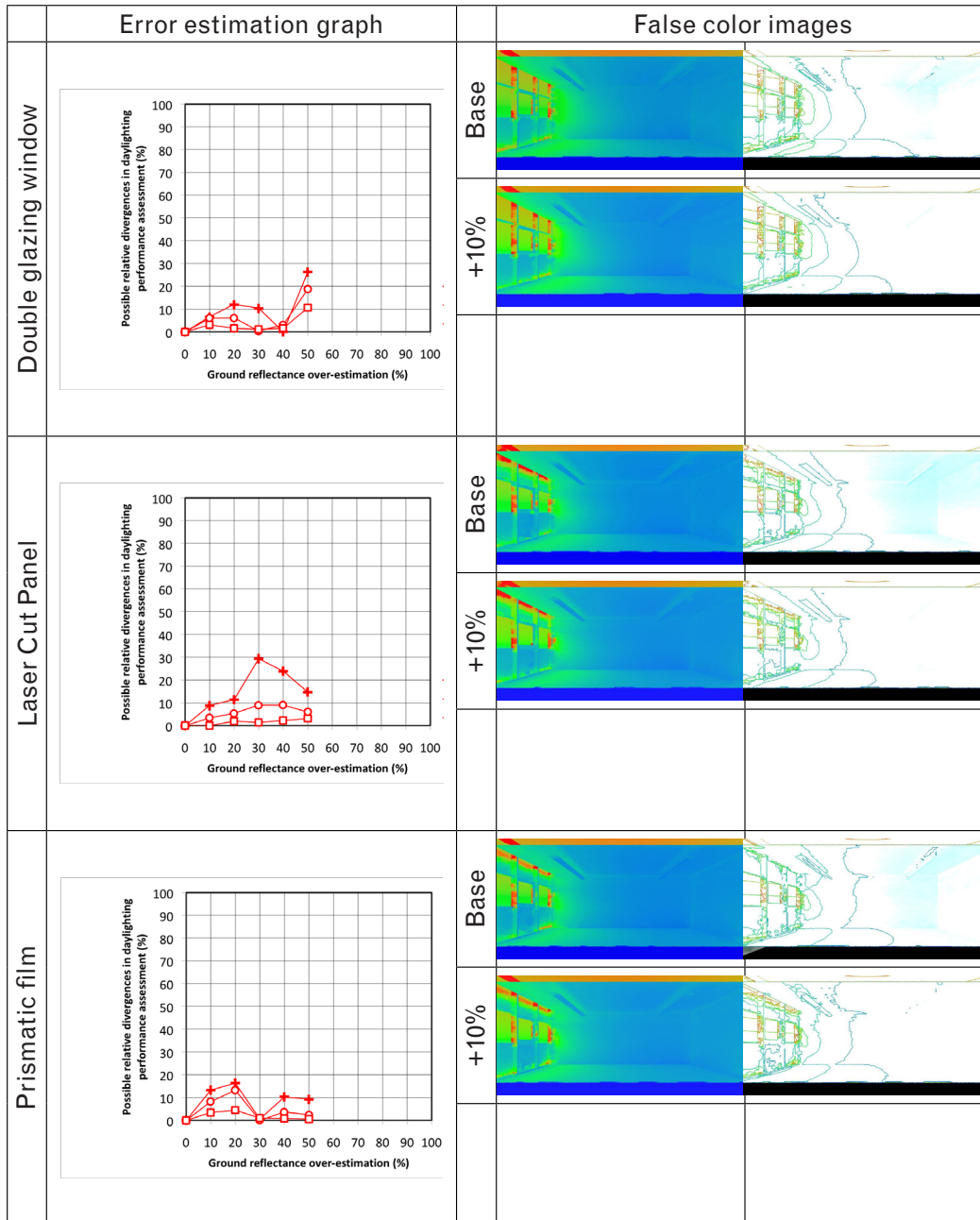
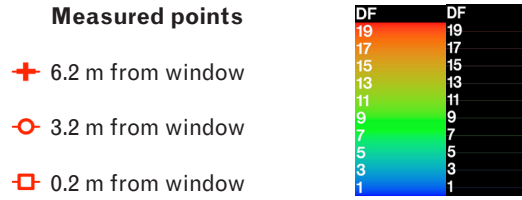
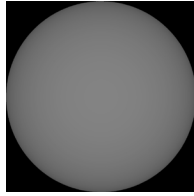
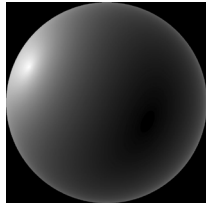


Fig. 5.15 CIE overcast sky; relative divergence (left) on daylight factors caused by overestimating ground reflectance. Comparative false-colour images (right) present the daylight daylight factor profiles in the room.

Ground reflectance over-estimation
CIE standard clear sky



- Measured points**
- + 6.2 m from window
 - 3.2 m from window
 - 0.2 m from window

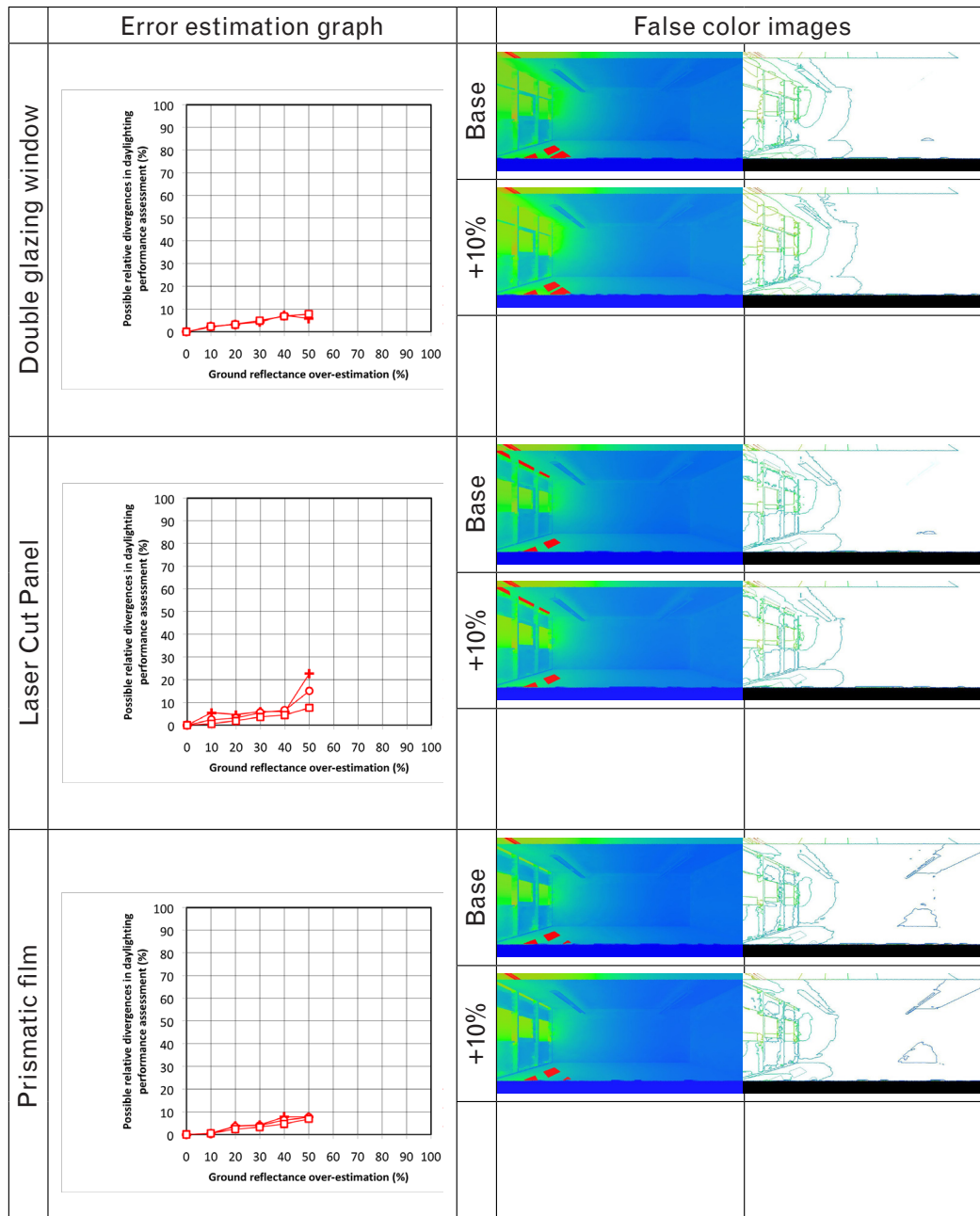
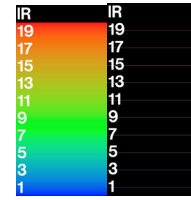


Fig. 5.16

CIE clear sky: graphs (left) present the level of assessment errors caused by overestimating ground reflectance. The comparative false-colour images (right) present the daylight properties (daylight factor profile) of the interior space.

Ground reflectance under-estimation
CIE standard overcast sky

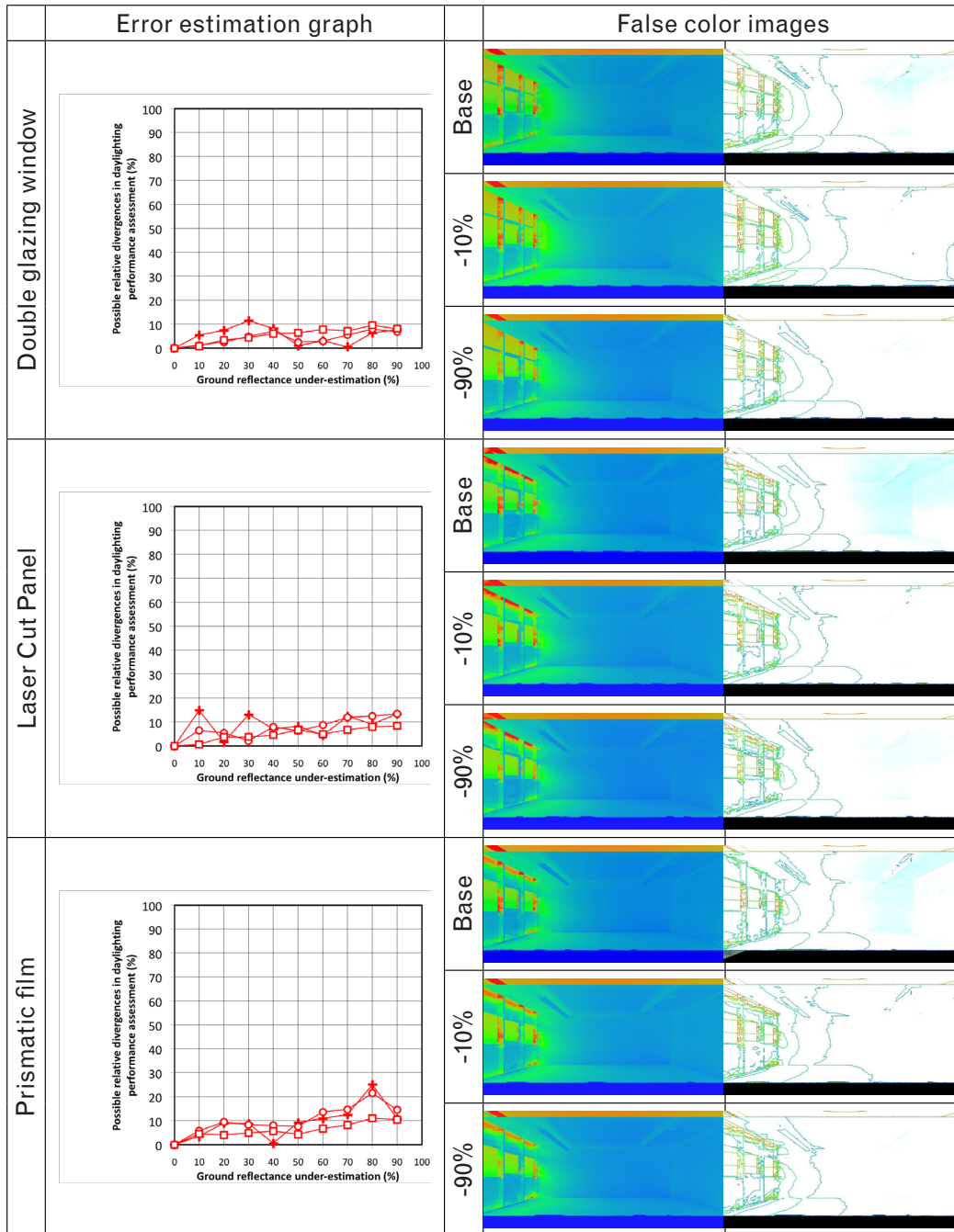
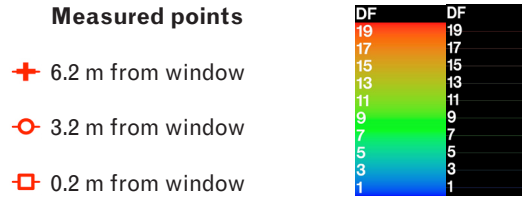
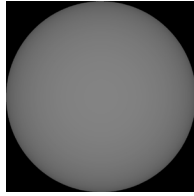


Fig. 5.17 CIE overcast sky; relative divergence (left) on daylight factors caused by underestimating ground reflectance. Comparative false-colour images (right) present the daylight daylight factor profiles in the room..

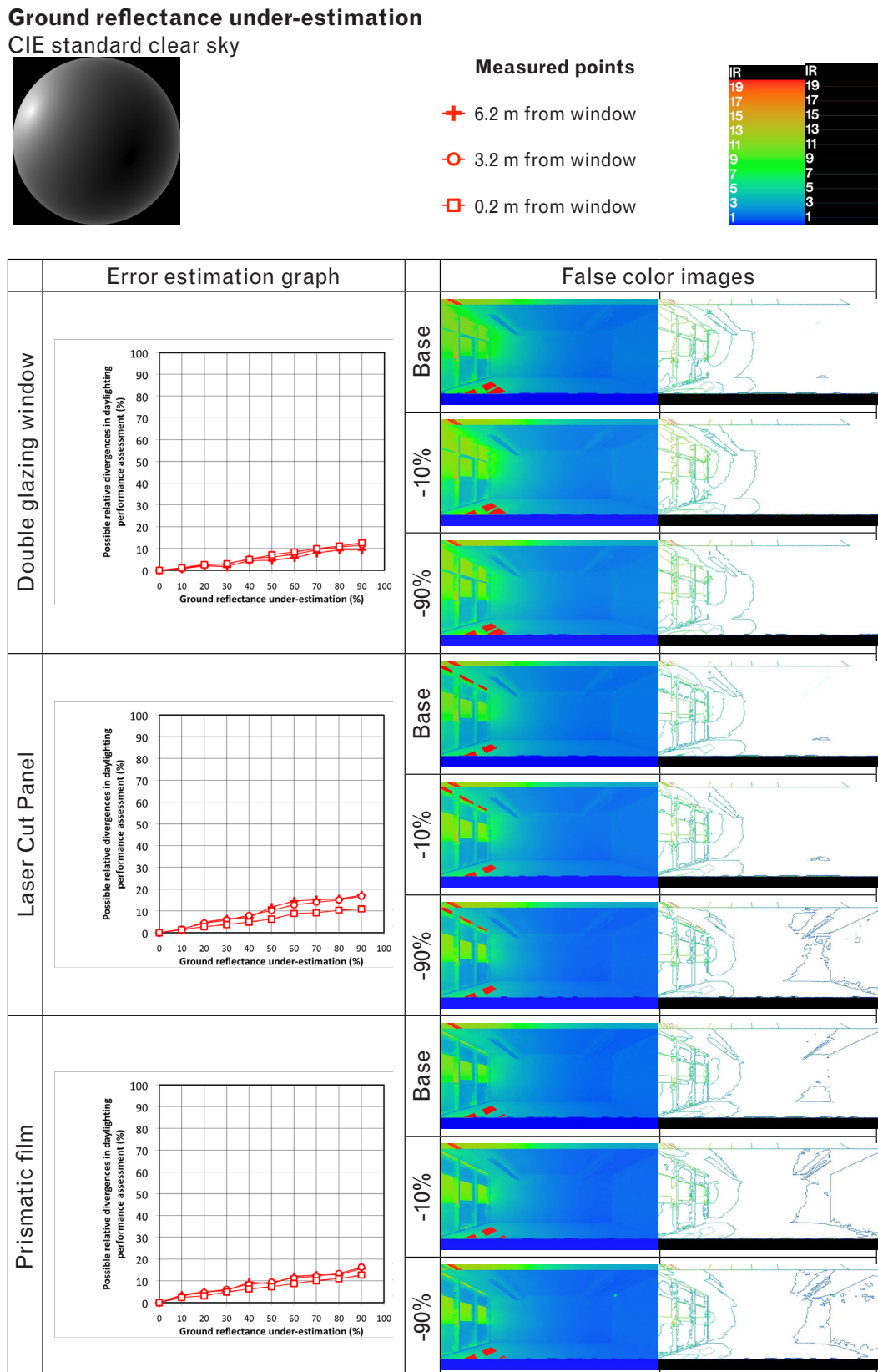


Fig. 5.18

CIE clear sky: graphs (left) present the level of assessment errors caused by underestimating ground reflectance. The comparative false-colour images (right) present the daylight properties (daylight factor profile) of the interior space.

Window transmittance

186

Window transmittance, which controls the penetration of the daylight flux into the room, is important in daylighting performance assessment so even slight imprecisions can lead to significant discrepancies. The analysis of window transmittance sensitivity was carried out using virtual models which were carefully designed to exactly match the geometric and photometric features of the ground reflectance of the real building (details in chapter 3). External sources of errors regarding the computer simulation parameters were not expected for this reason. The virtual models accurately simulated both CIE standard overcast sky and CIE standard clear sky in these studies.

Data set	Parameters in Radiance
Set 6: Window photometry	τ = Window transmittance
	$\tau_{\text{base case}} \times 0.1$
	$\tau_{\text{base case}} \times 0.2$
	$\tau_{\text{base case}} \times 0.3$
	$\tau_{\text{base case}} \times 0.4$
	$\tau_{\text{base case}} \times 0.5$
	$\tau_{\text{base case}} \times 0.6$
	$\tau_{\text{base case}} \times 0.7$
	$\tau_{\text{base case}} \times 0.8$
	$\tau_{\text{base case}} \times 0.9$
	$\tau = 100\%$

Table 5.8
Set of comparative data used to outline the effect of window transmittance on daylighting performance assessment

A sensitivity analysis of window transmittance was carried out for models including a double glazing window, as well as different CFS: window transmittance values, considered only on double glazing, (not on the CFS panels), were ranging from a 90% underestimation of the double glazing transmittance ($\tau = 80.5\%$) to a perfect transmittance ($\tau = 100\%$). Daylight factor and illuminance ratio profiles, observed in the models at 7 different locations at 1m intervals, were compared. The relative divergence observed between these figures were used to quantify the impact of window transmittance on model accuracy; large relative divergencies were noted.

Fig. 5.19 and 5.20 show for the virtual model with a double glazing a discrepancy of 2.5% for a 10% reduction in transmittance under overcast conditions (9.0% under clear sky). This increased to 24.1% for a perfect transmittance (overestimation) under an overcast sky and up to 41.9 % under clear sky conditions were observed.

For the virtual model with laser cut panel under overcast sky condition, the discrepancy was 4.3% for a 10% transmittance reduction; for 100% transmittance (an overestimation) the discrepancy was 28.5% under overcast sky conditions and 36.1 % under clear sky.

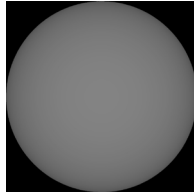
Divergences observed for the prismatic film, compared to 'Base case' reaches 6.1% for a 10% transmittance reduction; for perfect transmittance (an overestimation) the discrepancy was 24.1% under overcast sky conditions and 33.1 % under clear sky.

Appropriate window transmittance is consequently a very important parameter regarding the virtual model's accuracy, in any position in the room.

In all window systems the divergences can also be seen noticeably visible in the false-colour images, even for only 10% underestimation of the window transmittance, particularly under overcast sky conditions.

Since windows play an important role in controlling daylight flux into the building, its transmittance is a very important parameters in daylighting modelling. The tendency to errors caused by an inaccurate transmittance are rising up with the transmittance error : the reaction between them is moreover clear as can be explained by physical argument (linear relation with the daylight flux).

Window transmittance
CIE standard overcast sky



Measured points

- + 6.2 m from window
- 3.2 m from window
- 0.2 m from window

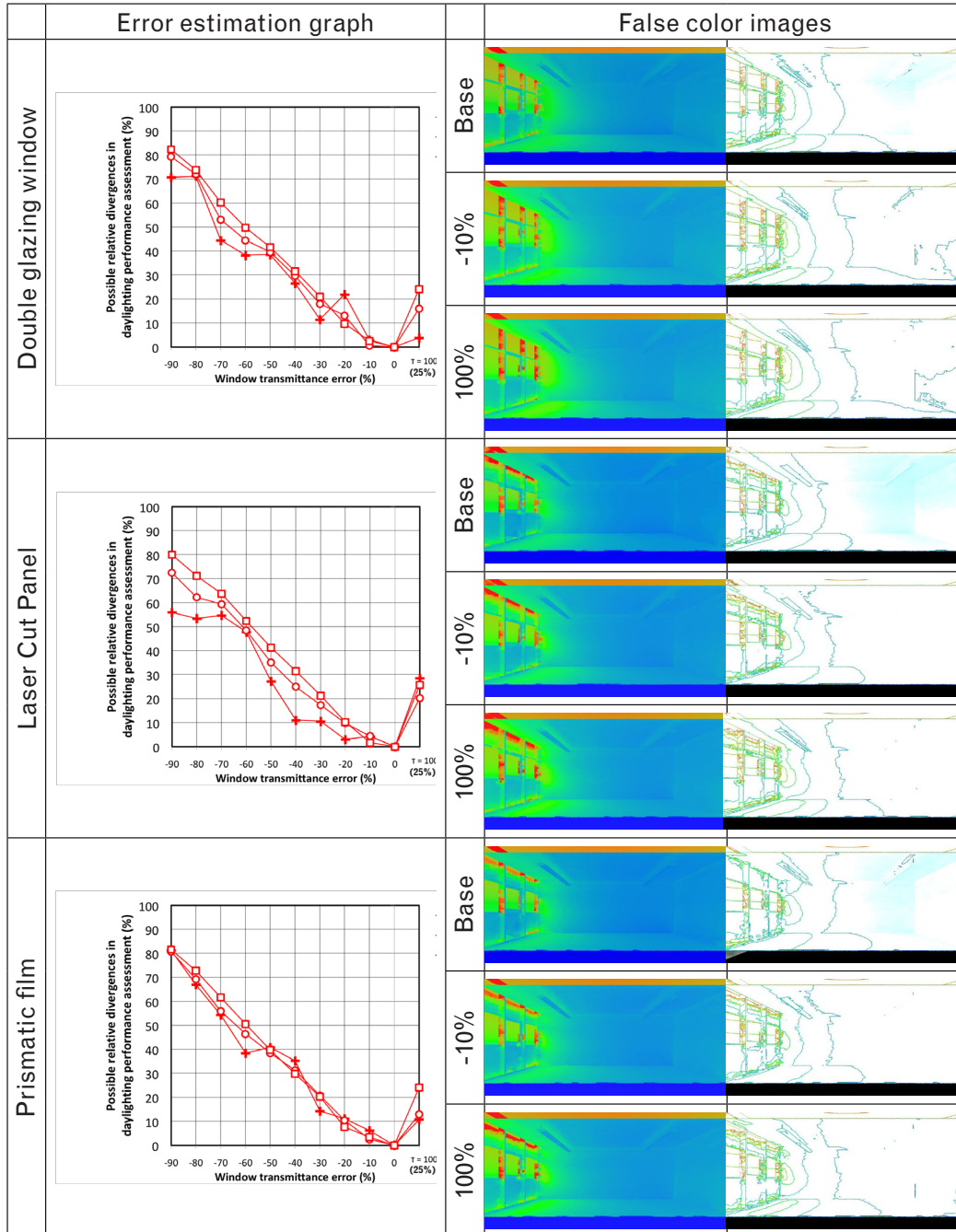
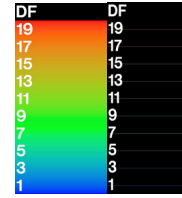
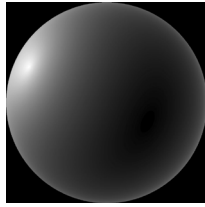


Fig. 5.19 CIE overcast sky; relative divergence (left) on daylight factors caused by window transmittance imprecisions. Comparative false-colour images (right) present the daylight daylight factor profiles in the room.

Window transmittance
CIE standard clear sky



- Measured points**
- + 6.2 m from window
 - 3.2 m from window
 - 0.2 m from window

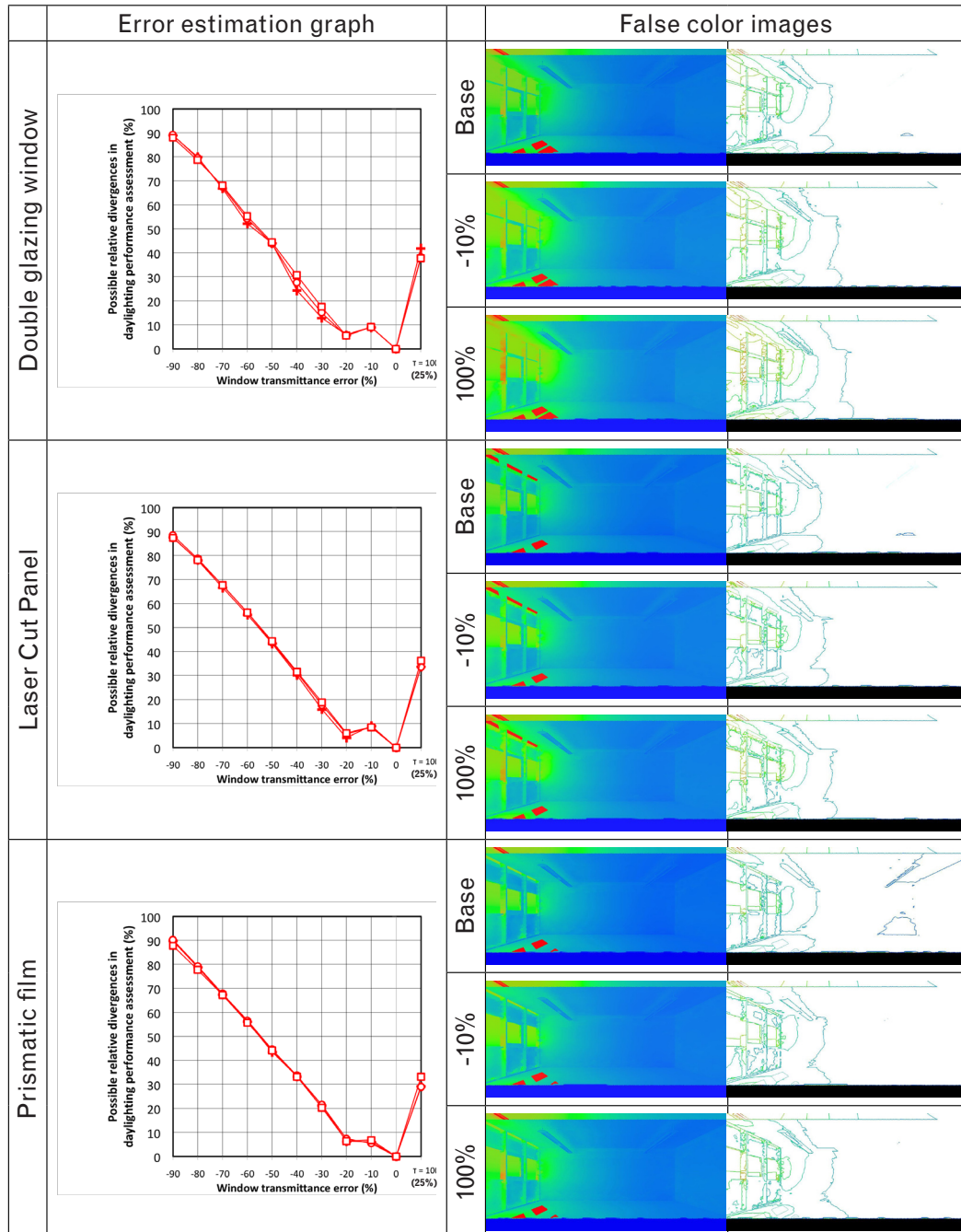
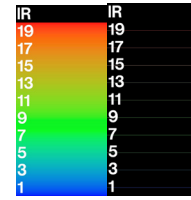


Fig. 5.20

CIE clear sky: graphs (left) present the level of assessment errors caused by window transmittance imprecisions. The comparative false-colour images (right) present the daylight properties (daylight factor profile) of the interior space.

5.5 Photometric sensors

190

The use of inappropriate photometric sensors can also lead to significant errors in daylighting performance assessment. A sensitivity analysis for this error was made using virtual models to test two important cases: the sensor's sensitive area and its position.

The sensitive area of the sensor

The analysis of the daylighting evaluation effect of the sensitive area of sensor (luxmeters) was carried out for models equipped with a glazing window and different CFS. Two different areas were considered in order to study the impact on daylighting evaluation of the difference in sensitive areas. The cases studied using different points definition in Radiance are presented in Table 5.9.

Data set	Parameters in Radiance
Set 7: Sensor's sensitive area	
Sensitive area 1	Illuminance = Illuminance measured on a single point
Sensitive area 2	Illuminance = Average illuminance measured on five points

Table 5.9
Set of comparative studies used to outline the effect of sensor area on daylighting performance assessment

A small sensitive area was simulated by considering only a one-point of measurement (Fig. 5.21a), a larger sensitive area was considered by accounting for a five-point of measurement (Fig. 5.21c)

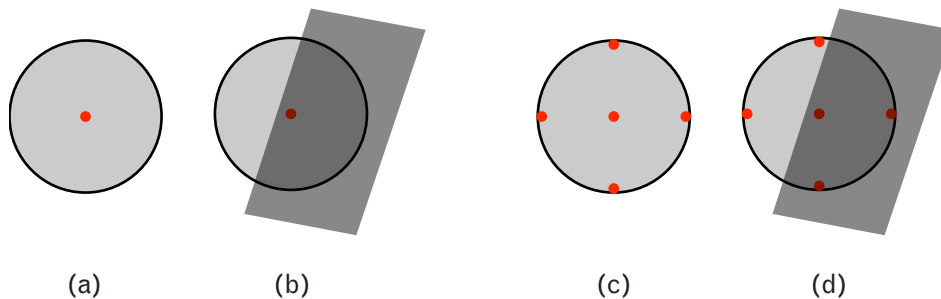


Fig. 5.21

(a) one-point measurement representing a small sensitive area, (b) one-point measurement when shadow was present, (c) 5-point measurement representing a larger sensitive area (d) 5-point measurement when shadow was present

For each studied case, three fenestration systems under both overcast and clear sky conditions, as presented in Fig. 5.22 and 5.23 were considered. Comparing the two sensitive areas showed little difference corresponding to less than 1% discrepancy.

This shows that differences in the sensitive area of the luxmeters are not the important cause of errors in daylight performance assessment (impact of illuminance gradient): illuminance are determined by dividing the light flux by the sensor area, so that only slight illuminance gradient differences can be sensed in this case. A remark can be made for situations where a measured point covered both direct shade and shadow from the window details. The light flux may differ from that expected (measured in the reality) since the average of the 5 points is different from the single point. As shown in Fig. 5.21b and 5.21d, the shadow plays an important role in the measurement; for the single point the value is collected from a point under shadow, while the 5-point measurement is averaged from 3 shadowed points and 2 points without shadow.

Sensor's sensitive area
CIE standard overcast sky

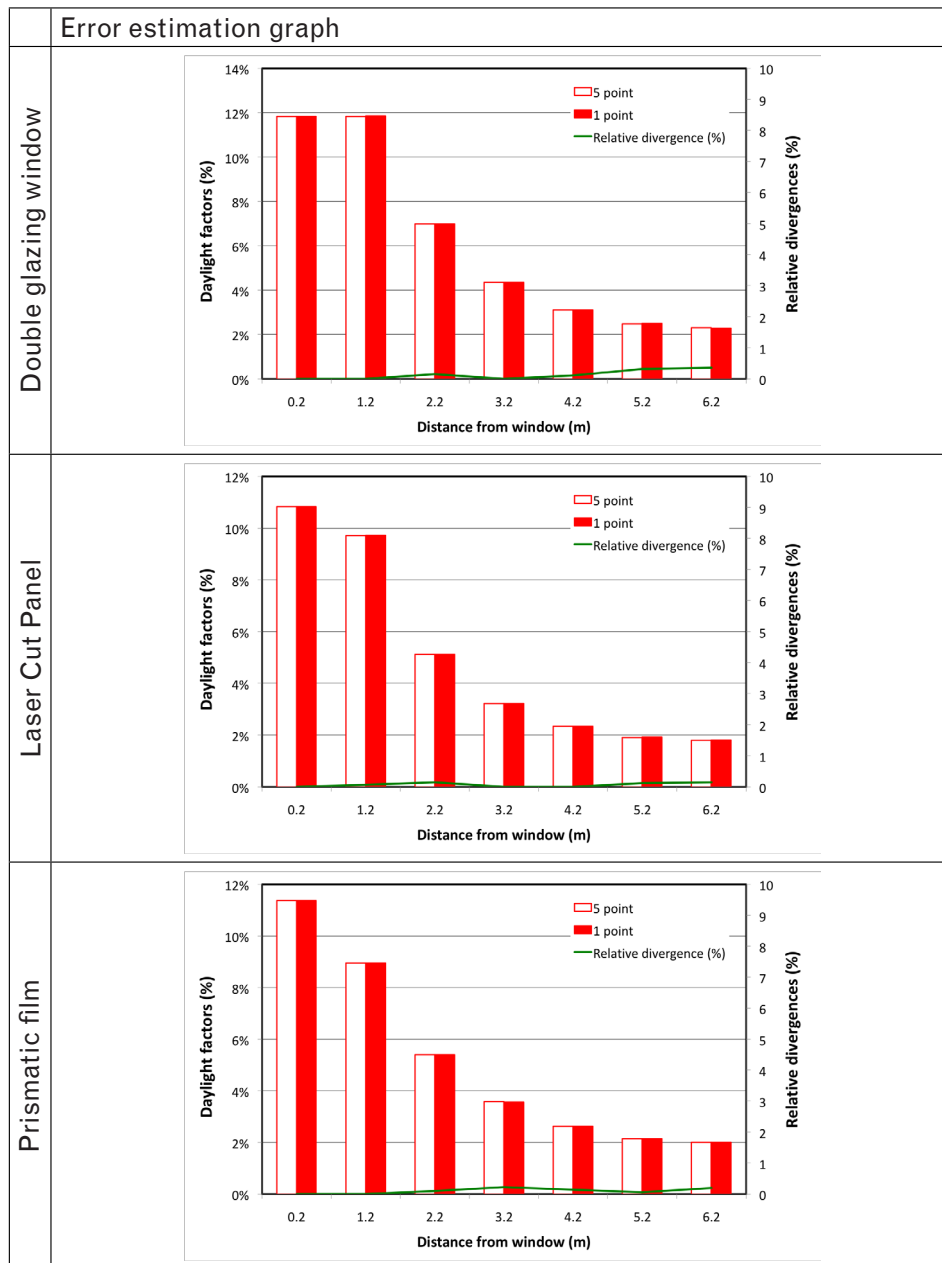
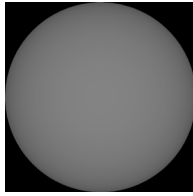


Fig. 5.22 CIE overcast sky: graphs presenting the level of daylighting performance assessment errors caused by the luxmeters's sensitive area

Sensor's sensitive area
CIE standard clear sky

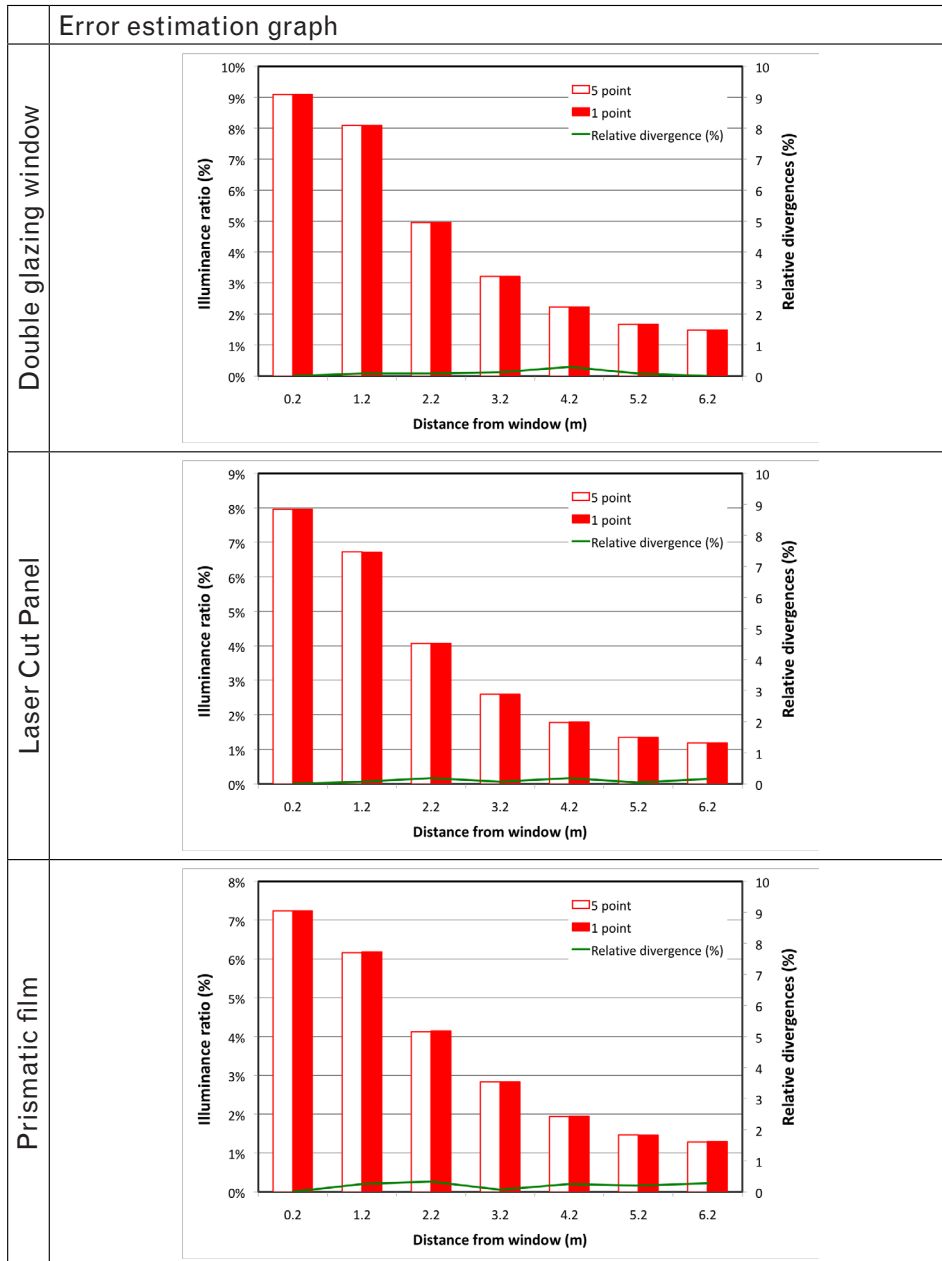
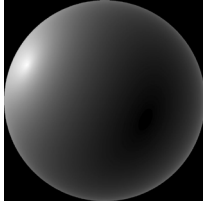


Fig. 5.23 CIE clear sky: graphs presenting the level of daylighting performance assessment errors caused by the luxmeters's sensitive area

Sensor positioning

When placing sensors in a physical model (or indicating sensor position in a virtual model), an error in levelling and orientation can easily happen. The study of positioning errors, in both the x axis (parallel to the window) and the y axis (perpendicular to the window) was considered (Fig. 5.24). Furthermore, errors caused by tilting the sensor in either axis were considered (Fig. 5.25).

A full description of the data sets is presented in Table 5.10 for sensor positioning and in Table 5.11 for sensor tilting.

Data set	Parameters in Radiance	Data set	Parameters in Radiance
Set 8: Sensor placement (x coordinate, parallel to window)	P_s = Sensor position in model	Set 9: Sensor placement (y coordinate, perpendicular to window)	P_s = Sensor position in model
	$P_{s \text{ base case}} - 0.05 \text{ m}$		$P_{s \text{ base case}} - 0.05 \text{ m}$
	$P_{s \text{ base case}} - 0.04 \text{ m}$		$P_{s \text{ base case}} - 0.04 \text{ m}$
	$P_{s \text{ base case}} - 0.03 \text{ m}$		$P_{s \text{ base case}} - 0.03 \text{ m}$
	$P_{s \text{ base case}} - 0.02 \text{ m}$		$P_{s \text{ base case}} - 0.02 \text{ m}$
	$P_{s \text{ base case}} - 0.01 \text{ m}$		$P_{s \text{ base case}} - 0.01 \text{ m}$
	$P_{s \text{ base case}}$		$P_{s \text{ base case}}$
	$P_{s \text{ base case}} + 0.01 \text{ m}$		$P_{s \text{ base case}} + 0.01 \text{ m}$
	$P_{s \text{ base case}} + 0.02 \text{ m}$		$P_{s \text{ base case}} + 0.02 \text{ m}$
	$P_{s \text{ base case}} + 0.03 \text{ m}$		$P_{s \text{ base case}} + 0.03 \text{ m}$
	$P_{s \text{ base case}} + 0.04 \text{ m}$		$P_{s \text{ base case}} + 0.04 \text{ m}$
$P_{s \text{ base case}} + 0.05 \text{ m}$	$P_{s \text{ base case}} + 0.05 \text{ m}$		

Table 5.10
Set of comparative studies used to outline the effect of sensor positioning on daylighting performance assessment

Data set	Parameters in Radiance	Data set	Parameters in Radiance
Set 10: Sensor positioning; tilting angle (x coordinate, parallel to window)	A_s = Sensor sensitive area angle and horizontal plane in model	Set 11: Sensor positioning; tilting angle (y coordinate, perpendicular to window)	A_s = Sensor sensitive area angle and horizontal plane in model
	$A_{s \text{ base case}} - 5^\circ$		$A_{s \text{ base case}} - 5^\circ$
	$A_{s \text{ base case}} - 4^\circ$		$A_{s \text{ base case}} - 4^\circ$
	$A_{s \text{ base case}} - 3^\circ$		$A_{s \text{ base case}} - 3^\circ$
	$A_{s \text{ base case}} - 2^\circ$		$A_{s \text{ base case}} - 2^\circ$
	$A_{s \text{ base case}} - 1^\circ$		$A_{s \text{ base case}} - 1^\circ$
	$A_{s \text{ base case}} = 0^\circ$		$A_{s \text{ base case}} = 0^\circ$
	$A_{s \text{ base case}} + 1^\circ$		$A_{s \text{ base case}} + 1^\circ$
	$A_{s \text{ base case}} + 2^\circ$		$A_{s \text{ base case}} + 2^\circ$
	$A_{s \text{ base case}} + 3^\circ$		$A_{s \text{ base case}} + 3^\circ$
	$A_{s \text{ base case}} + 4^\circ$		$A_{s \text{ base case}} + 4^\circ$
$A_{s \text{ base case}} + 5^\circ$	$A_{s \text{ base case}} + 5^\circ$		

Table 5.11
Set of comparative studies used to outline the effect of sensor tilting on daylighting performance assessment

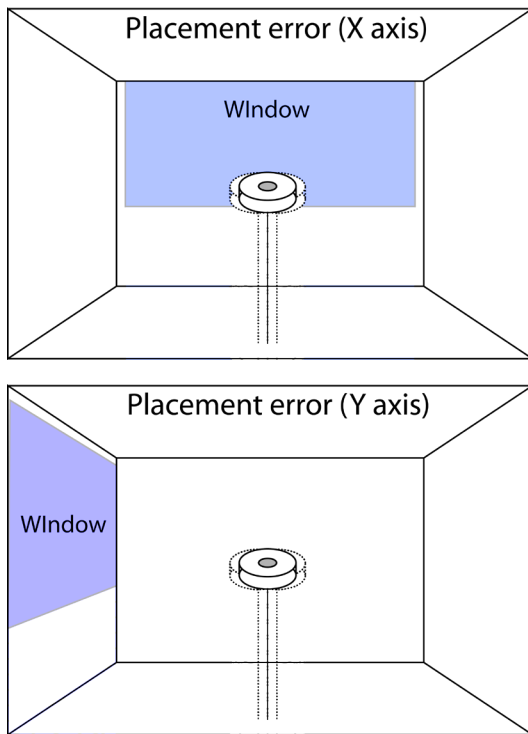


Fig. 5.24
Illustration of sensor positioning error

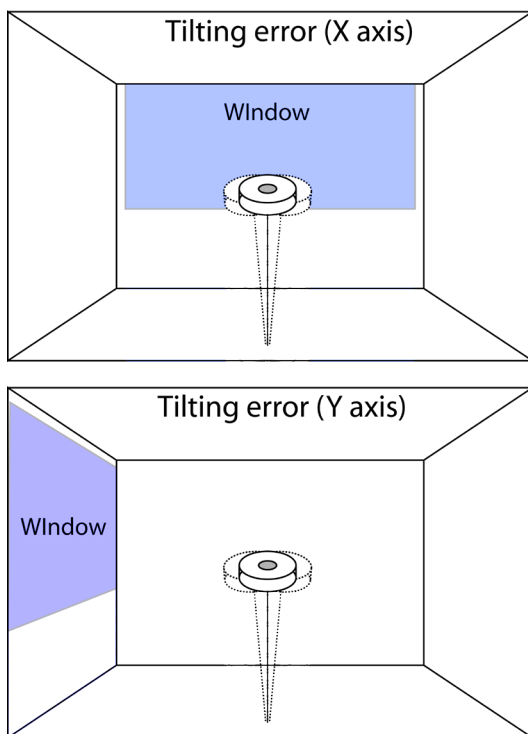


Fig. 5.25
Illustration of sensor tilting error

As shown in Fig. 5.26 to 5.29, the sensor's position or tilting can lead to significant errors - up to 20% relative divergence - particularly under overcast sky conditions. Errors generally increase as errors of position or tilting become greater. Sensor positioning errors are lower in clear sky conditions; the divergence is normally lower than 10%.

This result shows that inaccurate placement of the sensors is an important cause of error. Not only the model, but also the photometric sensor itself, can be cause of error in daylighting performance assessment.

Sensor's position

CIE standard overcast sky



Error estimation graph

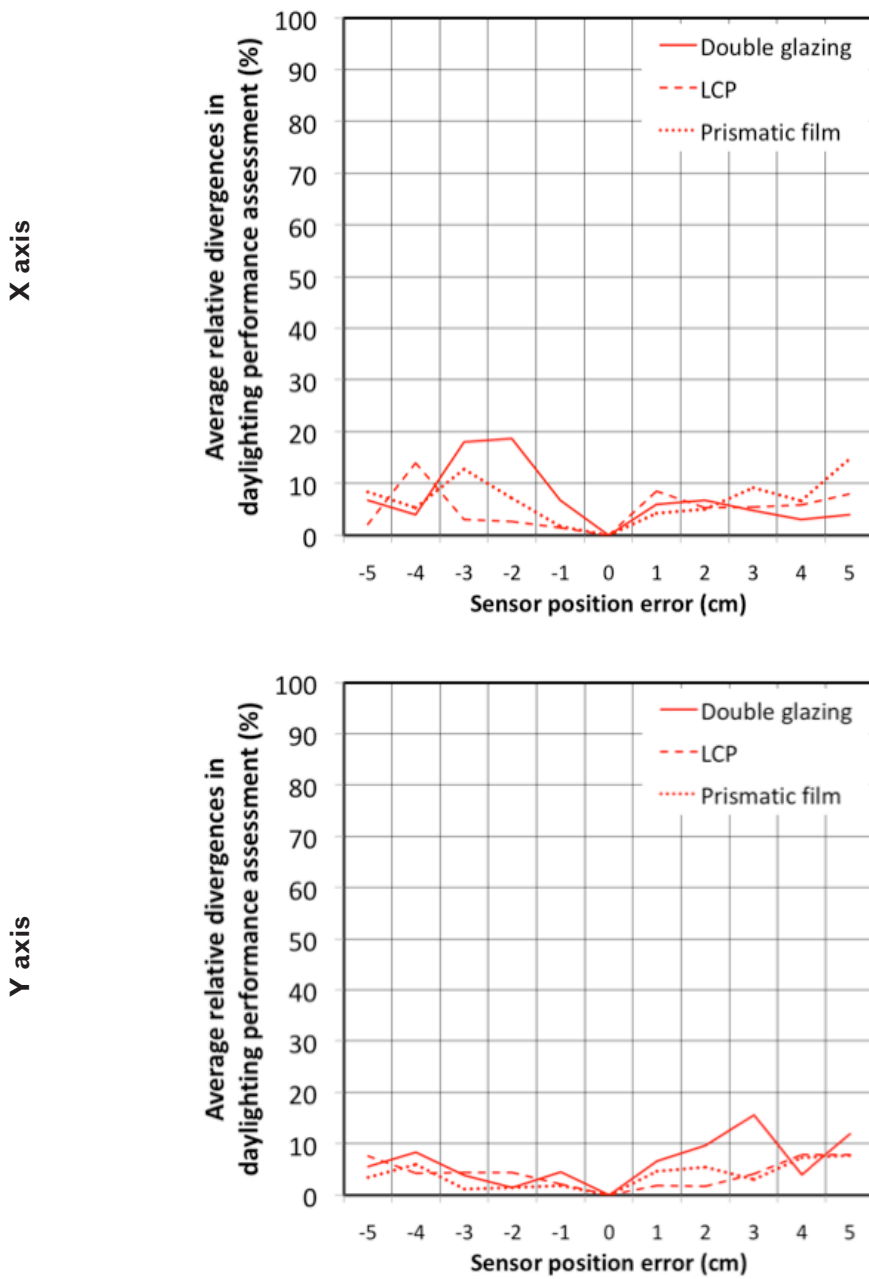
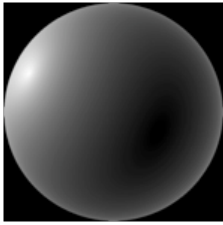


Fig. 5.26 CIE overcast sky: graphs present the level of model assessment errors caused by the sensor's position

Sensor's position
CIE standard clear sky



Error estimation graph

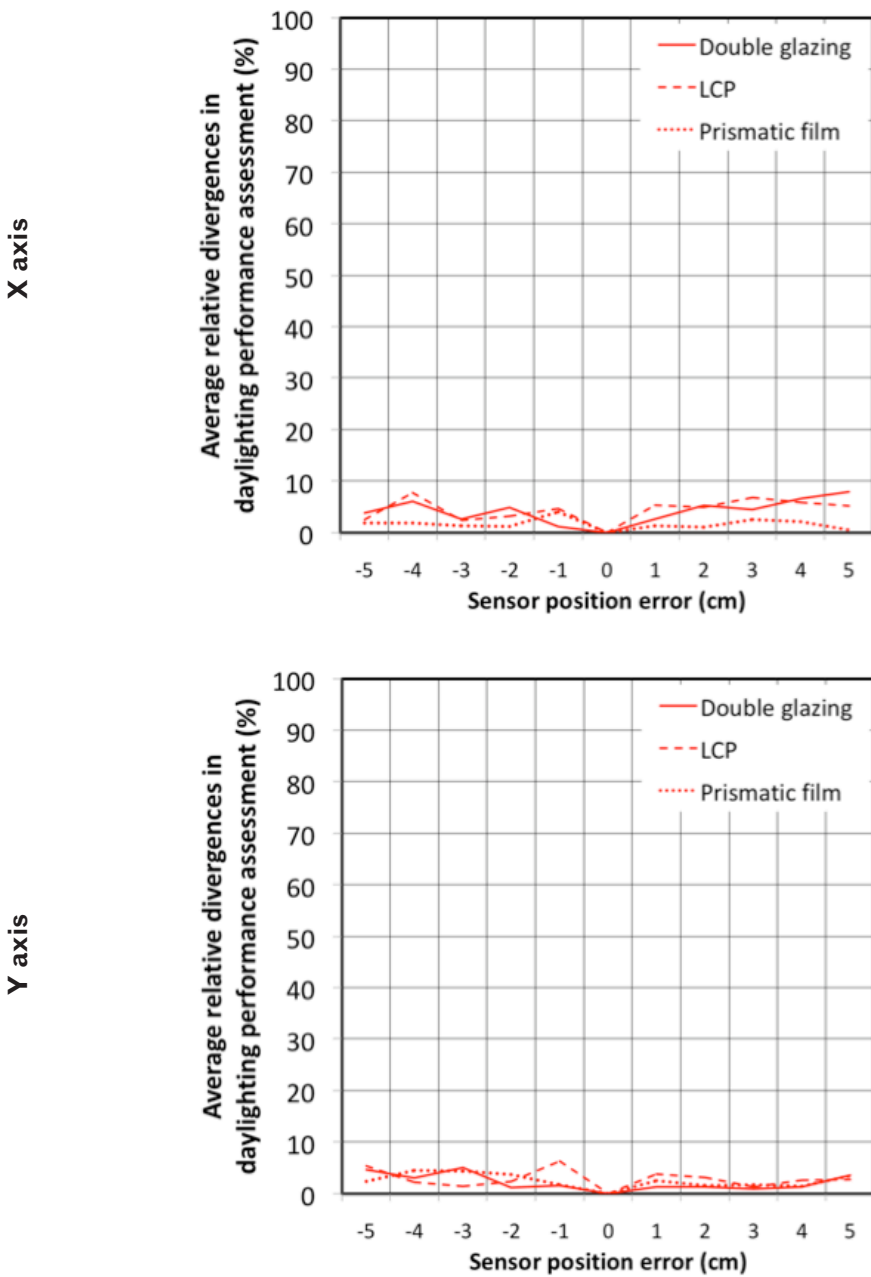


Fig. 5.27
CIE clear sky: graphs present the level of model assessment errors caused by the sensor's position

Sensor's position

CIE standard overcast sky



Error estimation graph

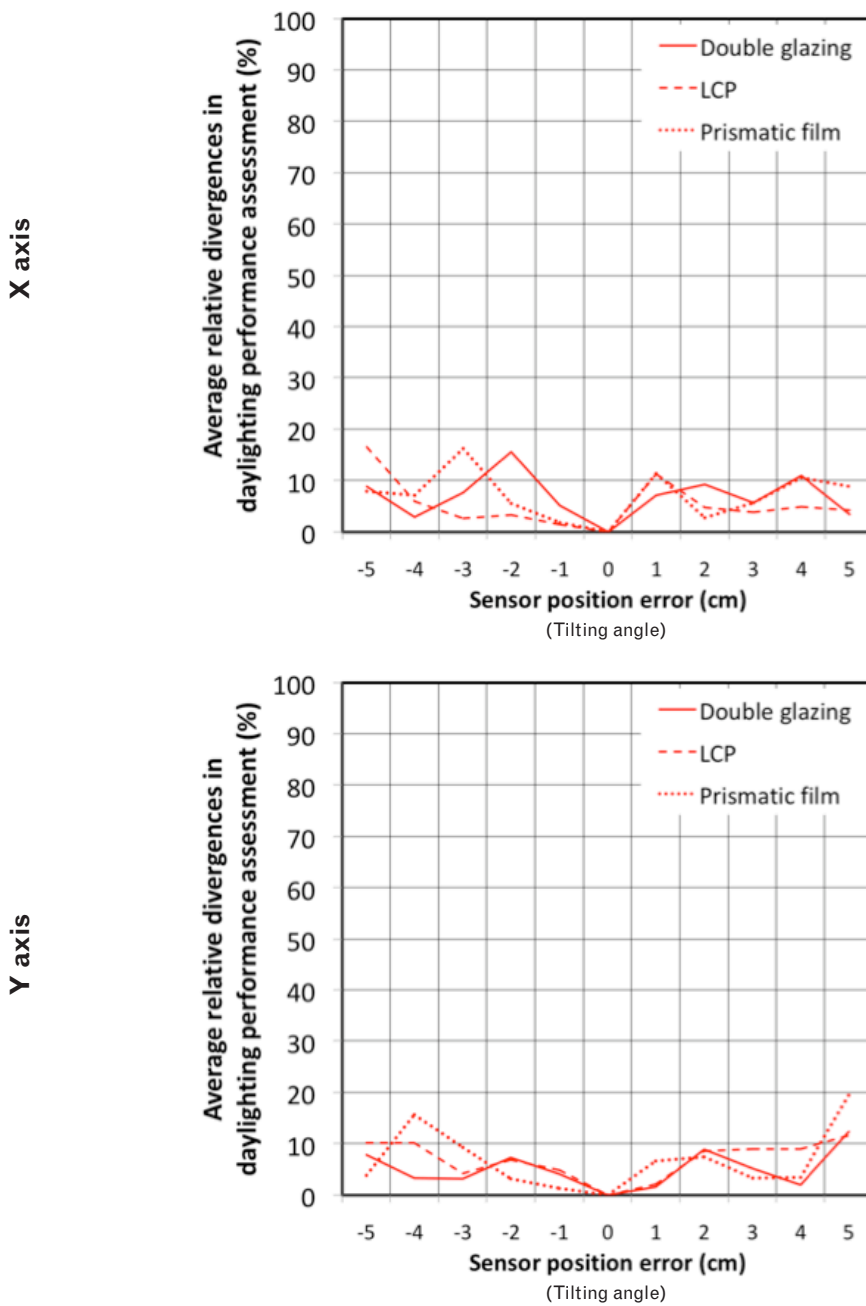
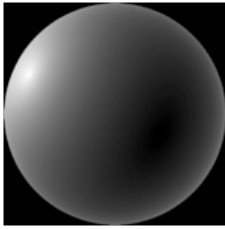


Fig. 5.28 CIE overcast sky: graphs present the level of model assessment errors caused by tilting the sensor

Sensor's position

CIE standard clear sky



Error estimation graph

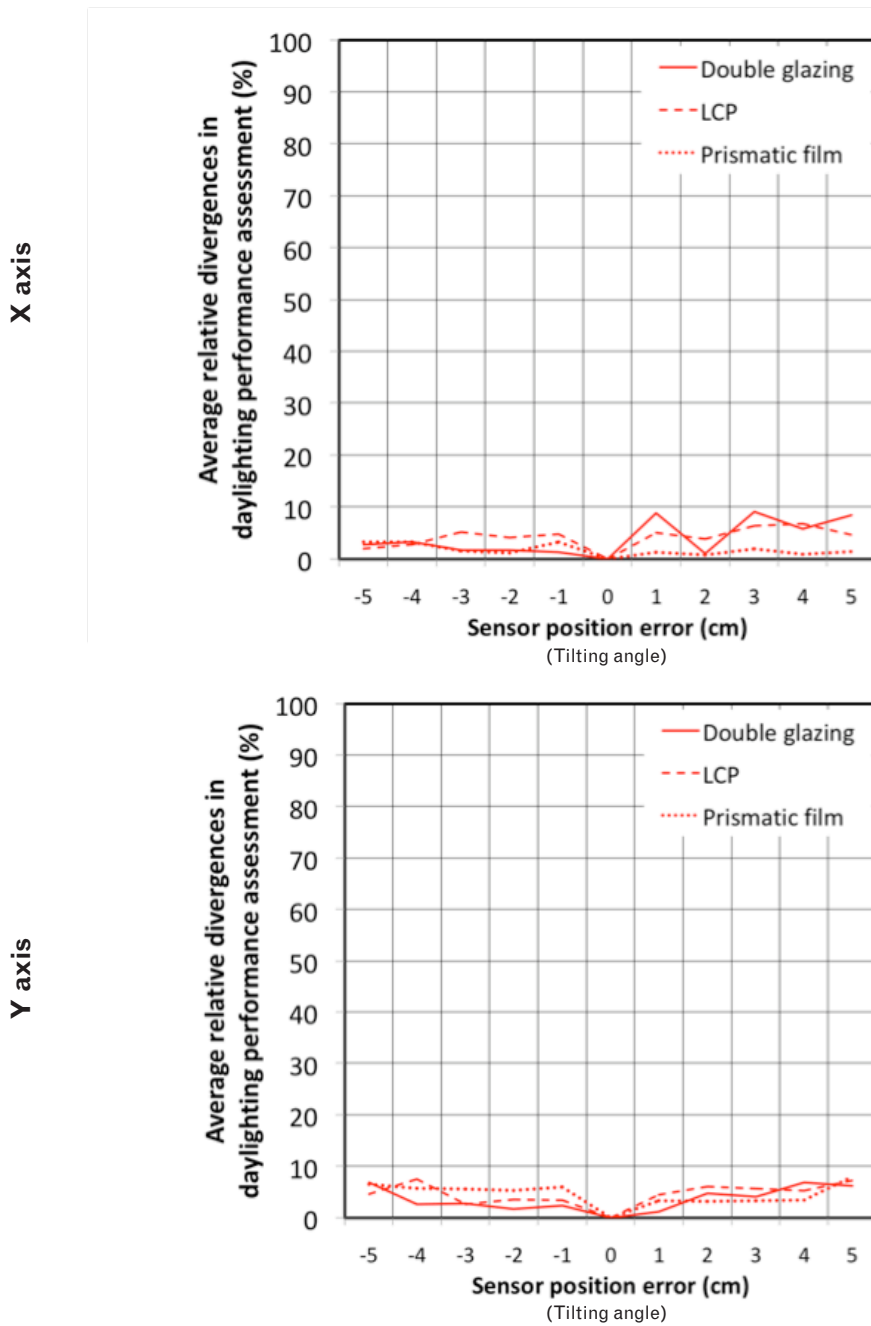


Fig. 5.29 CIE clear sky: graphs present the level of model assessment errors caused by tilting the sensor

5.6 Surroundings

A sensitivity analysis was carried out on surroundings of the EPFL campus using the real building (test module) and its scale model. The module, placed on a concrete platform, was surrounded by an open plain to the south and east and a car park towards the north. As a similar object was located on the west of it (Fig. 5.30), the window facades of the two modules were aligned, both facing due south, to avoid any mutual influence during the monitoring of daylighting performance.

The 1:10 scale model was placed close to the real building in order to benefit from identical outdoor daylighting conditions (sky view factor and luminance distribution). As a strictly identical position of the object and its scale model was impossible to achieve (this would have meant placing the model inside the module, thus affecting the latter's monitoring), the model was optimally positioned close to the module's facade (Fig. 5.30). The window side of the scale model was carefully aligned with the plane of the window facade of the building under consideration.



Fig. 5.30
Scale model location close to the real building (fixed to its western side)

Another, separate, scale model location was considered to investigate the impact of the daylight's ground reflection component and slightly different sky view factors. In this case the scale model was placed just inside the adjacent module (Fig. 5.31), its open facade perfectly aligned with the facade of the real building. Shadowing effects of the blind fixtures were avoided by having the scale model just out from the window by 10 – 20 cm.



Fig. 5.31
Scale model location close to the real building (in the adjacent module)

The daylighting performance monitoring was carried out during the winter (there was no snow) for different types of sky luminance distributions (clear skies).

As the real building and its 1:10 scale model were placed in slightly different locations, they experienced different sky view factors, which could lead to discrepancies between the assessed daylighting performance. As a consequence, a detailed analysis of the corresponding sky view factors in the scale model and the real building was carried out using a digital camera and fish eye views.

In both the real building and its scale model the camera was placed vertically at 6 different locations corresponding to the positions of the photometric sensors used to monitor daylighting performance (Fig. 5.32). The digital images corresponding to similar positions were compared one by one to identify possible significant differences of sky views.

Figure 5.33 presents the views taken from inside both the real building and the scale model for the two model locations under consideration (Fig. 5.30 and 5.31) and two different luxmeter positions close to the southern facade (0.22m and 0.42m from the model's window plane). For experimental reasons (the size of the camera), all model sides except the southern facade were removed when taking the pictures.

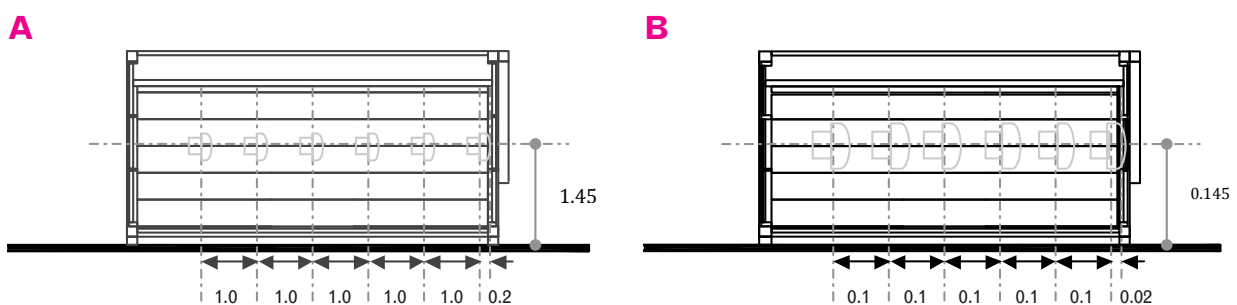


Fig. 5.32
Digital camera positions in the real building (test module) (a) and in the scale model (b) to assess the sky view factors of the 6 luxmeter positions (units: m)

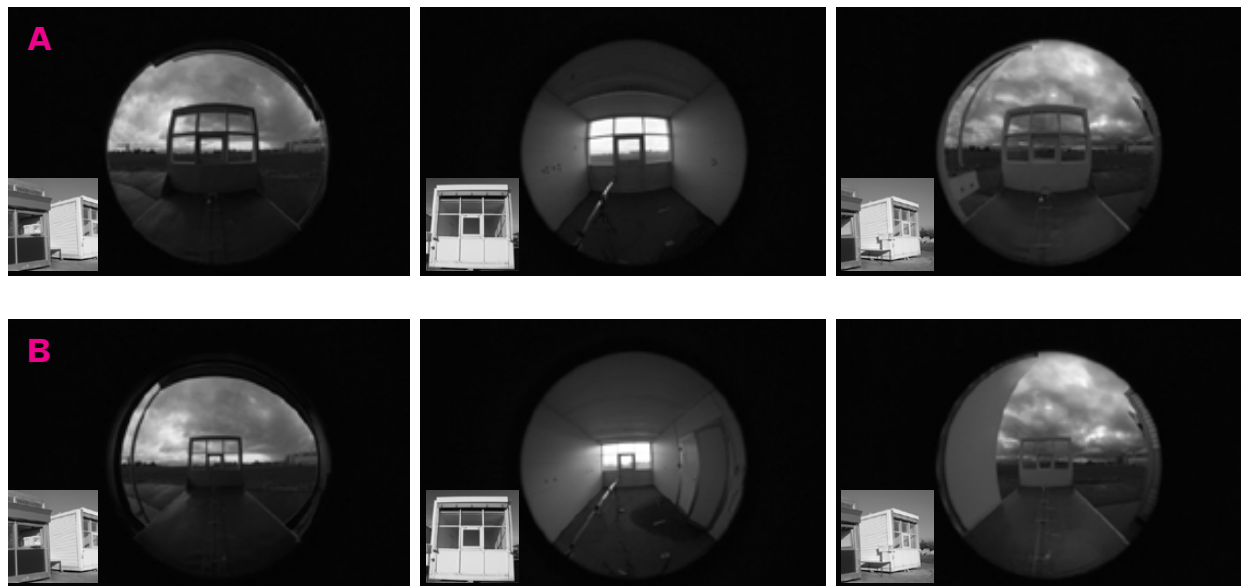


Fig. 5.33

Fish-eye views from inside the real building (centre) and the scale model (two model locations, left and right) corresponding to two different luxmeter positions: 2.2 m from the window (a) and 4.2 m from the window (b) (in Scale model; 0.22 m from the window (a) and 0.42 m from the window (b))

All pictures show identical solid angles both for the sky and for the ground visible up to the horizon line (Fig. 5.33). This observation, valid for all 6 luxmeter positions, indicates that all the corresponding photometric sensors placed in the model and the real building experience the same daylight contribution from sky and ground. As a consequence, differences in sky view factors should not be a cause of significant discrepancy in daylighting performance.

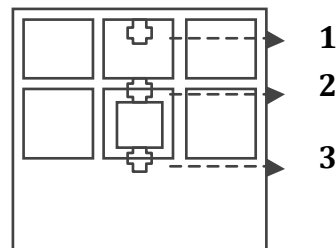


Fig. 5.34
Digital camera positions in the real building when assessing the sky view factors of its southern facade at three different heights (measured by 1, 2 and 3)

To test the sky view factors from the real building's windows, the camera was placed inside the module 1 m away from the glazing of its southern facade at 3 different heights (Fig. 5.34). Equivalent photographs were taken from inside the scale model at both of its locations.

As illustrated by the pictures shown in Fig. 5.35, all cases have identical sky and ground views, which confirms the earlier conclusion. Each glazing panel benefits from a comparable daylight flux from the sky vault, as well as from the ground, in all cases.

A more detailed analysis was carried out to assess the influence of the two locations of the scale model with regard to the contribution of the ground reflected component of daylight. These images were taken with the digital camera just outside the real building's window; the scaled-down equivalent was taken with the camera body inside the model, the lens jutting out slightly. Fig. 5.36 shows the camera mostly inside the model and its corresponding placement in front of the real building's window.

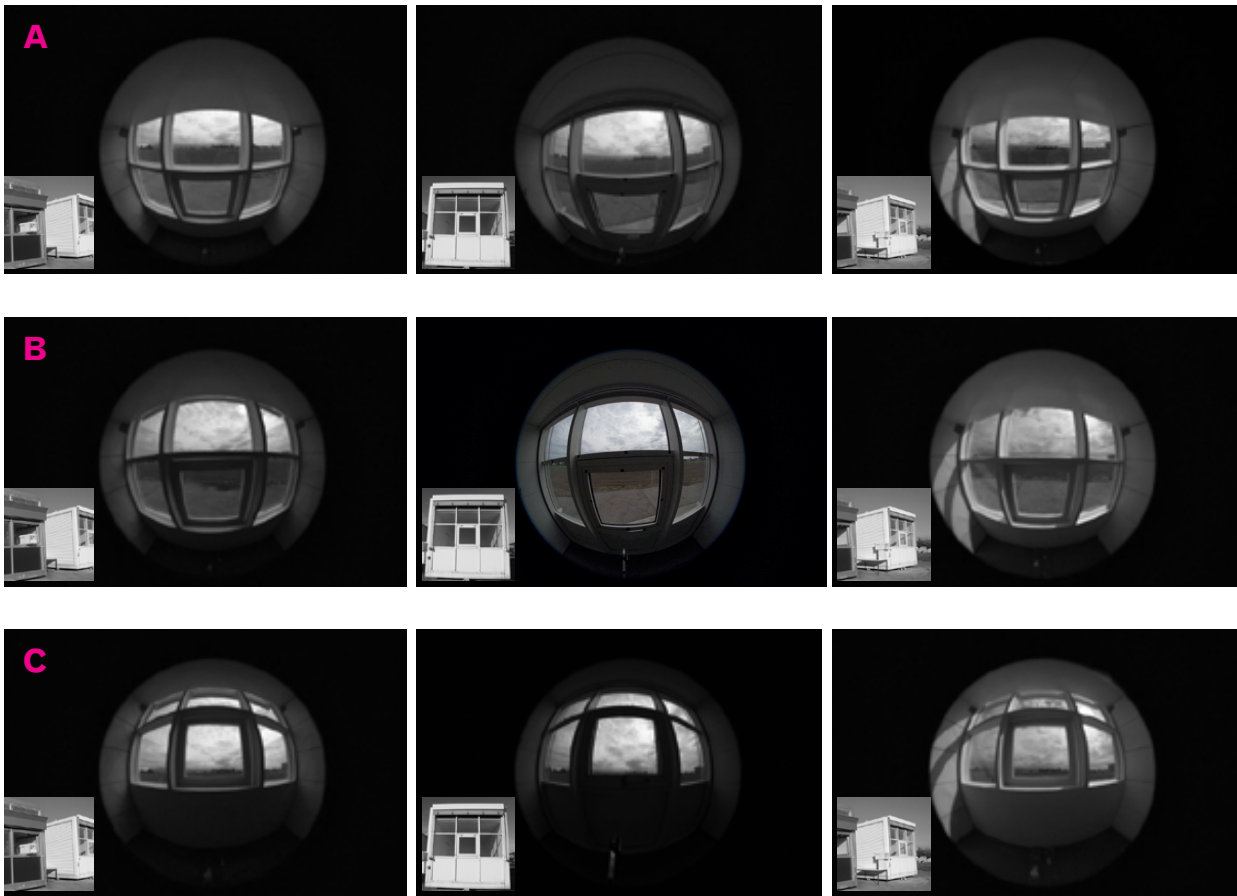


Fig. 5.35 Fish-eye views from inside the real building and its model (at the latter's two locations, left and right) taken at three different heights

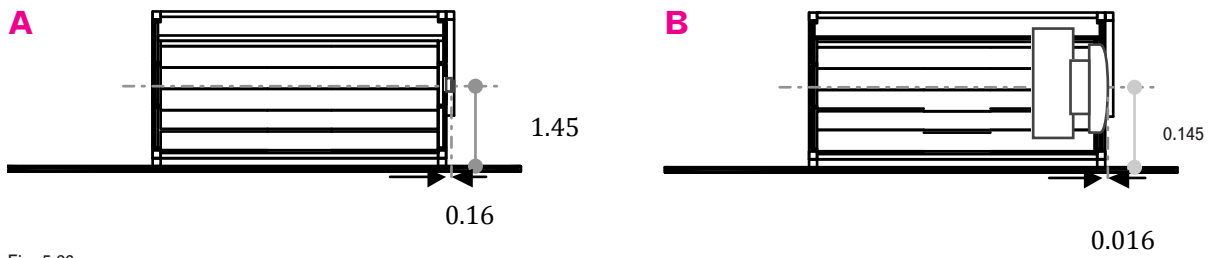
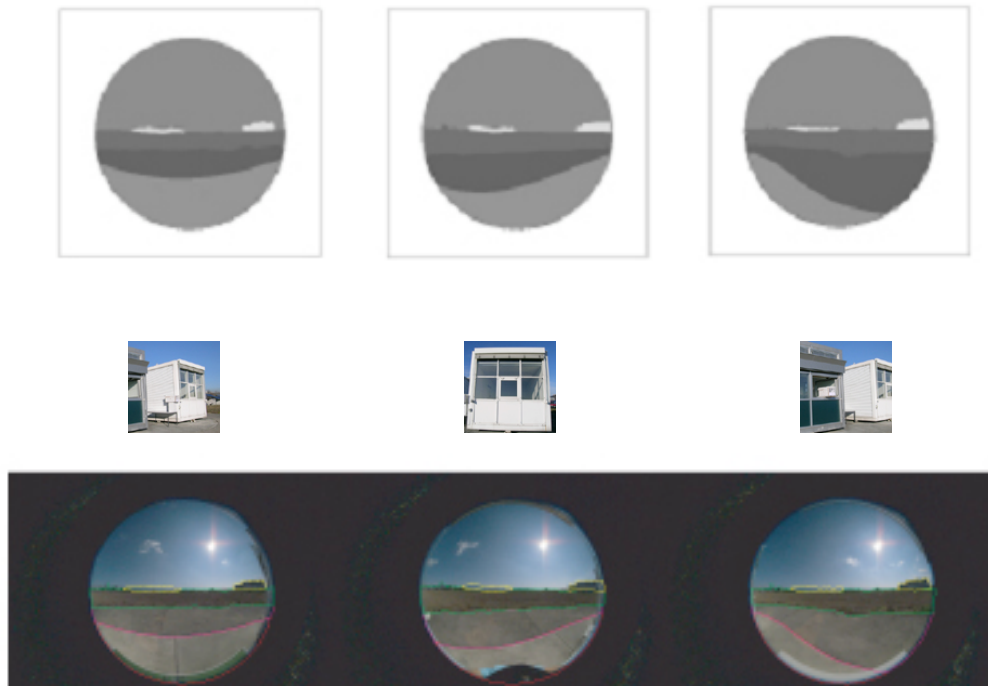


Fig. 5.36 Digital camera position outside the real building (a) and inside the scale model (b) to assess the sky view factors of the central window facade (units: m)

A



B

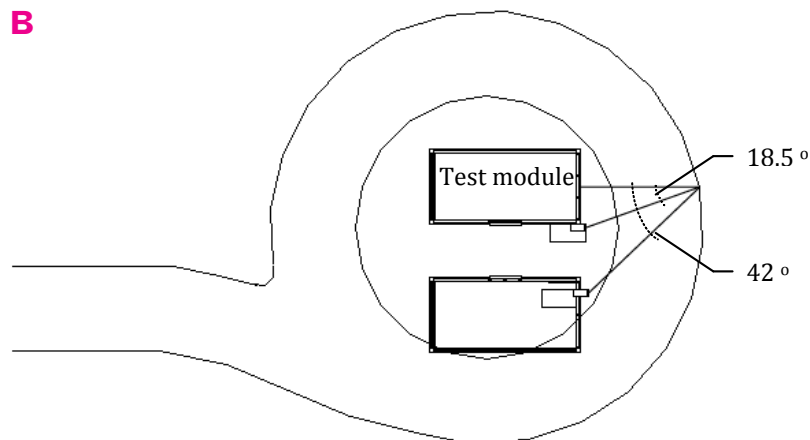


Fig. 5.37
 (a) Fish-eye views from the test module (centre) and from the scale model (two model locations, left and right) corresponding to the central window facade, (b) parallax angles of the two scale models (two locations).

Fig. 5.37 shows the corresponding pictures. The sky view as well as the position of the horizon line are identical for all three cases, indicating that their respective contribution to work plane illuminance and daylight factors can be considered as equal. This is not completely true for the external reflected component due to the concrete platform (seen as the lightest grey colour), which is clearly different in these pictures (especially from the model located in the adjacent test module). However, experimental results discussed below suggest that the ground reflected component is not a major contributor to the discrepancies observed.

The illuminance ratio was monitored in both the real building and the scale model at equivalent distances from their windows between 14:00 and 16:00 under clear sky and the relative divergences calculated. This was done with the model in two locations – next to the real building on one day, further away and jutting from the adjacent module on another (as can be seen in Figures 5.30 and 5.31).

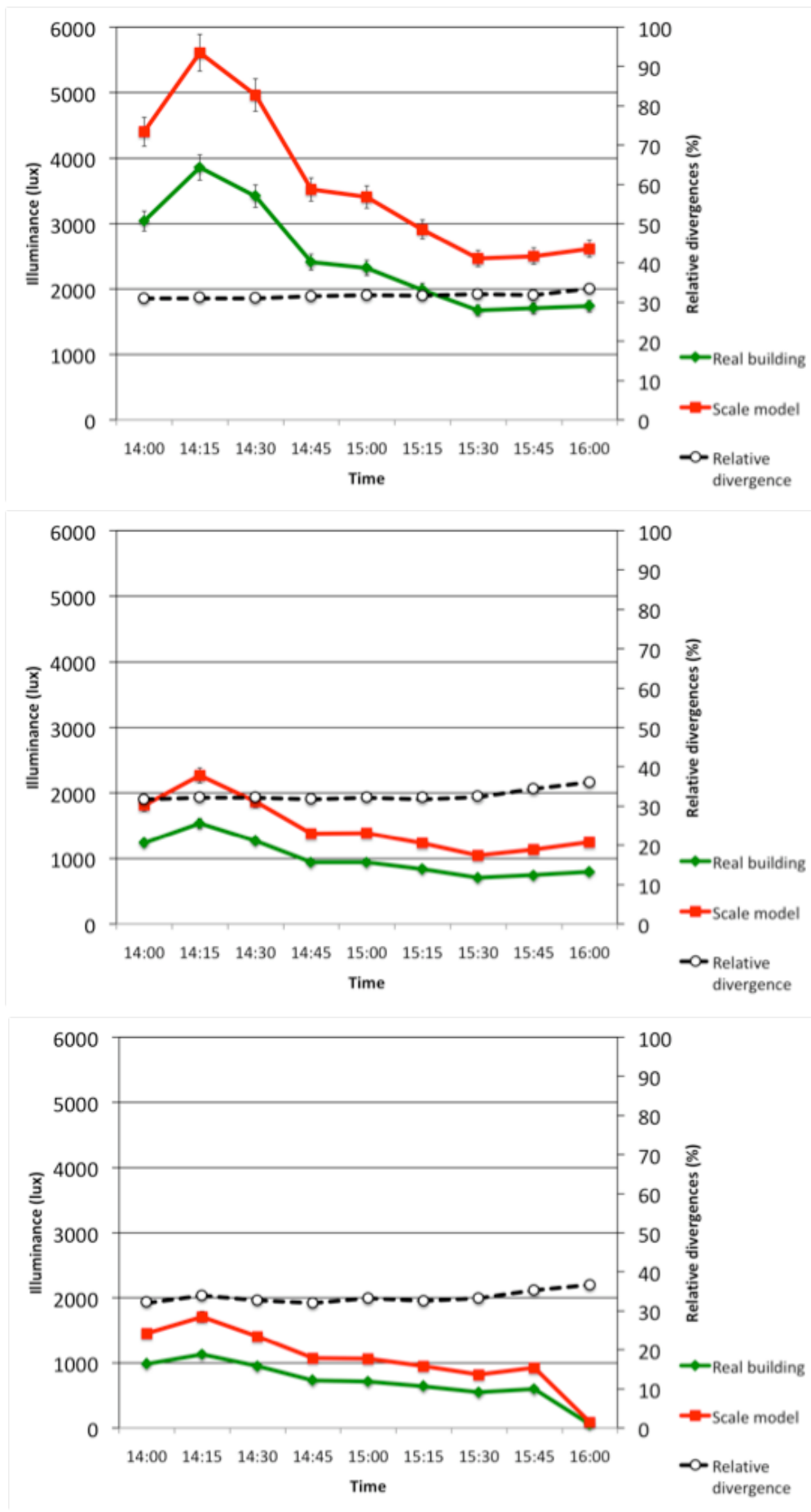
Fig. 5.38 shows the relative divergences observed between the model and real building work plane illuminances for the three different distances to the window, when the model was in the adjacent module. The relative divergence was on average 35%, almost constant at the three distances from the window, with a range of 32 to 37%.

Fig. 5.39 shows the corresponding work plane illuminances and relative divergences, when the model was positioned just outside the real building and therefore nearer to it than the previous case. A very small reduction of the average relative divergence was observed for the same three luxmeter positions when compared to the previous case (1 to 2 percentage points less).

Table 5.12 gives an overview of these figures, showing the minimal, maximal and average relative divergences observed for the two cases.

Clear sky condition	Relative divergence (%) of illuminance ratio: in neighbouring module			Relative divergence (%) of illuminance ratio: beside real building			Reduction in relative divergence: neighbouring module - beside real building		
	0.22 m from window	0.42 m from window	0.62 m from window	0.22 m from window	0.42 m from window	0.62 m from window	0.22 m from window	0.42 m from window	0.62 m from window
Average	34	35	35	32	33	34	2	2	1
Maximal	35	36	37	33	36	37	2	0	0
Minimal	32	34	33	31	32	32	1	2	1

Table 5.12
Impact of sky view factor and ground reflected component: comparison of the relative divergence between illuminance ratios of the real building and the model placed in two different locations



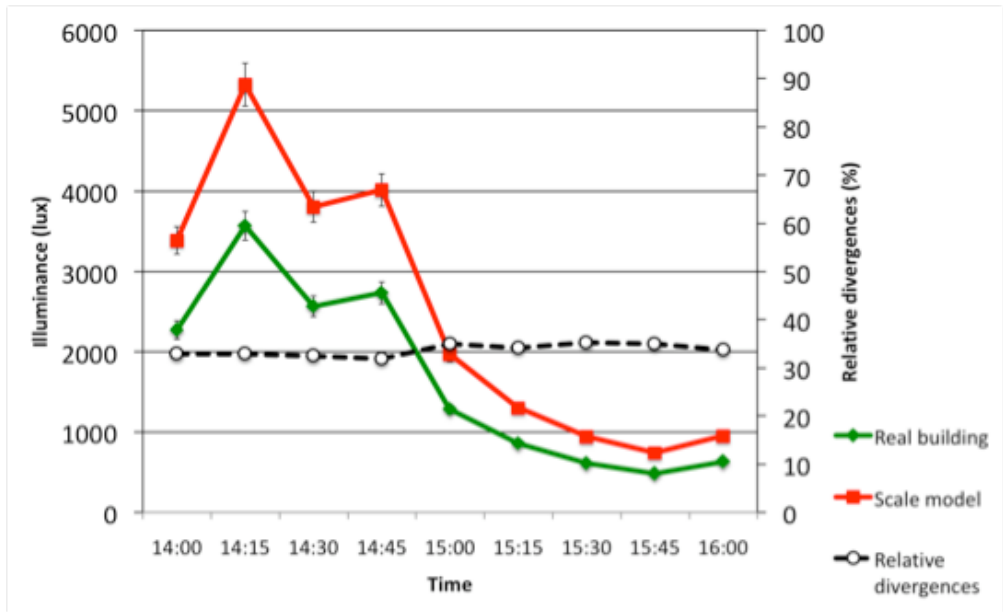
A

B

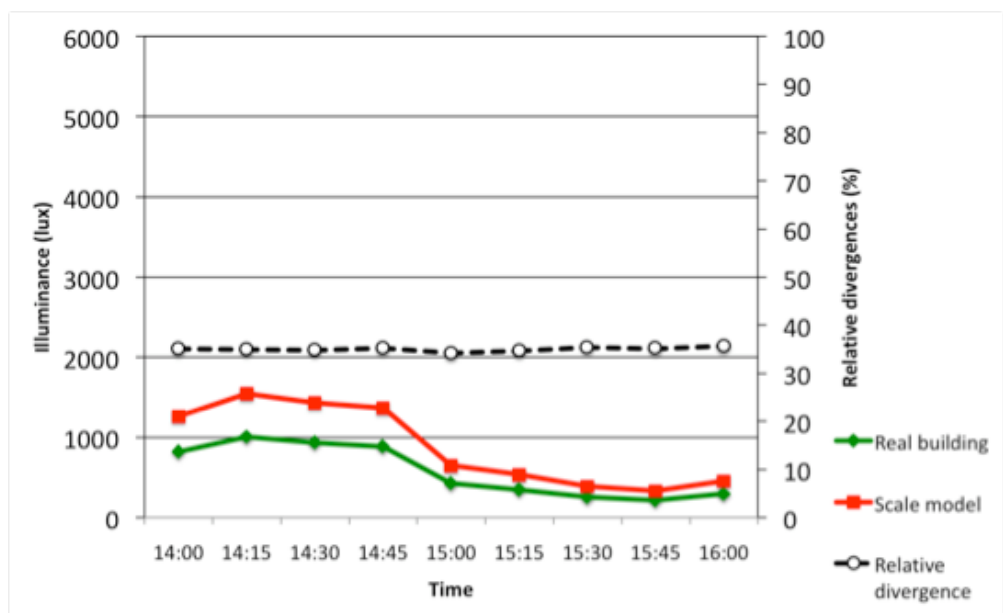
C

Fig. 5.38 Comparison of work plane illuminances monitored in the real building and its scale model at the more distant location (in the adjacent test module): (a) 2.2m from the window, (b) 4.2m from the window, (c) 6.2 m. from the window

A



B



C

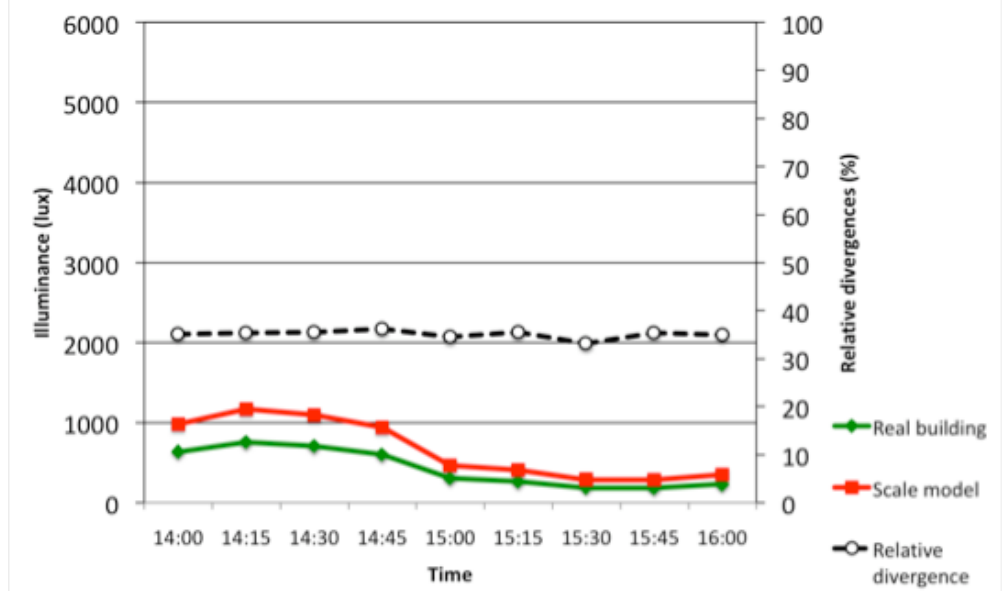


Fig. 5.39 Comparison of work plane illuminances monitored in the real building and its scale model at the closer location (next to the real building): (a) 2.2m from the window, (b) 4.2m from the window, (c) 6.2 m. from the window

Impact of sky view factor and ground reflected component

207

The hypothesis that a significant overestimation of the scale model's assessed daylighting performance is due to the differing sky view factors experienced by the module and its scale model was carefully examined by means of 360° photographs. These were taken at appropriate locations (six luxmeter positions, three window apertures), as illustrated by Fig. 5.33 and 5.35.

Both groups of pictures show identical solid angles for the visible part of the sky vault. The horizon lines, were in the same position in the pictures, indicating that no significant difference exist between the sky view factor experienced by the real building and the scale model. This was true for both model locations, whatever the distance from the real building.

The ground reflected daylight component was considered as another possible source of experimental error (Fig. 5.37). The quasi-constant relative divergences observed in the last case study when moving the scale model from one location to another on the concrete platform (Fig. 5.38 and 5.39) indicates that no significant influence can be assigned to the ground reflected components, beside a 2 percentage point impact (Table 5.13). As a consequence, this parameter was considered not to be responsible for significant performance overestimations.

According to the analysis in this study, the photometrical properties, window transmittance and reflectance factor inaccuracy are the main causes of errors. The model details can lead also to significant differences. The impact of photometric sensors displacement leads only to some differences in daylighting performance assessment. Slight displacement of model causes also very little errors. These discrepancies can be reduced by making an effort to mock up the geometric and photometric features of the models carefully.

chapter

6

conclusion

6.1 Putting the results into application

Models used to assess the daylighting performance of a building are expected to accurately reproduce the lighting environment of the final construction. However, it is difficult to produce a model that achieves this aim, particularly when complex fenestration systems (CFS) are to be used.

This study points out the significant sources of error in daylighting performance assessment. By rigorous study of the various types of model used in daylighting evaluation (both physical and virtual), one can see how they differ from the real building and to which types of error they are prone. Table 6.1 presents the dissimilarities and potential sources of error for each model type.

Model	How the model differs from the real case	Potential sources of error
Case A 1:10 physical scale model, real sky	—Modelling	—Geometric properties —Photometric properties —Photometric sensors —CFS scale
Case B 1:10 physical scale model, sky simulator, CIE standard sky	—Modelling —Sky luminance values —Daylight simulation	—Geometric properties —Photometric properties —Photometric sensors —CFS scale —Sky luminance distribution —Division of sky (145 circular sky sectors)
Case C 1:10 physical scale model, sky simulator, PDF method	—Modelling —Sky luminance values —Daylight simulation	—Geometric properties —Photometric properties —Photometric sensors —CFS scale —Sky luminance distribution —Division of sky (145 circular sky sectors) —Sky luminance acquisition using sky scanner
Case D Virtual model, standard sky (GenSky function)	—Modelling —Sky luminance values —Daylight simulation	—Geometric properties —Photometric properties —CFS property —Sky luminance distribution —Sky type
Case E Virtual model, sky simulation, PDF method	—Modelling —Sky luminance values —Daylight simulation	—Geometric properties —Photometric properties —CFS property —Sky luminance distribution —Division of sky (145 squared sky sectors) —Sky luminance acquisition using sky scanner

Table 6.1
Model types: their dissimilarities and potential sources of error in daylight performance assessment

A checklist to avoid daylighting modelling errors

212

The geometric and photometric properties of models must accurately mimic the real building in order to achieve a correct assessment. Sky luminance values and the daylight simulation type used in the assessments must also correspond to reality. A checklist of the possible errors that could occur at each step of modelling for daylighting evaluation follows. The sensitivity to error of the various parameters to which the modeller must take care is presented in Table 6.2, 6.3, 6.4 and 6.5.

Model scale and Dimensions

The scale and dimensions of a model should be appropriate to the assessment. If very accurate results are required a full-scale physical model should be used.

With physical models, the scale of the model can lead to inaccurate dimensions, for example a 1mm dimension inaccuracy in 1:10 scale model is equal to a 1cm inaccuracy in reality. In critical areas where light enters the building, details such as windows, CFS and objects obstructing or redirecting light, may produce a large error even if only a small error of dimension is made.

For virtual models created by an advanced daylighting simulation program such as Radiance, geometric properties such as scale and dimension are not major causes of error in daylight evaluation. The correct dimensions of the real case can be easily entered into the model.

Model details

In addition to its scale and dimensions, other critical details of the daylighting model should be carefully reproduced. Small complex details are often ignored due to the limitation of time and difficulty of modelling but they can cause significant errors in the assessment. For example, window details and daylighting systems such as CFS should be particularly considered. The details which can lead to noticeable shade, shadow, light transmission or redirection should be reproduced cautiously.

Model materials

The selection of the model's materials can be a major cause of error in daylight modelling. The photometric properties of a physical model's materials are often responsible for any errors incurred.

It is important to ensure accurate surface reflectance when making a model, particularly in zones of the building where reflected light plays an important role. Interior points furthest from the windows are particularly sensitive to inexact reflectance values because much of their light comes via surface inter reflection rather than from the direct component of daylighting. The effect of inaccuracy is more noticeable under overcast conditions than under clear skies. So the materials used for evaluation should be carefully selected to ensure a reliable daylighting model.

The impact of materials in a virtual daylighting assessment model is mainly linked to surface reflectance (of the interior surface when interior daylight properties are assessed). Normally the real reflectance values should be introduced if the simulation program allows it (as Radiance does). As with physical models, the surface reflectance plays an important role in virtual daylighting modelling, particularly in the deeper parts of the room. Errors caused by inaccurate reflectance are especially prevalent in these areas.

Glazing materials

Being the means by which daylight enters into the building, windows are always a very important factor in daylight modelling and evaluation. Not only must the details and dimensions of the window be

accurately modelled, but also the glazing material should be considered carefully when the daylighting model is built. An inaccurate window glazing property, often a photometric property such as the window transmittance, is a major cause of the errors coming from this source. Window transmittance is obviously very important in daylight assessment; its property has a direct impact on the daylight flux entering the space.

In a physical model, an appropriate material should be carefully chosen for the window glazing. Ignoring the window in the model or using a material with a different transmittance when modelling glazing lead to significant estimation in daylighting performance assessment. Even if it is impossible to precisely model double (or triple) glazing, to avoid this source of error the transmittance needs to be compared to the real situation and should be brought to the real value using neutral filters for instance.

In virtual models, the correct window transmittance must be entered in the simulation program together with the accurate dimensions and details of the window itself.

CFS modelling

Although accurate and reliable assessment results are required, Complex Fenestration Systems are not easy to model; their complex details and light redirecting properties are difficult to reproduce. A full-scale model is sometimes employed so that attaching a real scale CFS becomes possible. Scale or virtual models are alternatives, often required to facilitate the evaluation.

The CFS studied here, Laser-cut panel and prismatic film, are daylight-redirecting systems. Impossible to scale down, they were used at full scale in the 1:10 physical model to evaluate daylighting. Under a real sky the accuracy was not great; both had the tendency to raise the illuminance under clear sky, especially near the window. Under an overcast sky, however, the evaluated inaccuracy was only slight.

Under a scanning sky simulator the CFS evaluation showed greater errors, due to the different sky luminance distribution (continuous sky in the real case and circular sky division in the sky simulator). This study thus concludes that under real sky conditions a full scale CFS do not lead to significant errors when attached to a 1:10 scale model for daylighting performance assessment – lower accuracy is however attained when a sky simulator is used for daylighting simulation.

For virtual models the impact of CFS modelling inaccuracy is generally acceptable when direct sunlight is not strong and the sky luminance is continuously distributed. This was true of the simulations using real sky conditions (not divided into small sky elements), thanks to the integration of BTDF measurements (using a gonio-photometer) of the CFS under study. This is actually an important feature of Radiance program when combined to the outcome of a bidirectional gonio-photometer. The CFS modelling in the virtual model presents reliable simulations and leads to an acceptable result. It is not confirmed that CFS modellings in a virtual model will give acceptable results in daylighting performance assessment if the CFS does not include BTDF data.

Surroundings

The surroundings of the model can also cause error. For physical models the easiest ways to reproduce accurate surroundings is to place the model near the real situation, although this can only be done when the surroundings do not have a considerable elevation. Otherwise obstructions and reflections could lead to significant differences of assessment between the model and the reality it should represent. To have reliable daylight evaluation results, the important surrounding properties such as ground reflectance, buildings and trees should also be modelled.

If the model is placed under a sky simulator, the surrounding should be taken into account either by modelling the surroundings or using the surroundings simulation function within the sky simulator if one is available.

As with physical models, the virtual modeller should be cautious when including the surroundings. Surrounding buildings and obstructions should be reproduced and the correct exterior reflectance entered.

Daylight simulation

After the physical model and its surroundings have been built, the next step is simulating the source of daylight. Real sky conditions are the most convenient form of evaluation. Luminance measurement of the real sky is recommended; a luminance meter can be used for a quick measurements or a luminance sky scanner can be used for a more detailed measurement. However, one must remember light from the real sky is dynamic. The varying sky conditions require several measurements for a good evaluation, particularly with clear sky.

To avoid the difficulties of dynamic real skies while ensuring that all sky conditions are evaluated, a sky simulator, such as a scanning sky simulator, is used for daylight simulation. However, errors of simulation in this case may well come from the lighting quality and accuracy of the simulator used. Important errors may occur because the geometry of the sky divisions of the sky simulator differs from that of the real sky, which is characterised by a continuous luminance distribution. The sky luminance distribution values may be another cause of error in this case.

In virtual models, daylight simulation often employs CIE standard sky luminance distribution. Thanks to the advanced programs used nowadays, the daylight simulation in virtual models is mostly reliable and accurate. However, if real sky luminance must be reproduced in the computer simulation, errors can be introduced by the sky luminance acquisition method.

Monitoring equipment

To complete the daylighting evaluation process using a physical model, photometry measurement is needed. Photometric sensors and illuminance meters are often used for evaluation of daylight factors or illuminance profile. Apart from the need to calibrate the sensors, they must be accurately positioned, particularly in a small scale model. Errors of sensor position and direction can lead to slightly different results in the evaluation.

For luminance mapping within buildings, an HDR camera and luminance meters are recommended in addition to the illuminance sensors. They should be calibrated with a luminance calibrated sample in the view field and precisely positioned in order to have reliable luminance measurements.

	Errors in daylighting performance assessment							
Sky Conditions	Overcast sky							
Fenestration systems	Double glazing				CFS			
Modelling errors (%)	< ±10	±10	±30	>±30	< ±10	±10	±30	>±30
Window dimensions errors (cm)	< ± 6 cm	± 6 cm	> ± 6 cm		< ± 10 cm	± 10 cm	> ± 10 cm	
Model dimensions errors (cm)	< ± 6 cm	± 6 cm	> ± 6 cm		< ± 6 cm	± 6 cm	> ± 6 cm	
Details lamps	None				None			
Details window frame	With frame	None			With frame	None		
Surface reflectance under-estimation (%)	< 10	10	30	> 30	< 10	10	30	> 30
Surface reflectance over-estimation (%)	< 10			10	< 10			> 10
Glazing transmittance under-estimation (%)	< 20	20	40	> 40	< 20	20	40	> 40
Glazing transmittance over-estimation (%)	< 25	25	> 25		< 25		25	> 25
Ground reflectance under-estimation (%)	< 90	> 90			< 60	> 60		
Ground reflectance over-estimation (%)	< 50			> 50	< 20			> 20
Daylight simulation	Real sky	GenSky	Sky simulator		Real sky		GenSky	PDF
			PDF				Sky simulator	
Monitoring equipments	< ± 1 cm	± 1 cm	± 2 cm	> ± 2 cm	< ± 1 cm	± 1 cm	± 3 cm	> ± 3 cm

Table 6.2
Daylighting modeling checklist for the overcast sky

	Errors in daylighting performance assessment							
Sky Conditions	Clear sky							
Fenestration systems	Double glazing				CFS			
Modelling errors (%)	< ±10	±10	±30	>±30	< ±10	±10	±30	>±30
Window dimensions errors (cm)	< ± 10 cm	± 10 cm	> ± 10 cm		± 10 cm	± 10 cm	> ± 10 cm	
Model dimensions errors (cm)	< ± 10 cm	± 10 cm	> ± 10 cm		± 10 cm	± 10 cm	> ± 10 cm	
Details lamps	None				None			
Details window frame	None				with frame	None		
Surface reflectance under-estimation (%)	< 10	10	20	> 20	10	10	30	> 30
Surface reflectance over-estimation (%)	< 10			> 10	< 10			> 10
Glazing transmittance under-estimation (%)	< 10	10	40	> 40	10	10	40	> 40
Glazing transmittance over-estimation (%)	<25			> 25	< 25			> 25
Ground reflectance under-estimation (%)	< 80	> 80			< 60	> 60		
Ground reflectance over-estimation (%)	< 10				< 50			> 50
Daylight simulation	Real sky	GenSky		Sky simulator	Real sky	GenSky	GenSky	GenSky
				PDF				Sky simulator
								PDF
Monitoring equipments	< ± 5 cm	> ± 5 cm			< ± 5 cm	> ± 5 cm		

Table 6.3
Daylighting modeling checklist for the clear sky

Objective of daylighting models :

- < ±10% Full scale model, models for detailed study.
- ±10% Models for analysis of daylighting properties; glare analysis, daylight factors, surface luminance and detailed study.
- ±30% Models for daylight observation in buildings; interior space, shading device, daylighting systems, shade and shadow.
- >±30% Models for overall observation and preliminary study.

Overcast sky									
Source of error	Modelling precision								
	Accurate study model			Moderate study model			Preliminary study model		
Window dimensions									
Modelling precision	± 1 cm			± 5 cm			± 10 cm		
	min	average	max	min	average	max	min	average	max
Estimated errors (Double glazing)	2%	5%	7%	3%	6%	8%	10%	14%	17%
Estimated errors (CFS)	2%	8%	17%	1%	5%	8%	0%	8%	16%
Model dimensions									
Modelling precision	± 1 cm			± 5 cm			± 10 cm		
	min	average	max	min	average	max	min	average	max
Estimated errors (Double glazing)	6%	6%	6%	1%	9%	14%	13%	20%	26%
Estimated errors (CFS)	1%	7%	17%	4%	8%	17%	3%	18%	22%
Model details									
Modelling precision							Not very precise		
	min	average	max	min	average	max	min	average	max
Estimated errors (Double glazing)							0%	7%	34%
Estimated errors (CFS)							1%	14%	40%
Surface reflectance									
Modelling precision	+ 10%			+ 20%			+ 30%		
	min	average	max	min	average	max	min	average	max
Estimated errors (Double glazing)	32%	49%	65%	42%	77%	114%	78%	200%	334%
Estimated errors (CFS)	31%	58%	89%	37%	74%	136%	62%	153%	250%
Surface reflectance									
Modelling precision	- 10%			- 30%			- 50%		
	min	average	max	min	average	max	min	average	max
Estimated errors (Double glazing)	7%	12%	23%	6%	31%	56%	17%	46%	74%
Estimated errors (CFS)	5%	13%	18%	6%	36%	62%	15%	48%	75%
Window transmittance									
Modelling precision							+ 25% (No glazing)		
	min	average	max	min	average	max	min	average	max
Estimated errors (Double glazing)							4%	15%	24%
Estimated errors (CFS)							20%	25%	29%
Window transmittance									
Modelling precision	- 10%			- 20%			- 30%		
	min	average	max	min	average	max	min	average	max
Estimated errors (Double glazing)	1%	2%	3%	10%	15%	22%	11%	17%	21%
Estimated errors (CFS)	2%	3%	4%	3%	9%	11%	11%	16%	21%
Ground reflectance									
Modelling precision	+ 10%			+ 30%			+ 50%		
	min	average	max	min	average	max	min	average	max
Estimated errors (Double glazing)	3%	5%	7%	0%	4%	10%	11%	19%	26%
Estimated errors (CFS)	0%	6%	13%	0%	7%	29%	1%	6%	15%
Ground reflectance									
Modelling precision	- 10%			- 30%			- 50%		
	min	average	max	min	average	max	min	average	max
Estimated errors (Double glazing)	1%	3%	5%	4%	7%	11%	1%	3%	6%
Estimated errors (CFS)	1%	7%	15%	2%	6%	13%	4%	7%	9%
Daylight simulation									
Modelling precision	Real sky			Continuous sky			145 sky sectors		
	min	average	max	min	average	max	min	average	max
Estimated errors (Double glazing)				0%	11%	32%	3%	22%	58%
Estimated errors (CFS)				7%	26%	42%	4%	51%	117%

Table 6.4 Daylighting modeling checklist for overcast sky deduced from the sensitivity analysis

Clear sky									
Source of error	Modelling precision								
	Accurate study model			Moderate study model			Preliminary study model		
Window dimensions									
Modelling precision	± 1 cm			± 5 cm			± 10 cm		
	min	average	max	min	average	max	min	average	max
Estimated errors (Double glazing)	0%	1%	2%	1%	2%	4%	3%	5%	8%
Estimated errors (CFS)	1%	2%	2%	1%	3%	7%	2%	7%	13%
Model dimensions									
Modelling precision	± 1 cm			± 5 cm			± 10 cm		
	min	average	max	min	average	max	min	average	max
Estimated errors (Double glazing)	5%	8%	13%	3%	6%	8%	5%	9%	15%
Estimated errors (CFS)	2%	3%	4%	0%	4%	11%	5%	8%	19%
Model details									
Modelling precision							Not very precise		
	min	average	max	min	average	max	min	average	max
Estimated errors (Double glazing)							1%	8%	24%
Estimated errors (CFS)							0%	9%	31%
Surface reflectance									
Modelling precision	+ 10%			+ 20%			+ 30%		
	min	average	max	min	average	max	min	average	max
Estimated errors (Double glazing)	43%	60%	78%	64%	109%	156%	98%	195%	298%
Estimated errors (CFS)	40%	56%	72%	62%	108%	161%	92%	193%	300%
Surface reflectance									
Modelling precision	- 10%			- 30%			- 50%		
	min	average	max	min	average	max	min	average	max
Estimated errors (Double glazing)	6%	12%	16%	11%	53%	55%	29%	55%	75%
Estimated errors (CFS)	6%	12%	17%	9%	35%	56%	26%	54%	76%
Window transmittance									
Modelling precision							+ 25% (No glazing)		
	min	average	max	min	average	max	min	average	max
Estimated errors (Double glazing)							38%	39%	42%
Estimated errors (CFS)							34%	35%	36%
Window transmittance									
Modelling precision	- 10%			- 20%			- 30%		
	min	average	max	min	average	max	min	average	max
Estimated errors (Double glazing)	9%	9%	9%	5%	6%	6%	13%	15%	18%
Estimated errors (CFS)	8%	9%	9%	4%	6%	7%	16%	18%	19%
Ground reflectance									
Modelling precision	+ 10%			+ 30%			+ 50%		
	min	average	max	min	average	max	min	average	max
Estimated errors (Double glazing)	2%	2%	2%	4%	5%	5%	6%	7%	8%
Estimated errors (CFS)	0%	2%	5%	4%	5%	6%	7%	8%	11%
Ground reflectance									
Modelling precision	- 10%			- 30%			- 50%		
	min	average	max	min	average	max	min	average	max
Estimated errors (Double glazing)	1%	1%	1%	2%	2%	3%	4%	6%	7%
Estimated errors (CFS)	1%	2%	3%	4%	5%	6%	6%	9%	12%
Daylight simulation									
Modelling precision	Real sky			Continuous sky			145 sky sectors		
	min	average	max	min	average	max	min	average	max
Estimated errors (Double glazing)				0%	21%	31%	0%	87%	732%
Estimated errors (CFS)				0%	39%	63%	0%	107%	912%

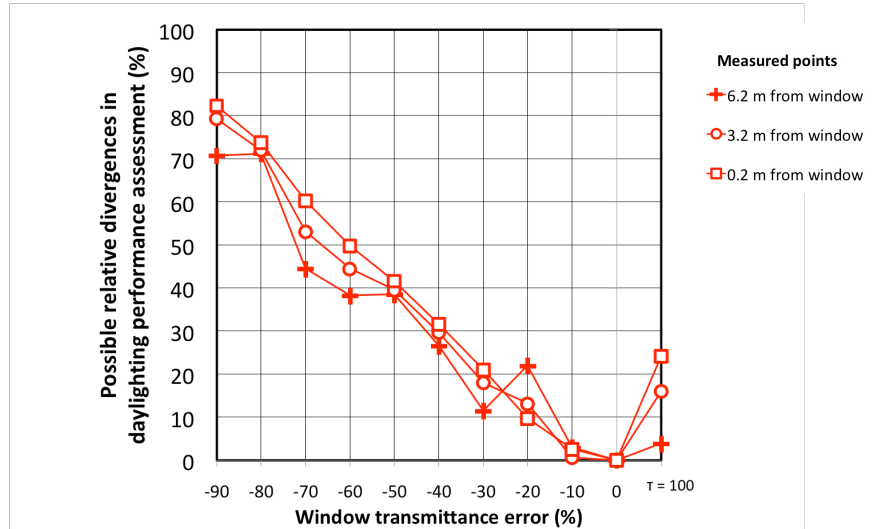
Table 6.5 5 Daylighting modeling checklist for clear sky deduced from the sensitivity analysis

Charts to help estimate the level of assessment inaccuracy

218

The sensitivity analysis of chapter 5 presents several charts of relative errors. They can be used to estimate the effects of model inaccuracy. The chart of one important parameter - window transmittance - is described here as an example (Fig. 6.1). Glazing does not transmit 100% of incident light, so if the model is made with no glazing (simply a window gap) daylighting will be overestimated. The chart shows in this case a 25% divergence under overcast sky condition and 40% under clear sky condition, meaning that assessments made using such a model will be inaccurate by those amounts. A model whose glazing is too opaque will be inaccurate by the amounts shown to the left of the chart.

A



B

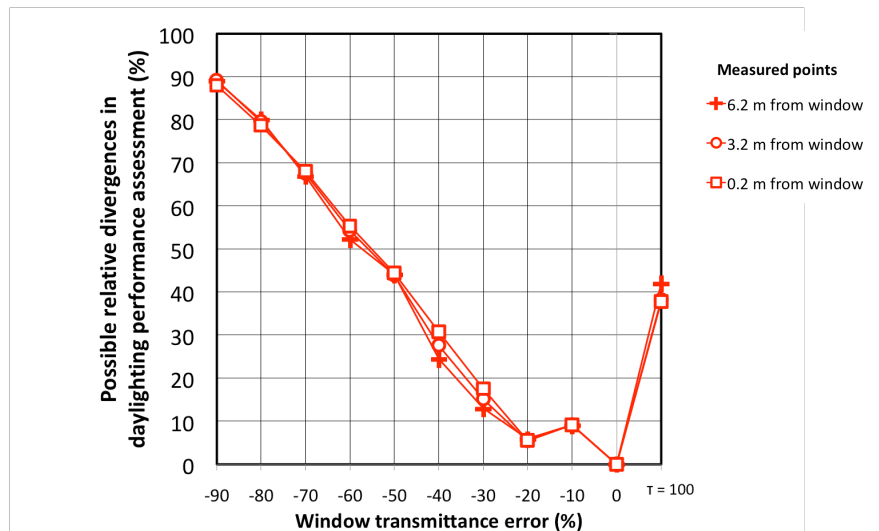


Fig. 6.1 Charts of relative divergence caused by window transmittance inaccuracies for (a) overcast sky conditions and (b) clear sky conditions

A further example (Fig. 6.2) shows the impact of window dimension inaccuracy when a CFS (in this case, prismatic film) is attached to the window. If a dimension of the model is inaccurate by 2 cm, one can expect the daylighting performance assessment to be inaccurate by 8% under overcast sky conditions or 5% under clear sky conditions.

An estimation of the level of errors in daylighting performance assessment that a model can cause should allow the modeller to see, right from the start, where greater exactitude is required for a particular daylighting evaluation, or where less may be acceptable.

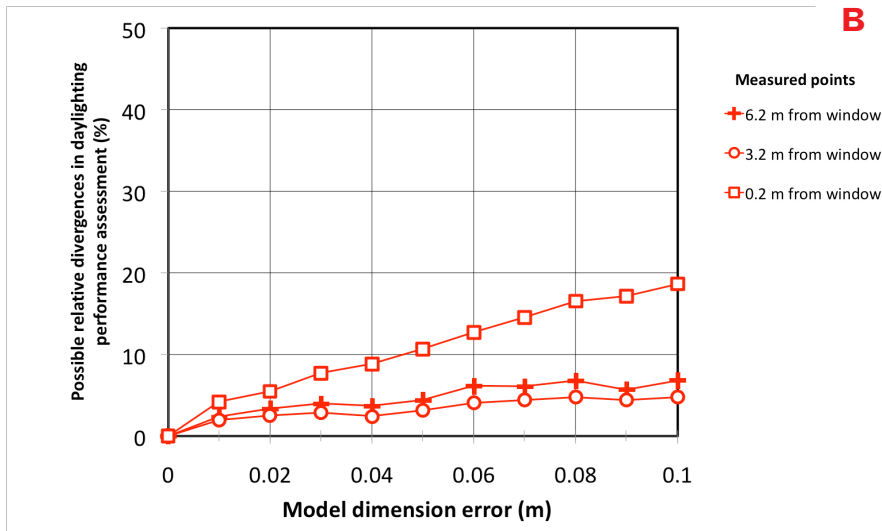
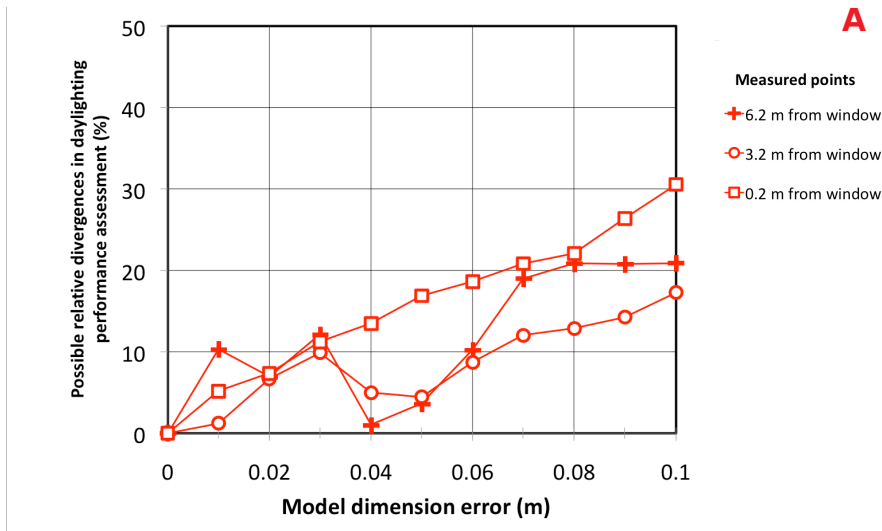


Fig. 6.2 Charts of relative divergence caused by model dimension inaccuracies for (a) overcast sky conditions and (b) clear sky conditions

Further study

220

This study could be extended in various ways. The qualitative sensitivity analysis, for example, could use the high dynamic range (HDR) imaging technique to evaluate the daylighting model in terms of luminance measurement. A comparative glare analysis assessment using different methods in both physical and virtual models could also be considered. Additionally, more CFS evaluations could be added to extend the checklist to other daylighting systems. Different commonly used daylight simulation techniques could be also evaluated. For virtual models, the various computer programs currently used in daylight research community or in lighting design community would make a very interesting study. Other daylighting simulation methods, such as the Daylight Coefficient methods (DAYSIM), as well as the other sky models like Perez model can also be employed in future study.

Daylighting performance assessment using models is an important way to develop daylighting systems which brings optimal lighting to a building and thus help reduce a building's electrical consumption. Daylighting research and study are obviously very important in designing buildings for sustainability. These building design strategies should be systematically developed and applied in building design and construction.

Appendices

Appendix A

CIE standard general sky (CIE, 2003)

Sky conditions vary according to the weather and sun position, both of which cause varying sky luminance distributions. The CIE standard general sky was created for two purposes: a) to classify the measured sky luminance distribution and b) to calculate the sky luminance in daylighting design.

15 CIE standard skies are listed whose luminance distributions are as follows:

- Type 1** – CIE Standard Overcast Sky, steep luminance gradation towards zenith, azimuthal uniformity
- Type 2** – Overcast, with steep luminance gradation and slight brightening towards the sun
- Type 3** – Overcast, moderately graded with azimuthal uniformity
- Type 4** – Overcast, moderately graded and slight brightening towards the sun
- Type 5** – Sky of uniform luminance
- Type 6** – Partly cloudy sky, no gradation towards zenith, slight brightening towards the sun
- Type 7** – Partly cloudy sky, no gradation towards zenith, brighter circumsolar region
- Type 8** – Partly cloudy sky, no gradation towards zenith, distinct solar corona
- Type 9** – Partly cloudy, with the obscured sun
- Type 10** – Partly cloudy, with brighter circumsolar region
- Type 11** – White-blue sky with distinct solar corona
- Type 12** – CIE Standard Clear Sky, low luminance turbidity
- Type 13** – CIE Standard Clear Sky, polluted atmosphere
- Type 14** – Cloudless turbid sky with broad solar corona
- Type 15** – White-blue turbid sky with broad solar corona

In addition, the spatial distribution of CIE standard general sky was noted as;

Type 16 – Traditional Overcast Sky

This sky may be used as an alternative to CIE overcast sky Type 1 when only an overcast sky is to be modelled.

Sky types are defined by their luminance distribution. The sky luminance distribution, as presented in Fig. A1, is characterised by:

1. The solar meridian and the angular distance between the sun and the zenith (Z_s)
2. Smooth continuous functions defining the sky luminance distributions which are typical cloudless skies or homogeneously cloud-covered skies.
3. The relative luminance at any point of the sky depending from the angle χ between the sun and sky element. The relative luminance at any point of the sky also depends on the angle Z between the sky element and the zenith. The relative scattering indicatrix ($f(\chi)$) and the luminance gradation between horizon and zenith ($\phi(Z)$) are the functions used for these two cases.

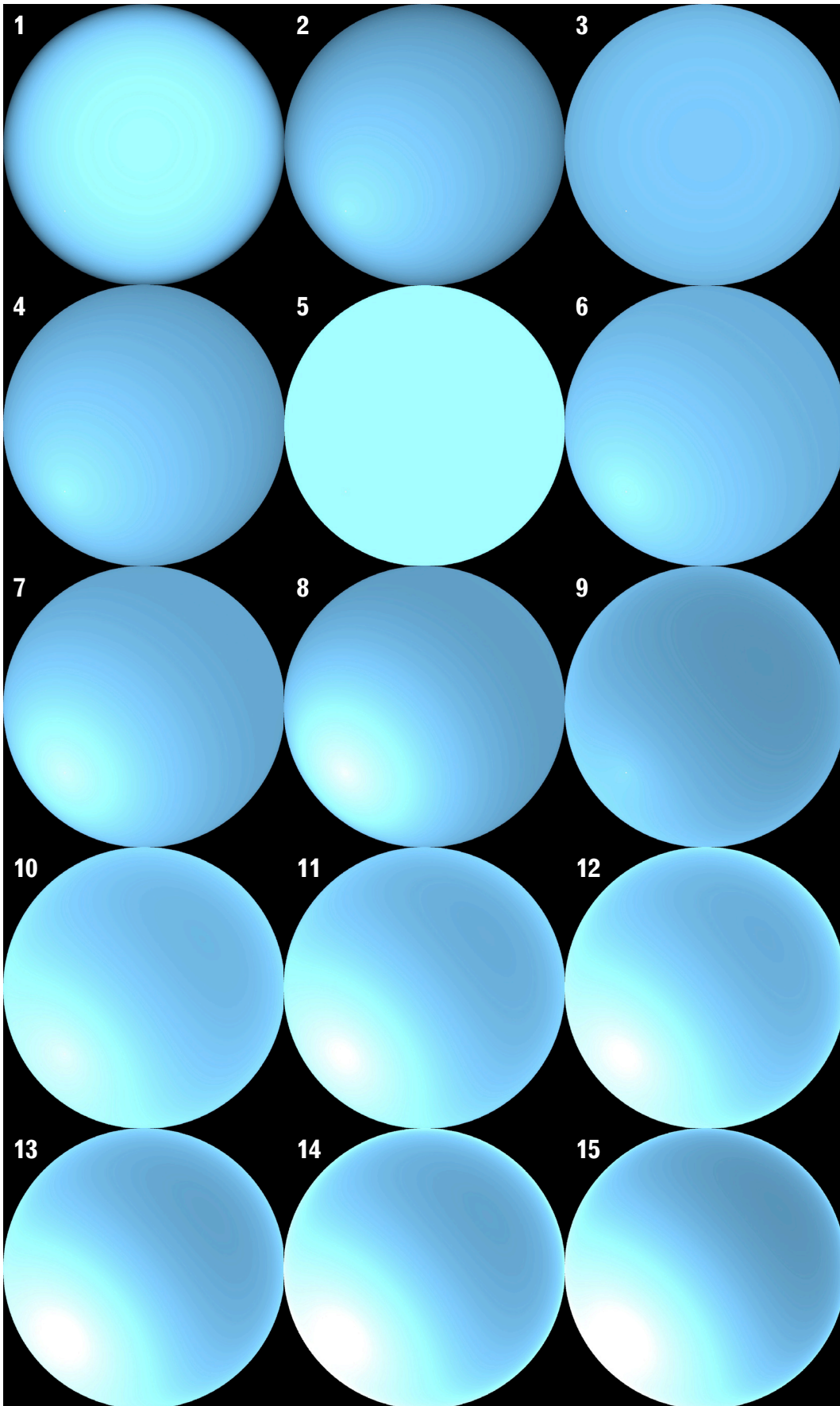


Fig. A 1
The relative luminance distributions of the 15 CIE standard skies

Solar meridian and angular distance between the sun and the zenith (Z_s)

As presented in Fig. A2, to specify the relative sky luminance distribution the position of the considered sky element is defined by the angular distance between the element and the sun (χ) using the zenith angle (Z), the zenith angle of the sun (Z_s), the difference of the azimuth of the sky element (α) (clockwise from north) and the azimuth of the sun (α_s) (clockwise from north).

$$\chi = \arccos(\cos Z_s \times \cos Z + \sin Z_s \times \sin Z \times \cos |\alpha - \alpha_s|) \quad \text{A.1}$$

Alternatively, the angles of elevation of the sun (γ_s) and of the sky element (γ) can be used using :

$$Z_s = \pi/2 - \gamma_s \quad \text{for the zenith angle of the sun} \quad \text{A.2}$$

$$Z = \pi/2 - \gamma \quad \text{for the zenith angle} \quad \text{A.3}$$

The ratio of the luminance of the considered sky element (L_a) to the zenith luminance (L_z) is:

$$L_a/L_z = f(\chi) \times \phi(Z) / f(Z_s) \times \phi(0) \quad \text{A.4}$$

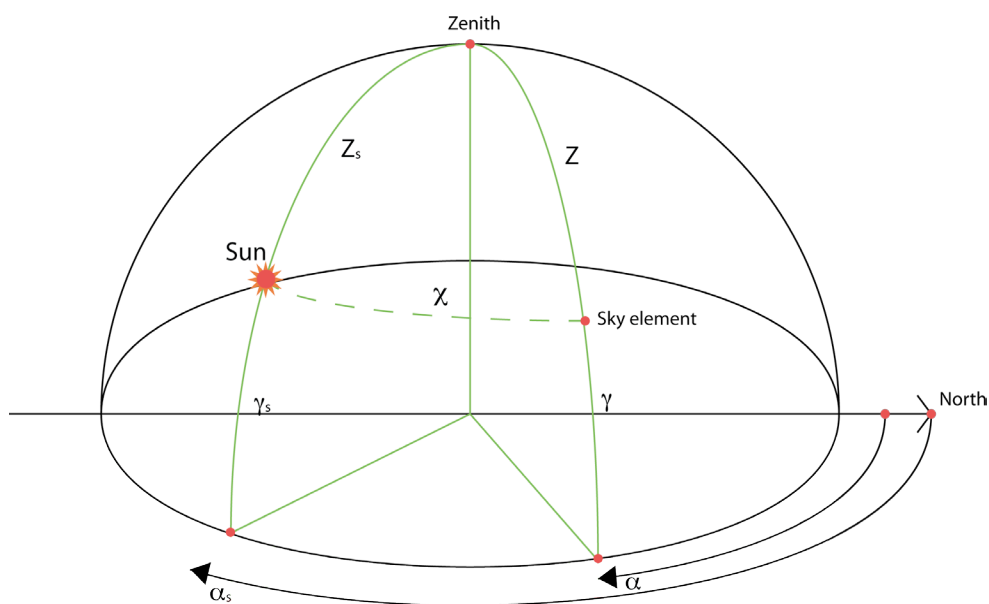


Fig. A 2
Positions of the sun and
a sky element

Luminance gradation function (ϕ)

The luminance gradation function (ϕ) is given by:

$$\phi(Z) = 1 + a \times \exp(b/\cos Z) \quad \text{when } 0 \leq Z < \pi/2 \quad \text{A.5}$$

$$\phi(\pi/2) = 1 \quad \text{at the horizon} \quad \text{A.6}$$

$$\phi(0) = 1 + a \times \exp b \quad \text{the value at the zenith} \quad \text{A.7}$$

This function is presented on Fig. A3.

Relative scattering indicatrix (f)

226

The relative scattering indicatrix (f) is given by:

$$f(\chi) = 1 + c \times \{\exp(d\chi) - \exp(d \pi/2)\} + e \times \cos^2 \chi \tag{A.8}$$

$$f(Z_s) = 1 + c \times \{\exp(d Z_s) - \exp(d \pi/2)\} + e \times \cos^2 Z_s \tag{A.9}$$

The parameters a, b, c, d and e used to classify the 15 standard relative luminance distributions are presented in Table 1.

Corresponding function is presented in Fig. A4.

Type	Gradation group	Indicatrix group	a	b	c	d	e
1	I	1	4.0	-0.70	0	-1.0	0
2	I	2	4.0	-0.70	2	-1.5	0.15
3	II	1	1.1	-0.8	0	-1.0	0
4	II	2	1.1	-0.8	2	-1.5	0.15
5	III	1	0	-1.0	0	-1.0	0
6	III	2	0	-1.0	2	-1.5	0.15
7	III	3	0	-1.0	5	-2.5	0.30
8	III	4	0	-1.0	10	-3.0	0.45
9	IV	2	-1.0	-0.55	2	-1.5	0.15
10	IV	3	-1.0	-0.55	5	-2.5	0.30
11	IV	4	-1.0	-0.55	10	-3.0	0.45
12	V	4	-1.0	-0.32	10	-3.0	0.45
13	V	5	-1.0	-0.32	16	-3.0	0.30
14	VI	5	-1.0	-0.15	16	-3.0	0.30
15	VI	6	-1.0	-0.15	24	-2.8	0.15

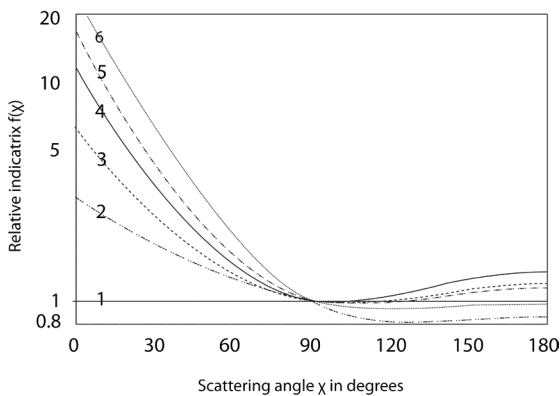


Fig. A 3
Standard gradation function groups

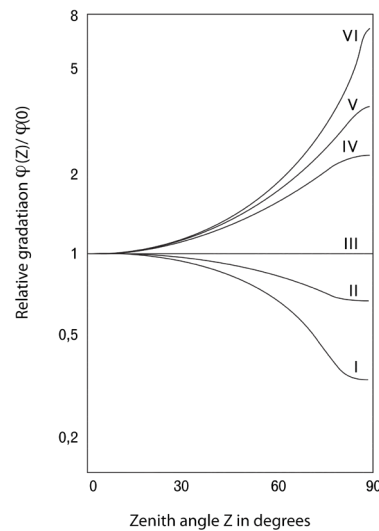


Fig. A 4
Standard indicatrix function groups

Appendix B

Impact on daylighting performance assessment of CFS placement within scale models

CFS were attached within real building and virtual model inside the window, those of the 1: 10 physical model were set up outside the window (Fig. B1 and B2). This was to avoid errors caused by frequent reinstallation and save time for experimentation. However, additional study presented in this appendix shows insignificant difference between the two cases.



Fig. B 1
Scale model: CFS attached on
the outside of the window



Fig. B 2
Real case: CFS attached on
the inside of the window

Two CFS (laser-cut panel and prismatic film) were tested using the scanning sky simulator under CIE overcast sky Type 1 and CIE clear sky Type 13. A CFS was first attached on the inside of the window and DF (and IR) monitored. Afterwards it was removed and attached on the outside of the window, DF and IR being monitored again. The second CFS was tested the same way.

As presented in Fig. B3 and B4, the comparison of DF under overcast sky and IR under clear sky conditions show very small divergences (less than 0.5% in every case).

Thus for the two CFS used in this study the placement of the CFS within the scale model caused no significant errors: it can be assumed that the CFS performing identical light redirecting properties for daylight within real buildings and models.

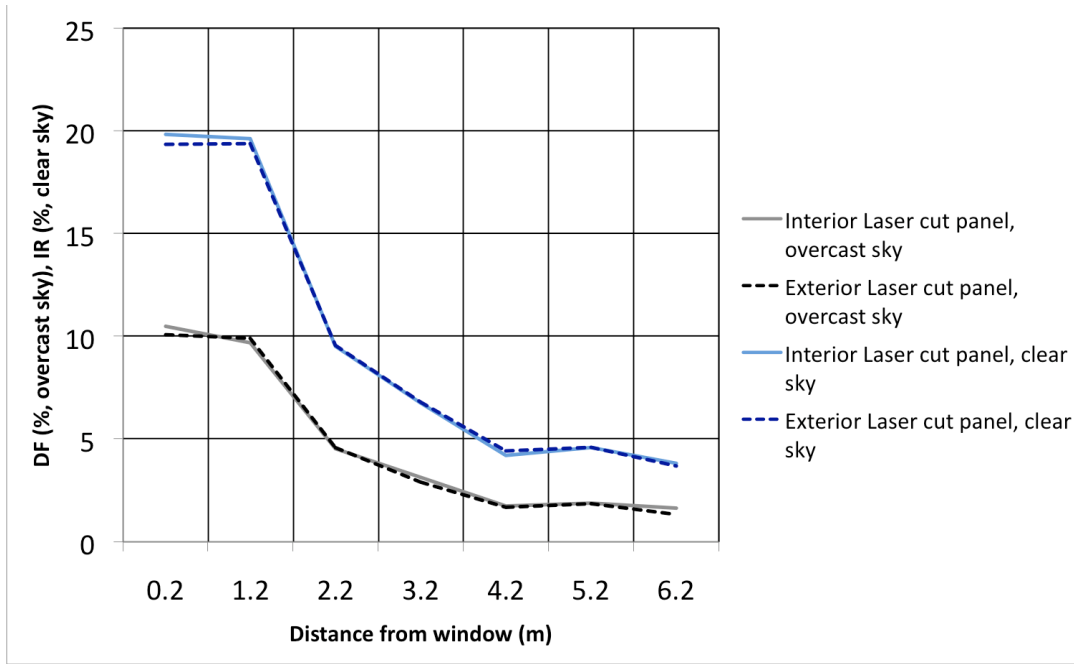


Fig. B 3 Daylight factor (DF) and illuminance ratio (IR) show insignificant difference when laser-cut panel is attached inside or outside the window under both overcast and clear skies

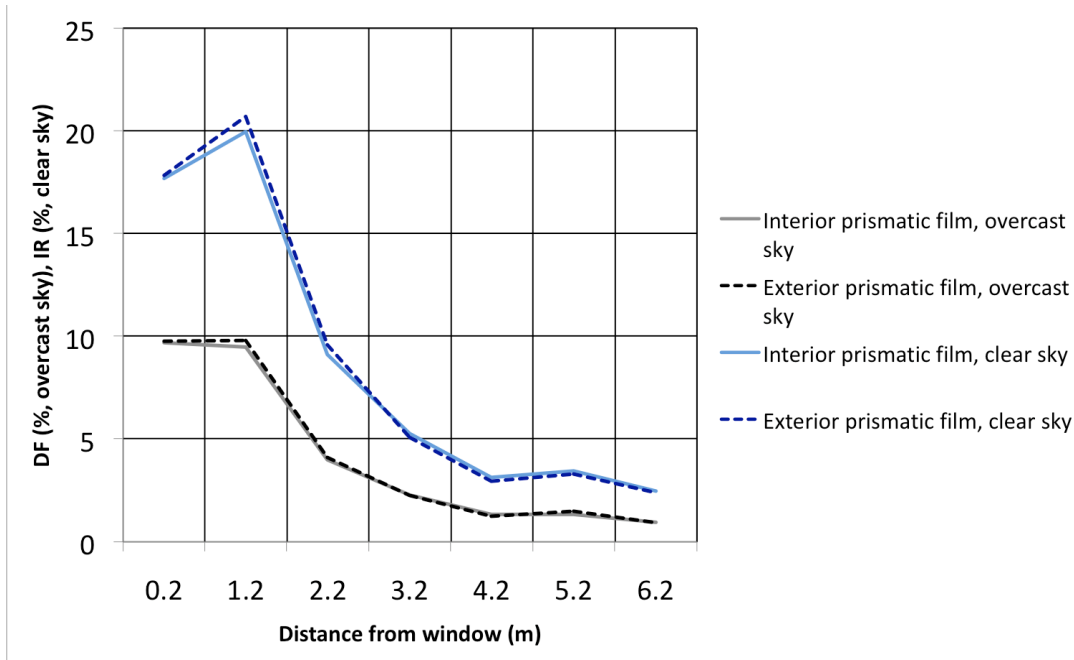


Fig. B 4 Daylight factor (DF) and illuminance ratio (IR) show insignificant difference when the prismatic film is attached inside or outside the window under both overcast and clear skies

Appendix C

Impact of the different CIE standard skies on daylighting performance assessment

At present there are certain difficulties and limitations in reproducing or simulating all 15 CIE standard skies when using several of the daylighting methods. Some general sky types, such as Type 1 (CIE Standard Overcast Sky, steep luminance gradation towards zenith, azimuthal uniformity) and Type 12 (CIE Standard Clear Sky, low luminance turbidity) are often used to mimic the overcast sky and the clear sky conditions.

Illuminance evaluations using virtual models were carried out to confirm that the slight differences of sky luminance distribution of the different sky types used in this thesis did not have any significant impact on the daylighting performance assessments. Three sky types were compared for each of two sky conditions. The illuminance were measured at the same 7 distances from the window as in the remainder of the thesis to ensure compatibility with the other results.

Group 1: overcast sky conditions

Type 1 – CIE Standard Overcast Sky, steep luminance gradation towards zenith, azimuthal uniformity

Type 2 – Overcast, with steep luminance gradation and slight brightening towards the sun

Type 3 – Overcast, moderately graded with azimuthal uniformity

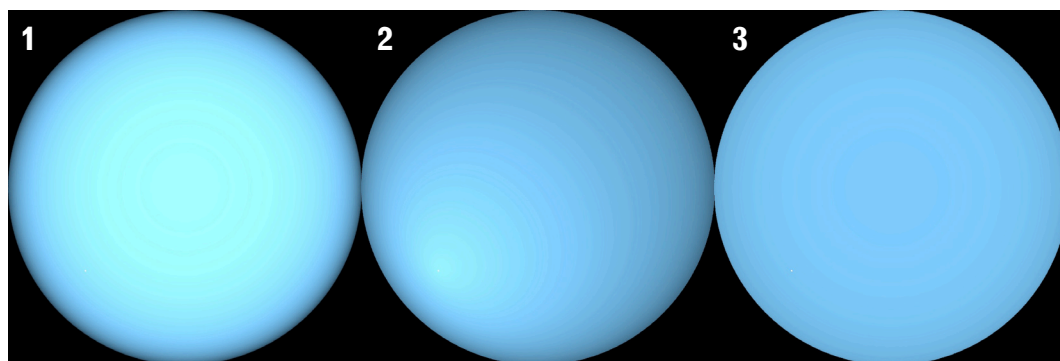


Fig. C 1
Virtual simulations of CIE standard overcast sky of Types 1, 2 and 3

Fig. C.5.2 presents three profiles of the model's illuminance, all very similar, showing less than 1% divergence. This result confirms that the slight differences of sky luminance distribution of the CIE standard sky Types 1, 2 and 3 did not induce significant errors in the daylighting performance assessment.

230

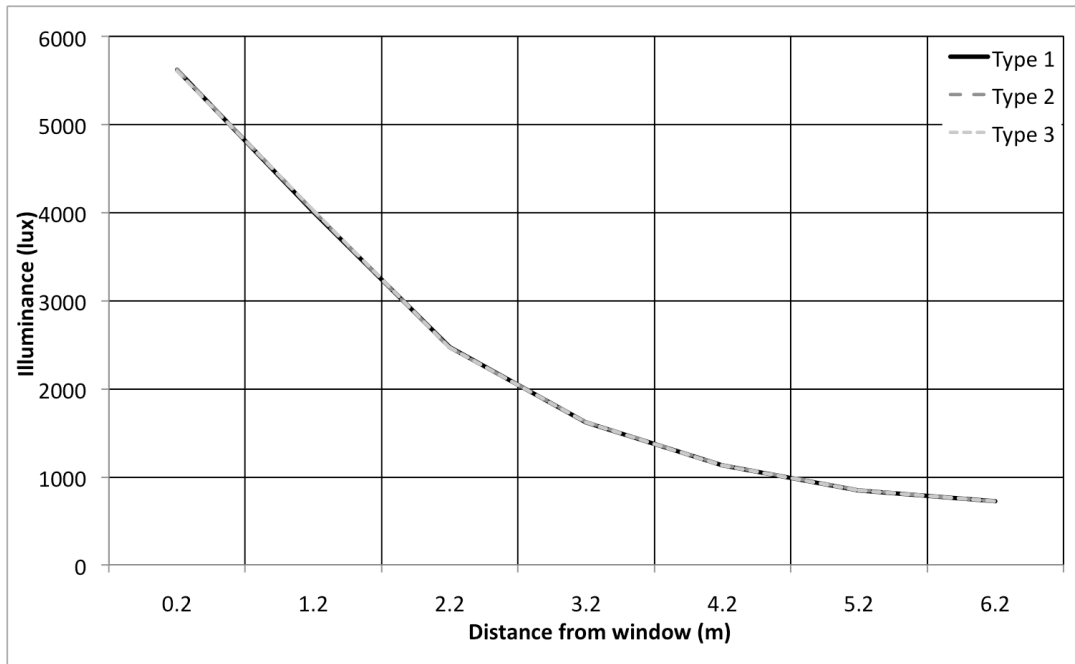


Fig. C 2
Comparison of the illuminance of the building under CIE standard overcast skies of Types 1, 2 and 3

Group 2: clear sky conditions

Type 11 – White-blue sky with distinct solar corona

Type 12 – CIE Standard Clear Sky, low luminance turbidity

Type 13 – CIE Standard Clear Sky, polluted atmosphere

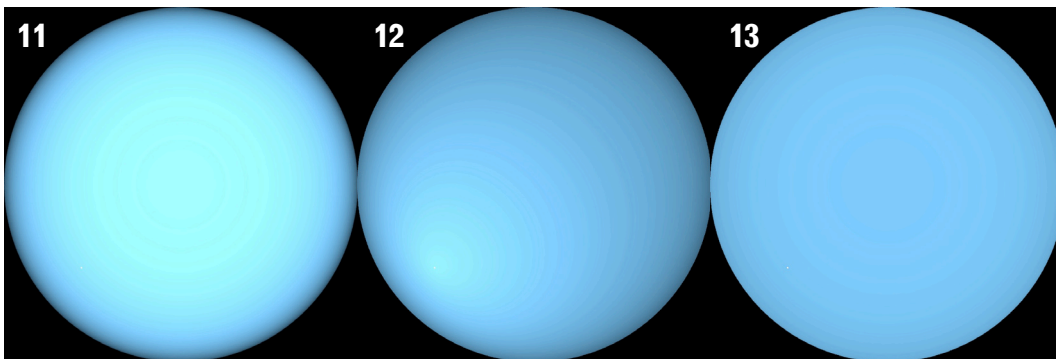


Fig. C 3
Comparison of the illuminance of the building under overcast skies of Types 1, 2 and 3

A similar study was made for clear sky conditions. Fig. C4 again presents three curves of the model's illuminance, all very similar, showing less than 1% divergence. In this case, too, the result confirms that the slight differences of sky luminance distribution of the CIE standard sky Types 11, 12 and 13 did not induce significant errors in the daylighting performance assessment.

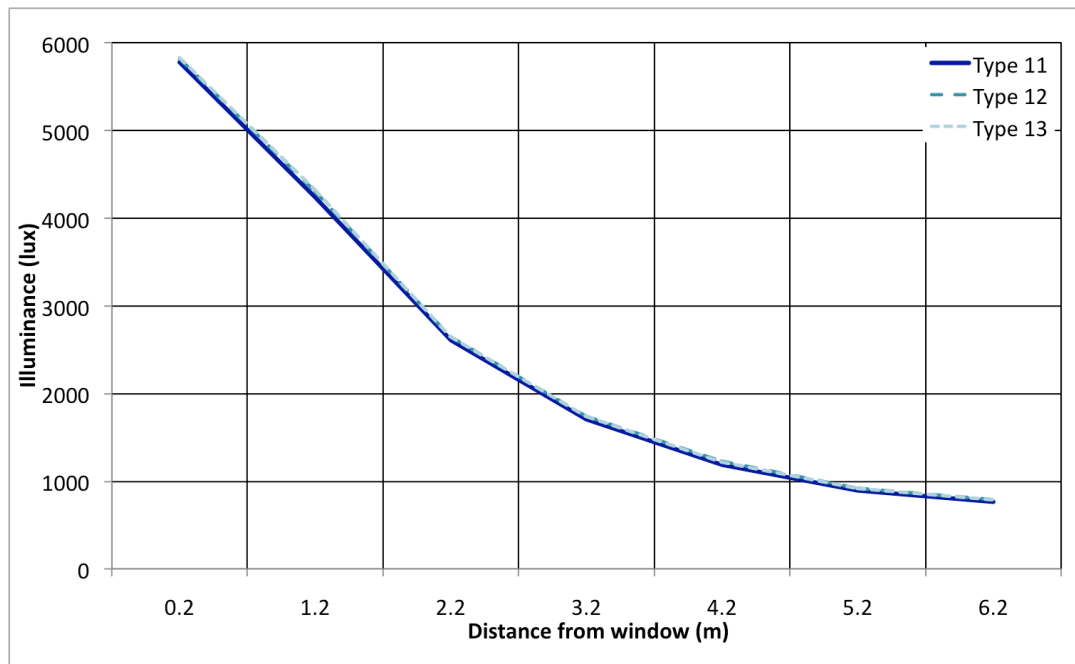


Fig. C 4
Comparison of the illuminance of the building under CIE standard clear skies of Types 11, 12 and 13

Nomenclature

General		
CFS	Complex fenestration system	
LCP	Laser-cut panel	
HDR	High dynamic range imaging technique	
VGA	Video graphics array	
SVGA	Super video graphics array	
CCD	Charge-coupled device camera	
IDMP	International Daylight Measurement Program	
PDF	Partial Daylight Factor method	
GenSky	Function for generate a RADIANCE description of the sky	

Geometric properties		
dA	Area	(m^2)
H	Window height	(m)
H_{model}	Window height of the model	(m)
$H_{base\ case}$	Window height of the base case model	(m)
D	Depth	(m)
D_{model}	Model depth	(m)
$D_{base\ case}$	Base case model depth	(m)
P_s	Sensor position	(m)
$P_{s\ model}$	Sensor position in model	(m)
$P_{s\ base\ case}$	Sensor position in base case model	(m)

Photometric properties		
BTDF	Bidirectional Transmission Distribution Function ($Cd \cdot m^{-2} \cdot lux^{-1}$) or (sr^{-1})	
BRDF	Bidirectional Reflection Distribution Function ($Cd \cdot m^{-2} \cdot lux^{-1}$) or (sr^{-1})	
ρ	Reflectance	(-) or (%)
ρ_s	Surface reflectance	(-) or (%)
$\rho_{s\ model}$	Model Surface reflectance	(-) or (%)
$\rho_{s\ base\ case}$	Base case model surface reflectance	(-) or (%)
ρ_g	Ground reflectance	(-) or (%)
$\rho_{g\ model}$	Model ground reflectance	(-) or (%)
$\rho_{g\ base\ case}$	Base case model ground reflectance	(-) or (%)
τ	Transmittance	(-) or (%)
τ_{model}	Model window transmittance	(-) or (%)
$\tau_{base\ case}$	Base case model window transmittance	(-) or (%)

Lighting figures

$d\Phi, F$	Luminous flux	(lumen)
Φ_r	Reflected light flux	(lumen)
Φ_i	Incident light flux	(lumen)
Φ_t	Transmitted light flux	(lumen)
Φ_a	Absorbed light flux	(lumen)
E	Illuminance	(lux)
E_i	Indoor illuminance on a horizontal surface	(lux)
E_e	Outdoor illuminance on a horizontal surface	(lux)
L	Luminance	(cd/m ²)
DF	Daylight Factor	(-) or (%)
IR	Illuminance Ratio	(-) or (%)
LR	Luminance Ratio	(-) or (%)
f	Fraction of the incident light flux	(lumen)
D_{ij}	Partial daylight factor	(-)
E_{ij}	Illuminance at considered point i (interior) from the luminous zone j	(lux)
E_{ej}	Illuminance at considered point e (exterior) from the luminous zone j	(lux)

Angles

Ω	Solid angle	(Steradian)
θ	Angle between the surface normal and the specified direction	(°)
i	Light ray incident angle	(°)
r	Angle of redirected light ray	(°)
A_s	Sensor sensitivity area angle (diviation from the base case)	(°)
$A_{s\text{ model}}$	Sensor angle in model (diviation from the base case)	(°)
$A_{s\text{ base case}}$	Sensor angle in base case model	(°)

Radiance parameters

ab	ambient bounces
aa	ambient accuracy
ad	ambient divisions
ar	ambient resolution

Others

R	Relative divergence	(%)
---	---------------------	-----

Bibliography

- Aghemo C., Pellegrino A., Lo Verso V.R.M., 2004. "Daylighting Design by means of a Scanning Sky Simulator: Applications to Different Typologies of Daylighting Systems", *Proc. Of EuroSun 2004*, Freiburg (Germany).
- Aghemo, C., Pellegrino, A., Lo Verso, V.R.M., 2002. "Scale Models Under an Artificial Sky as Tool for Daylighting Design: Possible Applications", *Proc. Of CIE Light and Lighting 2002*, Bucharest (Romania).
- Anaokar S., Moeck M., 2005. *Validation Of High Dynamic Range Imaging to Luminance Measurement*, Leukos: J. Illuminating Engineering Society of North America Vol2, No2, pp.133-144, IESNA (USA).
- Andersen, M., 2001. "Use of Matrices for the Adaptation of Video-Based Photogoniometric Measurement to a Variable Referential", *Proc. Of CISBAT 2001 Solar Energy in Buildings*, pp. 193 – 198, EPFL/ Lausanne (Switzerland).
- Andersen, M., 2004. *Innovative Bidirectional Video-Goniophotometer for Advanced Fenestration Systems*. PhD thesis, EPFL, Lausanne (Switzerland).
- Ando T. and Drew P., 1996. *Church on the Water, Church of the Light*, Phaidon Press, London (UK).
- Ashmore, J., Richens, Paul, 2001. "Computer Simulation in Daylight Design: A Comparison", *Architectural Science Review*, 44, pp 33-44, (UK).
- Augustesen C., 2006. *Detail Practice - Lighting Design: Principle, Implementation, Case studies*, Birkhäuser, Basle (Switzerland).
- Baker N. and Steemers K., 2002. *Daylight Design of Buildings*, James and James, London (UK).
- Begemann S. H. A. et al., 1996. "Daylight, Artificial Light and People in an Office Environment, Overview of Visual and Biological Responses", *Industrial Ergonomics*, 20, pp. 231-239, Elsevier (UK).
- Beltrán L., Mogo B., 2005. "Assessment of Luminance Distribution Using HDR Photography", *Proc of 2005 ISES Solar World Congress*, Orlando FL (USA).
- Bodart, M., de Penaranda, R., Deneyer, A., Flamant, G., 2007. "Photometry and Colorimetry Characterisation of Materials in Daylighting Evaluation Tools", *Building and Environment*, Elsevier Science (UK).
- Boesiger W. et al., 1970. *Le Corbusier 1946-52*, Les editions d'Architecture (Artemis), Zurich (Switzerland).
- Cannon-Brookes S. W. A., 1997. "Simple Scale Models for Daylighting Design : Analysis of Sources of Error in Illumination Prediction", *Lighting Research and Technology*, Vol. 29, pp. 135-142, CIBSE (UK).
- Chauvel P., Gracia M. and Brebion H., 1985. *Etude sur Maquettes en Ciel Artificiel*, Publication EN-ECL 85.11C, CSTB, Nantes (France).
- Cindy M. et al., 1984. "Modeling the Interaction of Light Between Diffuse Surfaces", *Computer Graphics*, Vol. 18(3), pp. 213-222, Siggraph'84.

- Commission Internationale de l'Eclairage, 1938a. Practical Methods for the Measurement of Reflectance and Transmittance, CIE, 130.
- Commission Internationale de l'Eclairage, 1938a. The Basis of Physical Photometry, CIE, 18.2 (TC-3-3).
- Commission Internationale de l'Eclairage, 1987. Method of Characterizing Illuminance Meters and Luminance Meters – Performance, Characteristics and Specifications, CIE, 69.
- Commission Internationale de l'Eclairage, 2003. Spatial Distribution of Daylight — CIE Standard General Sky, CIE, S 011/E.
- Compagnon R., 1993. *Computer Modelling of Side Daylighting Systems*, PhD Thesis N° 1193, Swiss Federal Institute of Technology (EPFL), Lausanne (Switzerland).
- Compagnon, R., 1993. *Simulations Numériques de Systèmes d'Eclairage Naturel à Pénétration Latéral*, PhD thesis, EPFL, Lausanne (Switzerland).
- Conway H. and Roenisch R., 2005. *Understanding Architecture: An Introduction to Architecture and Architectural history*, Routledge, London (UK).
- Courret, G., 1999. *Systèmes Anidoliques d'Eclairage Naturel*. PhD thesis, EPFL, Lausanne (Switzerland).
- De Boer, J., Erhorn, H. (Editor), 1998. Survey of Simple Design Tools, Final Report, IEA SChTask 21 Daylight in Buildings, Fraunhofer Gesellschaft, Stuttgart (Germany).
- De Gryse B., 1984. *Karnak: 3000 ans de gloire égyptienne*, Liège: Edition du Perron, Bruxelles (Belgium).
- Edmons, I., 1993. "Performance of Laser-Cut Deflecting Panels on Daylighting", *Solar Energy Materials and Solar Cells*, 29, pp. 1-26.
- Engels H. and Meyer U., 2001. *Bauhaus Architecture 1919-1933*, Prestel, München (Germany).
- Erhorn H. and Dirksmöller M. (Editors), 2000. *ADELIN 3 Software Documentation*, Fraunhofer-Institut für Bauphysik, Stuttgart (Germany).
- Fontoynt M. et al, 1999. "Validation of Daylighting Simulation Programmes within IEA Task 21", *Proc. of CIE Conference*, Warsaw (Poland).
- Fontoynt M., 1999. *Daylight Performance of Buildings*, James and James, London (UK).
- Fontoynt, M., 1987. *Prise en Compte du Rayonnement Solaire dans l'Eclairage Naturel de Locaux : Methode et Perspectives*. PhD thesis, L'Ecole Nationale Supérieure des Mines de Paris, Paris (France).
- Friemert C., 1984. *Die Gläserne Arche*, Prestel, München (Germany).
- Goral C., Torrance K., Greenberg D., Battaille B., 1984. "Modeling the Interaction of Light Between Diffuse Surfaces, ACM Siggraph", *Computer Graphics*, Vol.18, pp.213 - 222, New York (USA).
- Greenup, O., Edmonds, I., and Compagnon, R., 2000. "Radiance Algorithm to Simulate Laser Cut Panel Light Redirecting Elements", *Lighting Research and Technology*, 32(2), pp. 49-54, CIBSE (UK).
- Holmes, J., 1988. "Light Reflection by Prismatic Sheets", *CIBSE Research Note*, 20(3), pp. 115-117.

Hopkinson R.G., Petherbridge P. and Longmore J., 1966. *Daylighting*, Heinemann, London (UK).

Illuminating Engineering Society of North America, 1984. *Lighting Handbook – Application and Reference Volume*, IESNA, New York (USA).

Illuminating Engineering Society of North America, 2006. *Lighting Handbook*, IESNA, New York (USA).

Inanici M., 2006. "Evaluation of High Dynamic Range Photography as a Luminance Data Acquisition System", *Lighting Research and Technology*, Vol38, pp.123-136, CIBSE (UK).

Inanici M., Galvin J., 2004. *Evaluation of High Dynamic Range Photography as a Luminance Mapping Technique*, LBNL Report No.57545, Berkeley: Lawrence Berkeley National Laboratory, California (USA).

International Energy Agency, 1999. *Survey Simple Design Tools*, Report of IEA SHC Task 21 /ECBCS Annex 29, Stuttgart (Germany).

International Energy Agency, 2000. *Daylight in Buildings - A source book on daylighting systems and components*, Report of IEA SHC Task 21 /ECBCS Annex 29, Berkeley (USA).

Johnston S., 2001. *A history of Light and Colour Measurement: Science in the Shadows*, University of Glasgow, Crichton Campus, Institute of physics publishing Bristol and Philadelphia, London (UK).

Kaempf, J., 2003. Technical Report and User's Manual BTDF2prism2, LESO-PB/EPFL (Switzerland).

Kopylov, E., Dmitriev, K., 2000. "Light Propagation Visualization as a Tool for 3D Scene Analysis in Lighting Design", *Computer and Graphic*, Elsevier Science (UK).

Lechner N., 1991. *Heating Cooling Lighting- Design Methods for Architects*, John Wiley and sons, New York (USA).

Li, D., Lau, C., Lam J., 2003. "A Simplified Procedure Using Daylight Coefficient Concept for Sky Component Prediction", *Architectural Science Review*, 47, pp 287-294, (UK).

Linhart F. and Scartezzini J.-L., 2007. "Minimizing Connected Lighting Power in Office Rooms Equipped with Anidolic Daylighting Systems", *Proc. Of CISBAT 2007 Int'l Conference on Solar Energy and Buildings*, pp. 421 – 426, EPFL/Lausanne (Switzerland).

Littlefair, P., 1992. "Daylight Coefficients for Practical Computation of Internal Illuminances", *Lighting Research and Technology*, 24(3), pp. 127-135, CIBSE (UK).

Love J. A. and Navvab M., 1991. "Daylighting Estimation Under Real Skies : A Comparison of Full-Scale Photometry and Computer Simulation", *Illuminating Engineering Society*, 20(1), pp. 140-156, IESNA (USA).

Maamari, F., Fontoyont, M., 2003. "Analytical Tests for Investigating the Accuracy of Lighting Programs", *Lighting Research and Technology*, 35(3), pp. 225-242, CIBSE (UK).

Maammari F., Fontoyont M., Hirata M., Koster J., Marty C. and Transgrassoulis A., 2003. "Reliable Datasets for Lighting Programmes Validation: Benchmark results", *Proc. Of CISBAT 2003 Int'l Conference on Solar Energy and Buildings*, pp. 241 – 246, EPFL/Lausanne (Switzerland).

- Mardaljevic, J., 1999. *Daylight Simulation : Validation, Sky models and Daylight Coefficients*. PhD thesis, De Montfort university, Leicester (UK).
- Mardaljevic, J., 2004. "Verification of Program Accuracy for Illuminance Modeling: Assumptions, Methodology and an Examination of Conflicting Findings", *Lighting Research and Technology*, 36(3), pp. 217-242, CIBSE (UK).
- Martinell C., 1975. *Gaudi : his life his theories his work*, Editorial Blume, Barcelona (Spain).
- Mccarter R., 2005. *Louis I Kahn*, Phaidon, London (UK).
- Michel L., 2002, "Implementing the Partial Daylight Factor Method Under a Scanning Sky Simulator", *Solar Energy*, 72(6), pp. 473-492, Elsevier Science (UK).
- Michel L., Roecker C. and Scartezzini J.-L., 1995, "Performance of a New Scanning sky Simulator", *Lighting Research and Technology*, 27(4), pp. 197-207, CIBSE (UK).
- Michel, L., 1999. *Méthode Expérimentale d'Évaluation des Performances Lumineuse de Bâtiments*. PhD thesis, EPFL, Lausanne (Switzerland).
- Millet M. S., 1996. *Light Revealing Architecture*, Van Nostrand Reinhold, New York (USA).
- Nakamae E. and Tadamura K., 1995. "Photorealism in Computer Graphics- Past and Present", *Computer and Graphics*, 19(1), pp. 119-130, Pergamon press (UK).
- Pacciani R. et al., 1987. "Maquette", *Rassegna*, Rivista trimestrale, anno IX, 32/4 dicembre, Bologna (Italy).
- Perez., R., Seals, R., and Michalsky, J., 1993. "All-Weather Model for Sky Luminance Distribution: Preliminary Configuration and Validation", *Solar Energy*, 50(3), pp. 235 -245.
- Plant C., Archer D., 1973. "A Computer Model for Lighting Prediction", *Building Sciences* Vol.8, pp.351-361, Pergamon Press (UK).
- Reinhard E., Ward G., Pattanaik S, Debevec P., 2006, *High Dynamic Range Imaging*, Elsevier Inc., San-francisco (USA).
- Reinhart, C. and Herkel, S., 2000. "The Simulation of Annual Daylight Illuminance Distributions a State-of-the-Art Comparison of Six RADIANCE-Based Methods", *Energy and Buildings*, 72(1), pp. 167-187.
- Robbins C. L., 1986. *Daylighting Design and Analysis*, Van Nostrand Reinhold, New York (USA).
- Ryer A., 1997. *Light Measurement Handbook*, Technical publications department, International Light, Inc., MA (USA).
- Sauneron S. and Stierlin H., 1980. *Les Plus Beaux Temples Egyptiens*, MEDEA diffusion SA, Fribourg (Switzerland).
- Scartezzini J.-L. and Courret G., 2002. "Anidolic Daylighting Systems", *Solar Energy*, 73(2), pp. 123 -135, Elsevier Science (UK).
- Scartezzini J.-L., 2003. "Advanced in Daylighting and Artificial Lighting", *Proc. Of Research in Building Physics*, Technologisch Instituut, Leuven (Belgium).

Scartezzini J.-L., Paule B., Lousselet J., Perrottet C. and Simos S., 1994. *Office Lighting*, RAVEL Publication N° 724.329.2f, Swiss Action Programme on Rational Use of Energy, Bern (Switzerland).

Scartezzini, J.L., Compagnon, R., Citherlet, S., Courret, G., Michel, L., Paule, B., and Simos, S. Daylighting Design of European Buildings. UE project 93.0015, LESO-PB/EPFL, Lausanne (Switzerland).

Scartezzini, J.L., Compagnon, R., Ward, G., and Paule, B., 1994. Computer Daylighting Simulation Tools. Technical Report, University of Geneva / EPFL, Lausanne (Switzerland).

Schiler M. (Editor), 1987. *Simulating Daylight with Architectural Models*, Daylighting Network of North America, University of Southern California, Los Angeles (USA).

Seetzen H., Heidrich W., Stuerzlinger W., Ward G., Whitehead L., Trentacoste M., Ghosh A., Vorozcovs A., 2004. "High Dynamic Range Display Systems", *Proc. Of ACM SIGGRAPH Conference*, Los Angeles (USA).

Shen L., Deprettere E., Dewilde P., 1995. "A Parallel Image-Rendering Algorithm and Architecture Based On Ray Tracing and Radiosity Shading", *Computer & Graphics*, Vol.19, No.2, pp.281 - 296, Elsevier Science (UK).

Sthapitanonda N. and Mertens B., 2006. *Architecture of Thailand: a guide to traditional and contemporary forms*, Thames and Hudson, London (UK).

Thanachareonkit, A., Andersen, M., Scartezzini, J.-L., 2004. "Analysing Sources of Error in Building Daylighting Performance Assessment by Comparison of Test Modules and Scale Model", *Proc. of Eurosun 2004*, pp. 254 – 262, Freiburg (Germany).

Thanachareonkit, A., Andersen, M., Scartezzini, J.-L., 2003. "Comparing Daylighting Performances Assessment of Buildings within Scale Models and Test Modules", *Proc. of CISBAT 2003*, pp. 289 – 294, EPFL/Lausanne (Switzerland).

Thanachareonkit, A., Andersen, M., Scartezzini, J.-L., 2005. "Comparing Daylighting Performances Assessment of Buildings within Scale Models and Test Modules", *Solar Energy*, pp. 168 – 182, Elsevier Science (UK).

Thanachareonkit, A., Scartezzini, J.-L., "Modelling Complex Fenestration Systems", *Proc. of CISBAT 2007*, EPFL/Lausanne (Switzerland).

Thanachareonkit, A., Scartezzini, J.-L., 2006. "Comparing the Accuracy of Daylighting Physical and Virtual Models for Complex Fenestration Systems", *Proc. of PLEA 2006*, pp. 429 - 435, Geneva (Switzerland).

Thanachareonkit, A., Scartezzini, J.-L., Robinson, D., 2005. "Analysis of Error Sources within Daylighting Physical and Virtual Models of Buildings", *Proc. of CISBAT 2005*, pp. 429 – 434, EPFL/Lausanne (Switzerland).

Toman R. and Bednorz A., 1997. *L'Art Roman: Architecture, Sculpture, Peinture*, Könemann, Cologne (Germany).

Tragenza, P., 1987. "Subdivision of the Sky Hemisphere for Luminance Measurements", *Lighting Research and Technology*, 19, pp. 13-19.

Tyng A., 1984. *Beginnings: Louis I. Kahn's Philosophy of architecture*, Wiley, New York (USA).

Ward G., 1998. "The LogLuv Encoding for Full Gamut, High Dynamic Range Images," *Journal of Graphics Tools*, (USA).

Ward G., BrightSide Technologies, 2006. "Color in High Dynamic Range Imaging", *Proc. of 14th Color Imaging Conference*, Scottsdale AZ (USA).

Ward G., Simmons M., August 2004. "Subband Encoding of High Dynamic Range Imagery", *Proc. of First Symposium on Applied Perception in Graphics and Visualization (APGV)*, Los Angeles (USA).

Ward Larson, G. and Shakespeare, R., 1998. *Rendering with Radiance – The Art and Science of Lighting visualization*, Morgan Kaufmann Publishers, Inc., San Francisco, CA (USA).

Ward, G., 2002. "A Wide Field, High Dynamic Range, Stereographic Viewer", *Proc. of PICS 20.2*, Portland, Oregon (USA).

Wilkins A. J., 1993. "Health and Efficiency in Lighting Practice", *Energy*, 18(2), pp. 123 - 129, Pergamon press (UK).

Winkelmann, C.F. and Selkowitz, S, 1985, Daylighting Simulation in the DOE-2 Building Energy, *Energy and Buildings*, pp. 271- 286, Elsevier Sequoia (The Netherlands).

Anothai Thanachareonkit

Av. de Tivoli 8, 1007 Lausanne, Switzerland
anothai.thanachareonkit@epfl.ch
Phone +41 79 766 82 30

Education **Ph.D in Environment**, Swiss Federal Institute of Technology, Lausanne (EPFL), Switzerland, 2003—present
Thesis Title: "Comparison of Daylighting Performance Assessment of Complex Fenestration Systems"
Expected Completion date: June 2008

M.Arch. in Building Technology, Chulalongkorn University, Thailand, 2001
B.Arch. in Architecture, Chulalongkorn University, Thailand, 1999

Professional experience

Present	Research assistant Teaching assistant Swiss Federal Institute of Technology Lausanne (EPFL), Switzerland, Solar Energy and Building Physics Laboratory (LESO-PB)
2002—3	Trainee Swiss Federal Institute of Technology Lausanne (EPFL), Switzerland, Solar Energy and Building Physics Laboratory (LESO-PB)
2002	Architect , Division of Architecture, Department of Public Works and Town and Country Planning Ministry of Interior, Thailand
2001	Architect , Terra Architects Co., Thailand
1998	Trainee , Lands and Houses Co., Thailand

Professional activities

Conferences

Sep 2007	CISBAT 2007, "Renewables in a Changing Climate, Innovation in Building Envelopes and Environmental Systems," Lausanne, Switzerland
Sep 2006	Passive Low Energy Architecture (PLEA) 2006 Conference, Geneva, Switzerland
Sep 2005	CISBAT 2005, "Renewables in a Changing Climate, Innovation in Building Envelopes and Environmental Systems," Lausanne, Switzerland
Oct 2004	International Radiance Workshop, Fribourg, Switzerland
Jun 2004	EuroSun Conference, Freiburg, Germany
Oct 2003	CISBAT 2003 Conference, "Innovation in Building Envelopes and Environmental Systems", Lausanne, Switzerland

Seminars

Feb 2007	Environmental Energy Technologies Division Seminars, "Daylighting Research at the Swiss Federal Institute of Technology in Lausanne (Switzerland)," Lawrence Berkeley National Laboratory, University of California
Jun 2004	LESO-PB seminar, "Daylighting Performances Assessment of Buildings: Comparisons of Physical and Computer Models," Solar Energy and Building Physics Laboratory, Swiss Federal Institute of Technology, Lausanne

Visiting researcher

Feb 2007 High dynamic range imaging technique: Lawrence Berkley National Laboratory

Teaching

2005—8 Teaching assistant
Course: Building physics for architects 3 and 4 (second year students)

2006 Lecture: Lighting models for architects (Master's students in Architecture and Sustainable Development)

Fellowships

2002—5 Federal Commission for Scholarships for Foreign Students (Switzerland), Grants for postgraduate study

Publications

Modeling Complex Fenestration Systems, A. Thanachareonkit and J.-L. Scartezzini, in CISBAT Proceedings 2007, EPFL, Lausanne, 2007

Comparing the Accuracy of Daylighting Physical and Virtual Models for Complex Fenestration Systems, A. Thanachareonkit and J.-L. Scartezzini, in PLEA Proceedings 2006, pp. 429 – 435, Geneva, 2006

Comparing Daylighting Performance Assessment of Buildings within Scale Models and Test Modules, A. Thanachareonkit, M. Andersen and J.-L. Scartezzini, in Solar Energy, 73(2), pp. 168 – 182, Elsevier Science, UK, 2005

Analysis of Error Sources within Daylighting Physical and Virtual Models of Buildings, A. Thanachareonkit, J.-L. Scartezzini, and D. Robinson, in CISBAT Proceedings 2005, pp. 429 – 434, EPFL, Lausanne, Sep 28, 2005

Analysing Sources of Error in Building Daylighting Performance Assessment by Comparison of Test Modules and Scale Model, A. Thanachareonkit, M. Andersen, and J.-L. Scartezzini, in EuroSun Proceedings 2004, pp. 454 – 462, Freiburg i.B., June 20—23, 2004

Comparing Daylighting Performances Assessment of Buildings within Scale Models and Test Modules, A. Thanachareonkit, M. Andersen, and J.-L. Scartezzini, in CISBAT Proceedings 2003, pp. 289 – 294, EPFL, Lausanne, Oct 8—9, 2003

Skills

Radiance, Photosphere, Adobe Illustrator, Adobe Photoshop, Adobe InDesign, Autocad, Microsoft Office